Improving the understanding of platinum sensitivity and the tumour microenvironment in high grade serous ovarian cancer

Malcolm John Farquharson
MBChB, MSc, MRCS(Ed), MRCOG

Submitted in fulfilment of the requirements for the
Degree of Doctor of Philosophy

College of Medical, Veterinary and Life Sciences
University of Glasgow
May 2018

Abstract

Ovarian cancer is one of the most lethal malignancies and often presents at an advanced stage, resulting in a poor prognostic outlook. Platinum chemotherapy leads to an initial clinical response, however most patients will ultimately relapse and there remains a sub-group who are intrinsically resistant to platinum.

I focussed on high grade serous ovarian cancer (HGSOC), the most common subtype of ovarian cancer. The ID8 CRISPR-generated models represented a novel and simple tool to investigate the biology of HGSOC. By using this *in vivo* model, I aimed to further the understanding of platinum sensitivity in HGSOC by investigating the homologous recombination pathway and the tumour microenvironment.

In vitro work showed that sensitivity to PARP inhibitors was clearly correlated with defective homologous recombination but the relationship with platinum sensitivity was more complicated. Using the ID8 derivatives, *in vivo* cisplatin experiments identified *Pten* and *Nf1* loss to be associated with the worst prognosis with the knockout of *Brca1* or *Brca2* prolonging survival. A *Brca1* mutation in the PALB2 domain compared to the BRCT2 domain was found to be associated with a greater sensitivity to cisplatin.

The tumour microenvironment was shown to differ between genotypes and altered with the addition of platinum chemotherapy. Specifically, the loss of *Pten* was associated with an immunosuppressive microenvironment with increased levels of myeloid-derived suppressor cells (MDSCs) and tumour-associated macrophages (TAMs). The chemokines, *Ccl2* and *Ccl7* were shown to be significantly increased in the *Trp53-/-;Pten-/-* genotype.

I targeted both the cytokine/chemokine response directly by using a transgenic mouse model (CCR1, 2, 3, 5 receptors knockout) and the PI3K/AKT pathway by using a PI3K inhibitor (p110ß) (AZD8186) to attempt to reverse the effect of *Pten* loss. The transgenic mouse model (GGTACKO) showed encouraging early results with a reduction in MDSCs and TAMs in the knockout mice injected with

the *Trp53-/-;Pten-/-* genotype but a repeat experiment is required before valid conclusions can be made.

The AZD8186 *in vivo* experiment showed a significant reduction in MDSC levels in the ascites following AZD8186 treatment in mice injected with the *Trp53-/-; Pten-/-* genotype and a non-significant decrease in the tumour samples. There was also a reversal in the anaemia previously shown with the loss of *Pten* and a decrease in *Ccl2* and *Ccl7* expression.

I have used a transplantable *in vivo* model for HGSOC to investigate potential mechanisms of platinum sensitivity and identified poor prognostic genotypes (*Pten*, *Nf1*). I have found *Pten* loss to be associated with an immunosuppressive microenvironment and highlighted potential therapeutic targets. By targeting the PI3K/AKT pathway I have shown that the effect of *Pten* loss can be reversed. The next step will be to determine whether this reversal results in a prolonged survival.

Table of Contents

List of Tables

List of Figures

List of Appendices

Acknowledgements

I would firstly like to thank my supervisor, Professor Iain McNeish, for giving me the opportunity to be involved in this project and for his continued help and guidance. I could not have asked for a more supportive and encouraging supervisor. He was able to offer endless advice throughout the 3 years, and kept me enthused about my project even at my lowest points!

Thank you also to the members of Professor Iain McNeish's team – Pavlina, Alex, Melanie, Aula, Joana, Karen, Darren, Elaine and Josephine. You have all helped me at different stages along the PhD journey and I am extremely grateful. I particularly want to thank Suzanne Dowson for teaching me cell culture at the beginning and always being available whenever I needed help. Despite listening to your daily woes! I very much enjoyed working with you and you really helped me settle into the lab environment.

Finally, I would like to thank my family and friends for being there and also being available for a drink, whenever I needed a distraction! A special thank you to Katrina for her vital support and patience throughout.

Declaration

The work presented in this thesis was performed entirely by the author except as acknowledged at the Wolfson Wohl Cancer Research Centre, Institute of Cancer Sciences, Glasgow University. This thesis has not been previously submitted for a degree or diploma at this or any other institution.

Malcolm Farquharson

May 2018

Abbreviations

BMI	body mass index
BRCA1	Breast cancer 1
BRCA2	Breast cancer 2
BrdU	5-bromo-2'-deoxyuridine
BSA	bovine serum albumin
BSU	Biological Services Unit
CA-125	cancer antigen 125
CAF	cancer-associated fibroblasts
Ccl	chemokine ligand
CD	Cluster of Differentiation
cDNA	complementary deoxyribonucleic acid
Cdk	cyclin-dependent kinase
CKI	cyclin kinase inhibitors
CO_2	carbon dioxide
CRISPR	Clustered regularly interspaced short palindromic repeats
CRUK	Cancer Research UK
CSF-1	colony stimulating factor-1
Ct	cycle threshold
CT	computerised tomography
dH_2O	distilled water
DAPI	4',6-diamidino-2-phenylindole
DMEM	Dulbecco's Modified Eagle Medium
DMSO	dimethyl sulphoxide
DNA	deoxyribonucleic acid
dsDNA	double stranded deoxyribonucleic acid
DSB	double-strand breaks
ECM	extracellular matrix
EDTA	ethylenediaminetetraacetic acid
EGFR	epidermal growth factor receptor
ERCC1	excision repair cross-complementation group 1
FACS	fluorescence activated cell sorting

FBS	Foetal bovine serum
FIGO	International Federation of Gynecology and Obstetrics
FMO	fluorescence minus one
GC	guanine-cytosine
GFP	green fluorescent protein
HCT	haematocrit
H&E	haematoxylin and eosin
HEK	human embryonic kidney cell
HEPES	4-(2-hydroxyethyl)-1-piperazineethanesulfonic acid
HGB	haemoglobin
HGSOC	high grade serous ovarian cancer
HR	homologous recombination
HR	hazard ratio
HRT	hormone replacement therapy
ICGC	International Cancer Genome Consortium
IOTA	International Ovarian Tumor Analysis Group
IP	intraperitoneal
IC50	inhibitory concentration 50%
IHC	immunohistochemistry
IL	interleukin
ITS	Insulin, Transferrin, Sodium selenite
KO	knock-out
LG	L-Glutamine
MDSC	myeloid-derived suppressor cell
MHC II	major histocompatibility complex class II
MMR	mismatch repair pathway
MTT	3-(4,5-dimethylthiazol-2-yl)-2,5-diphenyltetrazolium bromide
NaCl	sodium chloride
NACT	neoadjuvant chemotherapy
NBF	neutral buffered formalin
NF1	neurofibromin 1
NER	nucleotide excision repair
NHEJ	non-homologous end joining
NICE	National Institute for Health and Care Excellence

NLS	nuclear localisation signal
NTC	no template control
PARP	poly (ADP-ribose) polymerase
PBS	phosphate buffered saline
PCR	polymerase chain reaction
PD-1	programmed death 1
PD-L1	programmed death ligand 1
PE	paired end
PFA	Paraformaldehyde
PLT	platelets
P/S	Penicillin/Streptomycin
PTEN	phosphatase and tensin homolog
RCT	Randomised control trial
RIN	RNA integrity number
RMI	risk of malignancy index
RNA	ribonucleic acid
RPMI	Roswell Park Memorial Institute (medium)
RT-qPCR	Quantitative reverse transcription PCR
SCNA	somatic copy number alterations
SD	standard deviation
SEM	standard error of the mean
SNP	single nucleotide polymorphism
SNV	single nucleotide variants
STIC	serous tubal intra-epithelial carcinoma
SV	structural variants
TAM	tumour-associated macrophage
TCA	trichloroacetic acid
TCGA	The Cancer Genome Atlas
TILs	tumour-infiltrating lymphocytes
TMA	tissue microarray
TME	tumour microenvironment
TNM	Tumour-Node-Metastases
TP53	tumour protein 53
TRAIL	TNF-related apoptosis inducing ligand
VEGF	vascular endothelial growth factor

WGC	whole genome sequencing
WT	wild-type
WT1	Wilms Tumour gene

Publications and Presentations

Publications

1. CRISPR/Cas9-derived models of ovarian high grade serous carcinoma targeting *Brca1*, *Pten* and *Nf1*, and correlation with platinum sensitivity; Walton J, **Farquharson MJ**, Mason S, Port J, Kruspig B, Dowson S, Stevenson D, Murphy D, Matzuk M, Kim J, Coffelt S, Blyth K, McNeish IA; Scientific Reports; 7: 16827; 2017

2. CRISPR/Cas9-mediated *Trp53* and *Brca2* knockout to generate improved murine models of ovarian high grade serous carcinoma; Walton J, Blagih J, Ennis D, Leung E, Dowson S, **Farquharson MJ**, Tookman LA, Orange C, Athineos D, Mason S, Stevenson D, Blyth K, Strathdee D, Balkwill FR, Vousden K, Lockley M, McNeish IA; Cancer Research; 76 (20); 2016

Presentations

1. Improving the understanding of the tumour microenvironment using an *in-vivo* model for high grade serous ovarian cancer; **Farquharson MJ**, Walton J, Dowson S, Ennis D, Mason S, Clark W, Bailey P, Upstill-Goddard R, Blyth K, McNeish I; RCOG World Congress, Singapore, March 21st-24th 2018

2. Loss of *PTEN* induces an immunosuppressive environment and influences survival and platinum sensitivity in high grade serous ovarian cancer; **Farquharson MJ**, Walton J, Dowson S, Ennis D, Mason S, Clark W, Bailey P, Upstill-Goddard R, Blyth K; McNeish I; British Gynaecological Cancer Society, Glasgow, June 15-16th 2017

1 Introduction

1.1 Incidence and Mortality Rates in Ovarian Cancer

Ovarian cancer is one of the most lethal malignancies and often presents at an advanced stage, resulting in a poor prognostic outlook for many patients. Worldwide, it is estimated that nearly 239,000 women were diagnosed with ovarian cancer in 2012 (Ferlay et al., 2015). Ovarian cancer is the 5th most common cancer in females in the UK with approximately 7000 new cases diagnosed each year. Overall the incidence of ovarian cancer has increased in the UK since the late 1970's. However, since 2000 the incidence has decreased by 11% (Figure 1.1) (CRUK). This decrease may be explained by the change in the classification of borderline tumours where prior to 2000 many borderline malignant ovarian tumours were classified as malignant. An additional explanation may also be the increased use of the contraceptive pill which reduces the risk of ovarian cancer (Beral et al., 2008).

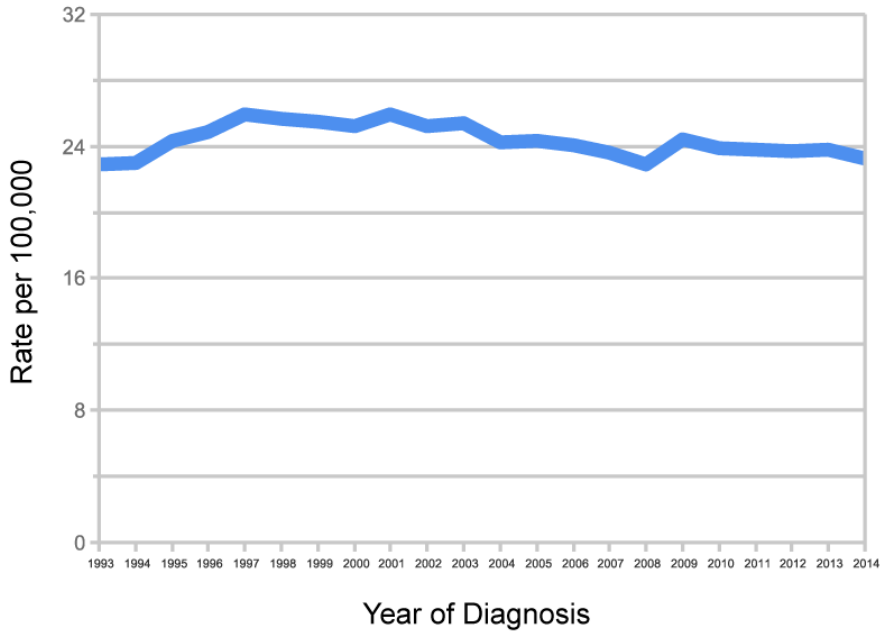

Figure 1.1: Ovarian cancer incidence rates in the UK between 1993-2014.

The figure demonstrates a decrease in incidence rates over the last 20 years (figure adapted from CRUK).

Approximately 152,000 women died worldwide from ovarian cancer in 2012 with around 4,300 women dying from the disease in the UK (Ferlay et al., 2015). Age-standardised mortality rates (Figure 1.2) have decreased between 1971-1973 and 2010-2012 with a 20% decrease over the last decade. However, this

reduction in mortality had been in women under 70, women aged 70 or over have seen a worsening of mortality over the last 30 years (CRUK). This increase in mortality may be due to a rise in incidence since the 1970s and specific to this age group an increase in nulliparity and the use of hormone replacement therapy (CRUK).

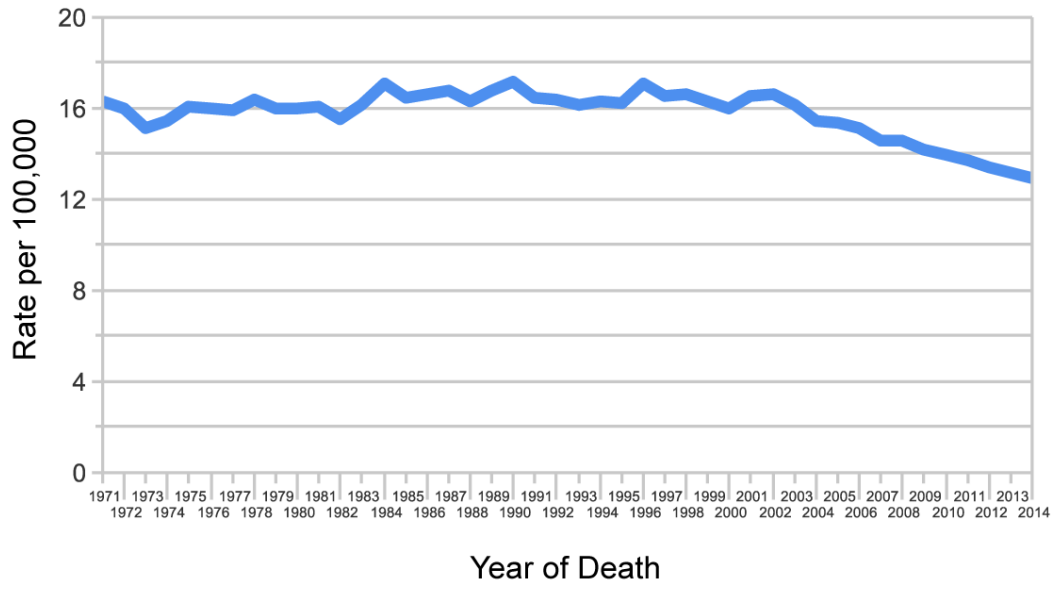

Figure 1.2: Ovarian cancer mortality rates in the UK between 1971-2014.

The figure demonstrates an overall decrease in mortality rates over the last 40 years (figure adapted from CRUK)

1.2 Risk Factors

The risk of developing ovarian cancer increases with age and usually occurs in women who have had their menopause. In the UK in 2012-2014 the age-specific incidence rates rise dramatically from 35-39, peaking in those aged 80-84 and then dropping sharply (Figure 1.3). On average each year more than half of cases were diagnosed in females over 65 (CRUK).

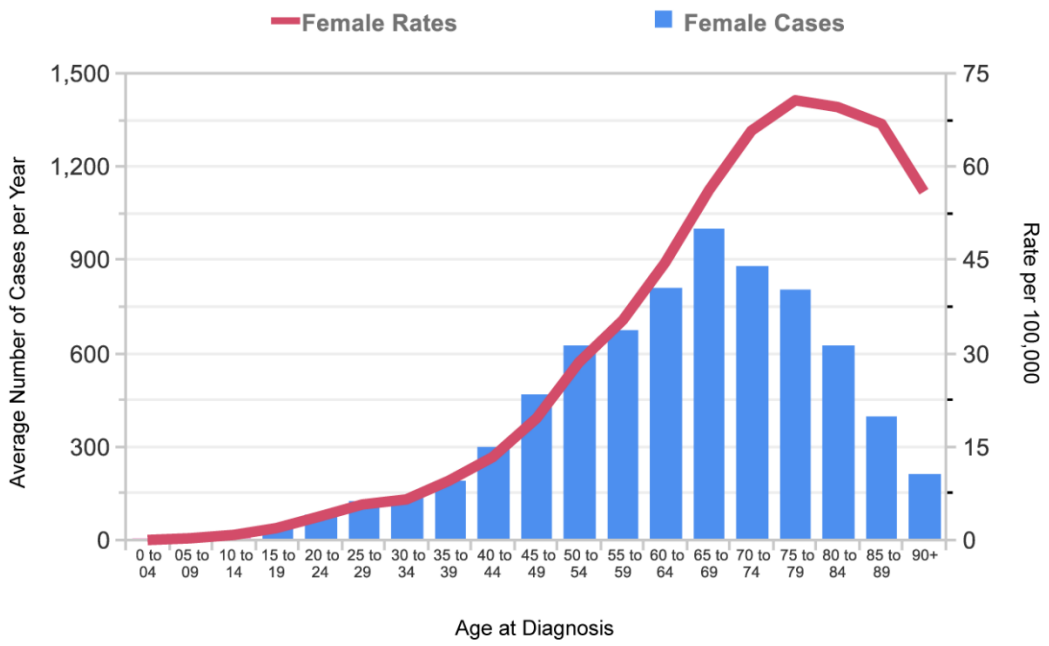

Figure 1.3: Average Number of New Cases per Year and Age-Specific Incidence Rates between 2012-2014.
The figure demonstrates the rise in incidence from 35-39 years (figure adapted from CRUK).

The 5-year survival rate is higher in younger women and decreases with increasing age. In England from 2007-2011 the 5-year survival ranged from 87% in those aged 15-39yrs to 17% in those aged 80-99yrs. Age-specific mortality in ovarian cancer increases sharply from 40-45yrs with the worst mortality in the over 85 age group. An average of 43% of deaths were in women over 75yrs and 72% were in those over 65yrs between 2010-2012 in the UK (CRUK).

Around 3% of all ovarian cancer cases occur in women with a family history of ovarian cancer (CRUK). The risk of ovarian cancer to any first-degree relative of patients with ovarian cancer is about 3-fold greater compared with the general population. There is also some evidence that the risk to relatives of

patients diagnosed younger than 50 years is as high as twice that to relatives of older patients with ovarian cancer. The most common sub-types of ovarian cancer, endometrioid and high-grade serous (HGSOC) have been shown to be associated with a significant increase in familial risk (Jervis et al., 2014). As *BRCA1* and *BRCA2* mutations are primarily associated with HGSOC it is not surprising the familial relative risk is higher for this subtype.

Inherited conditions are estimated to account for 5-15% of epithelial ovarian cancer. Hereditary Breast-Ovarian cancer syndrome with *BRCA1/2* mutations account for 65-85% and Lynch Syndrome with mismatch repair mutations account for another 10-15% (Lynch et al., 2013). There has been a wide range of figures quoted for ovarian cancer risk in women with *BRCA1/2* mutations. It is estimated that the risk is up to 65% higher in women with a *BRCA1* mutation and up to 35% higher in women with a *BRCA2* mutation (Ingham et al., 2013).

The risk of ovarian cancer is 24% higher in breast cancer survivors compared to the general population. The risk is higher in patients diagnosed with breast cancer at a younger age and also in oestrogen-receptor negative or oestrogen-receptor unknown breast cancer (Schonfeld et al., 2013). The risk of ovarian cancer is higher in bowel cancer survivors compared to the general population (Ahmed et al., 2006).

Evidence has shown that factors that alter the number of ovulations and/or sex hormone levels can affect the risk of ovarian cancer. Pregnancy, breastfeeding and oral contraceptives reduce the number of ovulations in a women's lifetime and have all been shown to decrease the risk of ovarian cancer (Lukanova and Kaaks, 2005).

HRT has been found recently to increase the risk of ovarian cancer by 43% in current users compared to women who have never used HRT (Beral et al., 2015). The use of HRT for <5 years had been previously thought to be a safe period however these women who had been on HRT <5 years at the time of diagnosis were also found to have a significant increased risk of ovarian cancer. The risk of ovarian cancer was significantly increased for both oestrogen-only and combined HRT with little difference between the types (Beral et al., 2015).

Although nulliparity is a known risk factor for ovarian cancer the association with infertility treatment has been less clear. A number of early cohort studies found an increased risk of borderline and invasive ovarian cancer following high doses and multiple cycles of clomiphene citrate (Rossing et al., 1994, Sanner et al., 2009). However in more recent and larger cohort studies there was no association found between malignancy risk and infertility medication (Jensen et al., 2009, Calderon-Margalit et al., 2009).

It has been suggested that 3% of ovarian cancer cases in the UK are linked to smoking (Beral et al., 2012, Faber et al., 2013). From meta- and pooled analyses there has been found to be significant variation in smoking-related risks between the tumour subtypes. In mucinous cancers, the incidence was increased in current versus never smokers however the increase was mainly in borderline malignant tumours. In both clear-cell and endometrioid cancers, studies have seen a reduction in cancer risk in current smokers however evidence for this is conflicting. There has been no significant association found between smoking and serous ovarian cancers (Beral et al., 2012, Faber et al., 2013).

Obesity is an important risk factor for many cancers. Some studies have shown a link between body size and ovarian cancer risk. The risk of ovarian cancer in HRT never-users is 10% higher per 5 unit BMI increment however the risk may only be increased in women with a BMI greater than 28 (Collaborative Group on Epidemiological Studies of Ovarian Cancer, 2012). Diabetes is associated with an increased risk of several cancer types although the exact mechanism of this link is not fully understood (Starup-Linde et al., 2013). A meta-analysis by Lee at al showed that the risk of ovarian cancer was increased by 55% in diabetics compared with non-diabetics when controlled for confounding variables (Lee et al., 2013).

The exact aetiology of endometriosis remains unclear. However, it is widely known to be associated with certain sub-types of ovarian cancer. A meta-analysis by Kim et al found that endometriosis increased ovarian cancer risk by 27-80% depending on study type (Kim et al., 2014). They also found that early stage disease, low-grade serous disease, endometrioid and clear cell sub-types

were all strongly associated with endometriosis-associated ovarian cancer. Whereas there was a relatively low incidence of high grade serous carcinoma in endometriosis-associated ovarian cancer and no association between endometriosis and mucinous carcinoma risk (Kim et al., 2014).

1.3 Pathology

1.3.1 Anatomy of the Fallopian Tube and Ovary

The ovaries consist of three components: the surface layer formed by cuboidal epithelium, the cortex containing stroma and ovarian follicles and the medulla containing stroma and neurovascular bundles. The anatomy of the female reproductive system is illustrated below (Figure 1.4).

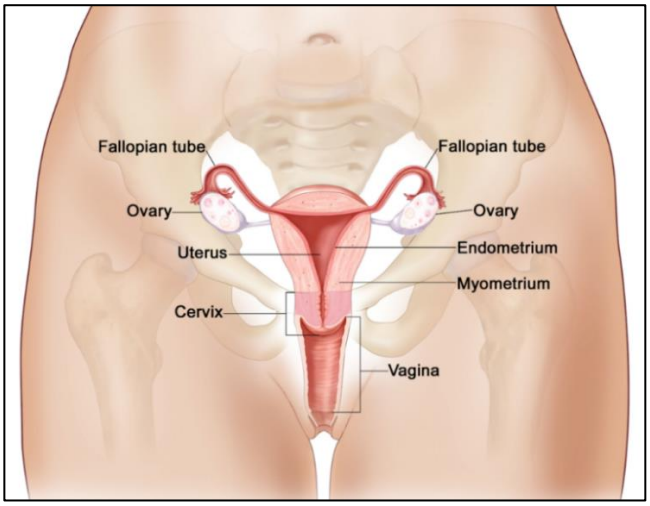

Figure 1.4: Anatomy of the female reproductive system.

The ovaries are located either side of the uterus within the broad ligament below the Fallopian tubes (http://seer.cancer.gov/statfacts/html/ovary.html).

The Fallopian tube consist of four parts the Isthmus, Ampulla, Infundibulum and Fimbriae. The inner mucosa is lined with ciliated columnar epithelial cells and non-ciliated secretory cells (Figure 1.5).

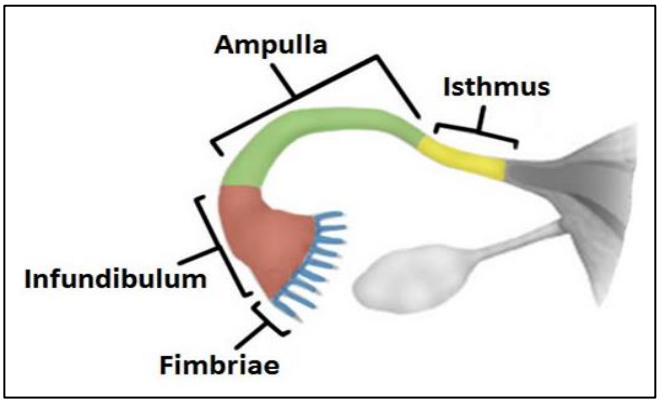

Figure 1.5: Anatomy of the Fallopian tube

(http://teachmeanatomy.info/pelvis/female-reproductive-tract/fallopian-tubes/)

1.3.2 Ovarian Cancer Histopathology

There are many different histological and molecular sub-types of ovarian cancer however they are often treated as a single disease. Nearly 10 years ago ovarian cancer surface epithelial tumours began to be classified into type I and type II tumours according to their pathway of tumourigenesis (Shih Ie and Kurman, 2004). Type I tumours included low grade serous, endometrioid, mucinous and clear cell types. Whereas Type II tumours at the time had no identified precursor lesion and included high-grade serous and carcinosarcoma (Shih Ie and Kurman, 2004) (Table 1.1 and Figure 1.6). However, between these subtypes there are significant genomic differences.

Recent genomic findings suggest that many ovarian cancers are derived from non-ovarian tissue and there are few molecular similarities between the histotypes. Immunological markers and genomic studies have shown that many tumours that were previously classified as high-grade endometrioid should be re-classified as high grade serous cancers (Madore et al., 2010).

This thesis focuses on high grade serous ovarian cancer, the most common sub-type of ovarian cancer.

Table 1.1: Ovarian cancer sub-types and associated mutations.

Ovarian cancer						
Epithelial					Non-epithelial	
High-grade serous	**Low-grade serous**	**Mucinous**	**Clear cell**	**Endometrioid**	**Sex cord-stromal**	**Others e.g germ cell**
TP53	*BRAF*	*KRAS*	*ARID1A*	*ARID1A*	Granulosa cell - *FOXL2*	
BRCA1/2	*KRAS*	*HER2*	*PIK3CA*	*PIK3CA*	Sertoli-Leydig cell - *DICER1*	
NF1	*NRAS*		*PTEN*	*PTEN*		
RB1	*ERBB2*		*CTNNB1*	*PPP2R1a*		
CDK12			*PPP2R1a*	MMR deficiency		
HR repair genes						

High-grade serous ovarian cancer (HGSOC) accounts for up to 70% of all ovarian cases. They have the highest frequency of *TP53* mutation of any solid tumour at 97%, which is the essential driver mutation in the pathogenesis of HGSOC (Ahmed et al., 2010). *TP53* is the only gene that is mutated in >10% of cases at the somatic level and it has been suggested that 100% of HGSOC are *TP53* mutant (Cole et al., 2016).

The increase in prophylactic salpingo-oophorectomy for familial risk has allowed pathologists to examine a larger number of specimens in women at higher risk of ovarian cancer.

The distal fallopian tube has relatively recently been identified as the likely source of HGSOC with early STIC (serous tubal intra-epithelial carcinoma) lesions with hallmark p53 signatures predominating in the fimbria and secretory cells (Cole et al., 2016). The first step in the transformation of benign tubal secretory cells is the 'p53 signature' with benign appearing cells showing evidence of strong nuclear p53 protein expression or absent p53 expression on IHC, in keeping with *TP53* missense and null mutations respectively. This is followed by the emergence of STIC lesions that are a multi-layered epithelium that lacks polarity and contains malignant secretory cells with DNA damage and p53 protein stabilisation in addition to a high proliferative index (Lee et al., 2007). The transformation of STIC lesions to HGSOC is thought to take approximately 7 years followed by the rapid development of metastases (Labidi-Galy et al., 2017b). Although a tubal origin of HGSOC is likely and widely accepted, STIC lesions are only seen in about half of HGSOC cases (Lee et al., 2007) and there have been mouse models of HGSOC that seem to primarily involve precursor cells in the ovary (Kim et al., 2012).

PAX8 is one protein that is consistently overexpressed in epithelial ovarian cancer compared to normal ovarian tissue. PAX8 is one of 9 transcription factors involved in embryogenesis and has been found to be expressed in non-ciliated secretory cells of normal healthy fallopian tubes but absent from ovarian surface epithelium (Di Palma et al., 2014).

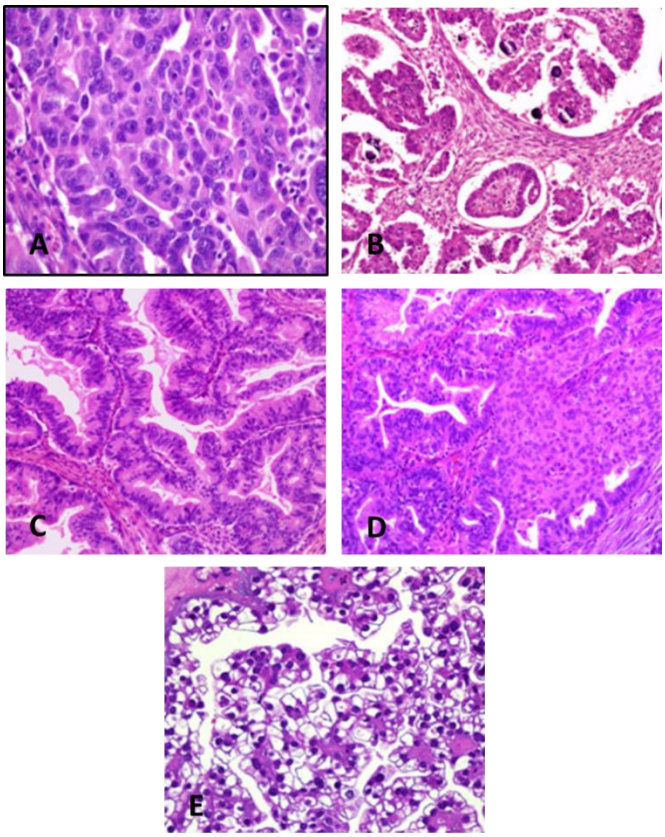

Figure 1.6: Five main sub-types of ovarian cancer.

A High-grade serous carcinoma; **B** Low-grade serous carcinoma; **C** Mucinous carcinoma; **D** Endometrioid carcinoma; **E** Clear cell carcinoma. Adapted from (Prat, 2012).

Recent studies have looked at the metastatic spread of HGSOC. HGSOC, like other intra-abdominal tumours, often metastasises to the omentum which is predominantly composed of adipocytes. The omental metastases ('omental cake') typically represent the largest tumour bulk in woman with ovarian cancer outside the pelvis. Nieman et al found that human omental adipocytes promote homing, migration and invasion of ovarian cancer cells and also act as an energy source (Nieman et al., 2011).

Epithelial ovarian cancer is believed to metastasize randomly by direct contact with intra-abdominal surfaces helped by the peritoneal circulation. However as discussed, ovarian cancer metastases have a predilection for the omentum. In addition to the omentum, pelvic and/or para-aortic lymph nodes can be involved and rarely brain and lung metastases. A recent study using a pre-clinical mouse model found haematogenous peritoneal dissemination of ovarian cancer cells with a tropism for the omentum, suggesting an additional mode of metastasis (Pradeep et al., 2014).

1.3.3 Mutations associated with high grade serous ovarian cancer

High grade serous ovarian cancer is characterised by genomic instability, in particular copy number abnormalities but with a low prevalence of recurrently mutated genes beyond *TP53* (2-6%) (Cancer Genome Atlas Research, 2011). Recent genomic studies have identified four gene expression clusters in high-grade serous cancer which have been termed: proliferative, immunoreactive, mesenchymal and differentiated according to the gene content in the clusters (Cancer Genome Atlas Research, 2011). This classification has not yet been applied clinically.

The Cancer Genome Atlas (TCGA) data suggested that up to 50% of HGSOC may have homologous recombination defects at the time of diagnosis (Cancer Genome Atlas Research, 2011). In addition to germline and somatic *BRCA1/2* mutations, these included a set of Fanconi Anaemia genes, *EMSY*, *RAD51, PTEN* and the DNA damage sensing genes *ATM* and *ATR* (Cancer Genome Atlas Research, 2011). However, these mutations were inferred and were not a functional assessment (Figure 1.7) and we specifically investigated the potential influence of *PTEN* loss on HR (see Chapter 3).

The frequency of *BRCA1* and *BRCA2* germ-line mutations had been unclear until recently with patient testing previously based solely on family history. Rust et al sequenced all newly presented non-mucinous ovarian cancer patients irrespective of family history and found 13.1% to have germline *BRCA1/2* mutations. They also found that 48% of patients selected would not have been offered sequencing based on the family history (Rust et al., 2018).

TCGA has analysed nearly 500 high grade serous ovarian cancer samples. They have reported 9 significantly mutated genes: *TP53, BRCA1, BRCA2, RB1, NF1, FAT3, CSMD3, GABRA6* and *CDK12* (Cancer Genome Atlas Research, 2011). As stated above, high grade serous cancer is characterised by near-universal *TP53* mutations as identified by Ahmed et al (Ahmed et al., 2010). *BRCA1/2* were mutated in 21% of tumours when combining both somatic and germline mutations. The remaining 7 mutated genes were only identified in 2-6% of high grade serous ovarian cancer cases (Cancer Genome Atlas Research, 2011).

The number of recurrent somatic copy number alterations (SCNAs) was analysed. The most common focal amplifications were *CCNE1, MYC* and *MECOM*, each of which was highly amplified in more than 20% of tumours (Cancer Genome Atlas Research, 2011). TCGA also identified 50 focal deletions, the tumour suppressor genes – *PTEN*, *RB1* and *NF1* were in regions of homozygous deletions in at least 2% of the tumours (Cancer Genome Atlas Research, 2011).

However, TCGA utilised whole exome sequencing (for SNV) rather than whole genome sequencing (WGS), and therefore did not evaluate over 95% of the genome. In addition, CNA was assessed using SNP arrays, which again will miss large portions of the genome. This is important because HGSOC is marked by extreme copy number abnormalities leading to structural variants (SV) and re-arrangement of large parts of the genome that alter gene integrity without specific mutations or large scale insertions/deletions, which will be missed by exome sequencing and SNP arrays (Patch et al., 2015). Critical genes whose function is altered by such SV include *PTEN, NF1* and *RB1*. Thus, an updated representation of the genomic landscape of HGSOC is given in Figure 1.7. However, it is important to appreciate that the alterations in this figure are rarely mutually exclusive – for example, over half (9/16) of cases with *NF1* loss in the ICGC WGS analysis (Patch et al) also had mutations in *BRCA1/2*. This makes classification of HGSOC genomes particularly challenging.

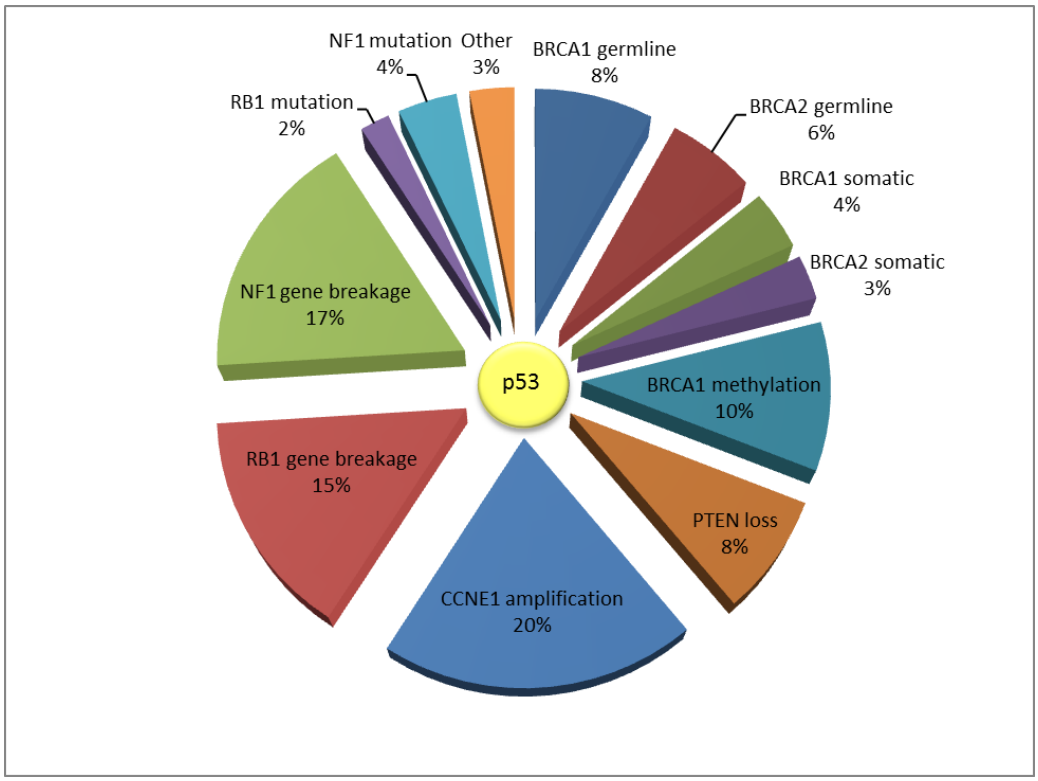

Figure 1.7: Mutational Landscape of High Grade Serous Ovarian Cancer. Adapted from (Patch et al., 2015) and (Cancer Genome Atlas Research, 2011).

1.4 Classification and Prognostic Factors

1.4.1 Anatomical Factors

The TNM (Tumour-Node-Metastases) classification and the FIGO (International Federation of Gynecology and Obstetrics) staging classification are both well-established classification systems accepted for the staging of ovarian cancer (Sobin, 2009, Prat, 2015).

The FIGO classification was updated in 2014 and the new TNM staging is awaiting publication. The FIGO classification emphasises surgical evidence, considers the likely tubal origin of HGSOC, and emphasises the importance of documenting the histologic subtype. It also correlates with the TNM system and is of prognostic significance (Table 1.2).

Patients with Stage I disease have a greater than 90% 5-year survival compared to a less than 5% 5-year survival for patients with Stage IV disease. The higher stage indicates more extensive disease and optimal debulking is less likely to be achieved when compared to a tumour that is only confined to the pelvis. For optimal debulking to be achieved in stage III/IV disease more radical surgery is often needed and this is associated with a higher incidence of perioperative morbidities (Ezzati et al., 2014).

The presence of a malignant pleural effusion in the absence of other stage IV criteria has a significantly worse prognosis when compared to stage III disease (Eitan et al., 2005). The presence of ascites is also an important component of the FIGO classification. Ascites in early-stage disease is a poor prognostic factor whereas smaller tumour volume and the absence of ascites in advanced disease are associated with a favourable outcome (Eitan et al., 2005).

The presence of lymph node metastases is a significant prognostic factor in ovarian cancer (Ozols et al., 1980). Retroperitoneal lymph node involvement occurs in up to 50-80% of women with advanced ovarian cancer (Omura et al., 1991). Women with tumours limited to the pelvis and positive lymph nodes have been found to have an improved 5-year survival (84%) compared to women with tumours that have spread beyond the pelvis (26%) (Ozols et al., 1980). There is

an on-going debate regarding the benefits of systematic lymphadenectomy versus lymph node sampling in advanced disease. The recent LION study concluded that systematic lymphadenectomy in patients with clinically negative lymph nodes and complete resection did not improve the overall and progression-free survival (Harter et al., 2017).

Optimal surgical debulking is the single most important prognostic factor in advanced ovarian cancer with studies showing a significant survival advantage with ≤ 1cm of residual disease (Shimizu et al., 1998). However, to achieve optimal cytoreduction there is often an associated surgical morbidity.

Table 1.2: The FIGO Ovarian Cancer Staging (2014).

Five-year relative percentage survival by stage between 2002 and 2006 (CRUK). Demonstrates the FIGO staging classification with the breakdown of each clinical parameter and corresponding TNM stage (Table adapted from similar in (Prat, 2015)).

Stage		5-year Survival
Stage I: Tumour limited to the ovaries (one or both)		
IA (T1a-N0-M0)	Tumour limited to one ovary; capsule intact, no tumour on ovarian surface; negative washings.	**90%**
IB (T1b-N0-M0)	Tumour limited to both ovaries; capsules intact, no tumour on ovarian surface; negative washings.	
IC	Tumour limited to one or both ovaries	
IC1 (T1C1-N0-M0)	Surgical spill	
IC2 (T1C2-N0-M0)	Capsule rupture before surgery or tumour on ovarian surface.	
IC3 (T1C3-N0-M0)	Malignant cells in the ascites or peritoneal washings.	
Stage II: Tumour involves one or both ovaries with pelvic extension (below the pelvic brim) or primary peritoneal cancer		
IIA (T2a-N0-M0)	Extension and/or implants on the uterus and/or tube(s)	**42.8%**
IIB (T2b-N0-M0)	Extension to and/or implants in other pelvic tissues	
Stage III: Tumour involves one or both ovaries with cytologically or histologically confirmed spread to the peritoneum outside the pelvis and/or metastasis to the retroperitoneal lymph nodes		
IIIA	(positive retroperitoneal lymph nodes and/or microscopic metastasis beyond the pelvis)	**18.6%**
IIIA1 (T1/2-N1-M0)	Positive retroperitoneal lymph nodes only IIIA1 (i) Metastasis ≤ 10mm IIIA1 (ii) Metastasis > 10mm	
IIIA2 (T3a2-N0/N1-M0)	Microscopic, extrapelvic (above the brim) peritoneal involvement +- positive retroperitoneal lymph nodes	
IIIB (T3b-N0/N1-M0)	Macroscopic, extrapelvic, peritoneal metastasis ≤ 2cm +/- positive retroperitoneal lymph nodes. Includes extension to capsule of liver/spleen.	
IIIC (T3c-N0/N1-M0)	Macroscopic, extrapelvic, peritoneal metastasis > 2cm +/- positive retroperitoneal lymph nodes. Includes extension to capsule of liver/spleen	
Stage IV (any T-any N-M1): Distant metastasis excluding peritoneal metastasis		
IVA	Pleural effusion with positive cytology	**3.5%**
IVB	Hepatic and/or splenic parenchymal metastasis, metastasis to extra-abdominal organs (including inguinal lymph nodes and lymph nodes outside of the abdominal cavity)	

1.4.2 Histological Factors

Tumour grade is thought to influence tumour behaviour however there have been conflicting studies over the association with clinical outcome (Ozols et al., 1980, Omura et al., 1991). Part of the difficulty is that there is no universally accepted grading system for ovarian cancer. Many pathologists use a FIGO system that characterises cellular architecture (AOGS, 1971) but a more recent system incorporates cellular architecture, nuclear grade and mitotic activity (Shimizu et al., 1998). This system correlates more accurately with lymph node metastasis and therefore survival. The histological sub-type is a much better predictor of survival than tumour grade (Bamias et al., 2012).

The tumour sub-type has been shown to be a more relevant histopathological prognostic factor in advanced ovarian cancer treated with the standard platinum-taxane combination (Bamias et al., 2012). Tumour grade was only significant between the low versus high grade serous tumours while the prognosis between grade 2 and 3 were similar. Tumour grade was found to be of no prognostic significance in mucinous, endometrioid and clear cell carcinomas (Bamias et al., 2012). The main challenge in determining the exact prognostic importance of tumour histology has been the previous misclassification of many ovarian cancer sub-types.

The histological sub-type has been generally thought to be associated with prognosis and studies have shown both mucinous and clear-cell carcinomas to be an adverse prognostic factor, but only in advanced stage (Zaino et al., 2011, Mackay et al., 2010).

1.4.3 Molecular Factors

A wide variety of molecular markers have been reported to influence prognosis in ovarian cancer including cell cycle regulators, mediators of proliferation, apoptosis and angiogenesis. However, most studies looking at prognostic markers have not differentiated between the subtypes and therefore it is difficult to make valid conclusions.

Tumour suppressor p53 has been one of the most investigated markers in ovarian cancer. A meta-analysis including 62 studies by (de Graeff et al., 2009) found wild-type p53 to be associated with a poor survival and when restricted to serous tumours there was a significant association with poor prognosis (HR 1.47, 95% CI 1.33-1.61). However there have been conflicting results in relation to p53 status and response to platinum-chemotherapy (Gadducci et al., 2009, Canevari et al., 2006). The lack of reproducible results makes it difficult to make any valid conclusions about the role of p53 as a reliable prognostic biomarker.

As discussed previously p53 has been found to be universally mutated in HGSOC therefore its potential as a prognostic marker is limited in this subtype. In addition, analysis of TCGA data suggest that type of *TP53* mutation (missense/gain-of-function vs null) also has no influence on outcome (PFS - p=0.0981, OS - p=0.0787; log-rank test) (Kang et al., 2013).

Wilms' Tumour gene (WT1) expression has shown differing patterns of expression among the ovarian cancer subtypes with a higher expression found in the serous subtype (Le Page et al., 2010). However, there have been conflicting reports over the role of *WT1* as a prognostic marker. Some studies report no prognostic advantage associated with *WT1* and others have shown a significantly worse prognosis when all histological subtypes are analysed (RR 1.7, 95% CI 1.2-2.3) (Kobel et al., 2008, Hogdall et al., 2007). *WT1* has been found to be a favourable marker in the cohort of patients with HGSOC and this may be because *WT1* is a marker of serous differentiation and therefore poorly differentiated serous carcinomas are less likely to express *WT1* and have a worse prognosis (RR 0.5, 95% CI 0.3-0.8) (Kobel et al., 2008). *WT1* is a good and

widely used diagnostic marker in serous carcinoma and helps in differentiating high-grade disease from a mixed carcinoma population (Le Page et al., 2010).

Ki67 is a proliferation marker commonly studied in cancer research as it is overexpressed in malignant tissue. It is a nuclear protein which is expressed throughout the cell cycle but absent in quiescent cells (G0) (Le Page et al., 2010). The overexpression appears to be in the serous histotype (Kobel et al., 2008) but this has not been found in all studies (Korkolopoulou et al., 2002). Again, there have been conflicting results on the prognostic value of Ki67, in the majority of reports high expression of Ki67 has been associated with a poor prognosis (Korkolopoulou et al., 2002). Kobel et al found that when retrospectively analysing all ovarian cancer subtypes for tissue-based biomarkers, Ki67 was associated with a negative prognosis (RR 1.7, 95% 1.2-2.4) however, HGSOC usually had a high Ki67 index. When the same subtypes were analysed individually, Ki67 was found to be of no prognostic significance (Kobel et al., 2008).

Many studies have shown that cell cycle regulators are involved in tumour progression in ovarian cancer. Cyclins are a family of proteins that co-ordinate the progression of cells through the cell cycle by activating cyclin-dependent kinase (Cdk) enzymes. Cyclin-Cdk complexes are regulated by kinase inhibitors (CKIs) (Le Page et al., 2010). The Cyclins appear and disappear at specific time points during the cell cycle. Oncogenesis can be caused by abnormal expression of cyclins (positive regulators) or loss of CKIs (negative regulators) (Le Page et al., 2010).

Cyclin E has been studied extensively in ovarian cancer and has been found to be associated with a poor prognosis in the serous disease subtype after retrospective IH analysis of 53 ovarian cancer samples ($p=0.054$ by Fisher test) (Rosenberg et al., 2001). A study by Etemadmoghadam measured genome wide copy number variation in 118 ovarian tumours and found CCNE1 expression to also be predictive of patient outcome and associated with resistance to platinum chemotherapy ($p=<0.001$ by Fisher test) (Etemadmoghadam et al., 2009).

Apoptosis is a process of programmed cell death. The extrinsic and intrinsic pathways mediate the process, and both lead to the activation of caspases. The extrinsic pathway is initiated by TRAIL, TNF and Fas-L whereas the intrinsic pathway is initiated by signalling events such as p53 and Bcl-2 activation.

TRAIL (TNF-related Apoptosis Inducing Ligand) is an extracellular protein that triggers apoptosis. The expression of different TRAIL receptors has been shown to enhance apoptotic ability of TRAIL (Duiker et al., 2006). The presence of stromal TRAIL in advanced disease has been shown to be associated with a favourable survival (p=0.049, log-rank test) (Horak et al., 2005) but this was not observed in patients treated with platinum chemotherapy (Duiker et al., 2010). Further studies have not seen any association between TRAIL and survival (p=0.09, log-rank test) (Ouellet et al., 2007). There have been conflicting results with Bcl-2. A high expression of Bcl-2 has been shown to be associated with an improved survival (p=0.0021, multivariate analysis) (Baekelandt et al., 1999) however this has not been found in the majority of studies (Geisler et al., 2000).

Poly (ADP-ribose) polymerase 1 (PARP1) is a key component in base excision repair, a significant pathway in the repair of DNA single-strand breaks. It also helps regulate both HR and NHEJ pathways (De Lorenzo et al., 2013). PARP inhibitors have an important role as a therapeutic agent in ovarian cancer. Although patients with BRCA1/2 germline mutations are associated with better outcomes which is most likely due to a greater sensitivity to platinum chemotherapy, Farmer et al found *BRCA1/2* mutant cell lines to be extremely sensitive to PARP inhibitors (Farmer et al., 2005). A recent randomised phase II trial by Ledermann et al found patients with platinum-sensitive relapsed serous ovarian cancer with BRCA-mutated disease to have a better progression free survival following the addition of a PARP inhibitor (11.2 months versus 4.3 months, HR 0.18 CI 0.10-0.31) (Ledermann et al., 2014). The *BRCA* status, although not universally used in clinical practice yet, may help as a predictor of disease response to therapeutic agents.

Vascular endothelial growth factor (VEGF) is a multifunctional cytokine that stimulates angiogenesis and increases microvascular permeability by binding to

receptors expressed on vascular endothelial cells (Neufeld et al., 1994). It is overexpressed in ovarian cancer when compared to benign tumours (Shen et al., 2000) and it has been shown to have a crucial role in neovascular formation in tumours (Ferrara, 1995). A high expression of VEGF on immunohistochemistry of 339 primary ovarian cancer samples has shown to improve survival in a study by Duncan et al ($p=0.04$, log-rank test) (Duncan et al., 2008) however a meta-analysis by Hefler et al found a high VEGF to be associated with a poor overall survival ($p=<0.001$, multivariate analysis) (Hefler et al., 2006).

The EGFR (epidermal growth factor receptor) is an extensively studied tyrosine kinase receptor and has been linked to a negative prognosis in many different cancers (Le Page et al., 2010). A meta-analysis found that EGFR and Her-2 had a limited impact on prognosis; however the analysis included a diverse number of tumour subtypes (de Graeff et al., 2009). This was further supported by the EORTC study that showed maintenance erlotinib (EGFR tyrosine kinase inhibitor) following first line chemotherapy in ovarian cancer did not improve progression-free or overall survival (PFS 12.7 (erlotinib) vs 12.4 months (observation) (HR 1.05, 95% CI 0.90-1.23) and OS 50.8 vs 59.1 months (HR 0.99, 95% CI 0.81-1.20) (Vergote et al., 2014).

1.4.4 Immunological Factors

The immune system has been shown to play an important role in ovarian cancer survival. Up to 50% of the cells within any solid tumour or metastasis are non-malignant (Balkwill et al., 2012). The complex tumour microenvironment includes many cells that have lost their protective function and operate in an immunosuppressive role. Cell types that retain their protective function are often inhibited by neighbouring cell types (Figure 1.8).

T and B cell lymphocytes

Zhang et al was the first to associate the presence of $CD3^+$ tumour-infiltrating lymphocytes (TILs) with improved clinical outcome in ovarian cancer (Zhang et al., 2003). A further study found $CD8^+$ TILs to be the only subtype associated with a favourable prognosis and that no stromal TILs of any subtype were associated with improved survival (Sato et al., 2005). The same study also found a high $CD8^+/CD4^+$ cell ratio improved survival although $CD4^+$ and $CD8^+$ alone had no association with prognosis (Sato et al., 2005). This finding implied that a further subpopulation of $CD4^+$ T cells might counteract the anti-tumour effects of $CD8^+$ cells (Sato et al., 2005).

A $CD4^+$ $CD25^+$ $FOXP3^+$ suppressor T cell (Treg) population has been found to be increased in late-stage ovarian cancer and associated with a worse prognosis (Curiel et al., 2004, Woo et al., 2001). Sato et al discovered that a high intraepithelial $CD8^+$/Treg ratio was associated with an improved survival and this indicates that the number of Tregs within the $CD4^+$ population influences the beneficial effects of $CD8^+$ T cells (Sato et al., 2005).

Myeloid-derived suppressor cells

Immune cells within the tumour microenvironment can limit and stimulate tumour growth. Myeloid-derived suppressor cells (MDSCs) are a heterogeneous population of immature myeloid cells that are recruited by tumour cells (Godoy et al., 2013). The two major MDSC subpopulations are granulocytic (human: $CD11b^+$ $CD14^-$ $CD15^+$ $CD66b^+$; murine: $CD11b^+$ $Ly6G^+$ $Ly6C^{low/-}$) and monocytic (human: $CD11b^+$ $CD14^+$ $HLA\text{-}DR^{low/-}$ $CD15^-$; murine: $CD11b^+$ $Ly6G^-$ $Ly6C^{high}$) (Godoy

et al., 2013). MDSCs have immunosuppressive properties and enhance tumour growth, invasion and metastasis (Obermajer et al., 2011).

In mice, changes in the phenotype of tumour-infiltrating dendritic cells have been found to influence disease progression in ovarian cancer. The depleting dendritic cells early in the disease accelerate tumour growth but the low dendritic cell number slow the aggressive progression in advanced disease (Scarlett et al., 2012).

Immune checkpoint inhibitors

Programmed death 1 (PD-1) is an inhibitory immune checkpoint receptor expressed by activated T cells (Hansen et al., 2016). PD-1 interacts with its ligands, PD-L1 and PD-L2 that are present on both tumour and stromal cells. Freeman et al found that binding of PD-1 by PD-L1 leads to inhibition of T cell lymphocyte proliferation and cytokine secretion (Freeman et al., 2000).

Tumour-associated macrophages

Macrophages are the most abundant immune cell in the tumour microenvironment. The two extreme states of macrophages are M1 and M2 with the latter correlated to poor prognosis in several human cancers (Dijkgraaf et al., 2013, Heusinkveld and van der Burg, 2011). Monocytes are recruited to the tumour microenvironment by a number of chemokines including CCL2, CCL5 and CXCL1 (Mantovani et al., 2004a), where they differentiate into tumour-associated macrophages (TAM). The survival of TAMs is sustained by cytokines within the tumour microenvironment such as CSFs and VEGF-A (Obermueller et al., 2004). TAMs produce either pro-tumour or anti-tumour properties depending on the types of cytokines to which they are exposed. Colony stimulating factor-1 (CSF-1) is a key cytokine in the recruitment and activation of macrophages by binding to a high-affinity receptor tyrosine kinase (CSF-1R) (DeNardo et al., 2011). TAMs acquire M2 properties, such as promoting tumour proliferation and progression in response to further cytokines such as TGF-ß, IL-10 and M-CSF (Obermueller et al., 2004). The terms M1 and M2 are too simplified as macrophages can adapt to a range of activation states between

the M1 and M2 phenotype depending on the signals within the microenvironment (Heusinkveld and van der Burg, 2011).

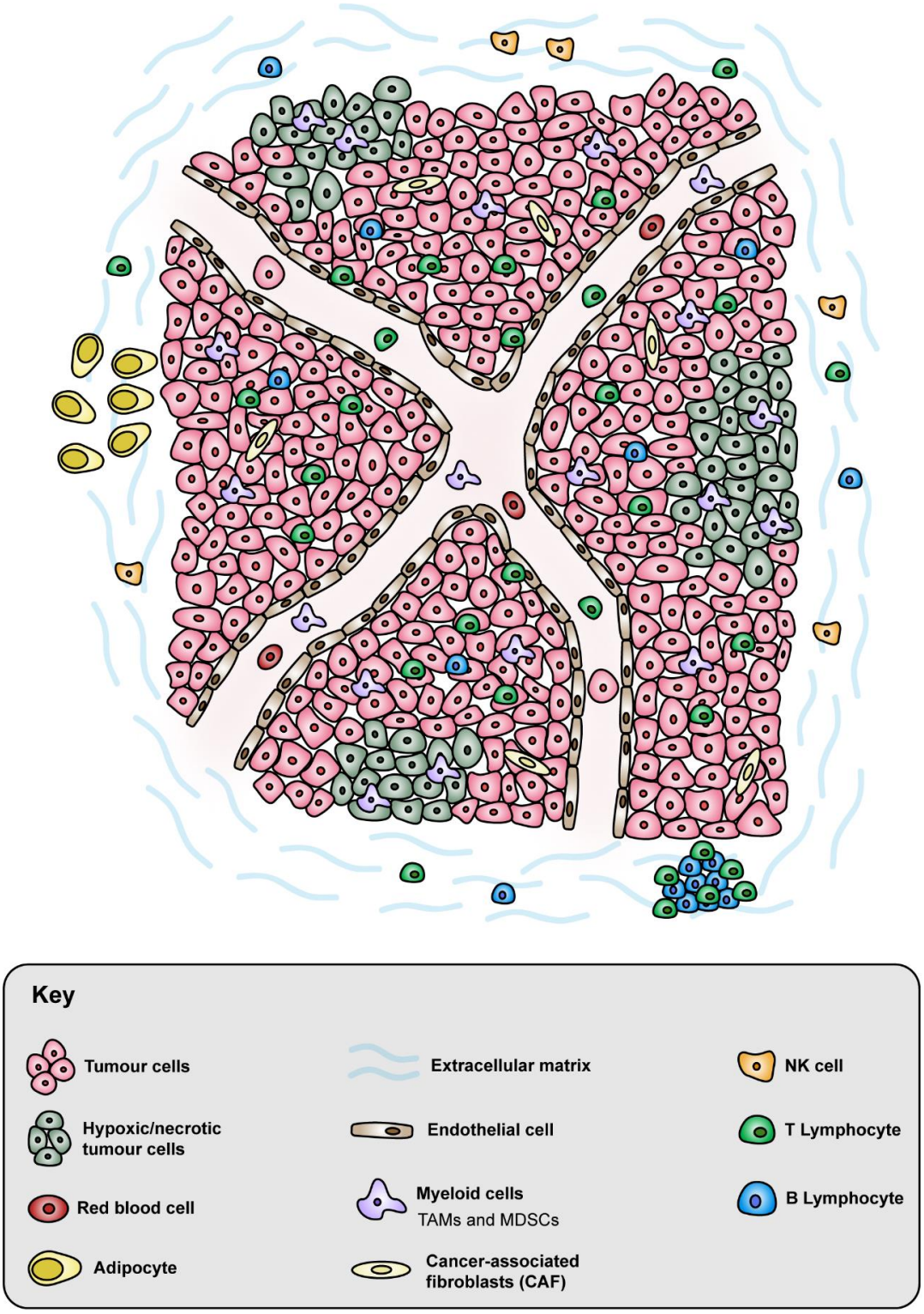

Figure 1.8: Illustration of the tumour microenvironment in ovarian cancer.
The figure shows the variety of cell types present (modified from (Balkwill et al., 2012))

1.5 Tumour Microenvironment (TME)

In addition to cells from the immune system several other components are involved in the tumour microenvironment. These include the tumour vasculature, lymphatics, fibroblasts, adipocytes and the extracellular matrix. (Figure 1.8).

Tumour vasculature

Many angiogenic signalling factors and specific cytokines are present within the tumour microenvironment, which may stimulate angiogenesis. The resulting blood vessels are leaky due to their abnormal structure and function. This, in turn, increases hypoxia and can influence drug distribution (Jain, 2005). As reviewed by Balkwill et al, VEGFA has been shown to be the predominant angiogenic factor in the tumour microenvironment (Balkwill et al., 2012).

Pericytes provide structural support to blood vessels. Studies in different cancer types have suggested that a key role of pericytes is to act as a negative regulator of metastases and that a low pericyte coverage correlates with a poor prognosis and increased metastases (Balkwill et al., 2012, O'Keeffe et al., 2008, Yonenaga et al., 2005).

In ovarian cancer the spread of disease is predominantly thought to be primarily via intraperitoneal 'seeding', although a study by Pradeep et al found preferential haematogenous metastasis to the omentum, albeit in a murine xenograft model, highlighting another important potential mode of metastasis (Pradeep et al., 2014).

Omentum

Ovarian cancer cells preferentially metastasise and proliferate in the omentum and as a result the 'omental cake' often represents the largest tumour bulk within the abdominal cavity. Nieman et al found that the secretion of adipokines aids with the recruitment of tumour cells and that adipocytes act as an energy source encouraging rapid tumour growth (Nieman et al., 2011).

Cancer-associated fibroblasts

Myofibroblasts are abundant within the tumour microenvironment and are referred to as cancer-associated fibroblasts (CAF). CAFs secrete growth factors such as EGF and IGF-1 which contribute to tumour progression (Spaeth et al., 2009, Tomasek et al., 2002). They also secrete key ECM components and remodelling enzymes. Depending on the tumour type, CAFs originate in a fibrovascular core and branch throughout the tumour mass or surround the tumour with dense stroma resulting in restricted chemotherapy distribution (Erez et al., 2010).

Lymphatics

Lymph nodes draining a tumour may protect the tumour from host immunity. The tumour-draining lymph nodes contain a high level of cytokines and antigens deriving from the tumour (Swartz and Lund, 2012). The lymph flow from tumours has been found to be increased compared to normal tissue in melanoma and increased lymph drainage has been positively correlated to metastasis in breast cancer (Harrell et al., 2007, Pathak et al., 2006). Lymphangiogenesis is driven by the production of VEGFC and VEGFD from the tumour and lymphatic endothelial cells within the tumour microenvironment have an important role in the dissemination of tumour cells (Alitalo, 2011).

Extracellular matrix (ECM)

The ECM is the non-cellular component present within all tissues and has a key role within the tumour microenvironment. In addition to providing scaffolding for many cells it is also crucial in the movement of cells into and out of the TME (Balkwill et al., 2012). The ECM is a highly dynamic structure that is constantly being remodelled (Frantz et al., 2010). The ECM interacts with cell surface receptors leading to signal transduction and gene transcript regulation (Frantz et al., 2010). A possible hypothesis for platinum-sensitive recurrence is that tumour cells can become chemotherapy resistant due to their contact with specific components of the ECM. These cells then persist after chemotherapy and go on to repopulate the tumour resulting in recurrence (Chien et al., 2013).

1.6 Management of Ovarian Cancer

1.6.1 Diagnosis

Ovarian cancer often presents with non-specific symptoms such as abdominal pain or distension, which can lead to a delay in diagnosis. The symptoms are frequently attributed to irritable bowel syndrome (IBS) and NICE guidelines recommend that women over 50 years with IBS symptoms should have a serum cancer antigen 125 (CA-125) performed (http://www.nice.org.uk/guidance/CG122).

Serum CA-125 is a glycoprotein that is most widely measured to detect ovarian cancer however; it can also be elevated in endometriosis, pelvic inflammatory disease, liver disease and other malignant tumours (Bast et al., 1983, Jacobs and Bast, 1989).

The CA-125 level and abdominal and transvaginal ultrasound are the key investigations when suspecting ovarian cancer. In the UK the risk of malignancy index (RMI) is used to help predict the risk of malignancy and to triage patients to the appropriate specialist. The RMI calculates a score according to ultrasound features, menopausal status and pre-operative CA-125 level (Geomini et al., 2009). The IOTA classification is an alternative system based on specific ultrasound findings and has similar sensitivity and specificity to RMI (Alcazar, 2016). A CT scan is routinely used to assess the site and spread of disease.

If chemotherapy is offered to women with suspected advanced disease, a tissue diagnosis should be confirmed by histology or cytology if histology is not appropriate (http://www.nice.org.uk/guidance/CG122).

1.6.2 Surgery

Surgery aims to remove as much tumour as possible and to establish the FIGO stage. It should include a total hysterectomy, bilateral salpingo-oophorectomy, tumour debulking and omentectomy (Jayson et al., 2014). Optimal debulking has been widely accepted as one of the most important prognostic indicators. A meta-analysis by Allen et al demonstrated a survival benefit for women with

advanced disease who had no macroscopic disease or tumour deposit <2cm (Allen et al., 1995). More recently, the survival advantage of complete debulking (no visible residual disease) was confirmed prospectively in a large adjuvant five-arm chemotherapy study (GOG182/ICON5) (Bookman et al., 2009). Thus, the aim of debulking surgery is to remove all visible macroscopic disease.

Increasingly radical surgery is being performed to free the patient of macroscopic disease, including diaphragmatic stripping, multiple bowel resections and resection of intrathoracic disease. However, the patient's condition and the extent of disease such as the involvement of the porta hepatis and small bowel mesentery limit the ability to achieve maximal debulking (Aletti et al., 2006).

Retroperitoneal lymphadenectomy has not been shown to confer a survival advantage in ovarian cancer but may be important for staging (Panici et al., 2005).

Primary surgery followed by adjuvant chemotherapy is considered the standard care in advanced ovarian cancer. The use of neoadjuvant chemotherapy when optimal surgical debulking is believed to be unachievable is now widely accepted, in the UK at least. This follows the publication of two trials in advanced disease that found no difference in survival between primary surgery and neoadjuvant chemotherapy (Vergote et al., 2010, Kehoe et al., 2015).

1.6.3 Chemotherapy

Adjuvant chemotherapy in early stage disease has been controversial with no clear consensus. Two RCTs, ICON1 and ACTION investigated the role of chemotherapy in early stage disease. With both studies combined, they demonstrated improved overall survival by 8% and progression-free survival by 11% at 5 years for those receiving adjuvant chemotherapy (Trimbos et al., 2003). Following extended follow-up from the ICON1 study, it was concluded that chemotherapy should be offered to patients with early disease and particularly patients with high-risk disease (stage 1B/1C grade 2/3, any stage 1 grade 3 or clear cell histology) (Collinson et al., 2014).

For the last 20 years, carboplatin and paclitaxel have been the standard of care for chemotherapy in ovarian cancer. The addition of paclitaxel to cisplatin was discovered to extend both overall survival and progression-free survival (McGuire et al., 1996) and currently six 3-weekly cycles of less toxic carboplatin combined with paclitaxel are given to women with advanced disease. Treatment response is monitored radiologically and by the CA-125 level (Rustin, 2003, Rustin et al., 2011).

Intraperitoneal chemotherapy has been found to significantly prolong survival in one study (Armstrong et al., 2006). However, toxic effects meant the regime was often intolerable and only 42% received all 6 cycles of intraperitoneal chemotherapy. Research is on-going into more tolerable regimes.

1.6.4 Recurrent disease

Most patients with recurrent disease receive second-line chemotherapy however a subset of women where surgical resection is achievable may have second surgery. The choice of chemotherapy regimen is dictated by the interval from the last platinum-based treatment to the point of recurrence (Eisenhauer et al., 1997).

Platinum-resistant disease is defined as disease progression within 6 months from the last platinum-based regime. Studies have found that <15% of women respond to second-line platinum if the 'platinum-free interval' is <6 months; this rises to >30% when the interval is greater than 6 months (Eisenhauer et al., 1997, Markman et al., 1991).

Randomised control trials have shown that platinum-sensitive recurrent disease is best treated with a combination of platinum-based chemotherapy with the addition of paclitaxel, gemcitabine or pegylated liposomal doxorubicin (Parmar et al., 2003, Pfisterer et al., 2006, Pujade-Lauraine et al., 2010).

1.6.5 New therapeutic options

There has been extensive research into Poly (ADP-ribose) polymerase (PARP) inhibitors for tumours with a defective homologous recombination pathway (Farmer et al., 2005, Bryant et al., 2005). PARP inhibitors have been found both by Phase I and by randomised trials to be of clinical benefit in women with *BRCA* mutations (Fong et al., 2009, Kaye et al., 2012). Further studies have found a prolonged progression-free survival with the addition of a PARP inhibitor as a maintenance therapy in recurrent disease following response to platinum-based chemotherapy (Ledermann et al., 2012, Mirza et al., 2016, Coleman et al., 2017).

Trials have also investigated angiogenesis as a target in ovarian cancer with most clinical studies involving bevacizumab (monoclonal anti-VEGF antibody). Two first-line trials have found that, in advanced disease, with residual tumour after surgery, the addition of bevacizumab to carboplatin and paclitaxel can improve progression-free survival (Perren et al., 2011, Burger et al., 2011). However, overall survival benefits are modest and restricted only to those with stage IV disease and/or bulky residual disease following primary dubulking surgery (Oza et al., 2015). Similarly, studies in platinum-sensitive and platinum-resistant relapse have also demonstrated that the addition of bevacizumab extends progression-free but not overall survival (Aghajanian et al., 2012, Pujade-Lauraine et al., 2014).

1.7 Platinum-based Chemotherapy

1.7.1 Mechanism of action

Cisplatin and Carboplatin are composed of a doubly-charged platinum atom surrounded by four ligands (Dasari and Tchounwou, 2014). Two amine ligands form strong interactions with the platinum atom, and the chloride ligands or carboxylate compounds form leaving groups allowing the platinum atom to form bonds with DNA bases (Goodsell, 2006).

Cisplatin becomes activated once it enters the cell and its chloride ligands are displaced by water molecules. It forms intrastrand and interstrand cross-links with purine bases to form DNA adducts. The cisplatin-DNA adducts block cell division and result in cell death (Dasari and Tchounwou, 2014). Carboplatin has a similar mechanism of action to Cisplatin (Figure 1.9).

Hongo et al demonstrated that carboplatin induced the same platinum-DNA adducts as those induced by cisplatin (Hongo et al., 1994). Carboplatin is less potent than cisplatin and the clinical standard dosage of carboplatin is usually 4:1 compared to cisplatin (Dasari and Tchounwou, 2014). The main benefit to carboplatin is reduction in nephrotoxic, neurotoxic and emetogenic effects; however myelosuppression limits the dosage (Dasari and Tchounwou, 2014).

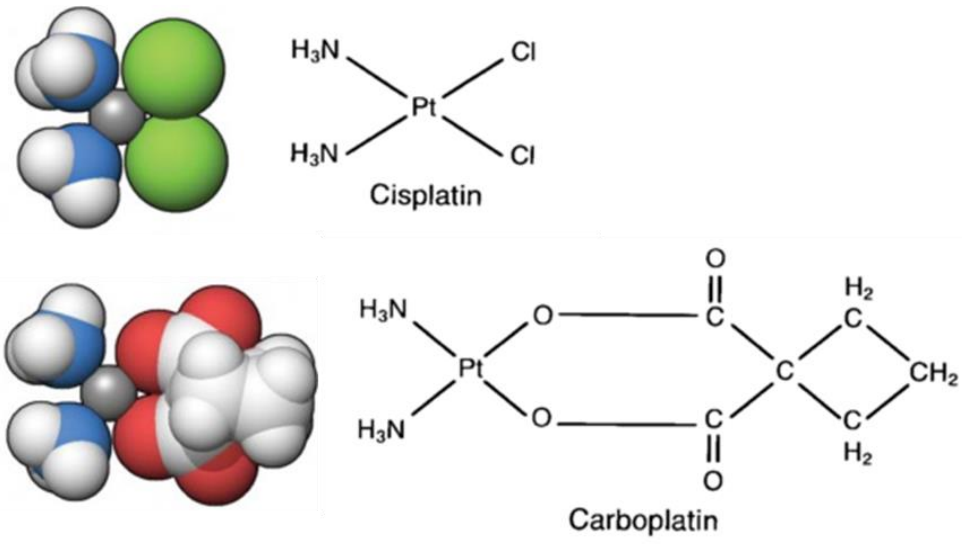

Figure 1.9: Chemical and molecular structures of Cisplatin and Carboplatin.

Both contain a doubly charged platinum atom with four ligands. Adapted from (Goodsell, 2006) and (Go and Adjei, 1999).

1.7.2 Mechanisms of resistance

A major factor in the low five-year survival in HGSOC is platinum resistance (tumour progression within six months of completion of platinum chemotherapy). Classically, in advanced ovarian cancer, patients respond initially to chemotherapy (approximately 65%). However, become increasingly resistant with more than two thirds relapsing within two years, of which half will present with platinum resistant disease (i.e. relapse within 6 months) (Vasey et al., 2004).

Multiple mechanisms are thought to contribute to drug resistance. The 'classical' mechanisms include (Vasey, 2003):

- Decreased drug uptake
- Increased drug efflux
- Increased repair of DNA damage induced by chemotherapy
- Reduced ability to undergo apoptosis

Newer molecular factors have been linked to platinum resistance that involve cell signalling pathways and the immune microenvironment.

1.7.3 Resistance and DNA repair pathways

The nucleotide excision repair (NER) pathway is responsible for repairing cisplatin bound to DNA. The excision repair cross-complementation group 1 (ERCC1) protein plays a key role in nucleotide excision repair (Martin et al., 2008). Increased *ERCC1* expression has been associated with the development of cisplatin resistance *in-vitro* (Ferry et al., 2000). A study by Kang et al found *ERCC1* mRNA levels in ovarian tumour samples to be inversely correlated to platinum response and survival (Kang et al., 2006).

Mismatch repair pathway (MMR) is a strand-specific repair pathway that is initiated with the recognition of DNA damage. When the pathway is deficient, damaged DNA accumulates, resulting in microsatellite instability (Martin et al., 2008). MMR deficiency allows cells to continue to proliferate despite DNA damage thus leading to resistance. Epigenetic silencing of MMR through Mut L

homologue 1 (hMLH1) promoter hypermethylation has been found in ovarian cancer. From mutational and expression data MMR deficiency is thought to be more common in non-serous ovarian cancer than serous subtypes (Xiao et al., 2014).

Homologous recombination (HR) plays a prominent role in the repair of DNA double-strand breaks. A number of studies have found that secondary mutations in both *BRCA1* and *BRCA2*-mutated tumours can restore the wild-type reading frame of the *BRCA1/2* protein and mediate acquired resistance to platinum-based chemotherapy (Swisher et al., 2008, Sakai et al., 2008, Lord and Ashworth, 2013).

1.7.4 Resistance and gene mutations

Amplification of Cyclin E1 (*CCNE1*), located on chromosome 19q12, is seen in approximately 20% of HGSOCs. CDK2 is the regulatory kinase of Cyclin E1 and binding of CDK2 to Cyclin E1 allows progression of the cell cycle from G1 to S phase and is essential for DNA replication (Etemadmoghadam et al., 2009). *CCNE1* amplification has been found to be associated with resistance in advanced serous ovarian cancer. The *CCNE1* copy number is specifically associated with chemoresistance and has been validated as a marker of patient outcome in ovarian cancer (Etemadmoghadam et al., 2009).

BRCA1/2 mutations and *CCNE1* amplification are known to promote genomic instability and tumour progression (Etemadmoghadam et al., 2013). They have been found to be mutually exclusive with a functional *BRCA1* selectively required in cancers that have *CCNE1* amplification. This requirement for *BRCA1* may offer a potential therapeutic approach for treatment resistant *CCNE1*-amplfied tumours (Etemadmoghadam et al., 2013).

p53 protein is involved in controlling the progression of cells through the cell cycle and helps cellular responses to DNA damage by mediating DNA repair, cell cycle regulation and activation of apoptosis (Vasey, 2003). There is increasing evidence that mutant p53 tumours lose wild-type p53 suppressor activity and gain functions to help with tumour progression (Muller and Vousden, 2014). In

ovarian cancer a significant correlation has been found between p53 accumulation, type of p53 mutation and poor response to platinum chemotherapy however, this data was found prior to accurate identification of disease subtype and before next-generation sequencing was available (Righetti et al., 1996). The high expression of both WT and mutant p53 in the cytoplasm of many tumours suggests that there is possible gain-of-function of p53 in driving oncogenesis (Chee et al., 2013). *TP53* as mentioned previously is universally mutated in high-grade ovarian cancer and as understanding of mutant p53 improves, it may offer a therapeutic target.

PTEN loss is a common event in HGSOC. TCGA previously showed homozygous deletion of *PTEN* in 6% of HGSOC cases (Cancer Genome Atlas Research, 2011), but following whole genome sequencing (Patch et al., 2015) and IHC studies (Martins et al., 2014), it was demonstrated that approximately 20% of HGSOC lose *PTEN* through complex SV and that up to 40% of tumour cells had loss of PTEN protein expression on IHC. *PTEN* is a phosphatase that inhibits cell proliferation induced by the PI3K/AKT pathway and acts as a tumour suppressor gene. Activation of the PI3K/AKT pathway is a critical step in cell survival through suppression of apoptosis, promotion of cell proliferation, migration, cell metabolism and protein translation (Martins et al., 2014). Studies have found that activation of the PI3K/AKT pathway may lead to chemotherapy resistance (Ohta et al., 2006, Lee et al., 2005).

1.7.5 Platinum Sensitivity

Women with *BRCA1/2* mutations tend to be hypersensitive to platinum chemotherapy and have a better prognosis compared to non-carriers (Foulkes, 2006). However, these patients still frequently develop platinum resistance. A recent paper from Candido-dos-Reis et al showed that *BRCA1/2* mutations were associated with an improved short-term survival. However over time in *BRCA1* carriers this advantage decreased and is reversed by 10 years (Candido-dos-Reis et al., 2015). This reversal in survival advantage for *BRCA1* carriers is difficult to explain at present. However, the short-term survival advantage of *BRCA1/2* carriers is a result of an increased sensitivity to platinum-based chemotherapy and impressive sensitivity to PARP inhibitors.

TCGA also found improved survival between patients with *BRCA1* and *BRCA2* mutations. In patients with a *BRCA2* mutation the 5-year survival rate was 61% versus 25% in the wild-type. Among the *BRCA2* mutated group 100% were platinum sensitive and this was compared to 80% of *BRCA1* mutated patients and 85% of wild-type cases (Cancer Genome Atlas Research, 2011). The *BRCA2* mutated patients also had a longer platinum-free survival when compared to both *BRCA1* mutated and wild-type patients.

Bolton et al observed that survival in *BRCA1* carriers depended on the mutation location. The N-terminal mutations on the *BRCA1* protein were associated with a worse survival compared to C-terminal mutations (Bolton et al., 2012). There is also evidence that a mutation in the RING domain (N-terminal) of *BRCA1* results in a poor response to Cisplatin and PARP inhibitors (Drost et al., 2011). A recent study by Labidi-Galy et al found that mutations in the RAD51 binding domain in *BRCA2* carriers was associated with a prolonged progression-free survival, platinum-free interval and overall survival (Labidi-Galy et al., 2017a). Further research into the location of the *BRCA1* and *BRCA2* mutations is required and particularly how this relates to survival and sensitivity to chemotherapy (Figure 1.10).

Increased platinum sensitivity is believed to occur in patients with mutations in other homologous recombination genes. This has been supported by Pennington et al that looked at 13 homologous recombination genes and found that patients with defects in these genes had an improved overall survival and increased sensitivity to platinum chemotherapy (Pennington et al., 2014). This was further supported by a recent study that found HR mutations including non-*BRCA* genes significantly prolonged both progression-free survival and overall survival in ovarian cancer (Norquist et al., 2017). As discussed previously the TCGA has found that up to 50% of HGSOC may have homologous recombination defects (Cancer Genome Atlas Research, 2011).

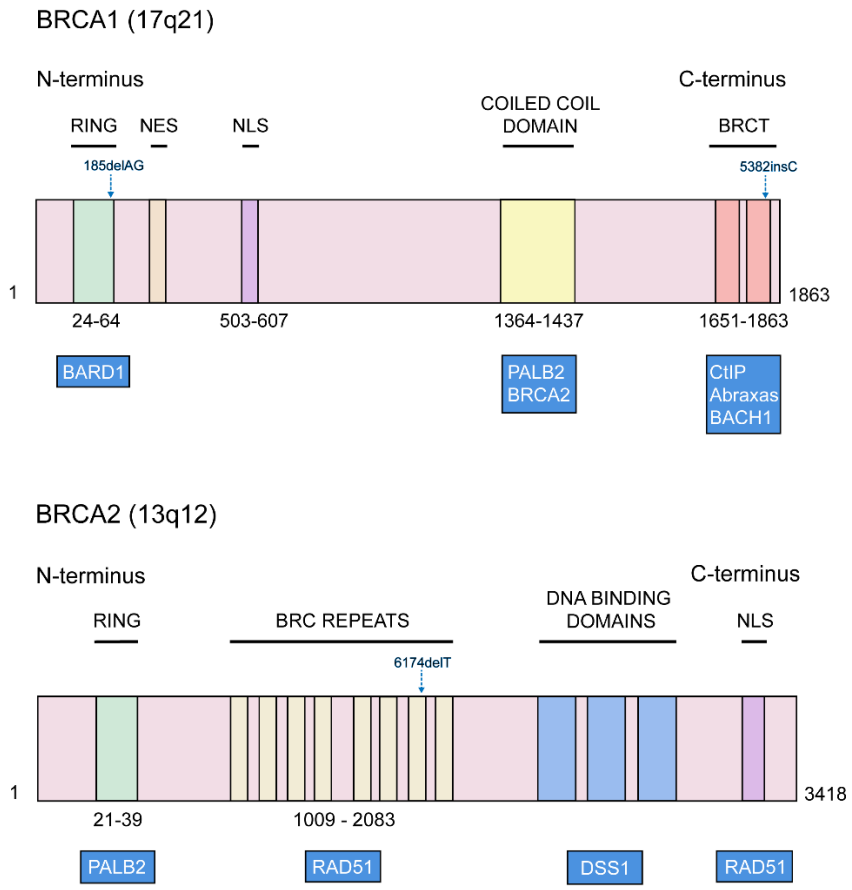

Figure 1.10: Schematic diagram of *BRCA1/BRCA2* binding partners.
Adapted from (Roy et al., 2011).
BRCA1 contains an N-terminal RING domain that is associated with BARD1, nuclear localisation signals (NLS), a coiled coil domain that is associated with BRCA2 via PALB2, and two C-terminal BRCT domains that bind ATM-phosphorylated abraxas, CtBP-interacting protein (CtIP) and BRIP1.
BRCA2 contains an N-terminal RING domain that binds PALB2, eight BRC motif repeats that bind RAD51, a DNA binding domain that bind both ssDNA and dsDNA and a C-terminal that contains an NLS that also binds RAD51.
Specific germline mutations found in Ashkenazi Jews (BRCA2 6174delT, BRCA1 185delAG and 5382insC) are illustrated in the above figure.

At present women with HR mutations including *BRCA1/2* are the only group of patients that we can predict are more likely to be sensitive to platinum chemotherapy. However, a study by Alsop et al found that of women with *BRCA1/2* mutations 85% were sensitive versus 68% and 15% of women with *BRCA1/2* mutations were resistant to platinum chemotherapy (Alsop et al., 2012). This study however defined sensitivity by the Ca125 and CT findings

whereas in clinical practice sensitivity and resistance are defined by the time to relapse. The reason for differences in cisplatin response in this group of patients in unclear and further research into the site and type of *BRCA1/2* mutation may offer an explanation.

1.7.6 Influence on tumour microenvironment

There is good evidence that HGSOC is an immunogenic tumour and recent *in-vivo* models have shown the immune system to play an important role in response to certain chemotherapy (Vacchelli et al., 2014, Michaud et al., 2011). The ability to take tumour biopsies at the time of diagnosis and following NACT gives us an opportunity to look at the influence chemotherapy has on the tumour microenvironment and whether the introduction of immunotherapy may be beneficial.

Böhm et al found that in omental biopsies after neoadjuvant chemotherapy there was evidence of T cell activation with significantly fewer $FoxP3^+$ T regulatory (Treg) cells and increased levels of immune-checkpoint molecules $PD\text{-}1^+$, $CTLA4^+$ and $PD\text{-}L1^+$. This suggests that platinum chemotherapy can initially enhance the host's immune response, but this effect is tempered by an increase in immune checkpoint molecules (Bohm et al., 2016).

A recent study by Lo et al found that neoadjuvant chemotherapy increased the densities of $CD3^+$, $CD8^+$, $TIA\text{-}1^+$ and $CD20^+$ tumour infiltrating lymphocytes in tumour samples (Lo et al., 2017). However, other than PD-1 that was increased, other immunosuppressive cell types were unchanged. They identified three major $PD\text{-}1^+$ TIL subsets: $PD\text{-}1^+$ $CD8^-$, $PD\text{-}1^+$ $CD8^+$ and $PD\text{-}1^+$ $FoxP3^+$. However, when analysed individually none of the subsets increased significantly so the overall increase may be due to small increases in all three subsets (Lo et al., 2017).

Pre-treatment tumours with increased densities of $CD3^+$, $CD8^+$, $CD20^+$ and $TIA\text{-}1^+$ have previously been shown to have a strong association with survival (Sato et al., 2005, Zhang et al., 2003). A feasible hypothesis is that post-neoadjuvant chemotherapy samples would have a greater prognostic significance given that

the altered microenvironment should influence the chance of disease recurrence. Lo et al found $CD20^+$ B cells to be significantly associated with survival however there was no significant association with $CD3^+$, $CD8^+$ and TIA-1^+ (Lo et al., 2017).

Lo et al also identified TIL response patterns using hierarchical clustering of the pre- and post-neoadjuvant chemotherapy samples. In the pre-NACT samples three subgroups of patients were identified. The first subgroup was positive for most of the immune markers ($CD3^+$, $CD4^+$, $CD8^+$, TIA-1^+, $CD20^+$, $FoxP3^+$ and PD-1^+) representing an immunoreactive tumour. The second showed low/intermediate levels of immune markers and the third was negative for most immune markers (Lo et al., 2017). Three response patterns were identified in the post-NACT samples. The pre-NACT samples that were positive for the immune markers generally showed a higher expression after NACT, samples with intermediate levels of immune markers also showed a higher expression and samples that were initially negative/low remained the same after NACT (Lo et al., 2017).

De Nardo et al found that in breast cancer an increased macrophage density correlated with a poor survival and that the ratio of macrophages/$CD68^+$ to $CD8^+$ was inversely correlated. They inhibited the tumour associated macrophages *in-vivo* and with the addition of chemotherapy showed an increase in the CD8 response and a positive influence on overall outcome (DeNardo et al., 2011).

There is evidence that treatment of cervical and ovarian cancer cell lines with platinum chemotherapy skews the monocytes to M2-like macrophages (Dijkgraaf et al., 2013).

1.8 Cancer Signalling Pathways

TCGA has identified both *PTEN* and *NF1* as common mutations in HGSOC. *PTEN* acts as a tumour suppressor gene and inhibits cell proliferation normally induced by the PI3K/AKT pathway. *NF1* is located at chromosome 17q11.2 and acts as a tumour suppressor gene that affects RAS-MAPK signalling. TCGA found *NF1* gene alterations in 12% of HGSOC patients (8% homozygous deletion and 4% mutations) (Yap et al., 2014).

1.8.1 PI3K/AKT Pathway

PI3K/AKT signalling pathway controls cellular processes such as proliferation, migration, apoptosis and metabolism. The Akt signalling cascade is activated by receptor tyrosine kinases and G-protein-coupled receptors that lead to production of PIP3 by PI3K. This results in phosphorylation of Akt that stimulates multiple pathways including mTOR signalling (Figure 1.11).

PTEN catalyses the dephosphorylation of PIP3 to PIP2 (membrane phospholipids) resulting in inhibition of the Akt activity.

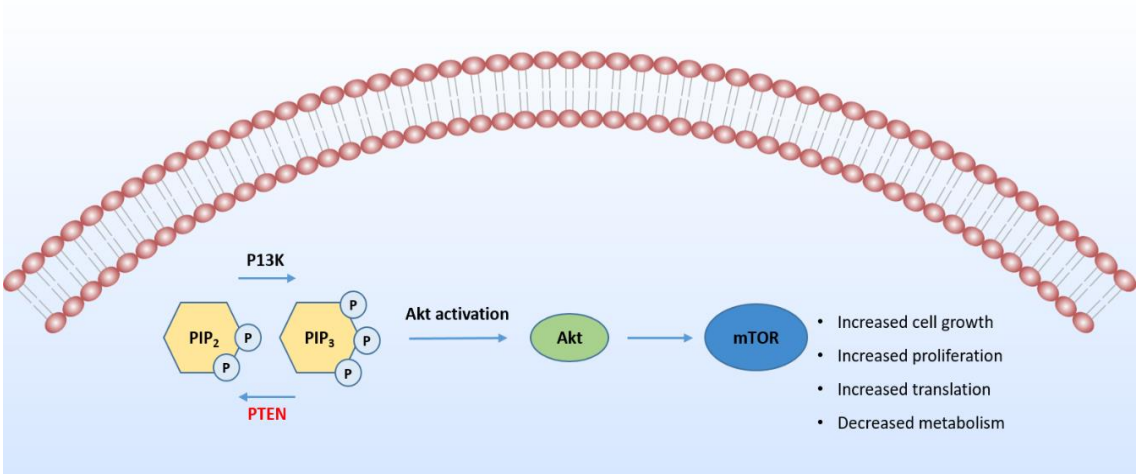

Figure 1.11: PI3K/AKT pathway illustrating the role of *PTEN*.

PI3K phosphorylates PIP2 to PIP3. Increases in PIP3 recruits AKT to the membrane where it is activated by other kinases. Akt phosphorylation mediates several important targets including mTOR which is responsible for up-regulation of protein synthesis. PTEN opposes PI3K by hydrolysing PIP3 to PIP2 (dephosphorylation) and resulting in inhibition of the PI3K/AKT pathway.

1.8.2 RAS/RAF/MEK/ERK Pathway

The RAS/RAF/MEK/ERK pathway is an important signalling pathway in cancer. Signalling through this pathway regulates several cellular functions including cell cycle regulation and migration that are crucial for tumorigenesis.

NF1 encodes for the neurofibromin protein and acts as a negative regulator of RAS. Neurofibromin inactivates Ras by accelerating the hydrolysis of active RAS-GTP to inactive RAS-GDP (Yap et al., 2014). As a consequence of RAS inactivation, downstream effectors of RAS are also suppressed, including PI3K, Akt, mTOR, RAF, MEK and ERK. In somatic NF1-associated tumours, biallelic loss of *NF1* is common and the main driver of oncogenesis whereas in non-NF1 associated tumours e.g. ovarian cancer, loss is not thought to act as an oncogene. In ovarian cancer, it is unknown whether biallelic loss of *NF1* or hemizygous loss is driving tumour progression (Ratner and Miller, 2015). The RAS/RAF/MEK/ERK and PI3K/AKT pathways interact with each other to regulate growth and tumour survival (Figure 1.12).

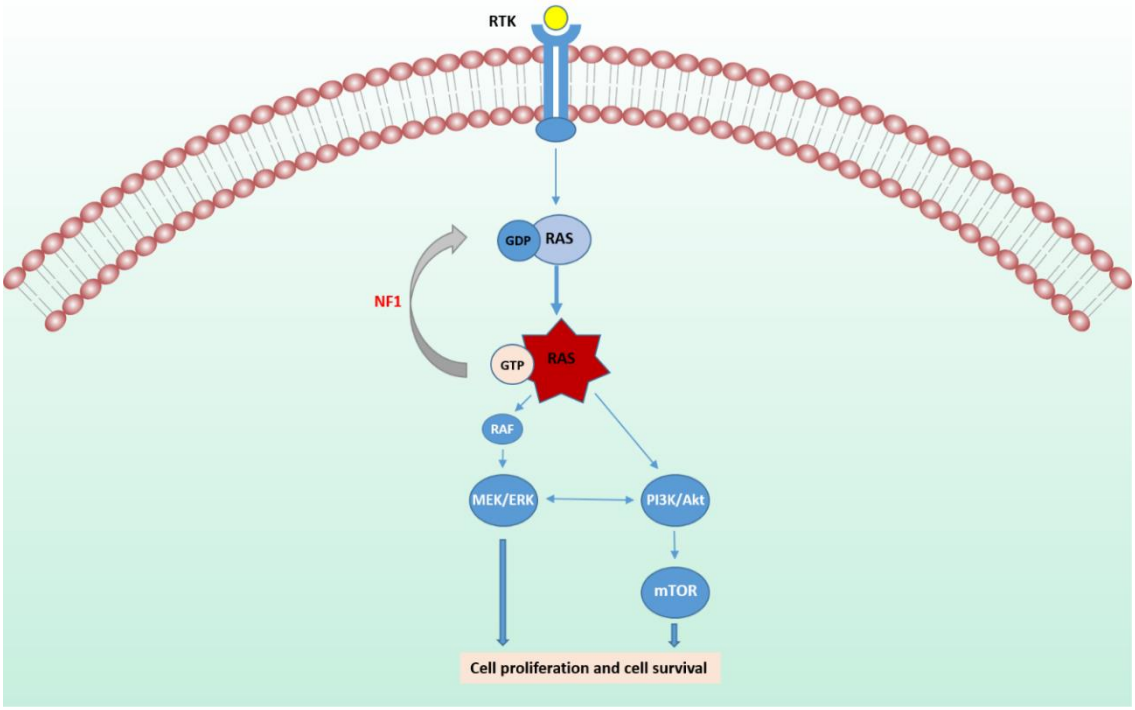

Figure 1.12: RAS/RAF/MEK/ERK pathway illustrating the role of *NF1*.

RAS is in its activated state when bound to GTP. Activated RAS activates the protein kinase activity of RAF kinase which subsequently activates MEK/ERK kinases. NF1 negatively regulates the RAS signalling pathway. Loss of NF1 results in increased levels of GTP-bound RAS levels and activation of signalling pathways downstream of RAS.

1.9 Homologous Recombination

DNA double-strand breaks (DSBs) are generally considered the most toxic of all DNA lesions. The repair of DSBs involves two complementary pathways – Homologous recombination (HR) and Non-homologous end joining (NHEJ). NHEJ is error-prone and promotes inaccurate re-ligation of DSBs, whereas HR is more precise and restores the genomic sequence by utilising sister chromatids as a template for repair (Ciccia and Elledge, 2010).

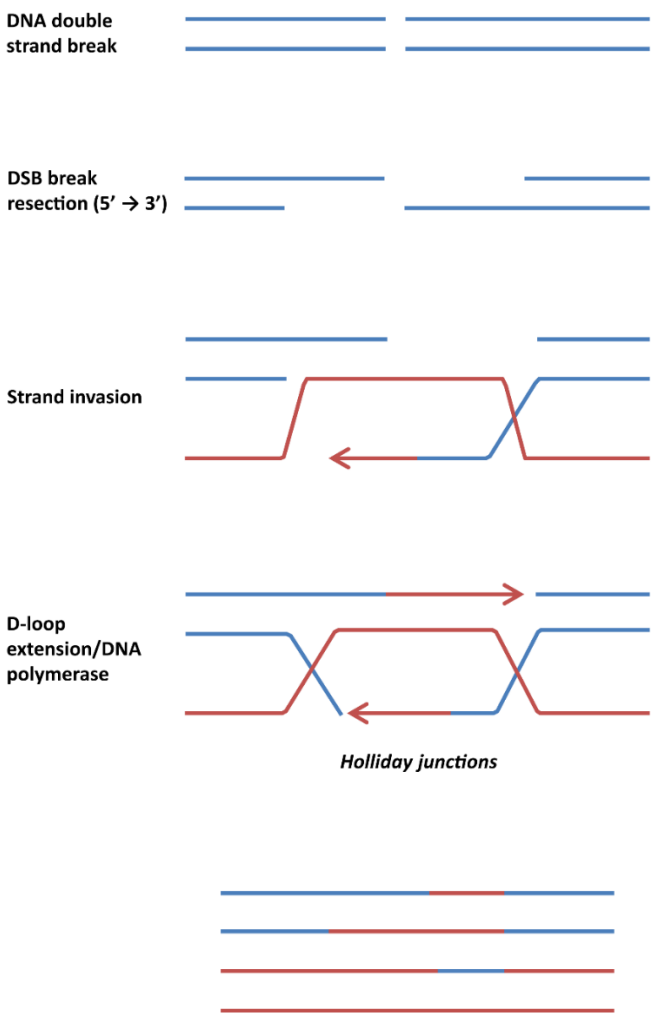

Figure 1.13: Illustration of double strand break (DSB) repair by HR.

DSB is initiated by 5' to 3' resection of the DNA ends. The resulting 3' strand invades an intact homologous duplex. A D-loop is formed and extended by DNA synthesis until it can pair with an exposed complementary sequence. The 3' strand of the second end serves as a primer for fill-in synthesis.

The HR pathway is activated when components of the MRN complex (MRE11/RAD50/Nbs1) bind to DNA double-strand breaks. The complex promotes activation of ATM and the preparation of DNA for HR (Ciccia and Elledge, 2010).

RAD50 contains ATPase domains that interact with MRE11. MRE11 stabilises DNA ends and has endonuclease and exonuclease activities involved in the initial DNA end resection. Nbs1 interacts with MRE11 and promotes the recruitment of ATM to DSBs (Williams et al., 2010).

DNA end resection is regulated by ATM through CtIP, which interacts with BRCA1 and MRN in the BRCA1-C complex (Huen et al., 2010). DSB resection and formation of 3' single stranded DNA (ssDNA) ends lead to RPA accumulation which help stabilise the ssDNA regions. BRCA1 associates with BRCA2 through PALB2/FANCN which is a major binding protein of BRCA2. BRCA1 has been found to be an upstream regulator of BRCA2 in DNA repair and the PALB2 is the main linker between BRCA1 and BRCA2 (Zhang et al., 2009).

RAD51 filaments assemble on RPA-coated ssDNA mediated by BRCA2. RAD51 induce strand invasion into the homologous DNA sequence and DNA polymerisation occurs using the sister chromatid as a template (Ciccia and Elledge, 2010). Further regulation of HR is provided by RAD51 phosphorylation mediated by CHK1, which is required for RAD51 recruitment to damage sites. BRCA2 is also phosphorylated by ATM/ATR (Figure 1.13 and Figure 1.14).

BRCA1/*BRCA2* mutations are the most common cause of defective homologous recombination in HGSOC. *BRCA1* and *BRCA2* mutations have been found to be associated with several clinical characteristics. Further analysis of the TCGA data found patients with *BRCA1* mutations were younger at diagnosis and the 5-year survival was significantly higher compared to wild-type patients.

Specific mutations in *BRCA1* and *BRCA2* occur more frequently in Ashkenazi Jews than in the general population. In Ashkenazi Jews, three mutations have been identified in breast/ovarian cancer families: 185delAG and 5382inC in *BRCA1* and 6174delT in *BRCA2* (Levy-Lahad et al., 1997). In a large population-based study of young Ashkenazi Jews the frequency of these mutations was 2.5% (*BRCA1* 185delAG 1%, *BRCA1* 5382inC 0.1% and *BRCA2* 6174delT 1.4%) (Roa et al., 1996).

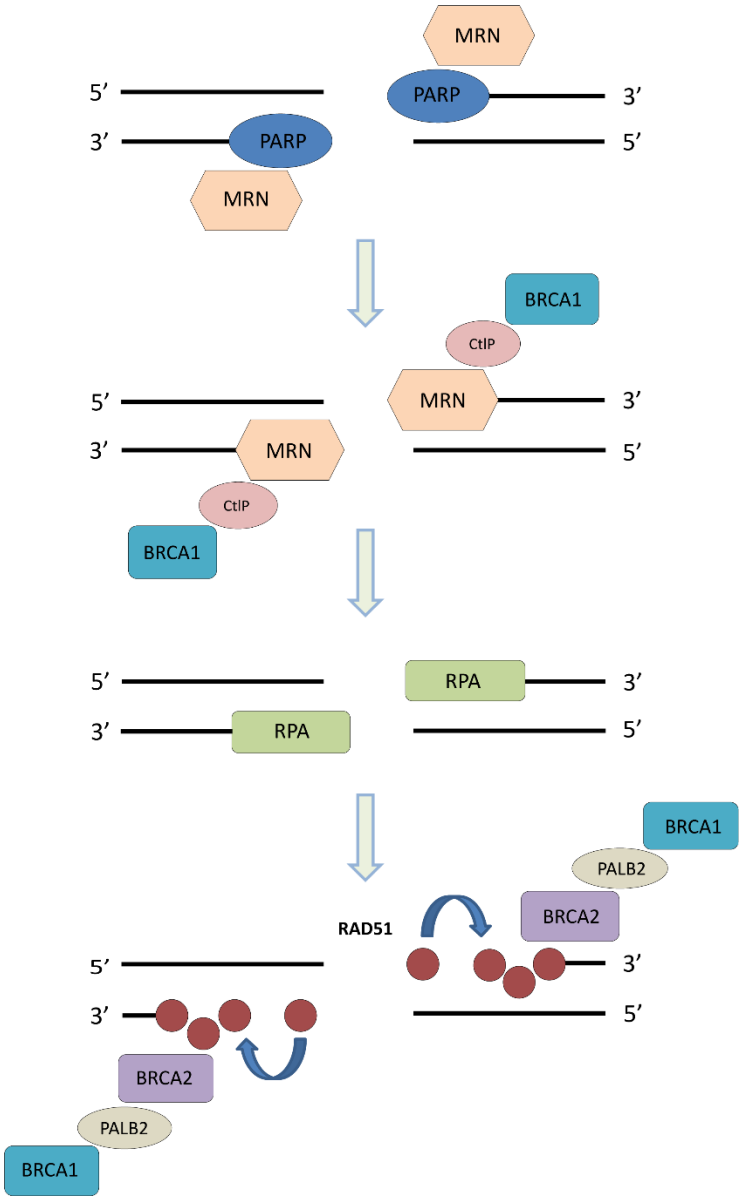

Figure 1.14: Homologous recombination pathway.

The MRN complex is recruited to DSBs by PARP and mediates the initial DSB resection together with CtIP and BRCA1. DSB resection leads to RPA accumulation and stabilises the ssDNA. Displacement of RPA and assembly of RAD51 filaments mediated by BRCA2 leads to strand invasion into homologous sequence. PALB2 links BRCA1/BRCA2 and BRCA1 acts as an upstream regulator of BRCA2.

The HR process is closely linked to the cell cycle. BRCA1 and RAD51 are only expressed in S and G2 phases of the cell cycle, therefore making HR impossible in G1. Also cells in G0 and G1 have not replicated their DNA and therefore lack sister chromatids that provide homologous sequences for HR (De Lorenzo et al., 2013).

1.10 Tumour Heterogeneity

The use of next-generation sequencing technology has helped us to understand that no two cancers are alike and that even different regions within the same tumour vary in their composition. Current evidence suggests that cancers evolve in a branched or punctuated pattern that results in temporal and spatial heterogeneity (Hiley and Swanton, 2014). This heterogeneity affects key pathways and presents a significant challenge to personalised medicine where a single biopsy is often used to guide management and develop biomarkers.

There are thought to be many factors that contribute to tumour evolution. These include intrinsic factors such as genomic instability and extrinsic factors such as the tumour microenvironment and cytotoxic chemotherapy (Hiley and Swanton, 2014). Widespread genomic instability is prominent in HGSOC. This instability generates a diverse cell population that can be subject to selection within the microenvironment and following chemotherapy.

Several studies have looked at genomic diversity within and between primary tumours and metastasis in ovarian cancer. Bashashati et al found widespread intratumoural variation in mutation, copy number and gene expression profiles and with key mutations only present in a subset of samples (Bashashati et al., 2013). *TP53* was the only somatic mutation consistently present in all samples (Bashashati et al., 2013).

A recent study looked at intra-tumour heterogeneity pre- and post-chemotherapy in HGSOC. They determined that subclonal tumour populations were present prior to chemotherapy and these can undergo expansion during chemotherapy resulting in relapse. Patients with high clonal expansion were associated with a worse survival. However due to the size of the patient cohort it is difficult to make any strong conclusions (Schwarz et al., 2015).

Interestingly, in most patients who relapse after chemotherapy they are platinum-sensitive. Therefore, the original concept of intratumoural heterogeneity and clonal selection of resistant cells by chemotherapy does not fit well in ovarian cancer. A possible hypothesis for platinum sensitive

recurrence is the presence of dormant chemo-sensitive stem cells that, following completion of chemotherapy, start to regrow and repopulate the tumour (Chien et al., 2013).

As discussed, the diverse tumour population includes a variety of different genotypes. The interaction between these different genotypes within a tumour and how this environment is altered following chemotherapy is not known.

1.11 ID8 Cell Line and Derivatives

The ID8 cell line is the most widely used transplantable murine model of ovarian cancer (Roby et al., 2000). This originated from cells from 5 C57Bl/6 mice ovaries that had been trypsin-digested. After about 20 passages, the cells lost contact inhibition and their classic cobblestone appearance. Ten different clones were derived, one of which, ID8, has been widely used in ovarian cancer research.

Following intraperitoneal injection of the ID8 cell line *in-vivo,* diffuse peritoneal tumour deposits with blood-stained ascites develop after approximately 110 days (Roby et al., 2000) (Figure 1.15).

Next generation sequencing by the host lab has shown that the parental ID8 cell line lack any of the characteristic mutations that you would expect in HGSOC (Walton et al., 2016). Using the CRISPR/Cas9 gene editing technique, single (*Trp53-/-*), double (*Trp53-/-;Brca2-/-*), double (*Trp53-/-;Brca1-/-*), double (*Trp53-/-;Pten-/-*), double (*Trp53-/-;Nf1-/-*), triple (*Trp53-/-;Brca1-/-; Pten-/-*) and triple (*Trp53-/-;Brca2-/-;Pten-/-*) knockout derivatives of ID8 have been generated by Dr Josephine Walton (post-doc, McNeish Lab) (Walton et al., 2017).

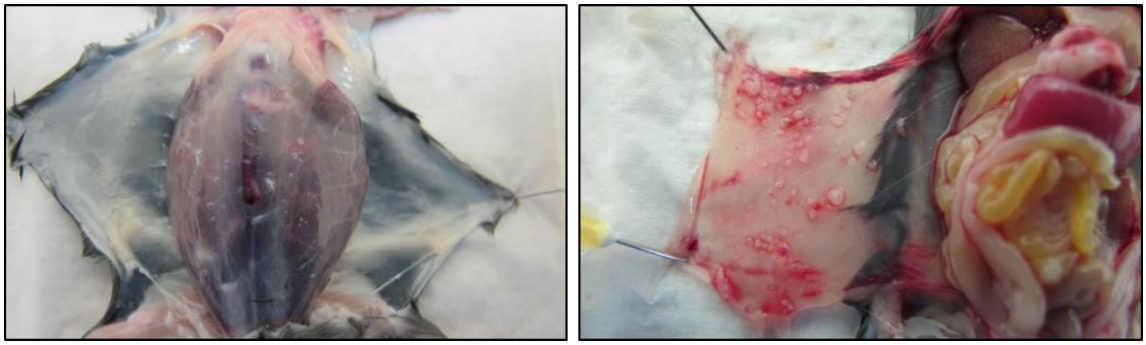

Figure 1.15: ID8 intraperitoneal injected mice.

The figure shows classical features of ovarian cancer with bloody ascites and widespread peritoneal tumour deposits.

The ID8 derivatives were used extensively in my research and the different cell lines are outlined below (Figure 1.16).

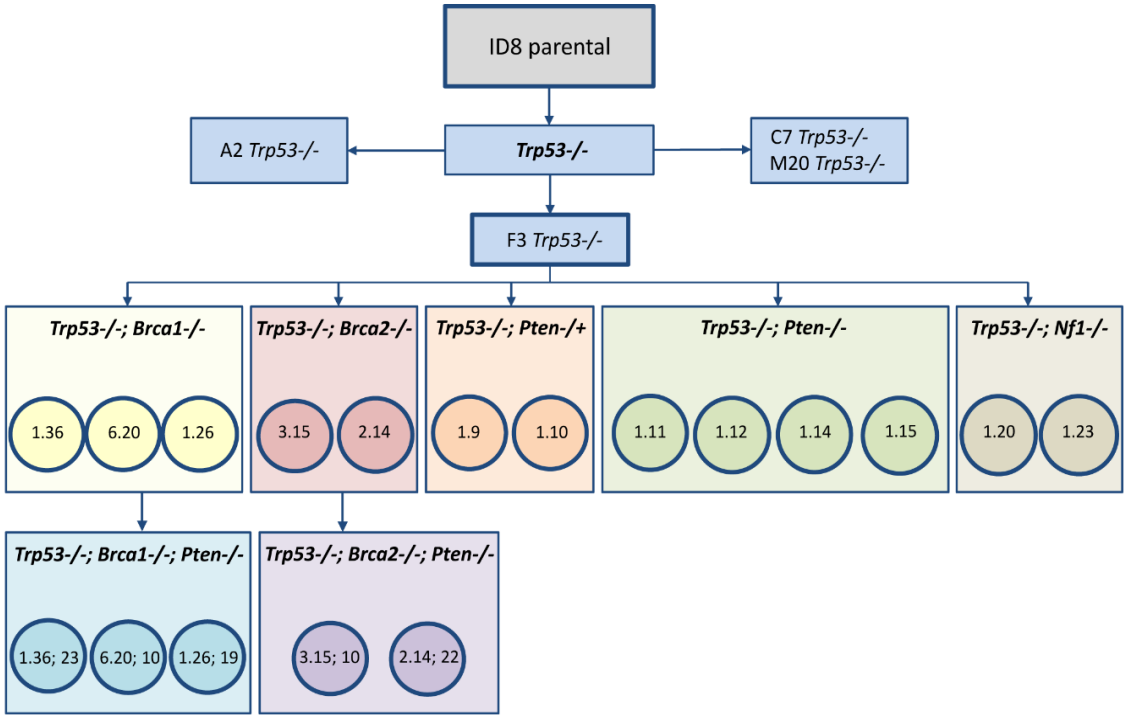

Figure 1.16: ID8 cell line and derivatives.

This illustrates the different ID8 derivatives generated by CRISPR/Cas9 gene editing technology. *Trp53-/-* knockout clones were generated from the original ID8 parental cell line and all subsequent knockouts originated from the F3 *Trp53-/-* clone. The circles show the different clones from each genotype that I used throughout this thesis.

1.12 Research Aims and Hypothesis

This thesis investigated the role of homologous recombination and the tumour microenvironment in HGSOC and how this environment is altered by platinum chemotherapy. By using a transplantable HGSOC mouse model the different immune cell populations and cytokines were assessed.

This tested the hypothesis that platinum chemotherapy alters the tumour microenvironment in different HGSOC genotypes supporting an immunosuppressive state. To test the hypothesis, the main objectives were to:

1. Establish the relationship between homologous recombination and platinum and PARP inhibitor sensitivity
    - Assess homologous recombination status on HGSOC cell lines and ID8 derivatives
    - Platinum and PARP inhibitor dose-response on cell lines

2. Assess *in vivo* cisplatin response in ID8 sublines
    - Determine differences in survival between the ID8 genotypes
    - Assess differences in the tumour microenvironment within the tumour and ascites between the ID8 genotypes

3. Assess *in vivo* tumour heterogeneity
    - Generate fluorescent ID8 sublines
    - Determine differences in tumour development between the ID8 genotypes and influence of platinum chemotherapy

By addressing these aims it is hoped that this project will further the understanding of platinum sensitivity in HGSOC and, by looking at the tumour microenvironment, offer attractive therapeutic targets for future research.

2 Materials and Methods

2.1 Cell Culture

High grade serous ovarian cancer (HGSOC) cell lines were cultured in T75 flasks in Dulbecco's Modified Eagle Medium (DMEM) (Thermofisher, 21969-035) supplemented with 10% foetal bovine serum (FBS) (Thermofisher, 10500-064), 100µg/ml Penicillin/100µg/ml Streptomycin (P/S) (Thermofisher, 15140-122), and 2mM L-Glutamine (LG) (Thermofisher, 25030-024) at 95% humidity, 5% CO_2 and 37°C.

ID8 cells (Roby et al., 2000) were cultured in T75 flasks in DMEM, supplemented with 4% FBS, 100µg/ml Penicillin/ 100µg/ml Streptomycin (P/S), 5µg/ml insulin, 5µg/ml transferrin and 5ng/ml sodium selenite (ITS) (Thermofisher, 41400-045) and 2mM L-Glutamine (LG) at 95% humidity, 5% CO_2 and 37°C.

ID8 cells were passaged 1:20 twice weekly; cells were washed once with PBS and detached using 1x 0.5% Trypsin-EDTA (Thermofisher, 15400-054) in PBS. The cells were cryopreserved for long-term storage: cells were centrifuged at 1200rpm and the cell pellet resuspended in FBS containing 10% DMSO. The cells were stored overnight in a Mr Frosty at -80°C prior to transfer to liquid nitrogen the next day.

OvidT 479 (*DICER*-/-;*Pten*-/-) cells were cultured in T75 flasks in Dulbecco's Modified Eagle Medium F12 (DMEM F12) (Thermofisher, 11320-074) supplemented with 10% FBS, 100µg/ml Penicillin and ITS at 95% humidity, 5% CO_2 and 37°C.

HGSOC cell lines were obtained from the National Cancer Institute (NCI, Frederick, MA, USA), OvidT 479 cells from Dr Seth Coffelt (CRUK Beatson Institute, Glasgow) and ID8 parental cells from Dr Katherine Roby (University of Kansas).

All cell lines were verified by Short Tandem Repeat profiling (STR) using the Promega GenePrint 10 system (Promega, UK) at the CRUK Beatson Institute. Cell lines were routinely tested for mycoplasma at the Wolfson Wohl Cancer Research Centre, University of Glasgow, using MycoAlert™, Mycoplasma Detection Kit (Lonza, LT01-318). The cell lines used throughout this thesis are outlined in Table 2.1.

Table 2.1: Outline of cell lines and corresponding mutations.

Human (HGSOC)	
PEO1	*BRCA2* mutation
PEO2	*BRCA2* wild-type
UWB1.289	*BRCA1* mutation
UWB1.289BRCA1	*BRCA1* wild-type
OVCAR3	/
OVCAR4	/
COV318	/
Mouse (ID8)	
Clones	
F3, A2, M20, C7	*Trp53-/-*
3.15, 2.14	*Trp53-/-;Brca2-/-*
1.36, 1.26, 6.20	*Trp53-/-;Brca1-/-*
1.11, 1.12, 1.14, 1.15	*Trp53-/-;Pten-/-*
1.9, 1.10	*Trp53-/-;Pten-/+*
1.20, 1.23	*Trp53-/-;Nf1-/-*
3.15.10, 2.14 22	*Trp53-/-;Brca2-/-;Pten-/-*
1.36.23, 6.20.10, 1.26.19	*Trp53-/-;Brca1-/-;Pten-/-*
Mouse (OvidT 479)	
DKO 4	*Dicer-/-;Pten-/-*
TKO 13	*Dicer-/-;Pten-/-;Trp53-/-*

2.2 Survival Assays

2.2.1 MTT assay

Thiazolyl Blue Tetrazolium Bromide powder, (Sigma Aldrich, M2128) was dissolved in PBS to give a 0.5% w/v solution. Medium was aspirated from cells in 24 well plates and replaced with 700µl of 1:10 MTT solution and incubated for 2 hours at 37°C. Medium was aspirated and formazan crystals dissolved in 300µl DMSO. Plates were read at 560nm on a Tecan, Infinite 200Pro plate reader and absorbance from a blank well was subtracted from all absorbances.

2.2.2 Sulphorhodamine B assay

Cells in a 24 well plate were washed in PBS and fixed with 250µl 10% Trichloroacetic acid (TCA) (Sigma Aldrich, T9159) for 30 minutes at 4°C. The cells were then washed three times in dH_2O, left to air dry and stained for 30 minutes with 250µl of Sulphorhodamine B (Sigma Aldrich, 230162) (0.4% w/v in 1% acetic acid). Following this, the Sulphorhodamine B was washed off with 1% acetic acid until running clear and left to air dry. Cells were dissolved in 500µl 1mM Tris pH9. Plates were read at 565nm on a Tecan Infinite 200Pro plate reader and absorbance from a blank well was subtracted from all absorbances.

2.2.3 Dose-response curves

Cisplatin (Accord Healthcare, Harrow, UK) was obtained from the chemotherapy pharmacy, Beatson West of Scotland Centre. Rucaparib was provided by Clovis Oncology (Boulder CO, USA). ID8 cells and derivatives were washed, trypsinised and plated at 3000 cells/well for Cisplatin and 10,000 cells/well for rucaparib in a 24 well plate. Four hours later, medium was removed and replaced with fresh medium (control) or medium containing cisplatin (0.01-1000µM) or rucaparib (0.003-30µM). Three wells were used for each drug concentration, with 5 wells used for a control and one well left as blank. 72 hours after initial plating, survival was determined by MTT assay (cisplatin) and sulphorhodamine B assay (rucaparib). Survival was expressed as a percentage of the control and IC50s were determined using Prism v6.0 (GraphPad, CA, USA).

HGSOC and OvidT 479 cell lines were plated at 10,000 cells/well (cisplatin and rucaparib) and the drug was added after 24 hours. The survival was determined 72 hours later by MTT or sulphorhodamine B assay.

2.2.4 Proliferation assay

ID8 and fluorescent ID8 cell lines were washed, trypsinised and plated at 3000 cells/well in a 24 well plate. At each time point (24h, 48h, 72h, 96h, 120h), an MTT assay was performed on a single row of three wells. Absorbances from blank wells were subtracted from absorbances at each time point. From these values the linear regression was calculated (Prism v6.0).

2.3 Homologous recombination assays

2.3.1 RAD51/γH2AX assay

The original assay was developed and published by the lab of Nicola Curtin and Richard Edmondson to assess HR competence (Mukhopadhyay et al., 2010). A cell line is deemed to be HR competent if cells can double the number of Rad51 foci in response to DNA double strand breakage (defined as ≥2-fold increase in γH2AX foci) induced by 24 hours of treatment with 10μM rucaparib. This assay was used to assess the HR status of HGSOC cell lines, OvidT 479 cell lines, parental ID8s and their derivatives.

Coverslips were sterilised in 70% ethanol and plated in 24 well plates. 500μl of 0.1% poly-L-lysine was added to each coverslip and incubated at 37° for 5 minutes. The poly-L-Lysine was aspirated and washed once with dH_2O and left for 2 hours before plating cells. HGSOC and DICER cell lines were plated at 5 x 10^4 per well and ID8 cells at 3 x 10^4 per well. The following day cells were treated either with 10μM rucaparib/medium or irradiation (10Gy)/medium.

Cells were stained 6 hours after exposure to irradiation or 24 hours following rucaparib treatment.

Cells were permeabilised for 1 minute in 0.2% Triton, and immediately fixed for 10 minutes in 3% PFA with 2% sucrose. Cells were washed in PBS (x3) using a cut pipette tip, before staining with primary antibodies in 2% BSA at 37°C for 30 minutes. Cells were washed with PBS (x3) and stained with secondary antibodies in 3% BSA at 37°C for 30 minutes (Table 2.2). Cells were washed a further three times with PBS before mounting using DAPI and kept at 4°C overnight. The slides were blinded to cell line, but with knowledge of treatment. All images were captured using a Zeiss 710 confocal microscope. Rad51 and γH2AX were counted, with at least 30 cells counted per cell line across multiple areas. Rad51 and γH2AX foci following rucaparib or irradiation treatment are expressed relative to medium control +/- SEM.

Table 2.2: Primary and secondary antibodies used for the RAD51/γH2AX assay.

Primary antibodies	Rad51	γH2AX
Supplier	Santa Cruz	Millipore
Catalogue No.	Sc8349	14-576
Dilution	1:100	1:800
Secondary antibodies	ALEXA 568 (anti-rabbit)	ALEXA 488 (anti-mouse)
Supplier	Invitrogen	Invitrogen
Catalogue No.	A-11011	A-11001
Dilution	1:200	1:200

2.3.2 DR-GFP assay

The GFP/ISce-I endonuclease assay is considered the gold standard for determining homologous recombination status. 5 x 10^5 HGSOC cells were plated per well in a 6 well plate. The following day 5μg of *p*DR-GFP plasmid was transfected into cells using a 3:1 FuGene 6 to plasmid ratio (Promega, E2691) and surviving colonies selected using puromycin (1 in 1000). Once surviving colonies were expanded, cells were replated and transfected with *p*ISce-I or pCAAGS (control plasmid) (FuGene 3:1). 48 hours following transfection, cells were trypsinised and GFP positivity assessed by flow cytometry (Figure 2.1).

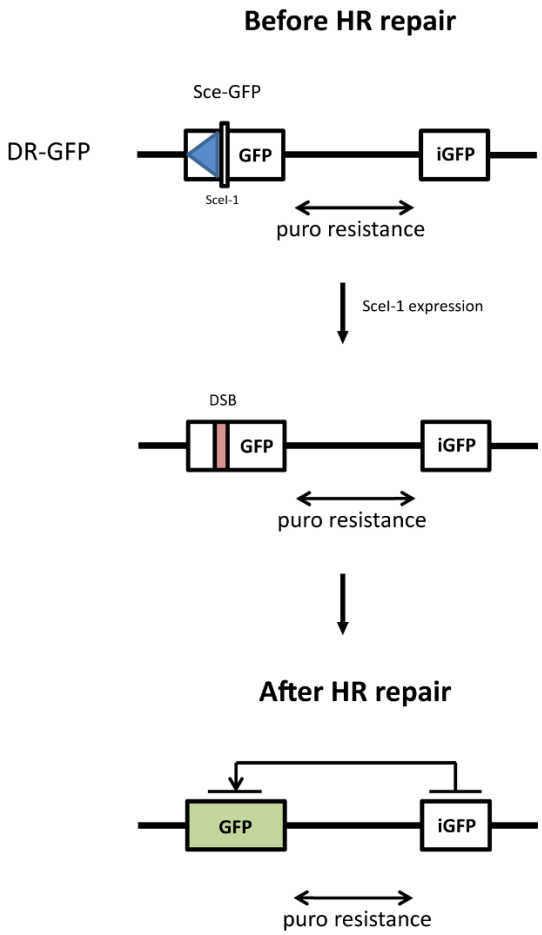

Figure 2.1: DR-GFP assay.

This assay uses the I-SceI rare-cutting endonuclease from Saccharomyces cerevisiae. I-SceI recognises an 18-bp DNA sequence not found in the human genome. It employs an inactive GFP plasmid (DR-GFP) containing a restriction site for I-SceI in the 5'GFP construct (SceGFP). Downstream of the SceGFP is an internal GFP fragment (iGFP), which is under an inactive promoter. The DR-GFP plasmid is transfected in the human cells and clones established by selection with puromycin. Cells expressing pDR-GFP are then transfected with pI-SceI which induce a single site-specific DSB in the 5'GFP construct (Golding et al., 2004).

Once a single site-specific DSB is introduced, the 3'copy of GFP DNA (iGFP) can be used as a template for repair by homologous recombination, resulting in a functional GFP gene. The GFP positive cells are easily quantifiable by flow cytometry and HR status determined.

2.4 Development of mCherry and GFP ID8 cell lines

2.4.1 GFP lentiviral transfection

2.5 x 10^6 HEK 293T cells were plated in a 10cm dish (DMEM, 5% FBS + no P/S) for a confluency of 50-70% the next day. Following day, 30µl FuGene 6 (Promega, E2691) added to 600µl of Opti-MEM (Thermofisher, 31985070) (serum-free medium), mixed with a pipette and incubated at room temperature for 5 minutes. 4µg GFP lentiviral plasmid (HIV-7-GFP), 4µg package plasmid (psPAX contains gag, pol, rev and tat) and 4µg envelope plasmid (VSV-G) mixed by inverting eppendorf and incubated at room temperature for 20 minutes. The contents were added to the dish and to ensure efficient mixing, plates were swirled in a figure of eight motion before incubation at 37°C.

The pHIV-7-GFP plasmid was obtained from Dr Vignir Helgason, Institute of Cancer Sciences, University of Glasgow, Glasgow, UK

2.4.2 mCherry retroviral transfection

2.5 x 10^6 Phoenix cells (encoding Gag-Pol-Env) were plated in a 10cm dish (DMEM, 5% FBS + no P/S) for a confluency of 50-70% the next day. Following day, 12µl FuGene 6 added to 200µl of Optimem (serum-free medium), mixed with a pipette and incubated at room temperature for 5 minutes. 4µg mCherry retroviral plasmid (Addgene, pMSCV-IRES-mCherry FP) (1:3 ratio) is added, mixed by inverting eppendorf and incubated at room temperature for 20 minutes. The contents were added to the dish and mixed as above before incubation at 37°C.

2.4.3 Lentiviral and retroviral harvest

The following day, medium was aspirated and replaced with serum-containing DMEM medium. 24 hours later the supernatant was removed using a 10ml syringe and then centrifuged at 3000rpm for 10 minutes to remove HEK293T or Phoenix cells. The remaining supernatant was filtered with a 2µM filter and frozen at -80°C. Medium was added to the cells, incubated for a further 24hr and the process repeated to obtain additional viral supernatant.

2.4.4 Infection of ID8 cells with mCherry retrovirus and GFP lentivirus

1 x 10^5 cells were plated on a 6cm plate. After 24 hours 250µl of viral supernatant was added and medium was changed the next day. 72 hours after incubation the cells were expanded into a T75 flask. GFP cells were visible under the microscope.

2.4.5 Sorting GFP and mCherry cell lines

As GFP positive cells were visible under the microscope, these cells were sorted by dilution cloning. A starting concentration of 2 x 10^4 cells (200µl) were plated in the first well of a 96 well plate. A multi-channel pipette was used for the dilution cloning. After 3-4 days, single cell GFP colonies were visible and were gradually expanded to T75 flasks before freezing at -80°C.

mCherry expression was not visible under our microscope. Positive mCherry single cells were sorted by flow cytometry using a negative control (3.15 clone) into a 96 well plate. These single cell colonies were again gradually expanded to T75 flasks before freezing at -80°C.

2.5 Immunohistochemistry

Three tissue microarrays (TMA) from the cisplatin *in-vivo* experiment were generated by the Histology Service, CRUK Beatson Institute. The TMA blocks were created using a 1mm punch set (Estigen Tissue Science, Estonia, Cat No: MP10) on a Manual Tissue Arrayer MTA-1 (Beecher Instruments Inc, Sun Prairie, WI, USA) using formalin-fixed paraffin-embedded tumours. Four blocks were used per genotype and each cisplatin treatment group, and three cores were taken per paraffin-embedded block. The cores were spread across three TMAs with the histology department generating a randomised map.

5µm sections from the TMAs and other paraffin-embedded tumours were optimised and stained at the Histology Service, CRUK Beatson Institute using a Dako Autostainer (Dako, UK) (Table 2.3).

Table 2.3: Antibodies used for immunohistochemistry staining.

Mouse antibodies	Supplier	Cat No.	Dilution
F4/80	Abcam	C1:A3-1	1/200, Proteinase K retrieval
CD3	Abcam	ab16669	1/50, pH6
CD8a	eBioscience	14-0808-82	1/75, pH8
p-Akt (Ser473)	Cell Signalling	4060	1/45, pH6
CD206	Abcam	Ab64693	1/1000, ER2 retrieval
iNOS	Abcam	Ab15323	1/50, ER2 retrieval
BrdU	BD Biosciences	347580	1/500, pH6
GFP	Cell Signalling	2555	1/50, pH8
mCherry	Cell Signalling	4060	1/100, pH9

Stained slides were digitised (Hamamatsu NanoZoomer NDP, Hamamatsu Photonics, Welwyn Garden City, UK). The slides were then uploaded onto HALO™ digital image analysis software v2.0.1061.3 (IndicaLabs) and classifiers created to differentiate tumour from non-tumour (Figure 2.2). Cellular staining algorithms for each marker (CD3, F4/80) were designed and the analysis was performed only on the tumour areas (Figure 2.3).

The slides were scored using the histoscore method as described in (Kirkegaard et al., 2006). This algorithm grades staining intensity as negative (0), weak (1),

moderate (2) and strong (3), multiplied by the percentage of tumour cells in each category giving a histoscore ranging from a minimum of 0 to a maximum of 300.

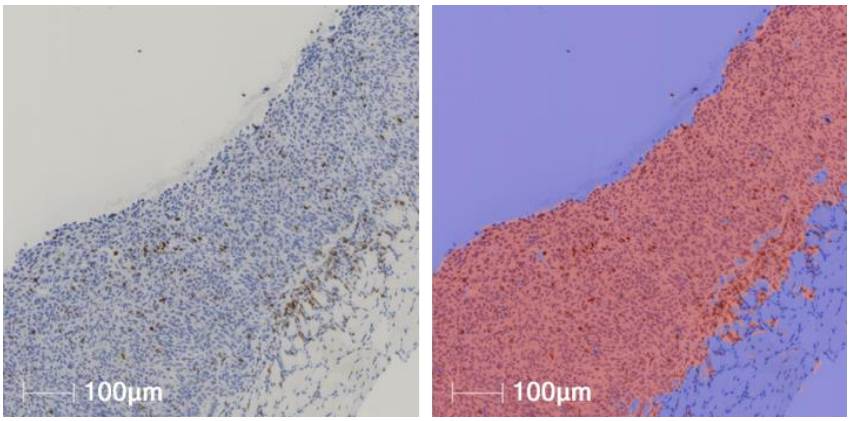

Figure 2.2: Classifier to differentiate tissue type.

Tumour (red) and non-tumour (blue) areas. Analysis of staining intensity was performed only on the tumour areas.

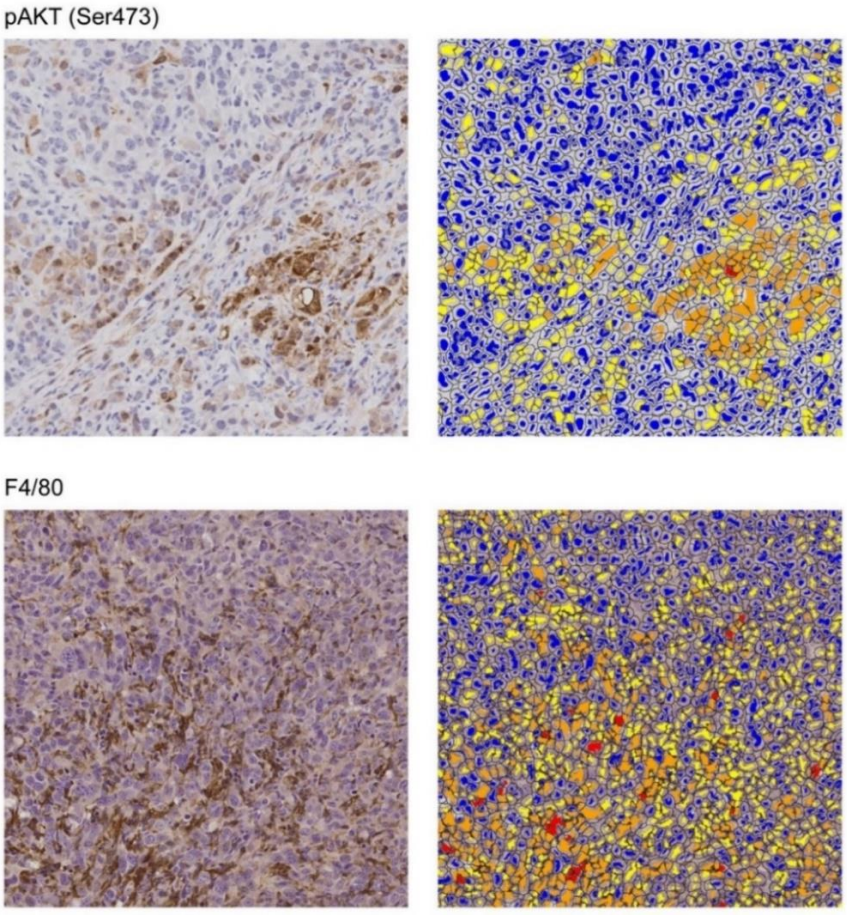

Figure 2.3: Example of the staining algorithm.

Mouse p-Akt (Ser473) and F4/80, staining intensity was scored as negative (0), weak (yellow - 1), moderate (orange - 2) and strong (red - 3).

2.6 Gene expression analysis

2.6.1 Tumour cellularity

A proportion of the tumours were assessed for tumour cellularity prior to RNA extraction. The samples had been initially placed in PBS prior to being snap frozen. To improve the quality of the haematoxylin and eosin (H&E) staining half the tumour was placed in 60% sucrose for 2 hours and transferred to 30% sucrose overnight and snap frozen again. RNA was then extracted from tumours with a cellularity >50%.

2.6.2 RNA extraction from tumours

A master mix of 10µl/ml β mercaptoethanol (Sigma Aldrich, M3148) in RLT buffer (Qiagen RNeasy Mini kit) was prepared and kept on ice for at least 30 minutes prior to RNA extraction. Snap-frozen tumours were placed in foil on dry ice, crushed and transferred to RLT/β mercaptoethanol mix. Tumours were homogenised using a Polytron® PT 1200 E homogeniser (Kinematica) and the resulting lysate frozen at -80 for no longer than 1 month before RNA extraction.

Homogenised lysates were thawed to room temperature prior to RNA extraction. RNA was extracted using the RNeasy RNA Mini kit (Qiagen). The lysate was centrifuged at 13,000rpm for 3 minutes. The supernatant was transferred to an eppendorf tube. 1 volume of 70% ethanol was added to the lysate, pipetted gently up and down to mix and a maximum of 700µl transferred to an RNA binding column collection tube. The column was centrifuged for 15 seconds at 8000rpm, the flow through discarded, any additional supernatant was added to another column, and the cycle repeated. A master mix of DNAase solution was made up (70µl RDD buffer and 10µl DNase stock) (RNase-free DNase set, Qiagen, 79254). 80µl of mix was pipetted directly onto the column and incubated for 15 minutes. Following this, 350µl buffer RW1 was added, centrifuged at 8000rpm for 15 seconds and the follow through discarded. 500µl of RPE buffer was added, centrifuged at 8000rpm for 15 seconds and flow through discarded. A further 500µl of RPE buffer was added, centrifuged for 2 minutes at 8000rpm and flow through discarded. The column was then placed in a new 2ml tube and centrifuged for 1 minutes at 13,000rpm to dry the membrane. The column was

transferred to a 1.5ml RNase free Eppendorf. 50µl RNase free dH_2O was pipetted onto the column and RNA was eluted by centrifugation at 9000rpm for 1 minute. RNA was quantified using the NanoDrop 2000 spectrophotometer (Thermo Scientific, Wilmington, DE, USA).

Immediately after quantification of RNA, the RNA was diluted with nuclease-free H_2O into 2 eppendorfs to minimise the number of freeze-thaw cycles. The first Eppendorf with 3µl of 50-100ng/µl for RNA quality check and the second at 1µg/50µl for the RNA library preparation/sequencing.

2.6.3 RNA quality

Prior to library preparation, each RNA sample was run through an Agilent 2220 TapeStation System (Agilent Technologies, Santa Clara, CA, USA) and a RNA integrity number (RIN) calculated. Samples were included for RNA sequencing if RIN >7.

2.6.4 Library preparation for RNA sequencing

'With-Beads' library preparation was done using TruSeq Illumina Stranded Total RNA Library Prep kit by the Sequencing Department, CRUK Beatson Institute.

Step 1: Purification of poly(A)-RNA from total RNA

50µl of oligo-dT magnetic beads were added to the 1µg/50µl total RNA and mixed well by pipetting. The samples were incubated in the thermocycler to bind poly(A)-RNA to the beads:

65°C for 5mins → 4°C for 1 mins → 25°C for 5 mins

The beads on the magnet were collected and supernatant removed. The beads were re-suspended with 200µl of Bead Wash Buffer and beads collected and supernatant removed. The beads were re-suspended again with 50µl of Elution buffer and samples incubated in the thermocycler to elute poly(A)-RNA from the beads:

80°C for 2 min → 25°C for 3 mins

Beads were re-suspended with 50µl of Bead Binding buffer and incubated for 5 mins at room temperature. The beads were then collected, and supernatant removed. The beads were re-suspended with 200µl of Bead Wash Buffer and beads again collected and supernatant removed.

Beads contain poly(A)-RNAs immobilised on their surface. Fragmentation and priming step was proceeded to immediately.

Step 2: Fragmentation and priming of poly(A)-RNA

The beads were resuspended with 19.5µl of Fragment Prime Finish Mix and samples incubated in the thermocycler to elute, fragment and prime RNA:

94°C for 8 mins → 4°C for 3 mins

This should result in RNA fragmentation to 120-210nt with median 155nt. The supernatant will contain fragmented and primed RNA ready for reverse transcription. The next step was proceeded to immediately.

Step 3: 1st Strand cDNA synthesis

A mix of 1µl of SuperScript III and 7µl of First Strand Synthesis Act D per sample. 17µl of fragmented and primed RNA was combined with 8µl of SuperScript III master mix. The samples were incubated in the thermocycler for reverse transcription:

25°C for 10 mins → 42°C for 15 mins → 70°C for 15 mins → 4°C hold

The samples were cooled to 4°C. The supernatant now contained RNA-DNA hybrid. The next step was proceeded to immediately.

Step 4: 2nd Strand cDNA synthesis

5µl of Resuspension Buffer and 20µl Second Strand Marking Master Mix were added to each sample. The samples were incubated in the thermocycler:

16°C for 60 mins → 25°C for 3 mins

90µl of well mixed RT Ampure XP beads were added to each sample. The samples were incubated for 5 mins at room temperature, beads on the magnet collected, washed twice with 180µl 80% Ethanol and allowed to air dry for 5 mins. DNA was eluted by adding 18.5µl of Resuspension Buffer and incubated for 5 mins at room temperature. The beads were pelleted to measure the DNA concentration by Qubit dsDNA HS (1µl into 200µl of Qubit dsDNA HS).
The RNA samples were converted to dsDNA and stored at -20°C overnight.

Step 5: Adenylation of 3' Ends and Adapters Ligation

12.5µl of A-Tailing Mix was added to 17.5µl of the sample and mixed well by pipetting. The samples were incubated in the hot-block:

37°C for 30 mins → 70°C for 5 mins → room temperature

2.5µl of indexed RNA Adapter was added to each sample. 2.5µl of DNA ligase Mix was combined with 2.5µl of Resuspension Buffer per sample and then 5µl of the resulting mixture was added to each sample and incubated in the hot-block:

30°C for 10 mins → room temperature

5µl of Stop Ligase Mix was added to each sample and vortexed/centrifuged to give a final volume of 42.5µl. 47µl (1.1x) of 20% PEG8000/2.5M NaCl was added to each sample and centrifuged at max rpm for 5 mins, the beads collected, washed twice with 80% Ethanol and air dried for 5 mins. The DNA was eluted in 50µl pf Resuspension Buffer (5mins at max rpm) and, without separating the beads and supernatant, 55µl (1.1x) of 20% PEG8000/2.5M NaCl was added to

each sample and centrifuged for 5 mins at max rpm. The beads were collected, washed twice with 80% Ethanol and air dried for 5 mins. The DNA was eluted in 25µl of Resuspension Buffer (5mins at max rpm).

The supernatant and beads were separated. The beads were washed twice with 0.05% Tween/TE and resuspended in 55µl (1.1x) of 20% PEG8000/2.5M NaCl. The eluted DNA was then quantified (1µl into 200µl of Qubit dsDNA HS) to determine the number of PCR cycles required for amplification.

Step 6: PCR amplification

5µl of PCR Primer Cocktail, 25µl of PCR Master Mix and 20µl of sample were combined and mixed well. The samples were incubated in the thermocycler for amplification (14 cycles for 5ng DNA, 11 cycles for 50ng DNA):

98°C for 30 secs → 98°C for 10 secs → 60°C for 30 secs →72°C for 30 secs → 72°C for 5 mins → 4°C hold

The 50µl samples were purified using 55µl (1.1x) of beads in 20% PEG8000/2.5M NaCl. The beads were collected on the magnet, washed twice with 80% Ethanol and air dried for 5 mins. The samples were eluted into 20µl of Resuspension Buffer and 18µl collected.

1µl of elute was analysed by Tapestation D1000 screen tape and DNA concentration measured by combining 1µl of elute and 199µl of dsDNA HS on Qubit.

2.6.5 Sequencing

The amplified library was sequenced on the NextSeq 500 (Illumina) with a paired-end sequencing strategy. The read length was a 2 x 36 cycle PE with an expected library size of ~260bp (median insert size ~150bp). There were 10-15 million reads per sample.

The analysis of the RNA sequencing data was performed by Rosie Upstill-Goddard (bioinformatician) at the Bioinformatics department, Wolfson Wohl Cancer Research Centre, Glasgow University. The primary sequencing reads produced were subjected to quality control. FASTQ files were clipped and the low-quality reads were removed by Cutadapt. Sequenced libraries were mapped to UCSC mouse mm10 reference genome using the STAR aligner. The sequencing alignment was performed using the bcbio-nextgen project RNAseq pipeline. Genes without at least 1 count per million in at least 3 samples were removed from downstream analysis.

Differential gene expression analysis was performed using R packages (edgeR, limmaR and DESeq2). Genes with p=<0.05 and absolute log fold change >1 were considered significantly differentially expressed. Heatmaps of differentially expressed genes with p=<0.05 and absolute fold change >2 were generated using an R package (ComplexHeatmap).

Enrichment analysis was performed on the significantly expressed genes using R (dnet). Genes were compared to genes associated with gene ontology terms: biological process (GOBP), molecular function (GOMF), cellular component (GOCC) and disease ontology (DO).

2.6.6 cDNA synthesis for RT-qPCR

Prior to cDNA synthesis, each RNA sample was quantified using the NanoDrop. The High-capacity cDNA reverse transcription kit (ThermoFisher, 4375222) was used for reverse transcription of RNA. The kit components and RNA samples were thawed on ice. A 2X RT master mix was prepared (without RNase inhibitor) including 2µl 10X RT buffer, 0.8µl 25X dNTP Mix (100mM), 2µl 10X RT Random Primers and 1µl MultiScribe™ Reverse Transcriptase per sample (5.8µl). A master mix was prepared without reverse transcriptase for the NRT (no reverse transcriptase control). Both mastermixes were vortexed and centrifuged.

The mastermix (5.8µl), nuclease-free H_2O and appropriate volume of RNA (for 2µg per sample) was pipetted into each q-PCR tube to a total volume of 20µl. For the NTC (no template control), nuclease-free H_2O was added instead of RNA.

The samples were vortexed and centrifuged prior to loading onto the thermocycler (Applied Biosystems).

The thermocycler was adjusted to the following settings:

1. 25° for 10 minutes
2. 37° for 120 minutes
3. 85° for 5 minutes
4. 4° (infinite hold)

The cDNA was stored at -20 prior to RT-qPCR.

2.6.7 Real Time quantitative PCR (RT-qPCR)

The cDNA was made to a concentration of 100ng/µl. The cDNA, primers and probes were thawed on ice. The cDNA was diluted by adding 80µl of dH_2O to 10µl of cDNA (50ng/9µl). Each reaction consisted of 10µl 2X Luna® Universal probe qPCR Mastermix (Biolabs, 003101), 1µl 20X primer and 50ng of cDNA. Into each well of a PCR plate, 11µl of primer/probe mix and 9µl of cDNA dilution were added to make a total volume of 20µl.

The PCR plate was sealed with adhesive, centrifuged and loaded onto a CFX96 Real Time System (BioRad).

The following settings were applied:

1. 2 minutes 50°
2. 10 minutes 95°
3. 40X (15 seconds 95°, 1 minute 60°)

Gene expression was calculated by subtracting the Ct value of the gene of interest from the Ct value of the housekeeper gene (*Rpl34*) (Table 2.4).

Table 2.4: Primer and probes.

Gene	Exon spanning region	Supplier	Cat No.
Ribosomal Protein L34 (*Rpl34*)	E1-E2	Applied Biosystems	Mm01321800_m1
Phosphatase and tensin homolog (*Pten)*	E4-E5	Applied Biosystems	Mm00477208_m1
Chemokine ligand 2 (*Ccl2)*	E1-E2	Applied Biosystems	Mm00441242_m1
Chemokine ligand 7 *(Ccl7)*	E1-E2	Applied Biosystems	Mm00443113_m1

2.7 *In vivo* experiments

2.7.1 Cisplatin experiment

ID8 cells and derivatives were washed, trypsinised, resuspended in complete medium and counted. Pellets were washed once in PBS and resuspended at 2.5 x 10^7 cells/ml in 37°C PBS. Each experiment routinely contained twelve C57BL/6 female mice, which were injected intraperitoneally (IP) with 5 x 10^6 cells in a volume of 200µl. The cages were randomised by the BSU staff to a treatment and control group. On days 28, 35 and 42, six mice were injected intraperitoneally with cisplatin (5mg/kg in PBS) and six mice injected with PBS. The PBS and cisplatin was given in a volume of 200µl and warmed to 37°C prior to injection.

Mice were monitored daily and killed when they reached UK Home Office limits. The defined endpoint was distended abdomen not exceeding that of pregnancy, high gait and pale feet. Experiments were performed at the Biological Services Unit at the CRUK Beatson Institute, Glasgow under suitable UK Home Office project and personal licence authority. All decisions about animal welfare were made by BSU staff.

2.7.2 GGTACKO pilot experiment

The GGTACKO mice are a transgenic mouse model that originate from C57BL/6n mice and have CCR1, 2, 3 and 5 knocked out. These mice were a gift from Professor Graham's lab, University of Glasgow. ID8 cells and derivatives were prepared and injected as above. The mice were culled once they reached the UK Home office limits.

2.7.3 PI3K inhibitor experiment

ID8 cells and derivatives were prepared and injected as above. The mice were given twice daily oral gavage of either 0.5% hydroxyl-propyl-methylcellulose + 0.1% tween-80 + ddH_20 (vehicle) or AZD8186 (PI3K p110ß inhibitor) (50mg/kg) (1.25mg/dose = 25g mouse) from day 37-42 in the *Trp53*-/- F3 mice or from day 25-30 in the *Trp53*-/-;*Pten*-/- 1.14 mice. On day 6 of treatment (day 30 or day

42) the mice were given a final treatment dose and a single IV injection of BrdU. One hour after the last dose of AZD8186/vehicle the mice were culled.

2.7.4 Harvesting of samples

Ascites

For the cisplatin experiment the ascites was harvested, total volume recorded and centrifuged at 2000rpm for 10 minutes. Supernatant was harvested, aliquoted and stored at -80°C. Ascites cells were treated with 5ml Red Blood Cell Lysis buffer (Sigma Aldrich, 11814389001) for 5 minutes at room temperature. PBS was added, and the tube centrifuged again at 2000rpm. Pellets were cryopreserved, aliquoted into four cryovials, and stored at -80°C.

In the GGTACKO and PI3K inhibitor experiments, the ascites was processed as above but used fresh for flow cytometry analysis (see section 2.9.3). If no ascites was present during the harvesting of the PI3K inhibitor mice, the peritoneal cavity was washed out with cold PBS.

Tumour and Mesentery for formalin fixation

Tumour and mesentery were immediately fixed in a maximum volume of 20mls 10% Neutral Buffered Formalin (NBF) and left at room temperature for 24 hours. The following day, NBF was replaced with 70% ethanol. Tumour and mesentery were paraffin embedded and an H&E stain was carried out. Both were performed by the Histology Service, CRUK Beatson Institute.

Only tumour was fixed in formalin as above in the GGTACKO and PI3K inhibitor experiment.

Tumour samples

A small sample of tumour was wrapped in foil and immediately placed on dry ice before transfer to -80°C and another tumour sample was initially put in PBS before it was snap frozen and transferred to the -80°C.

For the GGTACKO and PI3K inhibitor experiments, a small sample of tumour was snap frozen to be used for RT-qPCR and a small sample in PBS was used fresh for flow cytometry analysis (see section 2.9.4).

Full Blood Count (FBC)

A blood sample was taken from all mice that were culled in both the GGTACKO and PI3K inhibitor experiments and a FBC obtained using a Procyte Dx® Haematology Analyzer, IDEZZ Laboratories.

2.8 Operetta (Wt1 staining)

1 x 10^4 mouse ascites cells were plated in a clear-bottomed black 96 well plate. These were plated alongside the ID8 F3 (*Trp53-/-)* cell line (positive control) and the NIH/3T3 cell line (mouse fibroblast cell line) (negative control). 24 hours after plating, cells were initially washed once with PBS and fixed with 2% sucrose/3% PFA for 10 minutes. The cells were then washed with PBS (x3) and permeabilised with 0.5% triton for 10 minutes. Following further PBS washes (x3), the Wt1 primary antibody 1:100 in 2% BSA (Abcam, Cat No: ab89901) was added to the cells for 45 minutes at 37°C. The same amount of IgG isotype control (IgG rabbit) was added to the same cell lines on different wells. Again, the cells were washed with PBS (x3) and secondary antibody (Invitrogen, Cat No: A-11036, Alexa Fluor goat anti-rabbit 568) 1:500 in 2% BSA was added to all wells for 45 minutes at 37°C. The cells were washed with PBS (x3) and DAPI 1:10,000 in PBS added for 15 minutes at room temperature. The cells were finally washed with PBS (x3) and then read on the Operetta high-content imaging system at 10x magnification (Perkin Elmer).

2.9 Flow cytometry

2.9.1 Flow cytometry for DR-GFP assay

Cells were trypsinised, washed and re-suspended to a final concentration of 1 x 10^6 cells. The suspension was centrifuged at 1200rpm for 3 minutes and resuspended in 5ml of PBS. A final centrifuge was performed at 1200rpm for 6 minutes and then resuspended in 1ml of cold PBS. The suspension was passed through a strainer and taken on ice for flow analysis.

2.9.2 Cell sorting for mCherry expressing cells

Cells were trypsinised, washed and re-suspended in normal medium. The suspension was centrifuged for 3 minutes at 1200rpm and pellet washed with 2ml of cold sorting buffer followed by centrifuge at 1200rpm for 3 minutes. The cells were re-suspended in 2ml of cold sorting buffer to a concentration of 1 x 10^7 cells. A final centrifuge was performed at 1200rpm for 3 minutes and re-suspended in 1ml of sorting buffer before filtered through a 70-micron strainer. The suspension was taken on ice for sorting along with a 96 well plate containing ID8 medium.

Sorting buffer: PBS, 1mM EDTA, 25mM HEPES pH 7, 1% FBS (heat-inactivated), 0.2µm filter sterilised.

2.9.3 Flow cytometry for ascites

Flow cytometry analysis was performed using frozen ascites from the cisplatin experiment. Before antibody staining, cryopreserved ascites was thawed rapidly at 37°C and transferred to a 15ml tube containing pre-warmed ID8 medium. The tubes were centrifuged at 1200rpm 4°C and resuspended in 5ml of FACS buffer. Six FMO controls (Fluorescence minus one) (CD11b, F4/80, MHCII, CD86, PDL-1 and CD3) were created by using a spread of samples across different genotypes and treatments. 4 x 10^6 cells were plated on a v-bottom plate and kept on ice.

Flow cytometry analysis was performed using fresh ascites and tumour from both the GGTACKO and PI3K inhibitor experiment. Ascites was processed as previously described (see section 2.7.4) and resuspended in 5ml of FACS buffer before plating as above.

2.9.4 Flow cytometry for murine tumours

The tumour was transferred to a 6cm dish in PBS and chopped into small pieces (<1mm) before transfer to a 15ml tube and centrifuged at 1500rpm for 5 minutes. The PBS was aspirated and resuspended in 5ml of digestion mix (500µl trypsin, 50µl collagenase (Sigma, C7657), 50µl dispase (Sigma, Cat No: 42613-33-2), 0.1% BSA in RPMI medium). The 15ml tube was put on a roller and incubated at 37°C for 30 minutes. Following incubation, the sample was transferred to a 50ml tube and 10ml 0.1% BSA/RPMI added. The tube was then shaken vigorously up and down (about 20 times). This was repeated a further three times until a total volume of 45ml was reached.

The sample was then filtered using a 100µm filter into another 50ml tube, centrifuged for 5 minutes at 1500rpm and resuspended in FACS buffer. Depending on the number of mice a proportion of each mouse sample was used for the FMOs. The samples were plated on a v-bottom plate and kept on ice.

2.9.5 Antibody staining

50µl of Mouse Fc block (BD Biosciences, Cat No: 553142) was added at 1:200 to each well, cells resuspended and incubated at 4°C for 15 minutes. 50µl of the antibody mastermix or FMO mix was added to the samples and FMO controls and incubated at 4°C for 30 minutes. The mastermix contained a panel of 11 fluorescently conjugated antibodies against murine CD45, CD11b, F4/80, MHCII, Ly6C, Ly6G, CD3, CD8a, CD86, CD19, PDL-1. The concentrations had previously been optimised within the McNeish lab (Table 2.5). The samples were then washed with PBS and centrifuged at 1500rpm 4°C for 5 minutes followed by a further wash with PBS and centrifuged. 50µl of Zombie red viability dye (1:200 PBS) was added to the samples and incubated at 4°C for 20 minutes. Samples were then washed and centrifuged with FACS buffer before fixation with 100µl

of 1:1 solution of 4% PFA and FACS buffer. The samples were finally incubated at 4°C for 20 minutes. The samples were then washed with FACS buffer and centrifuged before resuspension in 350µl of FACS buffer and transferred to FACS tubes. The FACS tubes were kept at 4°C for no longer than 1 week before analysis.

FACS buffer: PBS, 0.5% BSA, 2mM EDTA

2.9.6 Compensation

Compensation with beads was used prior to the experiments with one tube per fluorochrome. Each tube contained positive and negative control beads. Anti-rat compensation beads for 10 fluorochromes (BD CompBeads, Cat No: 552845) and anti-mouse compensation beads for the F4/80 fluorochrome (BD CompBeads, Cat No: 552843). A separate tube was used to compensate for the viability dye again with positive and negative control beads (ArC™ Amine reactive compensation beads, Invitrogen, Cat No: A10628). In addition to beads, 100µl of FACS buffer and 1µl of antibody was added to each tube.

The samples were analysed by flow cytometry and used to set compensation for all subsequent experiments.

2.9.7 Flow analysis

Flow cytometry was performed on a BD Fortessa (BD Biosciences). For each sample, 30,000 CD45 events were collected and analysed with FlowJo software (Tree Star, Ashland, OR). A consistent gating strategy was applied to all experiments with the use of the 6 FMOs (Figure 2.4).

Table 2.5: 12 fluorochrome flow cytometry panel.

The panel was used to analyse the ascites and murine tumour by flow cytometry and shows the 6 FMOs (CD11b, F4/80, MHCII, CD86, PDL-1 and CD3) used.

Antibodies	Supplier	Catalogue No.	Fluorochrome	Filter	Dilution
CD45	Life Technologies	MCD4530	Pacific Orange	UV580/20	1 in 20
CD11b (FMO)	BD Biosciences	6245992	BUV 737	UV 785/62	1 in 300
Ly6G	Biolegend	127645	Brilliant Violet 785	V 780/60	1 in 50
Ly6C	Biolegend	128010	AlexFluor 647	R 670/14	1 in 1500
F4/80 (FMO)	Miltenyi Biotec	130-102-943	PE	YG 786/15	1 in 50
MHCII (FMO)	Miltenyi Biotec	130-102-910	FITC	B 530/30	1 in 50
CD86 (FMO)	Biolegend	105014	PE/Cy7	YG 780/60	1 in 20
CD8a	Biolegend	100742	Brilliant Violet 650	V 655/8	1 in 80
PDL-1 (FMO)	Biolegend	124315	Brilliant Violet 421	V 450/50	1 in 300
CD3 (FMO)	Biolegend	100217	PerCP-Cy5.5	B 685/35	1 in 150
CD19	Biolegend	218940	APC/Fire 750	R 780/60	1 in 300
Fixable viability dye	Biolegend	423110	Zombie red	YG 610/20	1 in 200

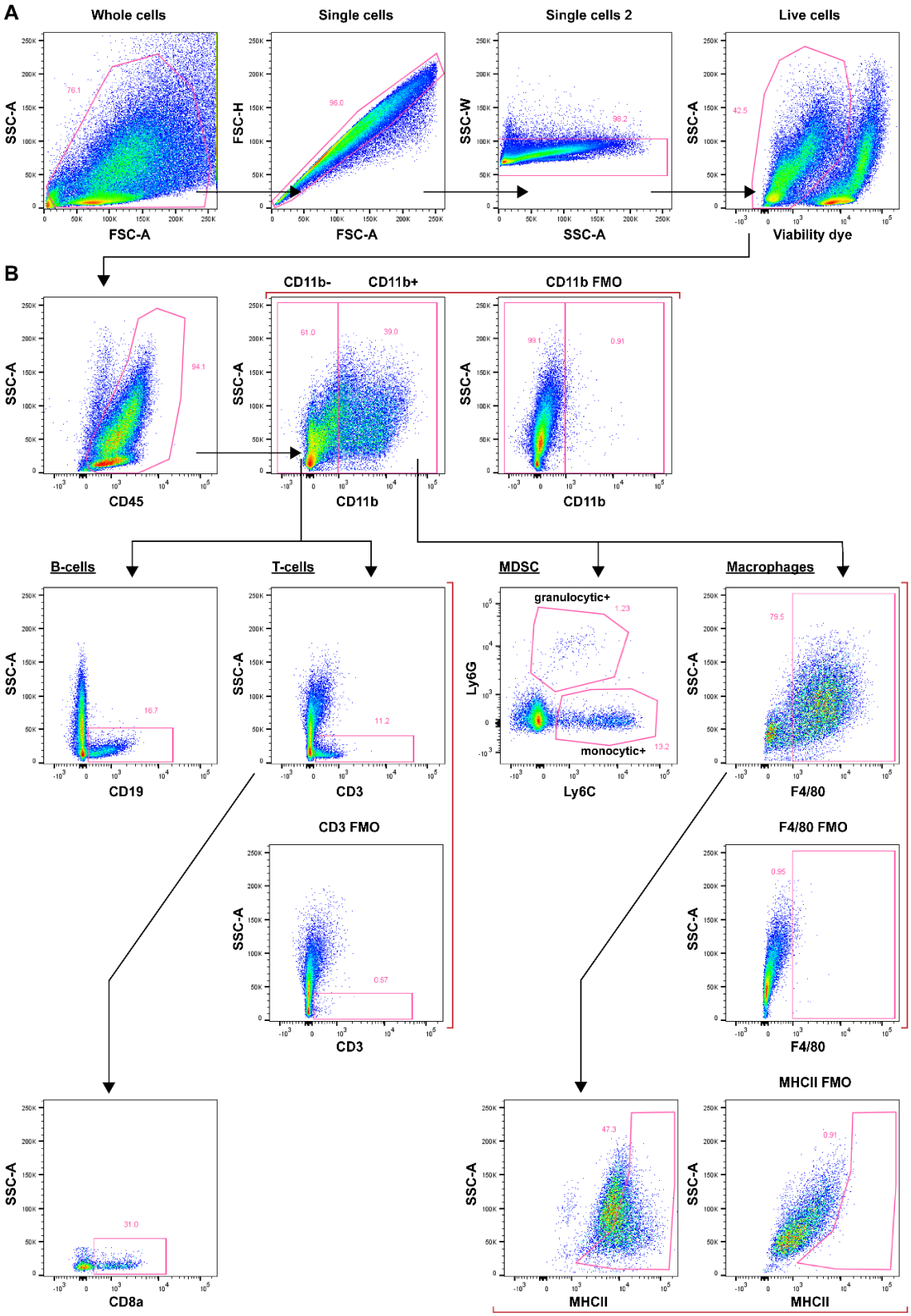

Figure 2.4: Gating strategy used for the flow cytometry.

The 6 FMOs (CD11b, F4/80, MHCII, CD86, PDL-1 and CD3) were used to assist with gating. The PDL-1 and CD86 gating is not shown in this example.

2.10 Statistical Analysis

All data are expressed as the mean, and error bars represent standard deviation of the mean (SD), apart from the Rad51/γH2AX assay, in which standard error of the mean (SEM) is used. Statistical tests were performed using Prism v6.0 (GraphPad, San Diego, CA). Pearson correlation (r) was used to determine the correlation between two variables.

Differences between groups of mice and lines were analysed using unpaired *t*-tests or One-Way ANOVA with Bonferroni's test for multiple comparisons. Differences in survival were calculated using log-rank test. A p value ≤0.05 (*) was considered significant. The level of statistical significance is indicated using asterisks (*p<0.05, **p<0.01, ***p<0.001, ****<0.0001).

Linear regression analysis was used to assess differences in cell proliferation. The Kruskal-Wallis test was used for RNA sequencing analysis to compare gene expression between genotypes. P values from differential gene expression were adjusted for multiple testing using the Benjamini-Hochberg procedure.

3 Homologous Recombination and platinum and PARP inhibitor sensitivity

3.1 Introduction

Platinum sensitivity in HGSOC is thought to be related to a multitude of factors but underlying defects in homologous recombination (HR) may be a strong predictor of sensitivity. Several studies including TCGA have consistently shown frequent genetic and epigenetic alterations of key HR genes in HGSOC, with *BRCA1* and *BRCA2* the most commonly mutated (Konstantinopoulos et al., 2015). This is further highlighted by the fact that acquired platinum resistance can be related to mutations in *BRCA1/2* that restore their function in HR. In the TCGA analysis, approximately 50% of HGSOC of cases were thought to exhibit defective homologous recombination. Although clinical trials consistently demonstrate high platinum sensitivity in *BRCA1/2* mutated tumours, there are still subgroups of patients with *BRCA1/2* mutations that are resistant to platinum chemotherapy and others that are sensitive that are *BRCA1/2* wild-type (Alsop et al., 2012).

HR-deficient cells have been shown to be extremely sensitive to PARP inhibitors. This has been supported by recent clinical trials in patients with *BRCA1/2* mutations, where 40% did not develop progressive disease for at least 3 years following treatment with maintenance olaparib therapy after responding to platinum chemotherapy (Ledermann et al., 2012, Ledermann et al., 2014). However, the exact mechanism of sensitivity remains poorly understood.

This chapter investigates the relationship between homologous recombination and both platinum and PARP inhibitor sensitivity. The HR status was established on HGSOC cell lines, ID8 knockout derivatives and a transgenic murine ovarian cancer cell line and then correlated with platinum and PARP inhibitor sensitivity. The aim was to determine whether defective homologous recombination was a strong predictor of sensitivity to both these drugs.

3.2 Assessment of Homologous Recombination status in cell lines

A cell line's ability to repair DSBs by homologous recombination was assessed using the Rad51/γH2AX immunofluorescence assay. This assay was developed in Newcastle by the lab of Nicola Curtin and Richard Edmondson (Mukhopadhyay et al., 2010). In the initial experiments with HGSOC and ID8 cell lines, cells were exposed to rucaparib (10μM) (PARP inhibitor) for 24 hours and, as described in the original assay, a two-fold increase in Rad51 foci defined HR competency in the presence of proven DNA DSB damage (two-fold increase in γH2AX foci following PARP inhibitor treatment).

As the Homologous Recombination status was being correlated with PARP inhibitor sensitivity it was felt that an alternative treatment should be used to induce DSBs. In subsequent experiments, cell lines were exposed to irradiation (10Gy) and γH2AX/Rad51 foci assessed 24 hours later.

The γH2AX foci seen following irradiation were more discrete and resulted in clearer confocal images. In terms of the HR status of cell lines the results between the rucaparib and irradiation showed complete concordance.

RAD51/γH2AX assay:

In all high grade serous ovarian cancer cell lines tested, treatment with 10μM of Rucaparib for 24hrs resulted in at least a 2-fold increase in γH2AX, showing DNA damage had occurred (Figure 3.2). In the ID8 derivatives treatment with 10Gy of irradiation resulted in at least a 2-fold increase in γH2AX foci in all cell lines showing again DNA damage had occurred (Figure 3.1, Figure 3.3, Figure 3.4, Figure 3.5, Figure 3.6). There was therefore adequate DNA damage to detect RAD51 foci and determine whether a cell line was HR-competent or deficient. The mean number of γH2AX and RAD51 foci per cell was calculated and compared to the control.

DR-GFP assay:

Following *p*DR-GFP transfection and puromycin selection, the surviving colonies were re-plated and transfected with *p*ISce-I or *p*CAAGS (control plasmid). 48 hours following transfection the cells were assessed for GFP positivity by flow

cytometry. An increase in GFP positivity in the *p*ISce-I group compared to *p*CAAGs demonstrates adequate HR-mediated DNA DSB repair has occurred (Figure 3.11).

Dose response for cisplatin and rucaparib:

The IC50 levels were taken from the cisplatin and PARP inhibitor dose response curves of each cell line and the mean IC50 from a triplicate experiment plotted (Figure 3.2 to Figure 3.10).

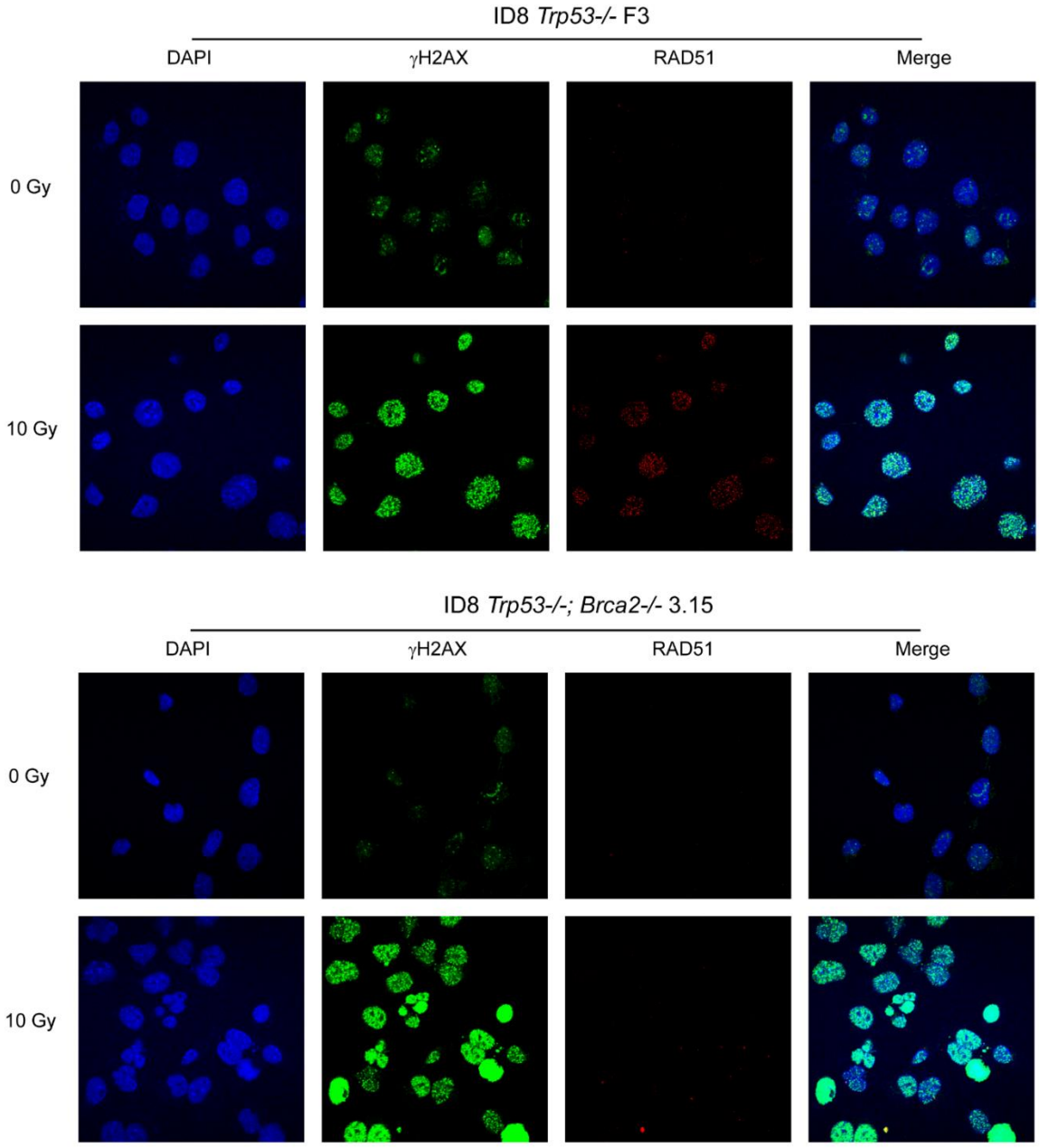

Figure 3.1: Assessment of HR status comparing the ID8 F3 *Trp53-/-* and the ID8 3.15 *Trp53-/-;Brca2-/-* cell lines.
The red dots correspond to the Rad51 foci and green dots to the γH2AX. The foci were quantified by manually counting 30 nuclei per condition. There was a 2-fold increase in γH2AX foci compared to the control in both cell lines following irradiation (10Gy) indicating adequate DNA DSB induction. There was a 2-fold increase in Rad51 foci compared to the control in the F3 *Trp53-/-* cell line but not in the 3.15 *Trp53-/-; Brca2-/-* cell line consistent with an HR-defective cell line.

3.2.1 High grade serous ovarian cancer cell lines

The HR-competent HGSOC cell lines (PEO4, OVCAR3, OVCAR4, COV318 and UWB1.289BRCA1) all showed at least a 2-fold increase in RAD51 foci in response to rucaparib over the untreated controls. HR-deficient HGSOC cell lines (PEO1 and UWB1.289) showed a less than 2-fold increase in RAD51 foci formation (Figure 3.2).

The *BRCA1/2* mutation status (and hence the theoretical HR competence status) of the HGSOC cell lines prior to the experiments was already known. PEO1 cell line has a *BRCA2* mutation and UWB1.289 cell line has a *BRCA1* mutation. The remaining cell lines (PEO4, OVCAR3, OVCAR4 and UWB1.289BRCA1) are *BRCA1/2* wild-type and thus theoretically HR competent.

There was considerable variability in the cisplatin and PARP inhibitor sensitivity between the cell lines. When comparing the matched cell pair PEO1 (HR deficient) and PEO4 (HR competent), PEO1 was more sensitive to both cisplatin and PARP inhibitor (cisplatin mean IC50 7.40 (PEO1), 14 (PEO4), p=0.02*; rucaparib mean IC50 2.7 (PEO1), 14.2 (PEO4) p=0.02*). However, comparing the UWB1.289 (HR deficient) and UWB1.289BRCA1 (HR competent) cell lines, UWB1.289 was more sensitive to PARP inhibition but showed similar sensitivity to cisplatin (cisplatin mean IC50 5.1 (UWB1.289), 2.4 (UWB1.289BRCA1), p=0.14; rucaparib mean IC50 10.3 (UWB1.289), 54.9 (UWB1.289BRCA1), p=0.03*) (Figure 3.2).

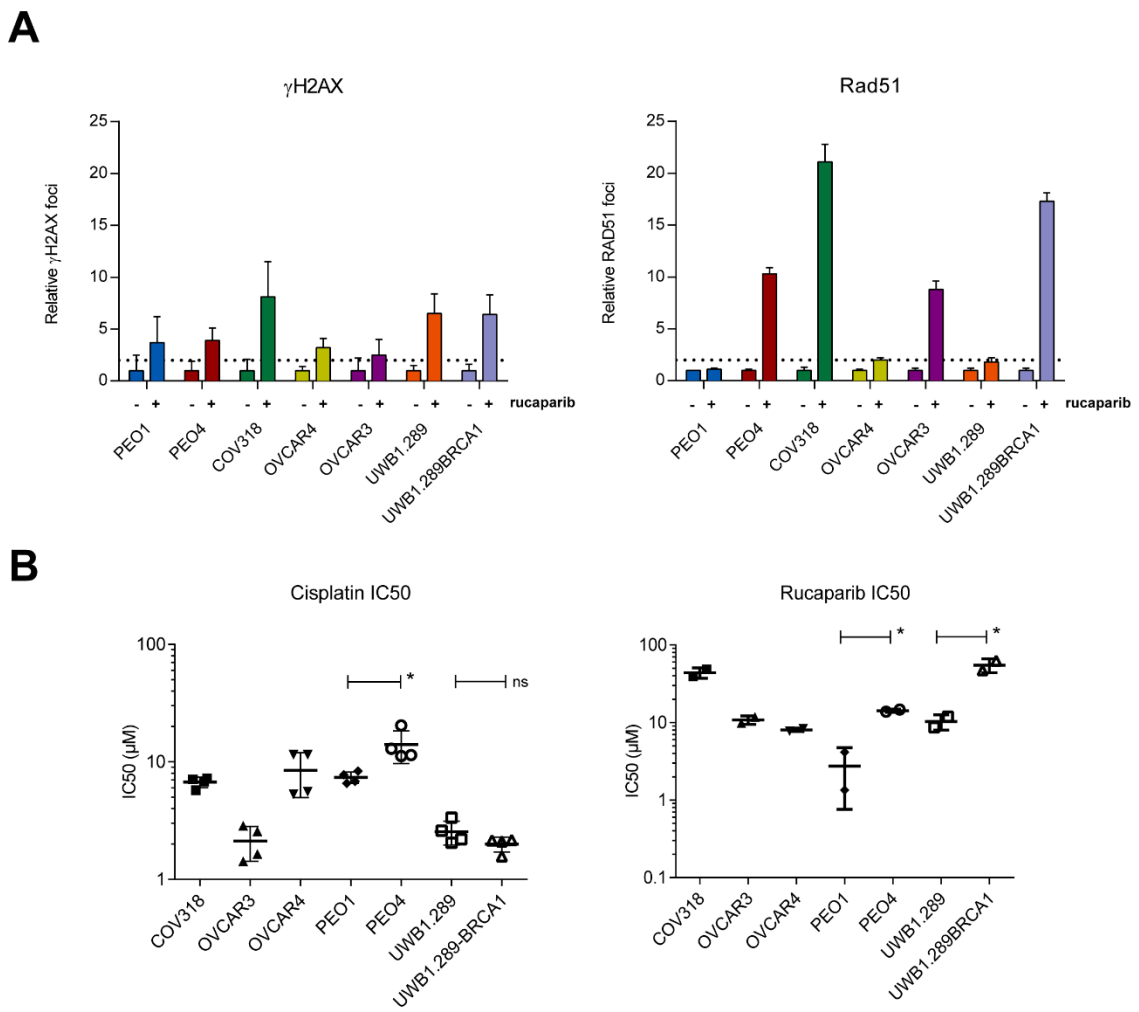

Figure 3.2: Assessment of HR status and cisplatin and rucaparib sensitivity in HGSOC cell lines.

A, HGSOC cell lines were treated with rucaparib (10μmol/L), fixed and stained for γH2AX and RAD51, and counterstained with DAPI. RAD51 foci were counted in 30 untreated and treated cells. Bars, mean (± SEM) foci per cell relative to untreated cells. The dotted line represents a two-fold increase in foci relative to untreated cells. **B**, Each dot represents the mean IC50 value from a triplicate experiment. Unpaired *t*-tests were performed on the matched cell lines with known HR status (PEO1 - *BRCA2* mutation, PEO4 - *BRCA2* wild-type, UWB1.289 – *BRCA1* mutation and UWB1.289BRCA1 – *BRCA1* wild-type).

3.2.2 ID8 derivatives

The ID8 cell line is a transplantable murine model of ovarian cancer originating from C57Bl/6 mice ovaries and created in 2000 by Dr Kathy Roby (Roby et al., 2000). Using the CRISPR/Cas9 gene editing technique, the McNeish lab has recently generated several knockout derivatives of the ID8 cell line to closer resemble the genetic background of HGSOC (Walton et al., 2016, Walton et al., 2017).

3.2.2.1 *Trp53-/-* and *Trp53-/-;Brca1* and *2-/-*

The *Trp53-/-* knockouts were generated using three different guide RNA constructs to target exon 5 of *Trp53*. F3 (guide G), A2 (guide K), C7 and M20 (guide R) clones were all found to contain bi-allelic deletions in *Trp53* exon 5. The F3 clone had a 43bp and A2 clone had a 280bp bi-allelic deletion. All clones showed absent basal p53 expression by immunoblot (Walton et al., 2016). The F3 *Trp53-/-* clone was used to create all the subsequent knockout derivatives.

The *Trp53-/-;Brca1-/-* knockout was generated using the F3 clone by targeting the *Brca1* PALB2-binding domain in exon 12 or the BRCT-2 domain in exon 19. Three different *Brca1-/-* clones had confirmed bi-allelic deletions (clones 1.26, 1.36 – PALB2-binding domain and 6.20 – BRCT2 domain) (Walton et al., 2017).

The *Trp53-/-;Brca2-/-* knockout again was generated from the *Trp53-/-* F3 clone by targeting the *Brca2* PALB2-binding domain in exon 3. Three clones (2.14, 3.15 and 1.4) derived from different guides had confirmed bi-allelic deletions (Walton et al., 2016).

Our data in the ID8 parental clone and ID8 *Trp53-/-* clone (F3) all showed at least a 2-fold increase in RAD51 foci in response to irradiation over the untreated controls. The ID8 *Trp53-/-;Brca2-/-* clones (2.14 and 3.15) and *Trp53-/-;Brca1-/-* clones (1.26, 1.36 and 6.20) showed a less than 2-fold increase in RAD51 foci formation (Figure 3.3).

The ID8 parental cell line has been shown to have no mutations in key HR genes and it has been previously found to be HR competent (Walton et al., 2016). This is consistent with my data that found the ID8 parental cell line to also be HR competent. p53 has not been found to play an important role in HR and therefore the ID8 *Trp53*-/- clones would also be expected to be HR competent.

The ID8 *Trp53*-/-;*Brca2*-/- clones (2.14, 3.15) and *Trp53*-/-;*Brca1*-/- clones (1.36, 1.26) all have distinct mutations in the region, which encodes the PALB2 binding domain. Whereas the *Trp53*-/-;*Brca1*-/- clone (6.20) has a mutation in the BRCT-2 domain. As both BRCA1 and BRCA2 are key genes in the HR pathway these clones should theoretically be HR deficient.

The *Trp53*-/-;*Brca1*-/- genotype was significantly more sensitive to both cisplatin and rucaparib compared to the F3 *Trp53*-/- clone (*Trp53*-/-;*Brca1*-/- cisplatin p=≤0.0001****; *Trp53*-/-;*Brca1*-/- rucaparib p=≤0.0001****). A similar pattern of sensitivity was also seen in the *Trp53*-/-;*Brca2*-/- genotype compared to the F3 (*Trp53*-/-;*Brca2*-/- cisplatin p=≤0.0001****; *Trp53*-/-;*Brca2*-/- rucaparib p=≤0.0001****) (Figure 3.3 and Table 3.1).

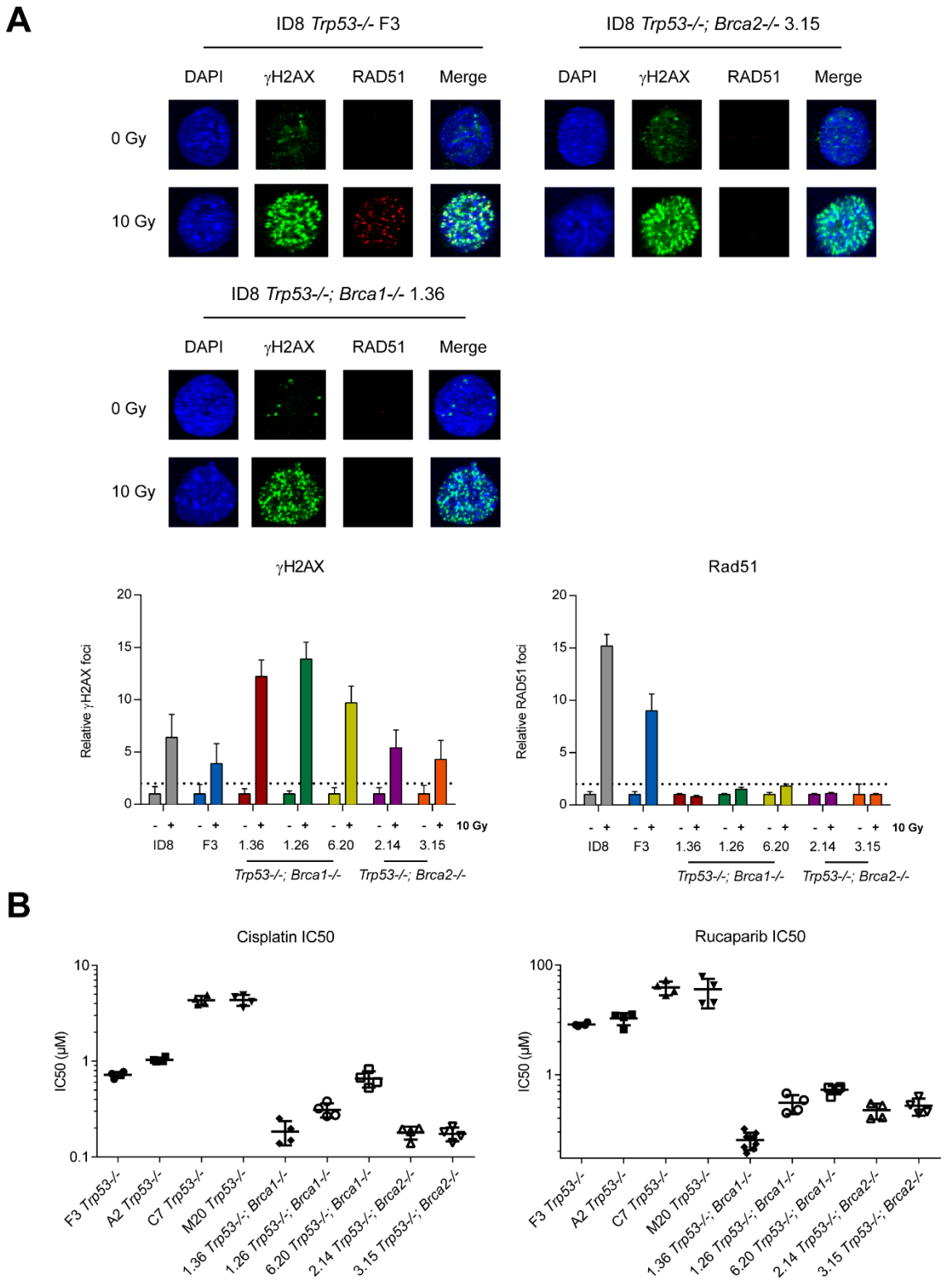

Figure 3.3: Assessment of HR status and cisplatin and rucaparib sensitivity in ID8 *Trp53-/-*, *Trp53-/-;Brca1-/-* and *Trp53-/-;Brca2-/-* knockouts.
A, ID8 derivatives were irradiated (10Gy), fixed and stained for γH2AX and RAD51, and counterstained with DAPI. **B**, Each dot represents the mean IC50 value from a triplicate experiment.

3.2.2.2 *Trp53-/-;Pten-/-* and *Pten+/-*

The *Trp53-/-;Pten-/-* knockout was generated using the F3 clone by targeting the *Pten* phosphatase domain in exon 5. Four clones (1.11, 1.12, 1.14, 1.15) had confirmed bi-allelic deletions and two clones (1.9, 1.10) had single allele deletions. PTEN was found to be absent on immunoblots in the *Trp53-/-;Pten-/-* clones and reduced in the heterozygote clones. There was also an increase in AKT phosphorylation following serum starvation in both the *Trp53-/-;Pten-/-* and *Pten+/-* clones (Walton et al., 2017).

The ID8 *Trp53-/-;Pten-/-* clones (1.11, 1.12, 1.14 and 1.15) and the ID8 *Trp53-/-;Pten-/+* clones (1.9 and 1.10) all showed at least a 2-fold increase in RAD51 foci in response to irradiation over the untreated controls and were therefore HR competent.

There have been conflicting reports of the possible role of PTEN in homologous recombination. Some reports have suggested that PTEN reduces RAD51 recruitment to double strand DNA breaks (McEllin et al., 2010) and sensitises cells to PARP inhibition (Mendes-Pereira et al., 2009); however more recent reports conclude no involvement in the HR pathway (Hunt et al., 2012, Fraser et al., 2012).

There was no significant difference in cisplatin and rucaparib sensitivity between the *Trp53-/-;Pten-/-* genotype and F3 *Trp53-/-*. There was a significant difference in cisplatin sensitivity between the *Trp53-/-;Pten-/+* clones and F3 *Trp53-/-* (cisplatin p=<0.0001) but no difference in rucaparib sensitivity (Figure 3.4 and Table 3.1).

3.2.2.3 *Trp53-/-;Brca1-/-;Pten-/-* and *Trp53-/-;Brca2-/-;Pten-/-*

The *Trp53-/-;Brca1-/-;Pten-/-* knockouts were generated using the 1.26 and 6.20 *Trp53-/-;Brca1-/-* clones and targeted the *Pten* phosphatase domain in exon 5. Two clones (1.26.19, 6.20.10) had confirmed bi-allelic deletions in exon 5.

The *Trp53-/-;Brca2-/-;Pten-/-* knockouts were generated using the *Trp53-/-; Brca2-/-* clones 2.14 and 3.15 and again targeted the same *Pten* domain. Two clones (2.14.22, 3.15.10) had bi-allelic deletions confirmed.

All the triple knockout clones (1.26.19, 6.20.10, 2.14.22, 3.15.10) had absent PTEN on immunoblot and an increase in AKT phosphorylation following serum starvation (Walton et al., 2017).

Both the ID8 *Trp53-/-;Brca1-/-;Pten-/-* and *Trp53-/-;Brca2-/-;Pten-/-* clones showed a less than 2-fold increase in RAD51 foci formation in response to irradiation over the untreated controls and therefore remaining HR defective.

The *Trp53-/-;Brca1-/-;Pten-/-* genotype was significantly more sensitive to both cisplatin and rucaparib compared to the F3 *Trp53-/-* clone (*Trp53-/-;Brca1-/-;Pten-/-* cisplatin p=≤0.0001; *Trp53-/-;Brca1-/-;Pten-/-* rucaparib p=≤0.0001). This was also seen in the *Trp53-/-;Brca2-/-;Pten-/-* genotype compared to the F3 clone (*Trp53-/-;Brca2-/-;Pten-/-* cisplatin p=≤0.0001; *Trp53-/-;Brca2-/-;Pten-/-* p=≤0.0001) (Figure 3.5 and Table 3.1).

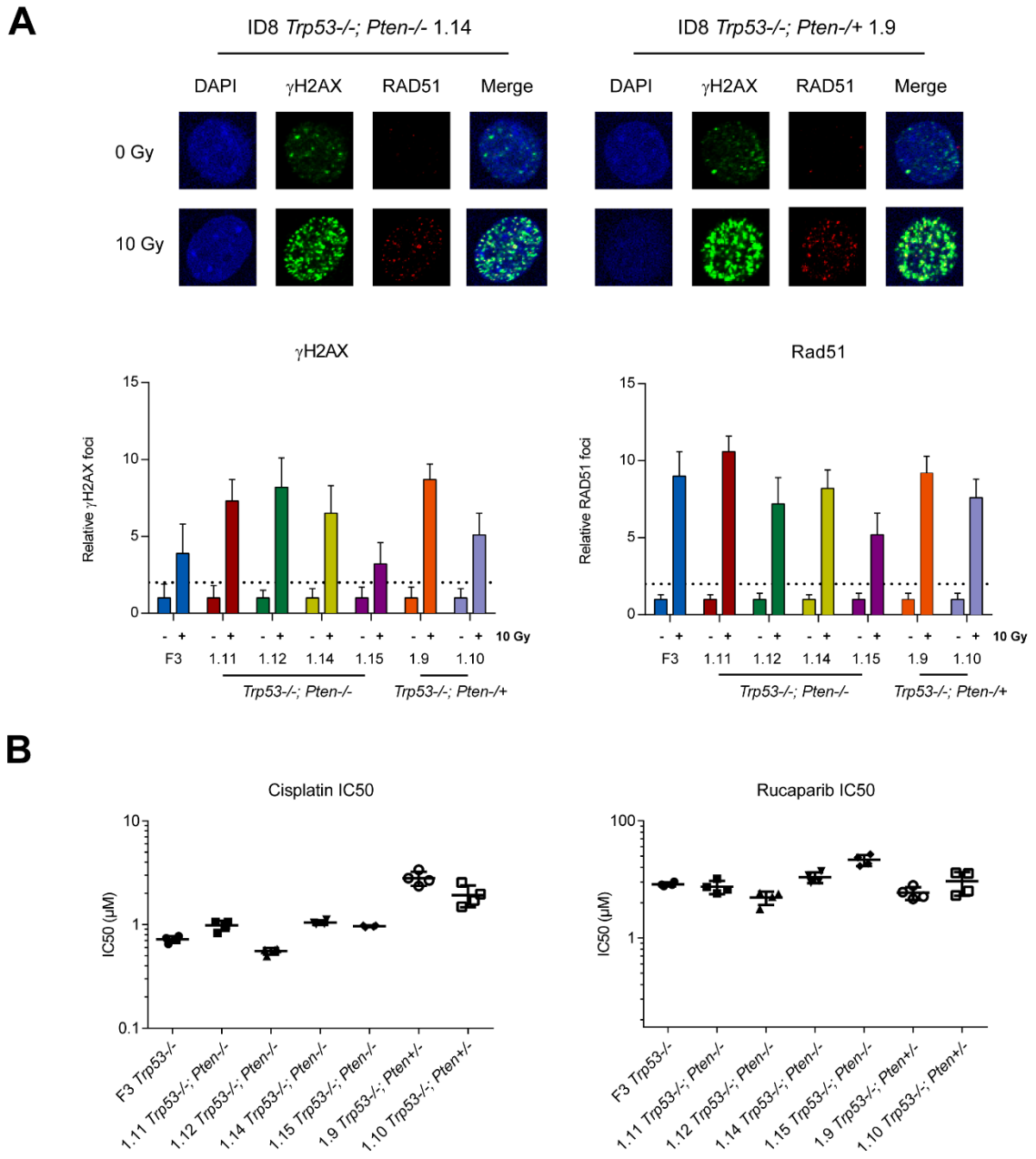

Figure 3.4: Assessment of HR status and cisplatin and rucaparib sensitivity in ID8 *Trp53-/-;Pten-/-* and *Trp53-/-;Pten+/-* knockouts.
A, ID8 derivatives were irradiated (10Gy), fixed and stained for γH2AX and RAD51, and counterstained with DAPI **B**, Each dot represents the mean IC50 value from a triplicate experiment.

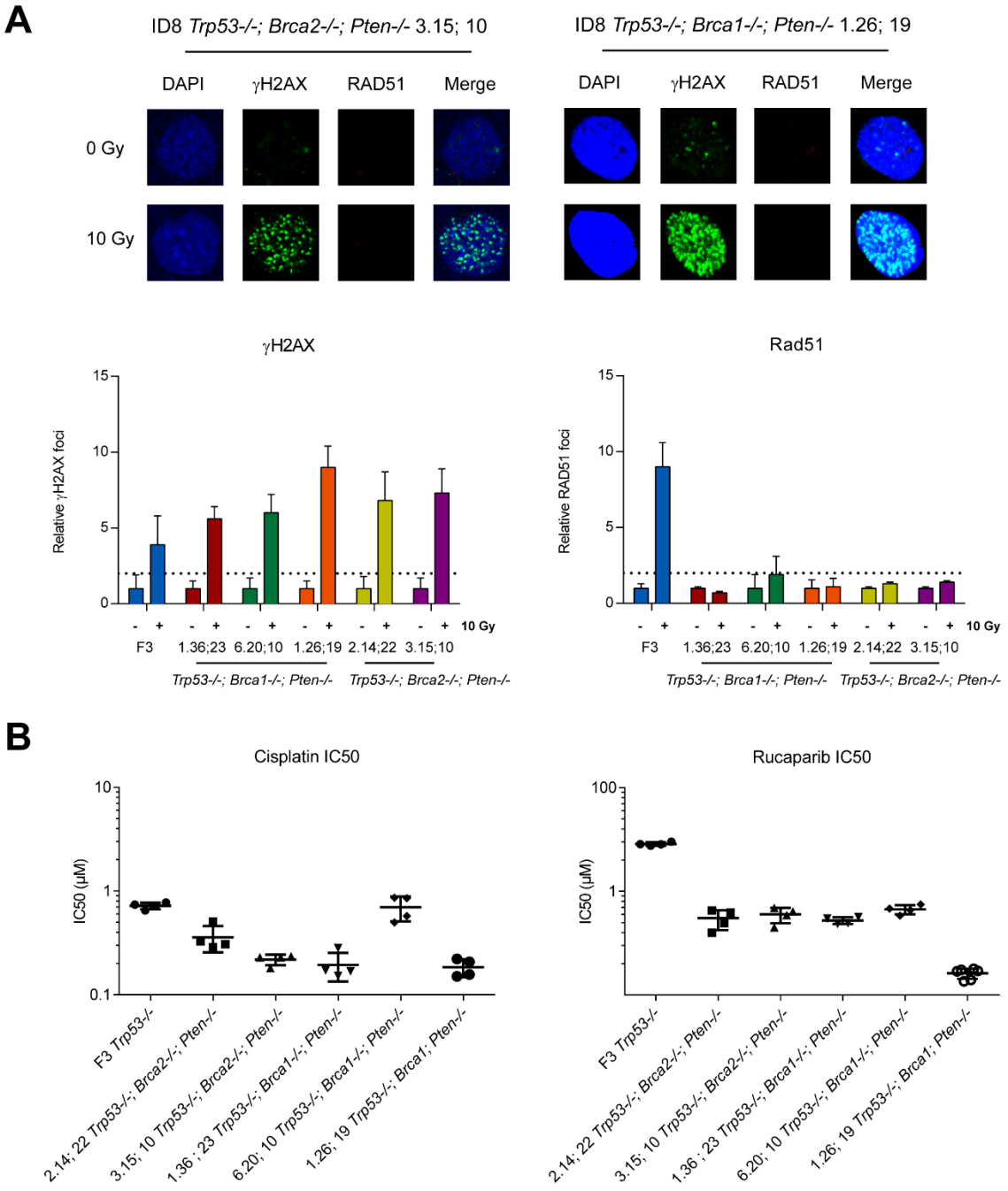

Figure 3.5: Assessment of HR status and cisplatin and rucaparib sensitivity in ID8 *Trp53-/-;Brca1-/-;Pten-/-* and *Trp53-/-;Brca2-/-;Pten-/-* knockouts
A, ID8 derivatives were irradiated (10Gy), fixed and stained for γH2AX and RAD51, and counterstained with DAPI **B**, Each dot represents the mean IC50 value from a triplicate experiment.

3.2.2.4 *Trp53-/-;Nf1-/-*

For the *Trp53-/-;Nf1-/-* knockouts, exon 2 was targeted in the F3 clone and the two generated clones (1.20, 1.23) had confirmed bi-allelic deletions. These clones showed evidence of activated RAS signalling with increased GTP-bound RAS and also increased ERK phosphorylation on immunoblot (Walton et al., 2017).

These two ID8 *Trp53-/-;Nf1-/-* clones (1.20, 1,23) all showed at least a 2-fold increase in RAD51 foci in response to irradiation over the untreated controls and were therefore HR competent.

There was no significant difference in cisplatin sensitivity between the *Trp53-/-;Nf1-/-* genotype and F3 *Trp53-/-* clone. However, the *Trp53-/-;Nf1-/-* genotype was significantly more sensitive to rucaparib compared to the F3 clone ($p=\leqslant 0.01$*). The reason for this difference in sensitivity is unclear (Figure 3.6 and Table 3.1).

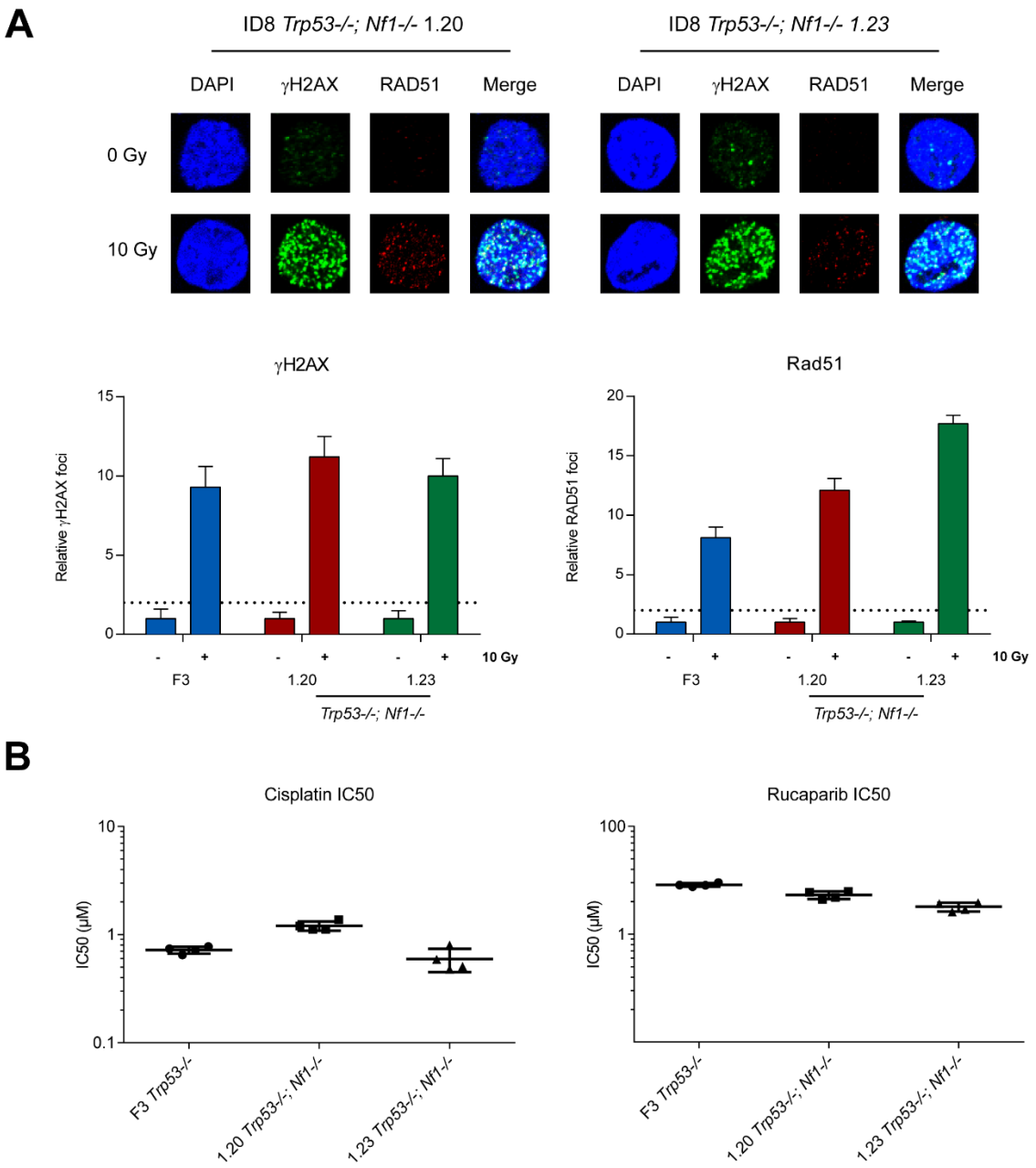

Figure 3.6: Assessment of HR status and cisplatin and rucaparib sensitivity in ID8 *Trp53-/-;Nf1-/-* knockouts.
A, ID8 derivatives were irradiated (10Gy), fixed and stained for γH2AX and RAD51, and counterstained with DAPI **B**, Each dot represents the mean IC50 value from a triplicate experiment.

3.2.3 OVIDT 479 cell lines

The *Dicer-/-;Pten-/-* cell line originated from a transgenic murine fallopian tube carcinoma model. Cre recombinase under the control of the anti-Mullerian hormone type 2 receptor promoter (*Amhr2-Cre*) was used to delete *Dicer* and *Pten* in the fallopian tube (Kim et al., 2012).

Dicer is a key processor of microRNAs and low Dicer expression has been correlated with poor clinical outcomes in ovarian cancer (Merritt et al., 2008).

The *Dicer-/-;Pten-/-;Trp53-/-* knockouts were generated by Dr Josephine Walton using the same guide RNA used to generate the ID8 F3 clone (targeting exon 5). Clone 13 was found to have a biallelic deletion in exon 5 and p53 expression was absent on immunoblot (Walton et al., 2017).

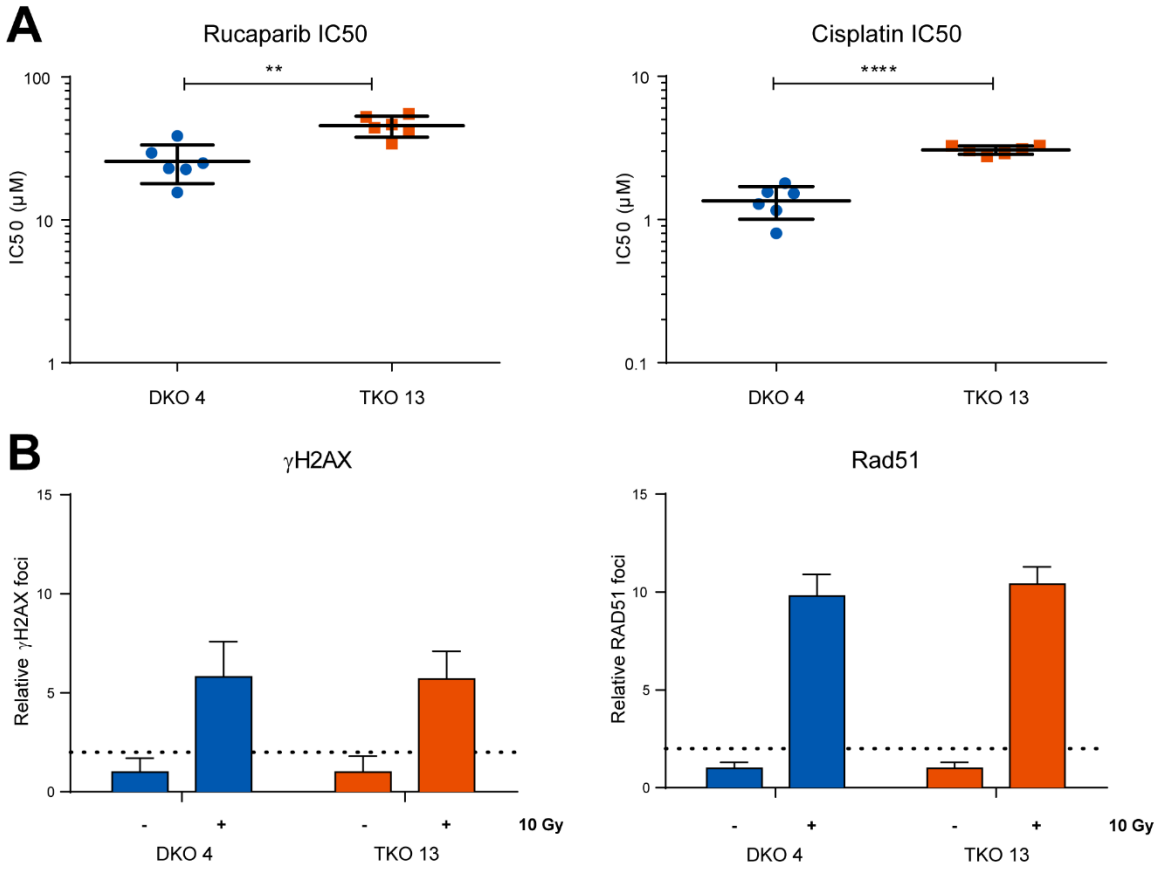

Figure 3.7: Assessment of HR status and cisplatin and rucaparib sensitivity in *Dicer-/-;Pten-/-* (DKO 4) and *Dicer-/-;Pten-/-;Trp53-/-* (TKO 13) knockouts.
A, Each dot represents the mean IC50 value from a triplicate experiment **B**, Dicer cell lines were irradiated (10Gy), fixed and stained for γH2AX and RAD51, and counterstained with DAPI.

The *Dicer-/-;Pten-/-* (DKO 4) and *Dicer-/-;Pten-/-;Trp53-/-* (TKO 13) all showed at least a 2-fold increase in RAD51 foci in response to irradiation over the untreated controls and were therefore HR competent.

The TKO 13 clone was significantly less sensitive to cisplatin and rucaparib compared to the DKO 4 clone (cisplatin p=≤0.0001****, rucaparib p=≤0.01**) (Figure 3.7).

3.3 All genotypes and HR/cisplatin/PARPi sensitivity

The cisplatin and rucaparib IC50 levels were plotted against the HR status for the ID8 cells (HR competent or defective) (Figure 3.8).

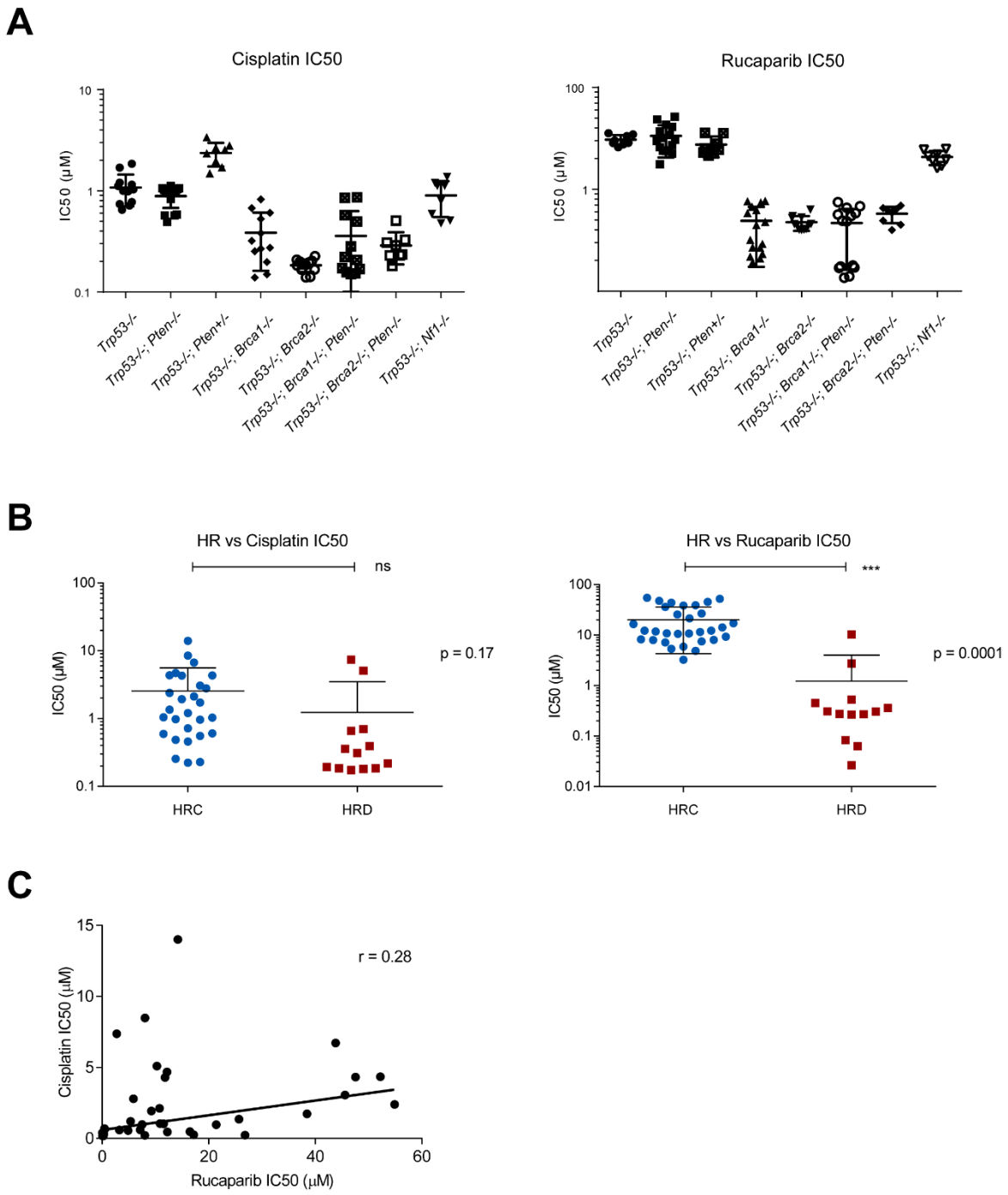

Figure 3.8: Cisplatin and rucaparib sensitivity of the ID8 genotypes and the relationship between HR and platinum and PARP inhibitor sensitivity.
A, Each dot represents the mean IC50 value from a triplicate experiment **B**, Each dot represents the mean IC50 from a triplicate experiment and plotted according to HR status determined by the γH2AX/RAD51 assay. ***, P < 0.001 **C**, Scatter plot showing a poor correlation between cisplatin and rucaparib sensitivity (r=0.28).

When the HR status of cell lines and cisplatin and rucaparib IC50 levels are analysed there is a significant difference between HR status and rucaparib sensitivity (p=<0.0001****) however there is no difference between HR status and cisplatin sensitivity (p=0.17). There is also a poor correlation between cisplatin and rucaparib sensitivity (r=0.28) (Figure 3.8).

3.4 Palb2 and BRCT2 binding domains

The *Trp53-/-;Brca1-/-* clones (1.26, 1.36) and both the *Trp53-/-;Brca2-/-* clones (2.14, 3.15) have mutations in the Palb2 domain whereas one *Trp53-/-;Brca1-/-* clone (6.20) has a mutation in the BRCT2 domain.

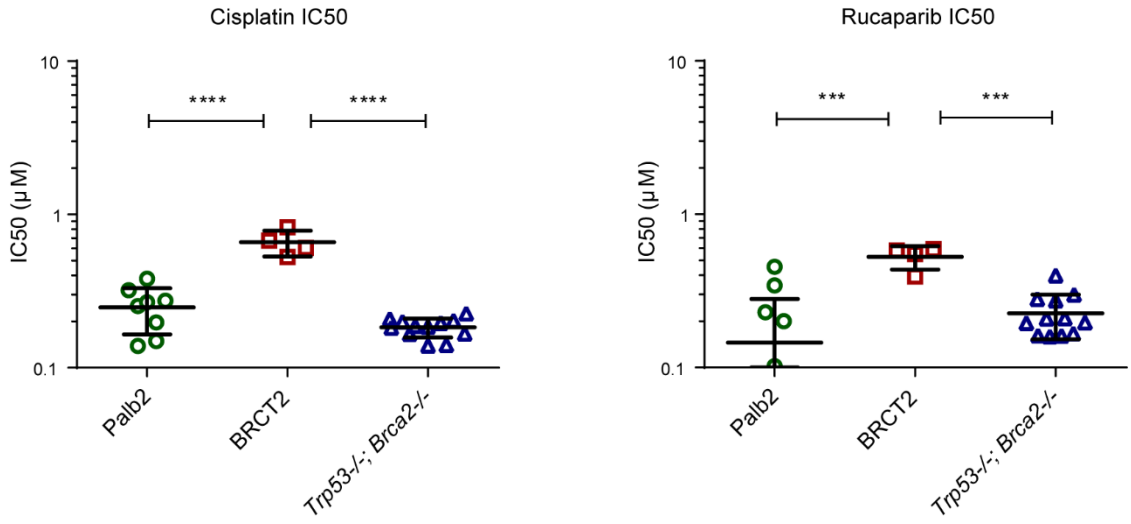

Figure 3.9: Cisplatin and rucaparib sensitivity comparing the different *BRCA1* and *BRCA2* binding domains.
Each dot represents the mean IC50 value from a triplicate experiment.

When comparing both cisplatin and rucaparib sensitivity between the *Trp53-/-;Brca1-/-* clones with mutations in the Palb2 domain (1.26, 1.36) and those with a mutation in the BRCT2 domain (6.20), the Palb2 clones are significantly more sensitive to both drugs (cisplatin p=≤0.0001; rucaparib p=≤0.0001). The same pattern is seen when comparing the *Trp53-/-;Brca1-/-* BRCT2 clone (6.20) with the *Trp53-/-;Brca2-/-* clones (2.14, 3.15) which also have mutations in Palb2 (cisplatin p=≤0.0001; rucaparib p=≤0.0001). However, when comparing *Trp53-/-;Brca1-/-* and *Trp53-/-;Brca2-/-* Palb2 clones there is no significant difference in cisplatin and rucaparib sensitivity (Figure 3.9 and Table 3.2).

3.5 *Trp53-/-;Brca2-/-;Pten-/-* and drug sensitivity

The triple deleted *Trp53-/-;Brca2;Pten-/-* clones (2.14.22, 3.15.10) were significantly more resistant to cisplatin compared to the *Trp53-/-;Brca2-/-* genotype (p=≤0.01); however there is no significant difference in rucaparib sensitivity between the two genotypes (Figure 3.10).

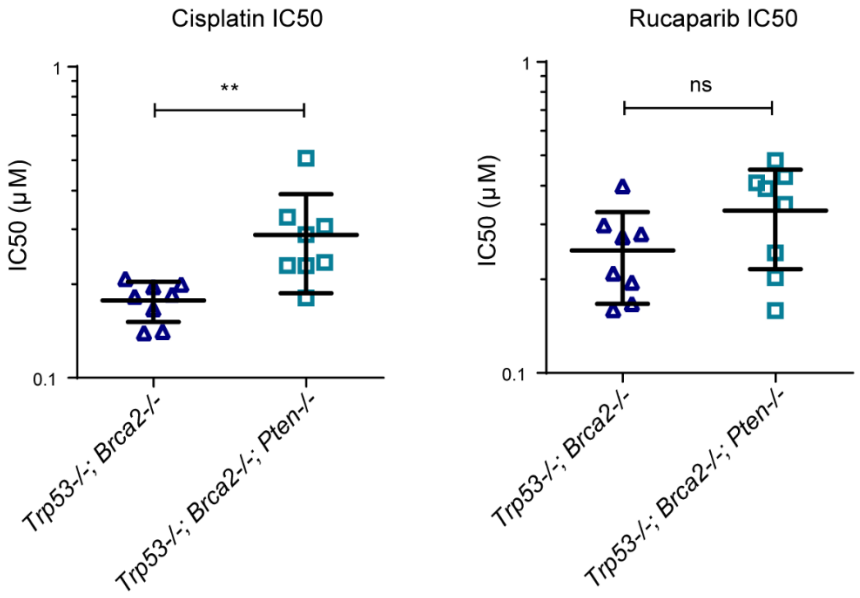

Figure 3.10: Cisplatin and rucaparib sensitivity comparing the *Trp53-/-;Brca2-/-* and *Trp53-/-;Brca2-/-;Pten-/-* genotypes.
Each dot represents the mean IC50 value from a triplicate experiment.

Table 3.1: *In-vitro* cisplatin and rucaparib sensitivity for the ID8 genotypes.

The table shows the mean IC50 value from a triplicate experiment. The IC50 values were compared using one-way ANOVA with Bonferroni's test for multiple comparisons with the *Trp53-/-* genotype.

Genotype	Rucaparib IC50 (μM) mean +/- sd	p=	Cisplatin IC50 (μM) mean +/- sd	p=
Trp53-/-	9.4 +/- 2.2		1.1 +/- 0.4	
Trp53-/-;Brca1-/-	0.2 +/- 0.2	<0.0001	0.4 +/- 0.2	<0.0001
Trp53-/-;Brca1-/-;Pten-/-	0.2 +/- 0.2	<0.0001	0.4 +/- 0.3	<0.0001
Trp53-/-;Brca2-/-	0.2 +/- 0.1	<0.0001	0.2 +/- 0.03	<0.0001
Trp53-/-;Brca2-/-;Pten-/-	0.3 +/- 0.1	<0.0001	0.3 +/- 0.1	<0.0001
Trp53-/-;Pten-/-	11.2 +/- 6.9	ns	0.9 +/- 0.2	ns
Trp53-/-;Pten-/+	7.6 +/- 3.3	ns	2.4 +/- 0.6	<0.0001
Trp53-/-;Nf1-/-	4.3 +/- 1.3	<0.01	0.9 +/- 0.4	ns

Table 3.2: *In-vitro* cisplatin and rucaparib sensitivity comparing the Palb2 and BRCT2 domains.

The table shows the mean IC50 values from a triplicate experiment. The IC50 values were compared between the Palb2 and BRCT2 domains using an unpaired t-test.

Genotype	Rucaparib IC50 (μM) mean +/- sd	Cisplatin IC50 (μM) mean +/- sd
Trp53-/-;Brca1-/- :	0.2 +/- 0.2	0.4 +/- 0.2
Palb2 (1.26 + 1.36)	0.2 +/- 0.1	0.3 +/- 0.1
BRCT2 (6.20)	0.5 +/- 0.1	0.7 +/- 0.1
Trp53-/-;Brca2-/- (Palb2)	0.2 +/- 0.1	0.2 +/- 0.03
	Rucaparib p=	**Cisplatin p=**
Palb2 vs BRCT2	<0.0001	<0.0001
Palb2 vs Trp53-/-;Brca2 (Palb2)	ns	ns
BRCT2 vs Trp53-/-;Brca2-/- (Palb2)	<0.001	<0.0001

3.6 DR-GFP assay

An attempt at optimising an alternative HR assay (DR-GFP) on HGSOC cell lines was performed.

The OVCAR4 cell line does not harbour mutations in any known HR gene and was shown to be HR competent in the RAD51/γH2AX assay (Figure 3.2). The OVCAR4 cell line showed a mean GFP positivity of 0.51% following *p*ISce-I transfection compared to 0.07% for control *p*CAAGS transfection (Figure 3.11).

However, although the GFP positivity in the OVCAR4 cell line was consistently increased compared to the control, the rates of GFP positivity were extremely low and variable. Using the assay in other HGSOC cell lines that were known to be HR competent (PEO1 and UWB1.289BRCA1) did not show similar results to OVCAR4. Therefore, I did not continue with the DR-GFP assay as the RAD51/γH2AX assay gave reliable and consistent results.

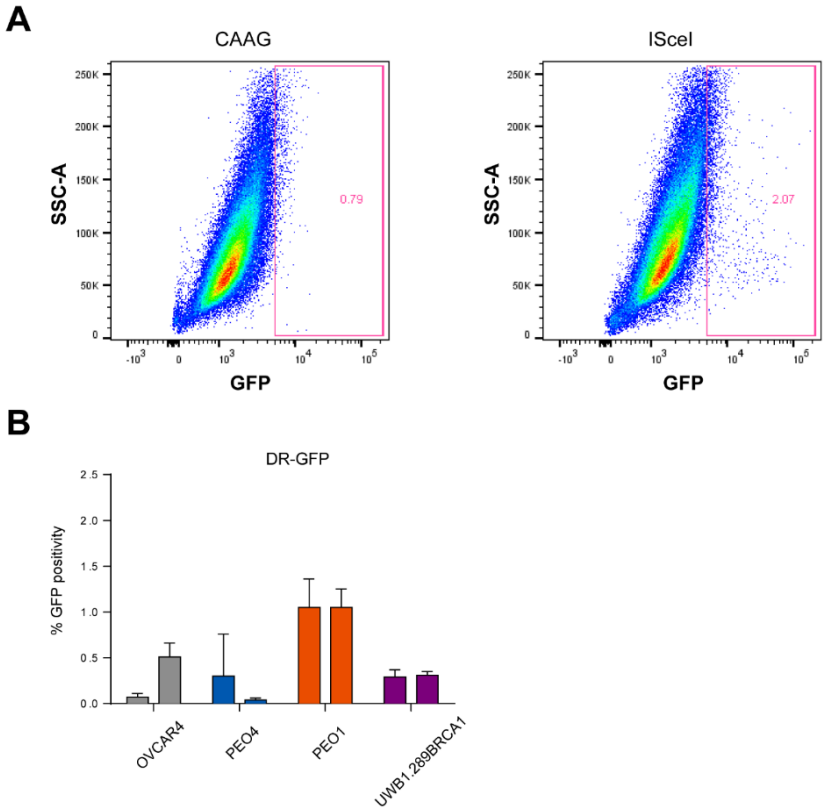

Figure 3.11: DR-GFP assay assessing HR-mediated DNA DSB repair in HGSOC cell lines.
A, GFP positivity determined by flow cytometry in a single experiment on OVCAR4 showing an increase in GFP positivity of pISce-I compared to the pCAAGS (control) **B**, Left bars correspond to the pCAAGS (control) and right bars to the pSce-1. Each bar represents the mean % GFP positivity of a triplicate experiment.

3.7 Discussion

The Rad51/γH2AX assay, as previously mentioned, was validated in Newcastle and is widely used to determine the homologous recombination status of cell lines (Mukhopadhyay et al., 2010). The assay however can show variation in the number and size of RAD51 foci and is unable to detect abnormalities downstream of RAD51. In addition, it requires culture of viable cells for at least 48 hours. These factors limit the long-term utility of the assay and there is a requirement for a functional HR assay that can be used in primary tissue. The DR-GFP assay is considered the gold standard for determining homologous recombination status. We attempted to optimise the DR-GFP assay initially on ovarian cancer cell lines with known HR status. However, we did not get reliable and consistent results that we had previously obtained with the Rad51/γH2AX assay. It was therefore decided not to pursue the DR-GFP assay further.

HGSOC cell lines with known *BRCA1/2* mutations were used to optimise the Rad51/γH2AX assay and correlate with cisplatin and rucaparib sensitivity. Although cell lines that were known to be HR deficient (PEO1 and UWB1.289) were more sensitive to rucaparib there was variation in cisplatin sensitivity (Figure 3.2). We performed the assay on primary ascites samples in an attempt to develop an assay with clinical utility (data not shown); however subsequent sequencing of cultured ascites cells found mutant *TP53* in <20% of samples, indicating that tumour cells were not being cultured.

Our data from the ID8 *Trp53-/-* clones show that the cell lines were HR competent (Figure 3.3). There is currently no evidence to suggest that p53 is associated with defective homologous recombination. It is established that mutant p53 not only results in loss of tumour suppressor function but also acquires additional oncogenic activity. This p53 gain-of-function contributes to genomic instability and there is evidence to suggest that DSB homologous recombination is stimulated in cells expressing mutant p53 resulting in 'hyper-recombination' (Muller and Vousden, 2013, Restle et al., 2008). However, the ID8 *Trp53-/-* clones are all loss of function null mutants as shown from previous work (Walton et al., 2016) rather than missense mutations with gain-of-function

and therefore further work is required to generate clones with missense mutations to investigate this further.

From previous experiments there was no significant difference in cisplatin and rucaparib sensitivity between the ID8 parental cell line and ID8 *Trp53*-/- clones (Walton et al., 2016). We found a significant variation in cisplatin and rucaparib sensitivity between the *Trp53*-/- clones (F3, A2, M20 and C7) with the F3 and A2 more sensitive to these drugs compared to the M20 and C7 clones (Figure 3.3). There is increasing evidence that different p53 mutants vary with respect to loss of wild-type p53 activity and gain of function as mentioned previously. Although the *Trp53*-/- clones resulted from the same guide RNA target (exon 5) there was variation in the size and site of mutation. There is minimal data regarding the type and location of p53 mutation and drug sensitivity. It is possible that subtle differences in mutation may result in alterations in structure and stability of the p53 protein and lead to differences in drug sensitivity (Muller and Vousden, 2014). We have not investigated this further but would require a significant range of different *Trp53*-/- clones to identify obvious patterns of sensitivity.

As expected, *Trp53*-/-;*Brca1*-/- and *Trp53*-/-;*Brca2*-/- clones were all found to be HR deficient using the Rad51/γH2AX assay (Figure 3.3). Both *BRCA1* and *BRCA2* genes play key roles in DNA double strand break repair via homologous recombination. However, they have distinct and complementary functions (Yang et al., 2011). *BRCA2* regulates the RAD51 protein by mediating the RAD51 filament assembly on ssDNA which is crucial for homologous recombination. *BRCA1* functions in both checkpoint activation and in DNA repair. *BRCA1* has been found to be an upstream regulator of *BRCA2* in DNA repair and the PALB2 is the main linker between *BRCA1* and *BRCA2* (Zhang et al., 2009). It is therefore expected that the loss of *BRCA1* or *BRCA2* function would result in a defective homologous recombination pathway.

We found that the *Trp53*-/-;*Brca1*-/- and *Trp53*-/-;*Brca2*-/- clones were significantly more sensitive to both cisplatin and rucaparib compared to the F3 *Trp53*-/- clone (Figure 3.3 and Table 3.1). It is now widely accepted that the loss of *BRCA1* or *BRCA2* results in greater sensitivity to cisplatin in most cases,

the hypothesis being that cells that have a defective homologous recombination pathway are unable to repair DNA double strand breaks effectively. Therefore, the tumour is unable to repair DNA cross-links formed by the introduction of chemotherapy such as cisplatin resulting in increased lethality. This is consistent with evidence from Alsop et al that found that patients with germline *BRCA1* or *BRCA2* mutations were less likely to have disease progression within 6 months compared to non-*BRCA1/2* carriers following cytotoxic chemotherapy (14.9% vs 31.7%; p=<0.001) (Alsop et al., 2012).

Interestingly it has been suggested that the location of mutations within *BRCA1* and *BRCA*2 may influence response to chemotherapy and overall survival. Several studies, although involving small numbers, have found a worse survival in patients with a mutation on the 5' end compared with the 3' end of *BRCA1* (Bolton et al., 2012). A recent study from Labidi-Galy et al found that *BRCA2* carriers with mutations in the RAD51 binding domain had a significantly prolonged 5-year overall survival (HR 0.36; 95% CI 0.20-0.64; p=0.001) (Labidi-Galy et al., 2017a).

The *Trp53-/-;Brca1-/-* clones were generated using two different RNA guides, one targeted the PALB2-binding domain (exon 12) and the other the BRCT-2 domain (exon 19). This resulted in the 6.20 clone (BRCT-2) and the 1.36 and 1.26 clones (PALB2) all with bi-allelic deletions in *BRCA1* but within different domains. These *Trp53-/-;Brca1-/-* clones offered an opportunity to investigate differences in cisplatin and rucaparib sensitivity *in-vitro*. Our data showed that the Palb2 clones (1.26, 1.36) were significantly more sensitive to both drugs compared to the BRCT-2 clone (6.20). This is further validated when comparing sensitivity with the *Trp53-/-;Brca2-/-* clones (2.14, 3.15) that also have deletions within the Palb2 domain. The Palb2 clones (1.26, 1.36, 2.14 and 3.15) have similar levels of sensitivity to both drugs but again the 6.20 (BRCT-2) clone is significantly less sensitive to cisplatin and rucaparib compared to the *Trp53-/-;Brca2-/-* clones (2.14, 3.15) (Figure 3.9 and Table 3.2).

PALB2 is a DNA-binding domain that binds ssDNA and interacts with RAD51 to stimulate strand invasion. It has been found to bind to *BRCA2* and function synergistically to further promote strand invasion (Buisson et al., 2010). PALB2,

as previously mentioned, is the link between *BRCA1* and *BRCA2* and the interaction between *BRCA1* and PALB2 is important for homologous recombination (Zhang et al., 2009). The BRCT domain (BRCA1 C-terminal) is involved in cell cycle signalling in the DNA damage response but is less important in homologous recombination (Leung and Glover, 2011). The differences in sensitivity between the *Trp53-/-;Brca1-/-* clones may be because of the varying importance of the domains in the homologous recombination pathway.

Alsop et al have shown that, although patients with *BRCA1/2* mutations respond well to platinum chemotherapy there remains a subgroup of patients that are resistant or refractory to chemotherapy despite having mutations in these genes (Alsop et al., 2012). The site of *BRCA1/2* mutation may explain differences in response to chemotherapy as well as mutations in other important genes e.g *PTEN* as described below.

Except for *BRCA1/2*, little is known about the prognosis of other prevalent mutations in high grade serous ovarian cancer. As discussed previously, *PTEN* is a tumour suppressor gene that inhibits cell proliferation induced by the PI3K pathway. TCGA identified *PTEN* loss in 7% of tumours; however following re-analysis by Martins et al, 36% of tumours showed heterozygous loss of *PTEN* (Martins et al., 2014). The *Trp53-/-;Pten-/-* and *Trp53-/-;Pten+/-* clones were all found to be HR competent using the Rad51/γH2AX assay (Figure 3.4). Despite early conflicting reports regarding the role of *PTEN* in homologous recombination it is now accepted that *PTEN* does not have an important role in the HR pathway (Hunt et al., 2012, Fraser et al., 2012).

In vitro, there was no difference in cisplatin and rucaparib sensitivity between the *Trp53-/-;Pten-/-* clones and F3 *Trp53-/-*. However, the *Trp53-/-;Pten+/-* clones were significantly more resistant to cisplatin compared to the *Trp53-/-* genotype (Figure 3.4 and Table 3.1). No difference was seen in rucaparib sensitivity. A possible explanation could be that heterozygous *Pten* loss has led to partial inactivation of Pten and altered gene expression resulting in an increase in cisplatin resistance.

The *Trp53-/-;Brca1-/-;Pten-/-* and *Trp53-/-;Brca2-/-;Pten-/-* clones all were found to be HR defective (Figure 3.5). They were also significantly more sensitive to cisplatin and rucaparib compared to the F3 *Trp53-/-* genotype. Interestingly the *Trp53-/-;Brca2-/-;Pten-/-* clones were significantly less sensitive to cisplatin compared to the *Tpr53-/-;Brca2-/-* genotype suggesting that *Pten* loss may contribute to platinum resistance without interfering with overall HR function (Figure 3.10).

NF1 is a tumour suppressor gene that encodes for neurofibromin-1, a RAS GTPase-activating protein (Ratner and Miller, 2015). Neurofibromin is an important negative regulator of the Ras pathway. *NF1* loss has been associated with chemotherapy resistance and a poor prognostic factor in glioblastoma multiforme and colorectal cancer (Yap et al., 2014). The *Trp53-/-;Nf1-/-* clones were all found to be HR competent (Figure 3.6). There is no evidence to suggest that *NF1* is involved in homologous recombination and therefore these results were expected.

There was no significant difference in cisplatin sensitivity between the F3 *Trp53-/-* genotype and *Trp53-/-;Nf1-/-* clones *in vitro*. However, the *Trp53-/-;Nf1-/-* clones showed a small but statistically significantly increase in sensitivity to rucaparib (Figure 3.6 and Table 3.1). DNA replication stress mechanisms such as serial replication stalling forks have been shown to result in genomic rearrangements with *NF1* loss (Hsiao et al., 2015). These rearrangements may explain the difference in PARP inhibitor sensitivity.

The *DICER-/-;Pten-/-* (DKO) and *DICER-/-;Pten-/-;Trp53-/-* (TKO) cell lines are additional transgenic *in vivo* models to further investigate the influence of *p53* loss in HGSOC. The *DICER* cell lines originated from fallopian tube carcinoma cells and *Trp53* was targeted using the same guide RNA used for the F3 *Trp53-/-* clone (Walton et al., 2017). The DKO and TKO were found to be HR competent (Figure 3.7). This is an additional HGSOC *in vivo* model that shows again that the loss of *Pten* does not alter the homologous recombination pathway.

Trp53 loss was associated with a significant reduction in sensitivity to both cisplatin and rucaparib (Figure 3.7). This contrasts with data using the ID8 *Trp53-/-* clones where no difference was seen in sensitivity when compared to the ID8 parental cell line. As mentioned previously this may be because of the type and position of *p53* mutation.

Interestingly, the loss of p53 function has been shown to significantly reduce the median survival *in vivo* (Walton et al., 2017). Similar findings were found with the ID8 derivatives. The DICER cell lines have not been used in any further experiments in this thesis as the ID8 derivatives offer a range of different knockouts that allow comparison between the genotypes.

When the HR status of cell lines is analysed with the cisplatin and rucaparib IC50 levels there is a significant difference between HR status and rucaparib sensitivity ($p=0.0001$). However there is no difference between HR status and cisplatin sensitivity ($p=0.17$). In addition, there is a poor correlation between cisplatin and rucaparib sensitivity ($r=0.28$) (Figure 3.8). Although many women with mutations in key HR genes e.g. *BRCA1/2* are more sensitive to platinum chemotherapy, the relationship between defective homologous recombination and platinum sensitivity is much more complicated and is likely to involve many different factors, including key mutated genes, chromosomal instability and the tumour microenvironment. The interaction between these variables and how it relates to platinum chemotherapy is not well known but hopefully a greater understanding of these factors will aid in predicting which patients will respond to chemotherapy in the future.

In summary, I have investigated the homologous recombination status of a range of ovarian cancer cell lines and how this relates to both cisplatin and rucaparib sensitivity. I have shown that the relationship between homologous recombination and cisplatin sensitivity is complicated and is likely to involve factors beyond HR status. By establishing the HR status, it may be possible to select patient subgroups that respond better to chemotherapy, but it does not identify poor prognostic groups. The next step was to assess platinum sensitivity *in vivo* to determine if this differs from *in vitro* data and to establish differences in survival between the ID8 derivatives.

4 *In-vivo* platinum sensitivity

4.1 Introduction

Mutations in key genes are thought to contribute to both platinum sensitivity and resistance. Although patients with *BRCA1/2* mutations tend to be extremely sensitive to platinum-based chemotherapy, this is not universal, and most patients will develop resistance. As discussed previously, Drost et al observed that N-terminal mutations on the BRCA1 protein was a poor prognostic factor and that mutations in the RING domain (N-terminal) were associated with a poor response to cisplatin and PARP inhibitors (Drost et al., 2011). The *BRCA1/2* mutation may explain differences in chemotherapy response and the *Trp53-/-;Brca1-/-* clones with mutations in the Palb2 and BRCT2 domains allowed us to begin to investigate this further.

The loss of *PTEN* is a common event in HGSOC and, following re-analysis of the TCGA data, 36% of tumours were found to have heterozygous loss of *PTEN* (Martins et al., 2014). As mentioned earlier, studies have found that activation of the PI3K/AKT pathway may be associated with chemotherapy resistance (Kolasa et al., 2009, Yang et al., 2008).

TCGA also found alterations in the *NF1* gene in 12% of patients but not much is known about platinum sensitivity in patients with an alteration in this gene (Cancer Genome Atlas Research, 2011). The loss of *NF1* results in activation of RAS/MAPK signalling with recent evidence showing the MAPK pathway to be a significantly mutated pathway in ovarian cancer (Kanchi et al., 2014). Further studies have suggested that MAPK activation is associated with a poor prognosis (Hew et al., 2016).

By using C57Bl/6 mice, I aimed to see if there was any difference in cisplatin sensitivity compared to previous *in-vitro* data and attempt to identify poor prognostic groups independent of HR status. The ID8 derivatives allowed us to look at the platinum sensitivity between the genotypes. As this was an immunocompetent model, it also allowed us to see how the tumour microenvironment was altered between genotypes and with the addition of cisplatin.

4.2 Cisplatin *in-vivo* experiment

The mice were treated with cisplatin (5mg/kg) or PBS (control) on days 28, 35 and 42. From previous *in-vivo* tumorgenicity experiments we knew that the *Trp53-/-;Brca2-/-* models had the longest survival (median survival 53 days) and the *Trp53-/-;Pten-/-* models had the shortest survival (median survival 34 days). The timing of treatment allowed the mice to get all 3 dosages of cisplatin and attempted to replicate clinical regimens i.e. multiple cycles of platinum-based chemotherapy.

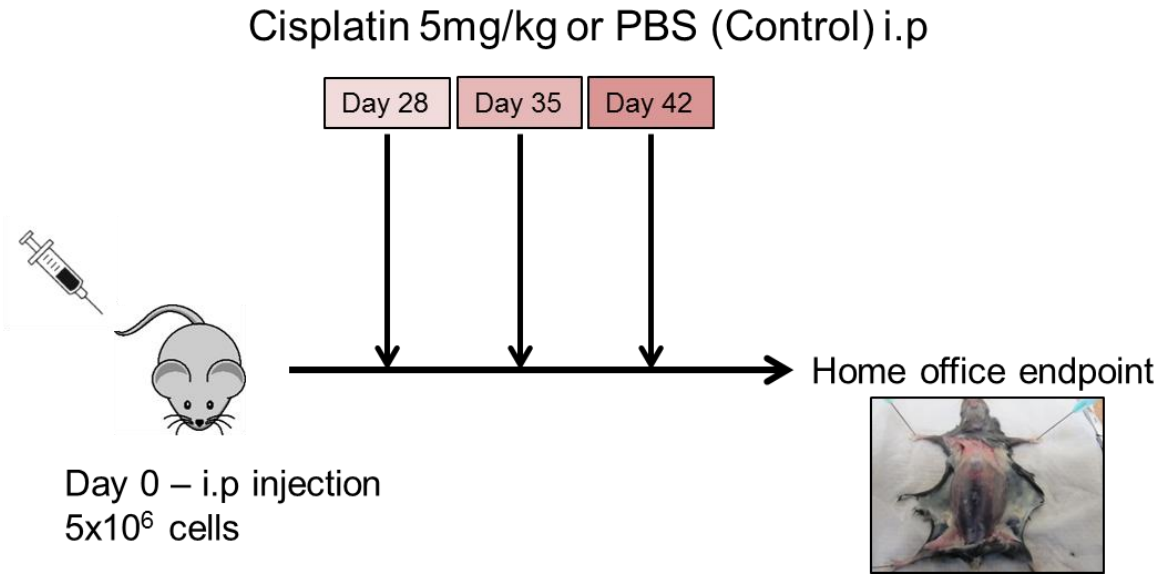

Figure 4.1: Protocol investigating *in vivo* cisplatin sensitivity using ID8 derivatives.
C57BL/6 (female) mice were injected i.p with $5x10^6$ ID8 cells, treated at Day 28, 35 and 42 with either cisplatin (5mg/kg) or PBS (control). The mice were then taken at the Home office endpoint.

4.2.1 Survival

The six different ID8 genotypes were injected intraperitoneally as described above (Figure 4.1). There were 24 mice per experiment (12 cisplatin treated, and 12 PBS treated), with at least two separate clones per genotype. The mice were monitored daily and killed when they reached UK Home Office limits.

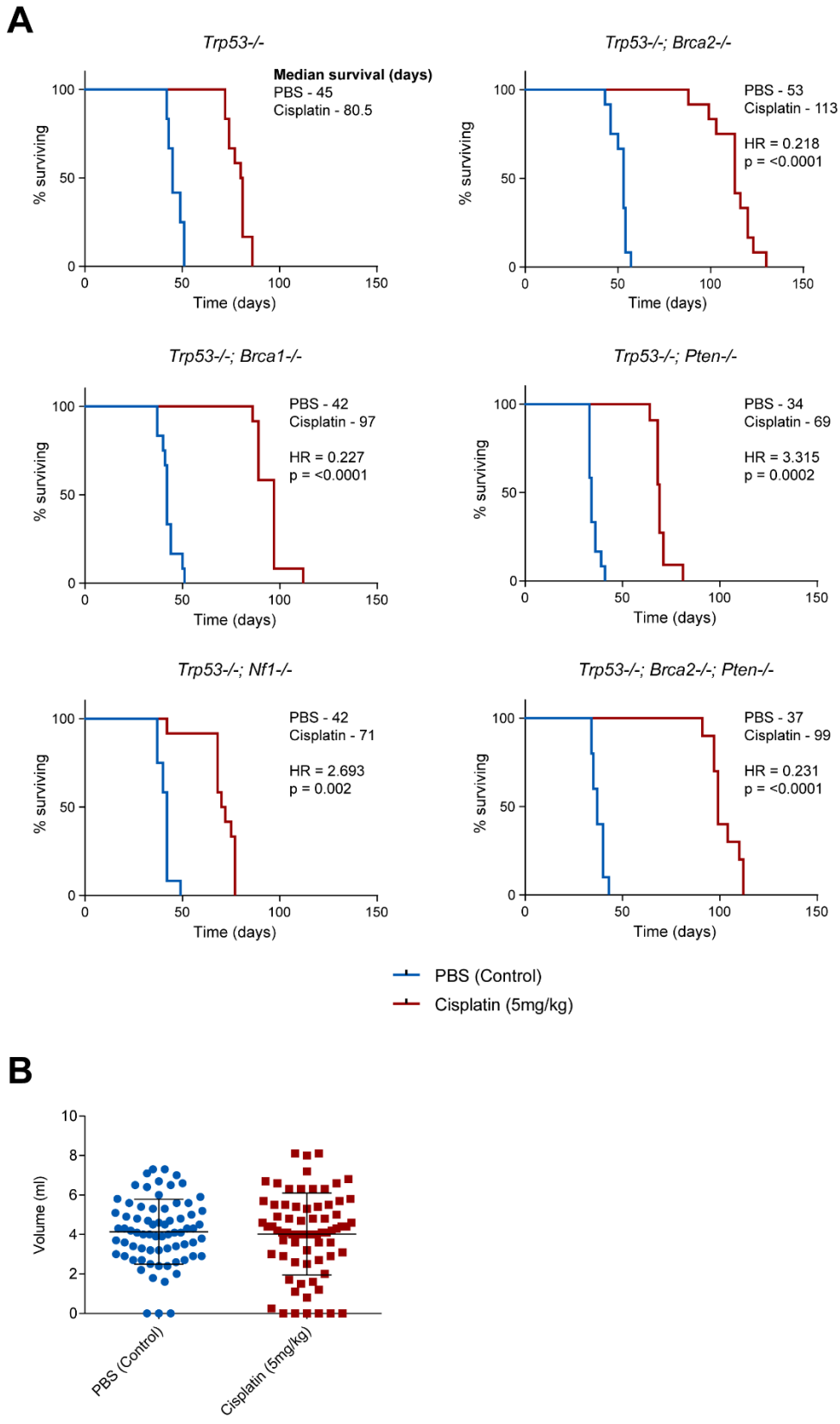

Figure 4.2: *In vivo* experiments investigating platinum sensitivity between different ID8 genotypes.
A, Kaplan-Meier survival curves comparing C57BL/6 (female) mice injected with different ID8 genotypes and treated with either cisplatin or PBS. Hazard ratios and p values are comparing the cisplatin treated groups with the *Trp53-/-* cisplatin group. **B**, Ascites volumes from all *in vivo* experiments comparing mice treated with either cisplatin or PBS.

The PBS treated groups had a median survival ranging from 34 to 53 days. The *Trp53-/-* genotype had a median survival of 45 days, *Trp53-/-;Brca1-/-* of 42 days, *Trp53-/-;Brca2-/-* of 53 days, *Trp53-/-;Pten-/-* of 34 days, *Trp53-/-;Nf1-/-* of 42 days and *Trp53-/-;Brca2-/-;Pten-/-* of 37 days (Figure 4.2). This data is consistent with previous *in vivo* data using the ID8 genotypes (Walton et al., 2016, Walton et al., 2017).

With the addition of cisplatin treatment, the survival was extended for all the genotypes. The cisplatin treated groups had a median survival ranging from 69 to 113 days. The *Trp53-/-* genotype had a median survival of 80.5 days. The *Trp53-/-;Brca1-/-* had a median survival of 97 days and when compared to the *Trp53-/-* genotype a hazard ratio of 0.227 (p=<0.0001). The *Trp53-/-;Brca2-/-* genotype had a median survival of 113 days (HR = 0.218, p=<0.0001), *Trp53-/-;Pten-/-* of 69 days (HR = 3.315, p=0.0002), *Trp53-/-;Nf1-/-* of 71 days (HR = 2.693, p=0.002) and *Trp53-/-;Brca2-/-;Pten-/-* of 99 days (HR = 0.231, p=0.0001) (Figure 4.2, Figure 4.3 and Table 4.1).

Two mice were excluded from the *Trp53-/-;Brca2-/-;Pten-/-* cisplatin experiment, one because the mouse only received one dose of cisplatin and in all previous experiments the mice had tolerated three doses of cisplatin. The other mouse was excluded because it survived greater than 2 weeks after the last culled mouse.

There was no significant difference in ascites volumes between the PBS treated and cisplatin treated groups (Figure 4.2).

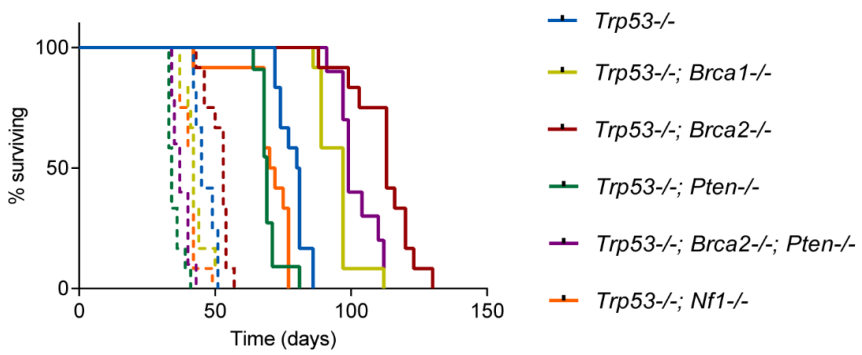

Figure 4.3: Kaplan-Meier survival curve comparing all the ID8 genotypes.
The dotted lines correspond to PBS treated groups and solid lines to cisplatin treated.

Table 4.1: *In vivo* survival in the cisplatin treated groups.

The median survival of the cisplatin treated groups are outlined in the table below and the hazard ratios (log rank) are compared to the *Trp53-/-* genotype.

Genotype	Median survival cisplatin (days)	Hazard ratio (log-rank)	p=
Trp53-/-	81	-	-
Trp53-/-;Brca1-/-	97	0.227	<0.0001
Trp53-/-;Brca2-/-	113	0.218	<0.0001
Trp53-/-;Brca2-/-;Pten-/-	99	0.231	<0.0001
Trp53-/-;Pten-/-	69	3.315	0.0002
Trp53-/-;Nf1-/-	71	2.693	0.002

4.2.2 Palb2 and BRCT2 binding domains

The cisplatin *in vivo* experiment used both the *Trp53-/-;Brca1-/-* (*BRCT2*) and *Trp53-/-;Brca1-/-* (*Palb2*) clones. Results for *Trp53-/-;Brca1-/-* clones were separated and the Kaplan-Meier curve illustrated below in Figure 4.4. The 1.36 *Trp53-/-;Brca1-/-* clone had a median survival of 97 days compared to 89 days in the 6.20 *Trp53-/-;Brca1-/-* clone. When compared to the *Trp53-/-* genotype (median survival 80.5 days) the 1.36 *Trp53-/-;Brca1-/-* clone had a hazard ratio of 0.2623 (p=0.0002) and the 6.20 *Trp53-/-;Brca1-/-* clone of 0.2788 (p=0.0004) (Figure 4.4 and Table 4.2). The difference between the two *BRCA1* clones was not significant (p=0.07).

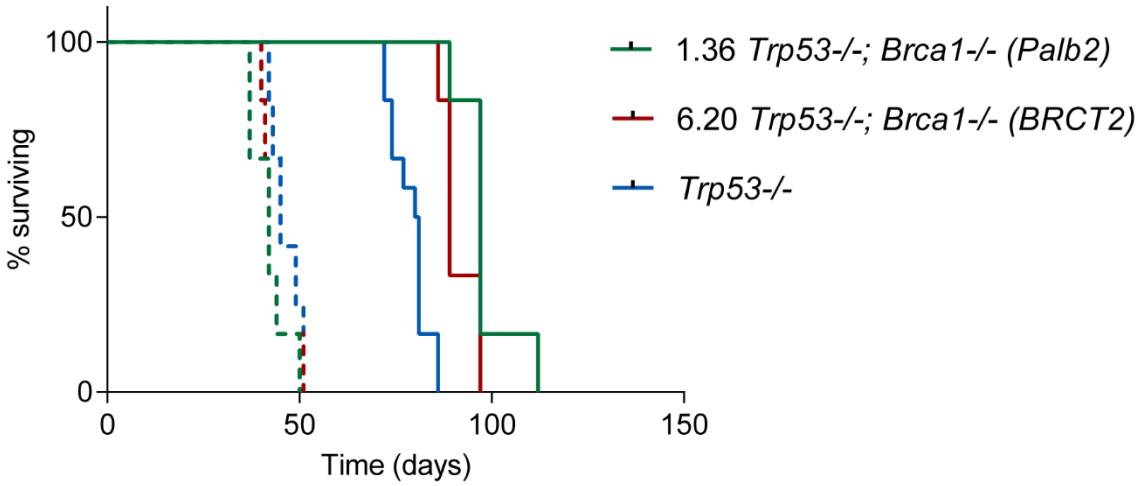

Figure 4.4: Kaplan-Meier survival curve comparing the binding domains.

The 1.36 *Trp53-/-;Brca1-/-* (*Palb2*) clone had a non-significant superior survival compared to the 6.20 *Trp53-/-;Brca1-/-* (*BRCT2*) clone.

Table 4.2: *In vivo* survival in the cisplatin treated Palb2 and BRCT2 clones.

The median survival of the cisplatin treated groups are outlined in the table below and the hazard ratios (log-rank) are compared to the *Trp53-/-* genotype.

Genotype	Median survival cisplatin (days)	Hazard ratio (log-rank)	p=
Trp53-/-	80.5	-	-
Trp53-/-;Brca1-/- (Palb2)	97	0.2623	0.0002
Trp53-/-;Brca1-/- (BRCT2)	89	0.2788	0.0004

4.3 Cell culture of ascites

The tumour cells in the ascites from the *in vivo* cisplatin experiment were cultured using ID8 medium (see Methods - section 2.8). The first aim was to determine if it was possible to culture tumour cells from frozen ascites whilst the second aim was to investigate potential differences in cisplatin sensitivity between the PBS and cisplatin treated groups.

Ascites cells from both PBS or cisplatin treated mice were cultured from the following clones - F3 *Trp53*-/-, 2.14 *Trp53*-/-;*Brca2*-/- and 3.15 *Trp53*-/-;*Brca2*-/-.

WT1 expression is used clinically as a diagnostic marker for HGSOC. Previous work has shown the ID8 cell line to be strongly positive for Wt1 and it was therefore used to determine whether tumour cells were specifically being cultured (Walton et al., 2016).

The Wt1 antibody concentration was initially optimised by culturing ascites cells from a mouse bearing F3 *Trp53*-/- tumour. The murine fibroblast cell line 3T3 was used as a negative control and the F3 *Trp53*-/- cell line as a positive control. A high-content imaging system (Operatta, Perkin Elmer) was used to visualise the cells following staining with Wt1 and DAPI.

The cells were positively stained with Wt1 confirming that tumour cells were being cultured from the ascites. The optimal Wt1 antibody concentration was determined to be 1 in 100 (Figure 4.5).

4.3.1 Cisplatin sensitivity

The ascites samples all had positive Wt1 staining. The *Trp53*-/-;*Brca2*-/- clones (2.14 and 3.15) cultured from the ascites remained significantly more sensitive to cisplatin compared to the F3 *Trp53*-/- cell lines. However, there was no significant difference in cisplatin sensitivity between the PBS treated and cisplatin treated ascites (Figure 4.6).

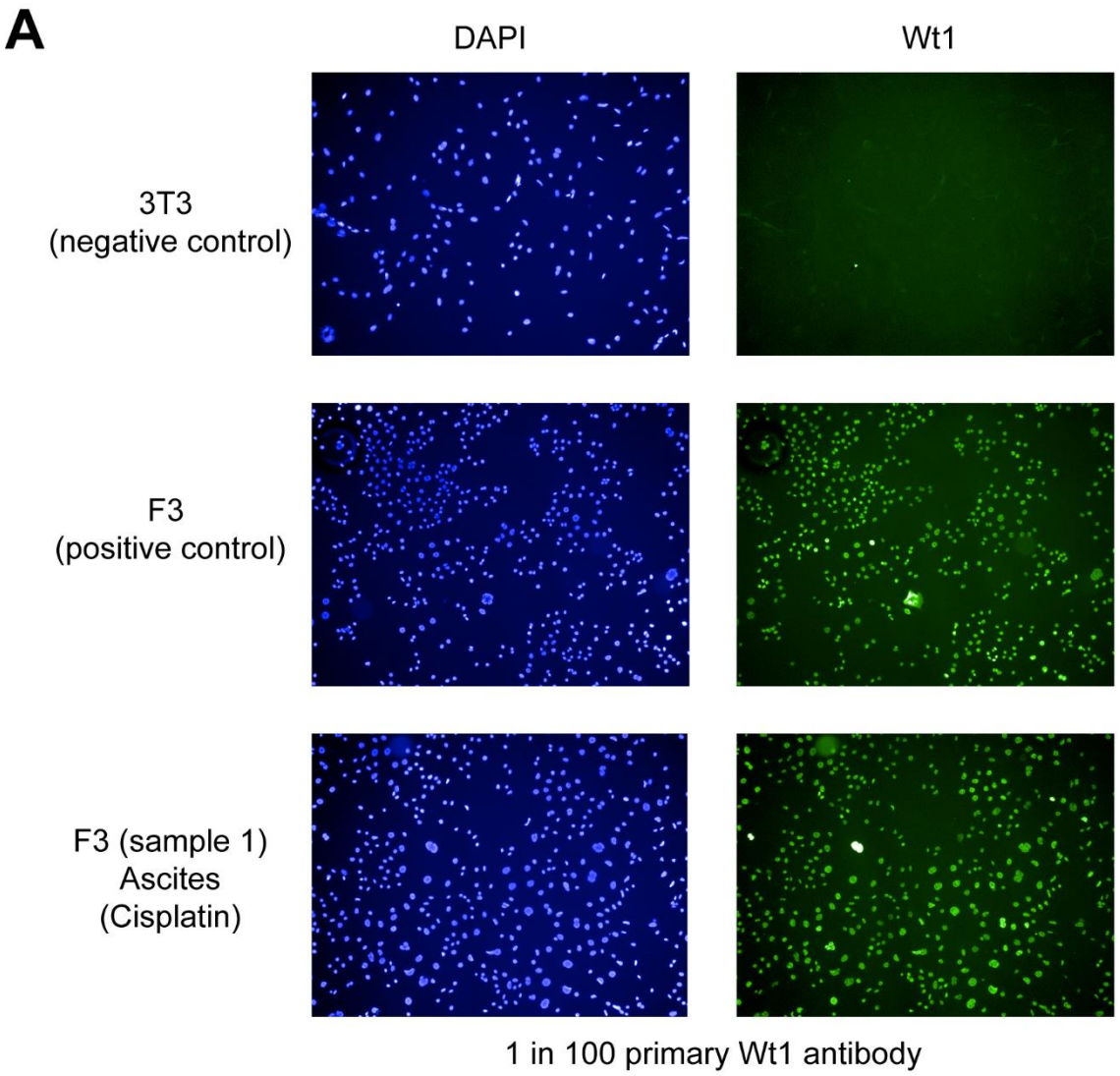

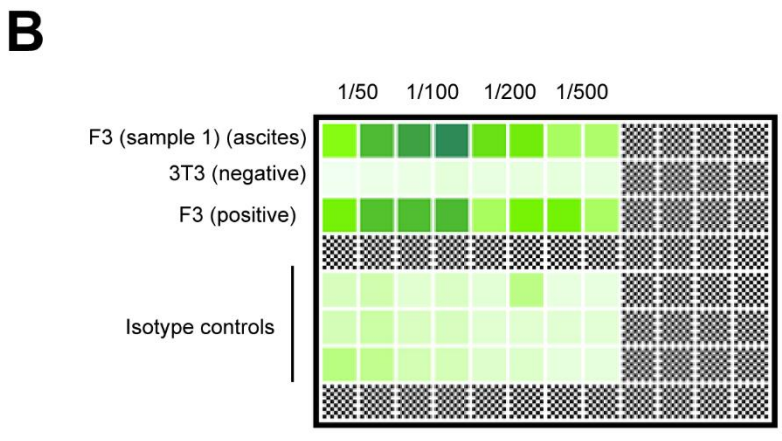

Figure 4.5: Wt1 primary antibody optimisation of cultured ascites.

A, Wt1 (1/100) and DAPI staining of 3T3 cell line (negative control), F3 (positive control) and F3 (sample 1) (cisplatin treated ascites sample) with positive staining in the ascites sample confirming the presence of tumour cells. **B**, The green corresponds to the mean Wt1 nuclear intensity per well (Alexa 488) showing 1 in 100 as the optimal Wt1 concentration. There was no Wt1 staining present in the negative control (3T3) or isotype controls.

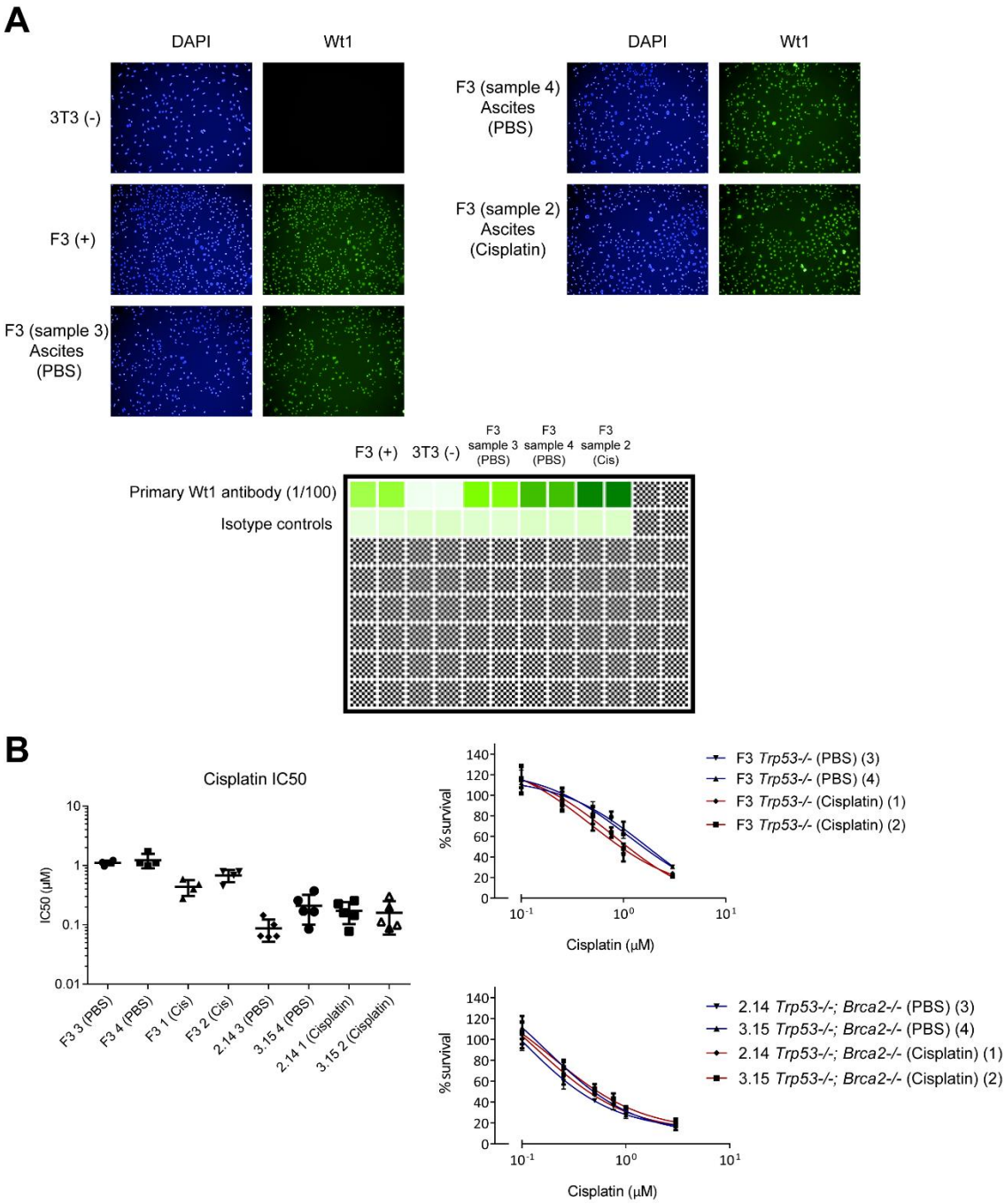

Figure 4.6: Wt1 and DAPI staining of ascites and cisplatin sensitivity.

A, Wt1 and DAPI staining of ascites confirming the presence of tumour cells. No Wt1 staining was present in the negative (3T3) or isotype controls. The sample numbers correspond to different ascites samples. **B**, Cisplatin sensitivity comparing the PBS and cisplatin treated groups of each genotype. Each dot represents an IC50 value. The *Trp53-/-;Brca2-/-* clones were significantly more sensitive to cisplatin but no difference was shown between the treated and untreated groups.

4.4 Generation of fluorescent ID8 cell lines

To try to investigate tumour heterogeneity further and how dominant clones develop in HGSOC, we generated a GFP-expressing F3 *Trp53*-/- cell line and an mCherry-expressing 3.15 *Trp53*-/-;*Brca2*-/- cell line (see Methods – section 2.4). These cell lines were characterised to ensure they were as close as possible in terms of growth and drug sensitivity to non-expressing cells prior to undertaking *in vivo* experiments.

4.4.1 *In vitro* growth and drug sensitivity

There was no significant difference in *in vitro* growth using linear regression analysis between the F3 and GFP-expressing F3 cell line (p=0.52) and between the 3.15 and mCherry-expressing 3.15 cell line (p=0.76). There was also no difference found in *in vitro* cisplatin sensitivity between the F3GFP and F3 cell line and in cisplatin and rucaparib sensitivity between the 3.15mCherry and 3.15 cell lines (Figure 4.7).

4.4.2 *In vitro* confocal and flow cytometry analysis

The fluorescent ID8 cell lines were visualised using confocal microscopy to confirm the expression of GFP in the F3 *Trp53*-/- cell line and mCherry in the 3.15 *Trp53*-/-;*Brca2*-/- line. This was also confirmed by flow cytometry (Figure 4.7). In preparation for *in vivo* experiments, flow cytometry analysis was performed on fixed (2% PFA) and non-fixed GFP-expressing F3 and mCherry-expressing 3.15 cell lines. There was no difference in GFP or mCherry fluorescence shown between the fixed and non-fixed samples. The two cell lines were also mixed 50:50, and two different fluorescent populations were able to be identified (Figure 4.8).

These experiments showed that there was no difference *in vitro* in growth and drug sensitivity with the expression of GFP and mCherry. The *in vitro* flow cytometry also showed we would be able to identify and analyse the different populations which would be required for *in vivo* experiments.

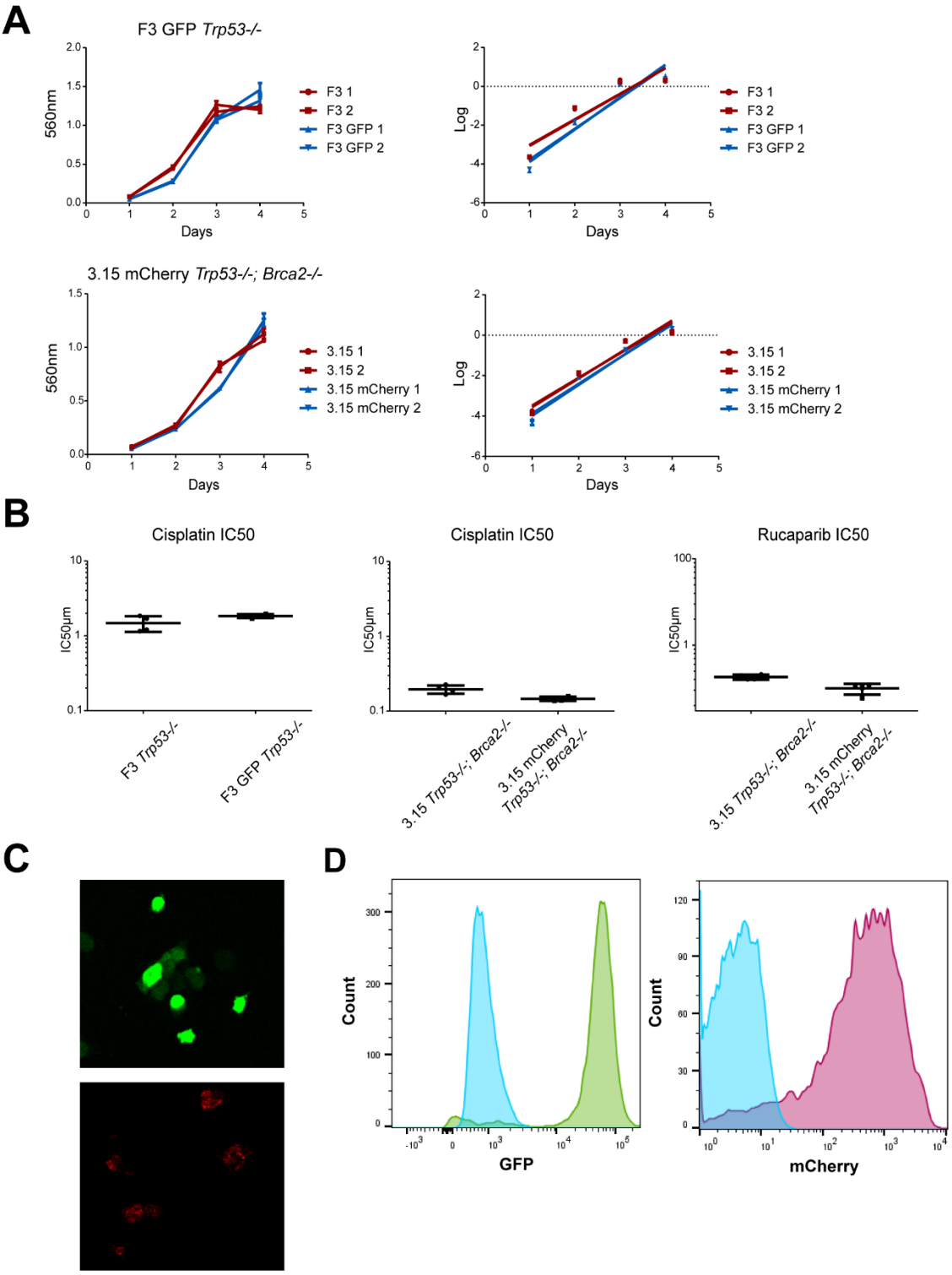

Figure 4.7: *In vitro* characterisation of ID8 fluorescent cell lines.

A, Cell proliferation assay comparing the GFP-expressing F3 and mCherry-expressing 3.15 with non-expressing cells. Using linear regression analysis, no difference in growth was shown (F3GFP p=0.52, 3.15mCherry p=0.76). **B**, Cisplatin sensitivity comparing the F3GFP and F3 cell line and showing no difference. Cisplatin and rucaparib sensitivity comparing the 3.15mCherry and 3.15 cell line again showing no difference. Each dot represents an IC50 value. **C**, **D**, Confocal microscopy and flow cytometry analysis showing the expression of both GFP and mCherry in the F3 and 3.15 cell line respectively.

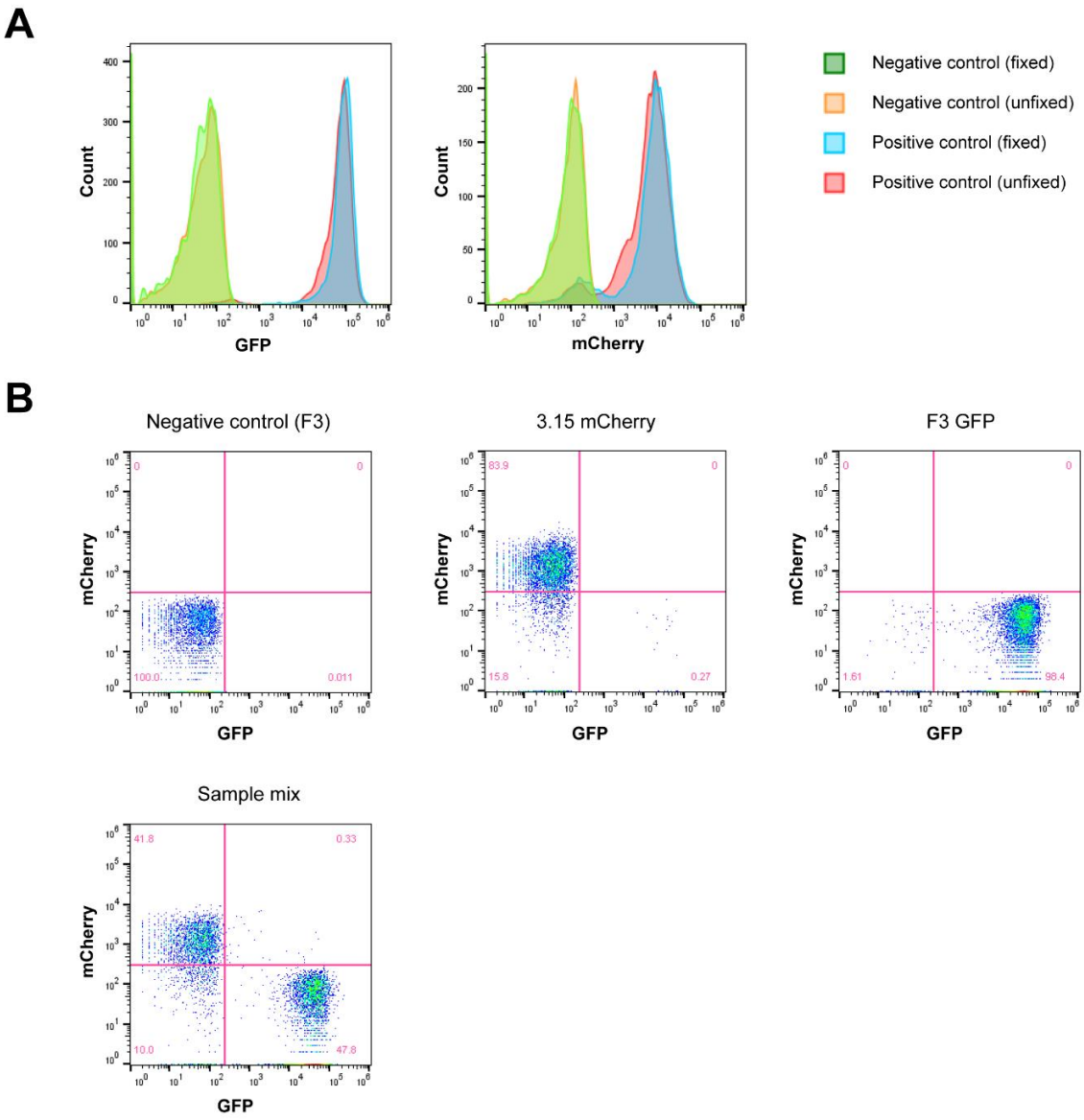

Figure 4.8: *In vitro* flow cytometry analysis of the ID8 fluorescent cell lines.

A, Flow cytometry comparing fixed (2% PFA) and unfixed samples of the F3GFP and 3.15mCherry cell lines, showing no difference in fluorescence intensity between the samples. **B**, Flow cytometry showing identification of both F3GFP and 3.15mCherry from a mixed population. F3 (negative), F3GFP (positive) and 3.15mCherry (positive) were used as controls.

4.4.3 *In vivo* data

The F3GFP, 3.15mCherry and equal mix of F3GFP/3.15mCherry cell lines were injected intraperitoneally as described previously (see Methods – section 2.7). There were 4 mice per cell line. The mice were monitored daily and killed when they reached UK Home Office limits.

The F3GFP cell line had a median survival of 57 days, 3.15mCherry of 48 days and the F3GFP/3.15mCherry mix of 56.5 days (Figure 4.9). This compared to the previous *in vivo* experiment where the non-expressing F3 *Trp53*-/- cell line had a median survival of 45 days and the 3.15 *Trp53*-/-;*Brca2*-/- cell line of 53 days (Figure 4.2).

Flow cytometry analysis was performed on the ascites. Only 1 of the 4 mixed samples (F3GFP/3.15mCherry) had ascites at endpoint and there were <1% positive mCherry cells present compared to 30.4% GFP positive cells. The four 3.15mCherry ascites samples had 0.81, 0.85, 8.74 and 9.61% positive mCherry cells. Only 3 of the 4 F3GFP samples had ascites at endpoint with 4.17, 51.4 and 47.1% GFP positive cells following analysis (Figure 4.9).

The murine tumour samples were visualised using the confocal microscope with obvious areas of tumour expressing GFP and more subtle areas expressing mCherry in the mixed samples (Figure 4.10). A concern was that the mCherry expressing cells had a low intensity of fluorescence and was therefore difficult to identify with flow cytometry and confocal analysis.

Staining the tumour samples for mCherry and GFP by immunohistochemistry would identify any weakly positive cells. The F3GFP tumour samples were almost 100% positive for GFP and the 3.15mCherry samples were also nearly 100% for mCherry suggesting that the confocal had underestimated the number of mCherry positive cells. We therefore stained the F3GFP/mCherry mixed tumour sample for GFP and any unstained tumour was assumed to be mCherry positive. The four mixed samples had an average % mCherry positivity of 24% (inferred) and an average % GFP positivity of 76% (Figure 4.10).

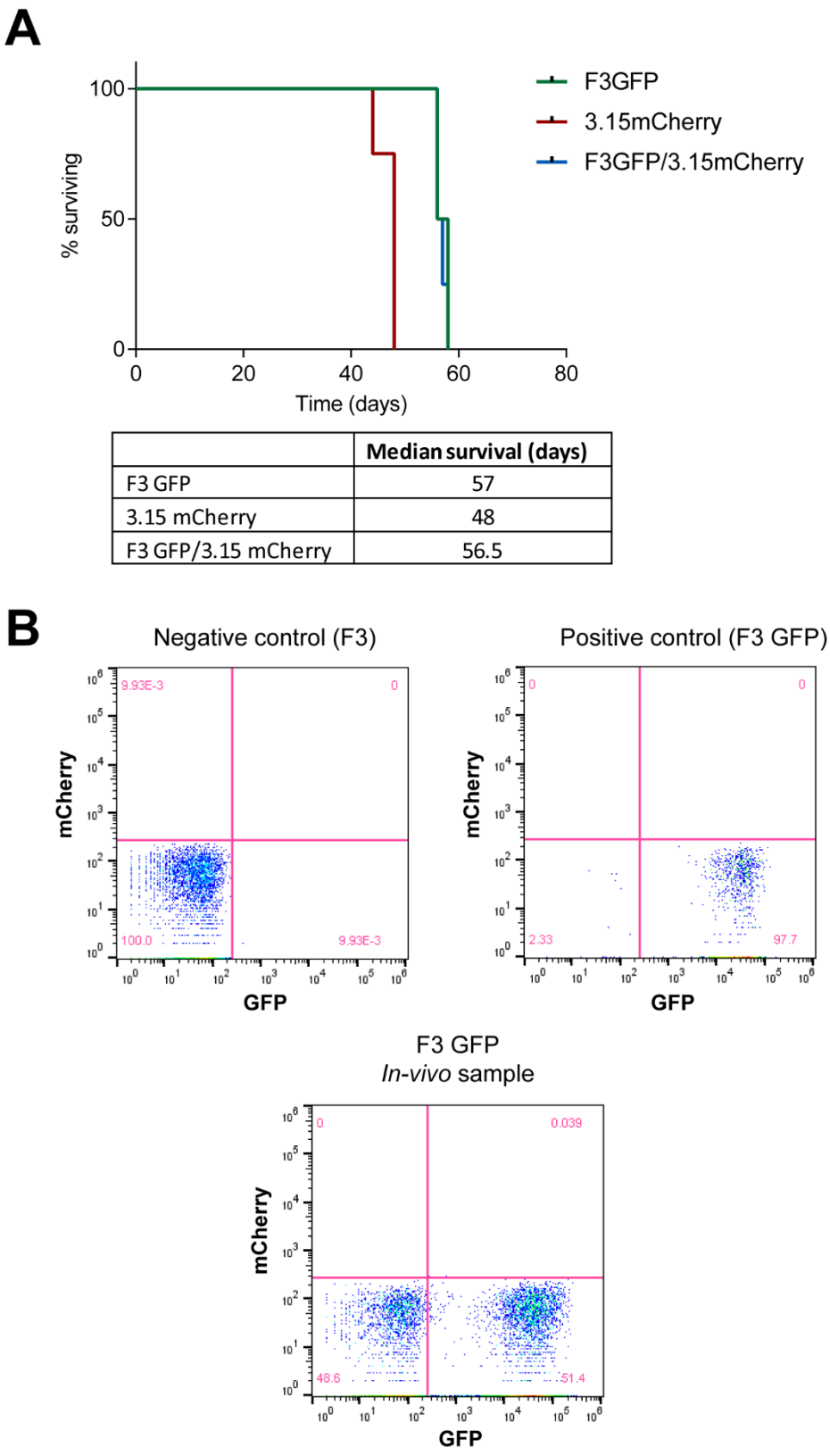

	Median survival (days)
F3 GFP	57
3.15 mCherry	48
F3 GFP/3.15 mCherry	56.5

Figure 4.9: *In vivo* experiments using the ID8 fluorescent cell lines.

A, Kaplan-Meier survival curves comparing the F3GFP, 3.15mCherry and mixed F3GFP/3.15mCherry cell lines. **B**, Example of flow cytometry analysis on an F3GFP ascites sample, showing 51.4% GFP positivity.

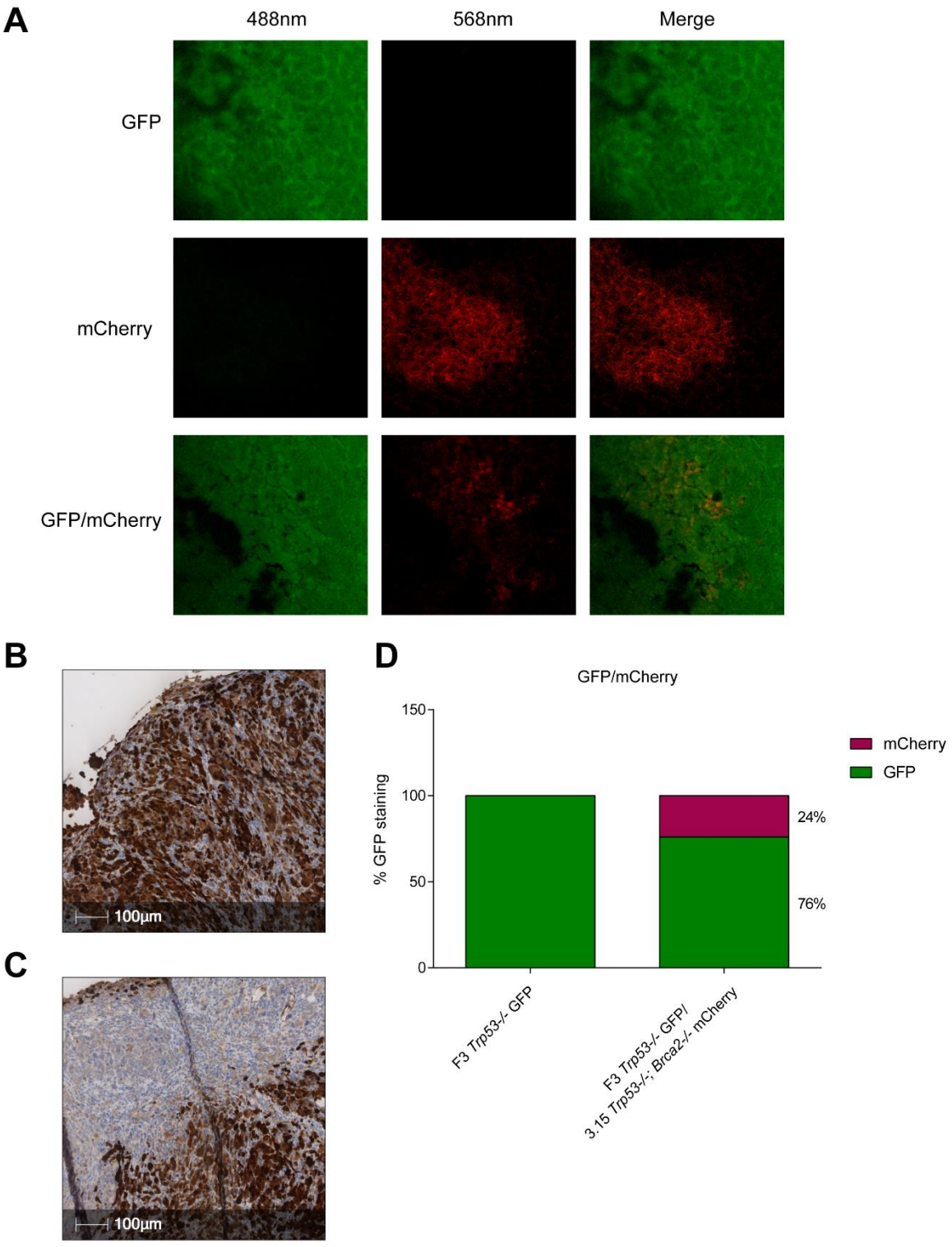

Figure 4.10: *Ex vivo* analysis of fluorescent tumour samples.

A, Confocal microscopy of murine tumour samples showing obvious areas of GFP positivity and small areas of mCherry positivity. **B**, GFP immunohistochemistry staining of an F3GFP tumour showing 100% GFP staining. **C**, GFP immunohistochemistry staining of a mixed F3GFP/3.15mCherry sample showing non-stained areas assumed to be mCherry positive. **D**, Bar chart illustrating the average % of mCherry (inferred) and GFP positivity within the four mixed samples. mCherry staining was not performed on the mixed samples but areas not stained by GFP were inferred to be mCherry positive.

4.5 Discussion

Bolton et al have found that patients with a germline *BRCA1* or *BRCA2* mutation have an improved overall survival compared to non-carriers, with loss of *BRCA2* offering the best prognosis (Bolton et al., 2012). This contrasts with the TCGA that found that *BRCA2* carriers had a positive prognosis, but they found no difference in prognosis between *BRCA1* carriers and non-carriers. However, this is now thought to be due to a lack of power in the TCGA data to detect survival differences (Bolton et al., 2012). A follow up study by Candido-dos-Reis et al confirmed a short-term survival benefit in patients with a *BRCA1* or *BRCA2* mutation. However, this survival benefit was found to reduce over time with an eventual reversal in *BRCA1* carriers after approximately 10 years (Candido-dos-Reis et al., 2015).

Our cisplatin *in vivo* data correlate closely with what has been found in patients. Clinically most patients with HGSOC receive platinum-based chemotherapy and therefore the *in vivo* survival following cisplatin treatment is relevant to patient survival data. The *Trp53-/-* genotype had a median survival of 80.5 days following cisplatin treatment. Like clinical data, the *Trp53-/-;Brca1-/-* and *Trp53-/-;Brca2-/-* genotypes had the greatest extension in survival after cisplatin treatment compared to the *Trp53-/-* genotype. The *Trp53-/-;Brca1-/-* genotype had a median survival of 97 days (HR 0.227; p=<0.0001). The *Trp53-/-;Brca2-/-* genotype had a median survival of 113 days (HR 0.218; p=<0.0001) (Figure 4.2 and Figure 4.3).

As discussed previously the site of *BRCA1* mutation may influence cisplatin sensitivity and survival. By separating the two *Trp53-/-;Brca1-/-* clones we found that the 1.36 *Trp53-/-;Brca1-/-* clone (Palb2) had a median survival of 97 days (HR 0.2623; p=0.0002) and the 6.20 *Trp53-/-;Brca1-/-* clone (BRCT2) had a median survival of 89 days (HR 0.2788; p=0.0004) (Figure 4.4). From our previous *in vitro* data, we showed that *BRCA1* mutations in the PALB2-binding domain were more sensitive to cisplatin compared to clones with mutations in the BRCT2 domain (Chapter 3 – Figure 3.9). These *in vivo* findings are consistent with what was found *in vitro* and suggest that cisplatin sensitivity and therefore overall survival can be influenced by the site of *Brca1* mutation. We have not

looked at exact mechanisms behind the differing cisplatin sensitivities between the two clones, but a possible explanation may be the greater functional role of the PALB2 domain compared to the BRCT2 domain in the homologous recombination pathway. A mutation within the PALB2 domain could result in a lower overall Brca1 expression.

TCGA was the first to identify *PTEN* homozygous deletion in 6.7% of cases and a small fraction of the homozygous deletions were intragenic i.e. only part of the gene affected (Cancer Genome Atlas Research, 2011). The TCGA data were reanalysed by Martins et al, who found *PTEN* loss to be a common event with heterozygous loss found in 36% of tumours. They found during IHC analysis that the downregulation or loss of PTEN was strongly associated with a poor overall survival and even a weak PTEN expression had a negative impact on survival (Martins et al., 2014). Thus, loss of *PTEN* is a relatively common event in HGSOC and is associated with a negative prognosis.

Our cisplatin *in vivo* data correlate with previous clinical data that have found *PTEN* to be a poor prognostic factor. The *Trp53-/-;Pten-/-* genotype had the shortest extension in survival compared to the *Trp53-/-* genotype with a median survival of 69 days (HR 3.315; p=0.0002) following cisplatin treatment (Figure 4.2 and Figure 4.3).

TCGA analysis found co-existing mutations of either single and/or double copy deletions of *BRCA1* and *PTEN* in 31% of cases and *BRCA2* and *PTEN* in 25% of cases. They also found homozygous *PTEN* loss in 7% of *TP53; BRCA2* cases (Cancer Genome Atlas Research, 2011). This highlights the importance of the ID8 triple knockouts as a relevant model of HGSOC. From our *in vivo* data the *Trp53-/-;Brca2-/-;Pten-/-* genotype had a median survival of 99 days (HR 0.231; p=<0.0001) after cisplatin treatment which is a significant reduction in survival compared to the *Trp53-/-;Brca2-/-* genotype (median survival 113 days) (Figure 4.2 and Figure 4.3). This shows that the loss of *Pten* not only has a negative impact on survival in the *Trp53-/-;Pten-/-* genotype but also on the background of *Brca2-/-* loss following cisplatin treatment. This also means that *BRCA1* and *BRCA2* mutated tumours are not a homogenous group and may partially explain the wide variation in survival seen in patients with these mutations.

The TCGA identified loss of *NF1* in 12% of cases (deletion 8%, mutation 4%) (Cancer Genome Atlas Research, 2011). Patch et al looked at inactivating mutations caused by gene breakage that would result in copy number neutral loss of transcription in the absence of single nucleotide variation. They found that inclusion of gene breakage increased the frequency of *NF1* loss to 20% (Patch et al., 2015). Alterations in *NF1* are thought to result in resistance to chemotherapy with recent studies showing MAPK activation to be associated with a poor prognosis in ovarian cancer (Hew et al., 2016).

Our cisplatin *in vivo* data are consistent with what has been found in other non-ovarian tumours with *NF1* loss. The *Trp53-/-;Nf1-/-* genotype had a shorter extension in survival compared to the *Trp53-/-* genotype with a median survival of 71 days (HR 2.693; p=0.002) (Figure 4.2 and Figure 4.3). Although no difference in cisplatin sensitivity was found *in vitro* in the *Trp53-/-;Nf1-/-* genotype, we found that the loss of *Nf1* was associated with poor outcome following platinum chemotherapy *in vivo*.

Culturing of the tumour cells from ascites offered an opportunity to investigate whether the cells had acquired resistance to cisplatin and if so by what mechanism e.g. *BRCA1/2* reversion. The cells were stained for Wt1 to confirm tumour cells were being cultured prior to undertaking assessment of *in vitro* cisplatin sensitivity. All the ascites samples cultured had positive Wt1 staining however no difference was found in cisplatin sensitivity between the cisplatin and PBS treated samples (Figure 4.5 and Figure 4.6). A possible explanation for this is that the mice only received 3 dosages of cisplatin over 3 weeks (day 28, 35 and 42) and were taken at the Home office endpoint to determine survival. Multiple continuous cisplatin dosages may be required for the tumours to begin to acquire resistance.

The generation of different ID8 genotypes expressing fluorescent proteins would allow us to start looking at the tumour heterogeneity of tumours in more detail. It is known that there is a diverse population of different genotypes within a primary tumour but also within and between metastatic deposits (Bashashati et al., 2013). Patch el al found *BRCA1/2* reversion events within

different individual tumour deposits following selection pressure from chemotherapy (Patch et al., 2015). The aim was to try and determine using the ID8 fluorescent cell lines whether dominant clones form within a tumour in response to cisplatin treatment.

The F3GFP *Trp53*-/- and 3.15mCherry *Trp53*-/-;*Brca2*-/- cell lines were characterised *in vitro* prior to undertaking *in vivo* experiments. There was no difference found in the growth and cisplatin sensitivity between the expressing and non-expressing cell lines (Figure 4.7). However, the expression of GFP and mCherry seemed to affect the *in vivo* survival. The F3 GFP had a median survival of 57 days and this compared to 45 days in the non-expressing F3 cell line (p=0.005, **). The 3.15mCherry had a median survival of 48 days, compared to 53 days in the non-expressing 3.15 cell line (p=0.17, ns) (Figure 4.9). There was also concerns that the fluorescence intensity of mCherry was low, making it difficult to identify mCherry positive cells. We therefore used GFP and mCherry IHC staining that identified weakly positive mCherry tumour. The IHC determined that about a quarter (24% - inferred) of the mixed tumour was mCherry positive (*Trp53*-/-;*Brca2*-/-) and the remaining tumour (76%) was GFP positive (*Trp53*-/-) (Figure 4.10). It is unclear whether this cell fraction is correct from IHC alone, next generation sequencing to look at the *BRCA2* mutant allele fraction would be required to determine whether this cell mix is genuine.

It was decided not to continue with further *in vivo* experiments using the fluorescent cell lines because it was not possible to identify the mCherry positive cells reliably using flow cytometry and due to concerns that the fluorescent protein expression was having an effect upon survival.

In summary, we have identified good and poor prognostic groups and shown that the cisplatin *in vivo* sensitivity for different ID8 genotypes closely correlate with clinical data. The *Trp53*-/-;*Brca1*-/- and *Trp53*-/-;*Brca2*-/- genotypes have the longest survival whereas the loss of *Pten* or *Nf1* has a negative impact on survival. This transplantable *in vivo* model offers a unique opportunity to further understand the biology of HGSOC and why these key genetic mutations influence survival. The next step was to investigate the tumour

microenvironment between the genotypes and following cisplatin treatment to attempt to explain the difference in prognosis between genotypes.

5 Tumour microenvironment and influence of platinum chemotherapy

5.1 Introduction

The dissemination of tumour throughout the peritoneal cavity with the development of widespread ascites and the predisposition of the tumour for the omentum are unique features of high grade serous ovarian cancer (Thibault et al., 2014). The tumour microenvironment has a complex interaction between the malignant and non-malignant cells. These non-malignant cells have a dynamic and often tumour-promoting function (Hanahan and Coussens, 2012).

HGSOC is an immunogenic tumour with evidence of activated T cells in both the tumour microenvironment and ascites (Ioannides et al., 1991, Zhang et al., 2003). Increased levels of tumour-infiltrating leukocytes (TIL) have been associated with an improved overall survival in patients (Zhang et al., 2003). Non-malignant cells can make up over half the tumour microenvironment but with unanswered questions regarding their tumour promoting or inhibitory functions. As described previously, tumour-associated macrophages (TAMs) can have either pro-tumour or anti-tumour properties depending on the surrounding cytokines present (Balkwill et al., 2005). Myeloid-derived suppressor cells (MDSCs) are thought to contribute to an immunosuppressive environment and have been found to accumulate in ascites in patients with ovarian cancer (Obermajer et al., 2011).

It is now believed that chemotherapy can be immune stimulatory in some circumstances with evidence of immunogenic cell death following treatment by both taxane and platinum chemotherapy (Galluzzi et al., 2015). Böhm et al and Lo et al have both shown that platinum chemotherapy can influence the tumour microenvironment and alter the different immune populations. Both studies showed increased levels of CD3+ and CD8+ but this was counteracted by an increase in expression of the immune checkpoint molecule PD-1 (Bohm et al., 2016, Lo et al., 2017).

This chapter uses the tumour and ascites samples from the cisplatin *in vivo* experiments described in the previous chapter to investigate the tumour microenvironment. I used flow cytometry, immunohistochemistry, RT-qPCR and RNA sequencing to look at how the environment is altered between the genotypes and following cisplatin treatment. The aim was to establish an explanation for the poor prognosis in the *Trp53-/-;Pten-/-* and *Trp53-/-;Nf1-/-* genotypes.

5.2 Flow cytometry

Flow cytometry analysis was performed on frozen ascites from the *in vivo* cisplatin experiment using a 12 colour fluorochrome panel (see Methods – Table 2.4). The gating strategy was consistent across the experiments (see Methods – Figure 2.4). We focussed on three genotypes – *Trp53-/-*, *Trp53-/-;Brca2-/-* and *Trp53-/-;Pten-/-*, which had marked differences in *in vivo* survival.

5.2.1 Overall cisplatin effect

We started with an unselected analysis where the PBS-treated, and cisplatin-treated groups from all genotypes were combined which is similar to analysis of an unselected patient population. This allowed us to investigate whether there were any subtle differences in immune cell populations following the treatment with cisplatin. We then went on to analyse the individual genotypes separately.

The CD45+ (*) and CD11b+ (**) populations were significantly increased with cisplatin treatment. In addition, the monocytic (Ly6C+G-) levels were significantly decreased (****) and the granulocytic (Ly6C-G+) levels significantly increased (*) following treatment. However, there was no difference in Ly6C+Ly6G+ (Gr-1+) expression between the PBS and cisplatin treated groups (Figure 5.1).

CD3+ and CD8a+ populations were significantly increased in cisplatin treated samples (CD3+***, CD8a+*). The F4/80+ population was significantly increased in the cisplatin group (**) but there was no difference in MHCII+ expression and CD19+ levels between the two groups. (Figure 5.1 and Figure 5.2).

There was a non-significant decrease in PDL-1 expression on CD3 cells after cisplatin treatment (p=0.05) but no significant difference in CD8 PDL-1 expression and a significant decrease on CD19 cells (****). CD86+ expression was significantly decreased on both CD3+ and CD19+ populations (****) (Figure 5.2).

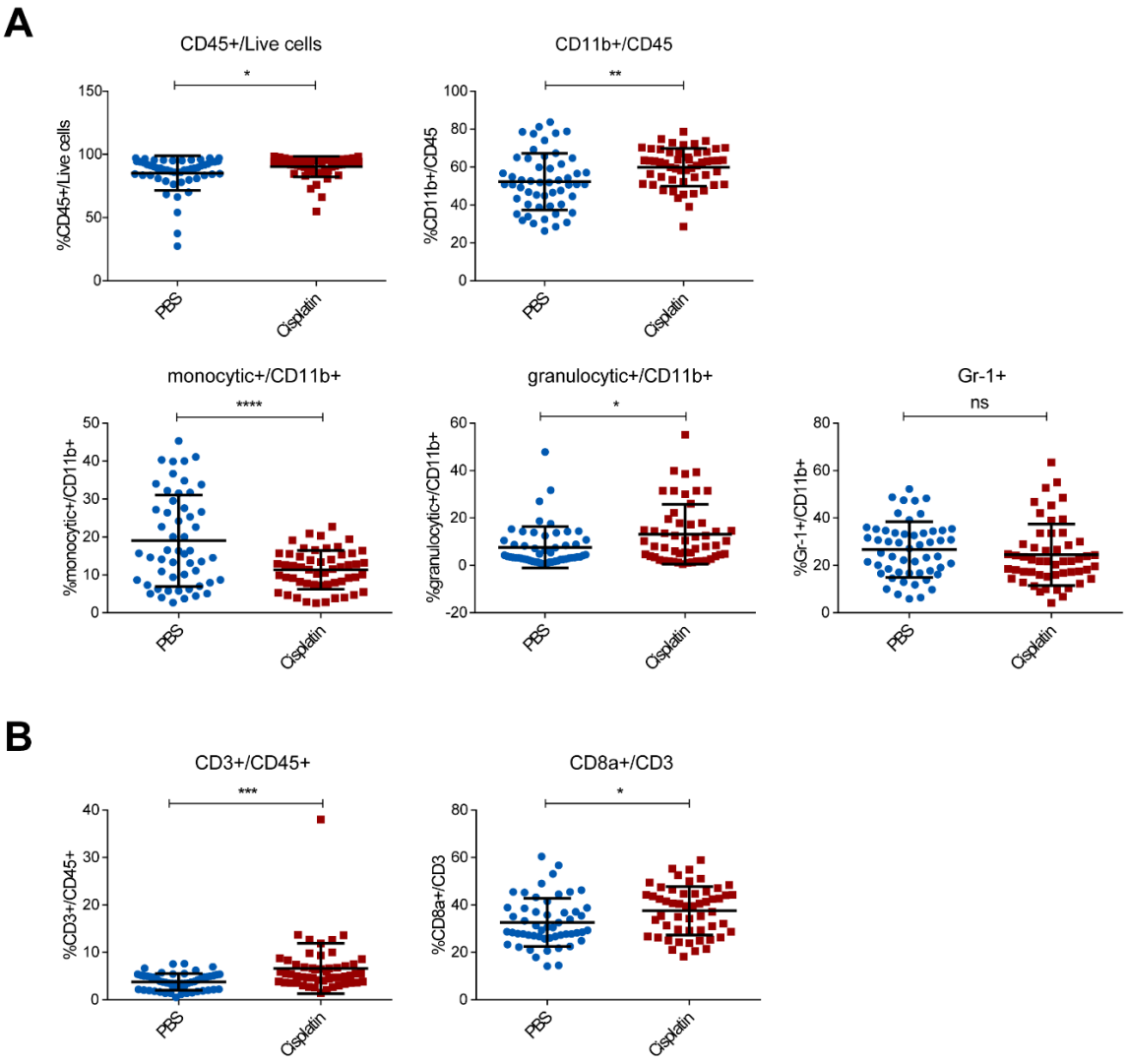

Figure 5.1: Flow cytometry analysis of ascites comparing the untreated PBS and treated cisplatin groups.
The figure shows the overall cisplatin effect with the different genotypes combined. **A,** Flow analysis showing a significant increase in CD45+ (*), CD11b+ (**) and granulocytic MDSC (*) in the cisplatin treated group, with a significant decrease in the monocytic MDSC (****) population in the cisplatin group. There was no significant change in Ly6C+Ly6G+ (Gr-1) between the groups. **B,** Flow analysis showing a significant increase in CD3+ (***) and CD8a+ (*) in the cisplatin treated group compared to the PBS treated group.

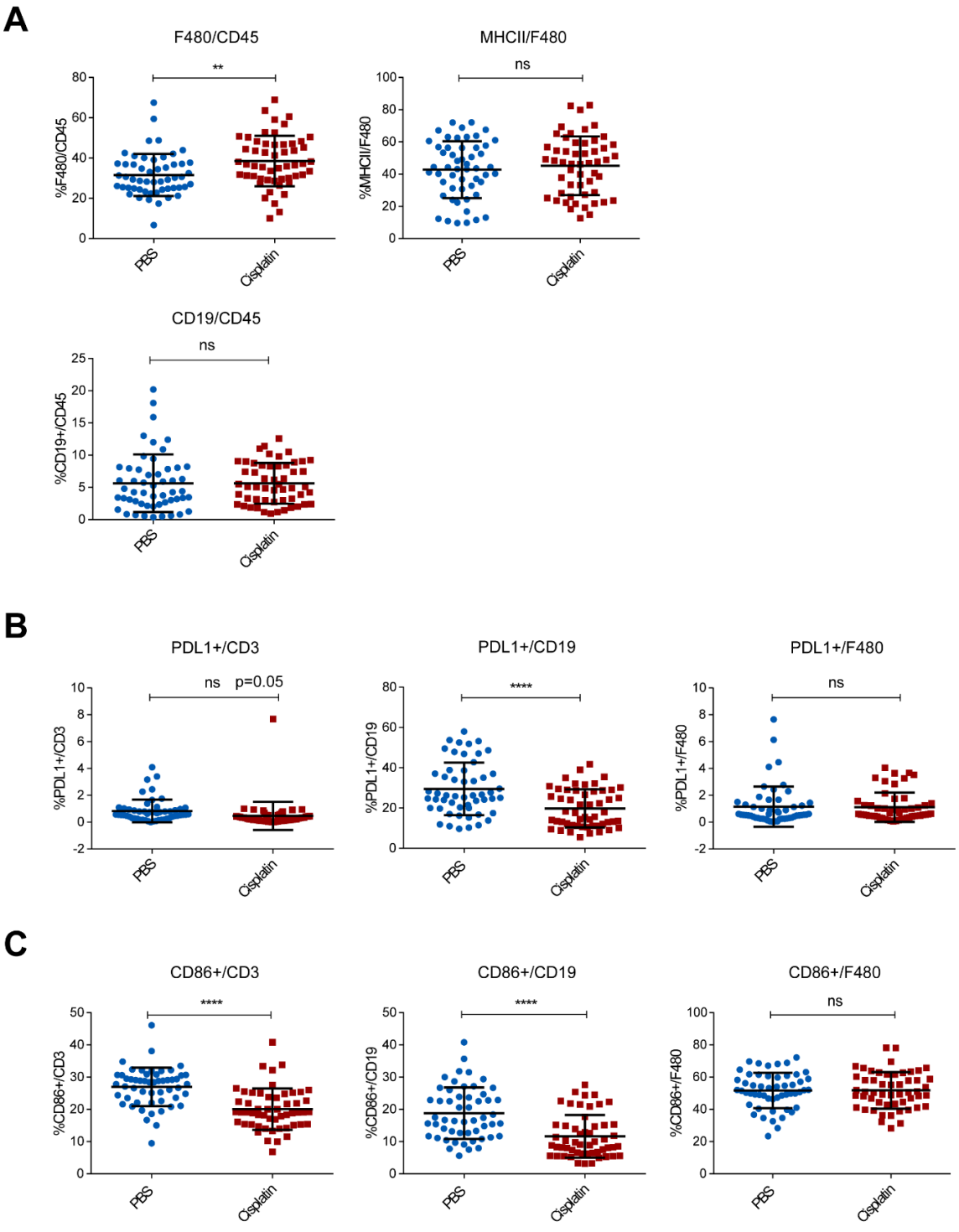

Figure 5.2: Flow cytometry analysis of ascites comparing the untreated PBS and treated cisplatin groups.
This figure again shows the overall cisplatin effect with the different genotypes combined.
A, Flow analysis showing a significant increase in F4/80+ (**) in the cisplatin treated compared to PBS treated groups and no difference in MHCII+/F480 levels between the groups. **B,** Flow analysis showing a significant decrease in PDL1+ expression on CD19 cells (****) in the cisplatin group. **C,** Flow analysis showing a significant decrease in CD86+ expression on CD3 and CD19 cells (****) in the cisplatin groups.

5.2.2 Differences between genotypes

There were similar levels of CD45+ and CD11b+ cells between the genotypes. The proportion of CD45+ cells within the live cell population was >90% in most samples, of which >50% were CD11b+. There was an increase in the monocytic MDSC (Ly6C+G-; CD11b+) population but no obvious increase in granulocytic (Ly6C-G+) cells in the *Trp53-/-;Pten-/-* genotype compared to the *Trp53-/-* genotype. However, the Ly6C+Ly6G+ (Gr-1+) (combined monocytic and granulocytic) population was significantly increased in the *Trp53-/-;Pten-/-* genotype (*). The proportion of Ly6C+Ly6G+ cells was also significantly lower in the *Trp53-/-;Brca2-/-* genotype compared to the *Trp53-/-;Pten-/-* genotype (**).

There were no significant differences between the genotypes in proportions of CD3+, CD8a+ and F4/80+ cells. However, there was a non-significant reduction in number of CD19+ cells in the *Trp53-/-;Brca2-/-* compared to the *Trp53-/-* genotype (Figure 5.3 and Figure 5.4).

5.2.3 Influence of cisplatin between genotypes

Treatment with cisplatin did not significantly change the proportion of CD45+ and CD11b+ cells between the different genotypes. There was also no change in monocytic and granulocytic MDSC populations after treatment (Figure 5.3). However, the number of CD3+ cells were significantly increased between the *Trp53-/-;Pten-/-* (PBS treated) and *Trp53-/-;Pten-/-* (cisplatin treated) groups (*) and a non-significant increase was seen in the other cisplatin treated genotypes. There was no difference in CD8a+ populations after treatment but the cisplatin-treated *Trp53-/-;Pten-/-* genotype had a significantly higher number of CD8a+ cells compared to the treated *Trp53-/-* (*) and *Trp53-/-;Brca2-/-* (*) groups (Figure 5.3).

The number of F4/80+ cells was non-significantly increased in the *Trp53-/-;Pten-/-* cisplatin treated group compared to the PBS treated group. There was no difference in MHCII/F480 expression between the genotypes and following cisplatin treatment (Figure 5.4).

CD19+ cells were significantly increased in the *Trp53-/-;Brca2-/-* (PBS treated) and *Trp53-/-;Brca2-/-* (cisplatin treated) groups (*) (Figure 5.4).

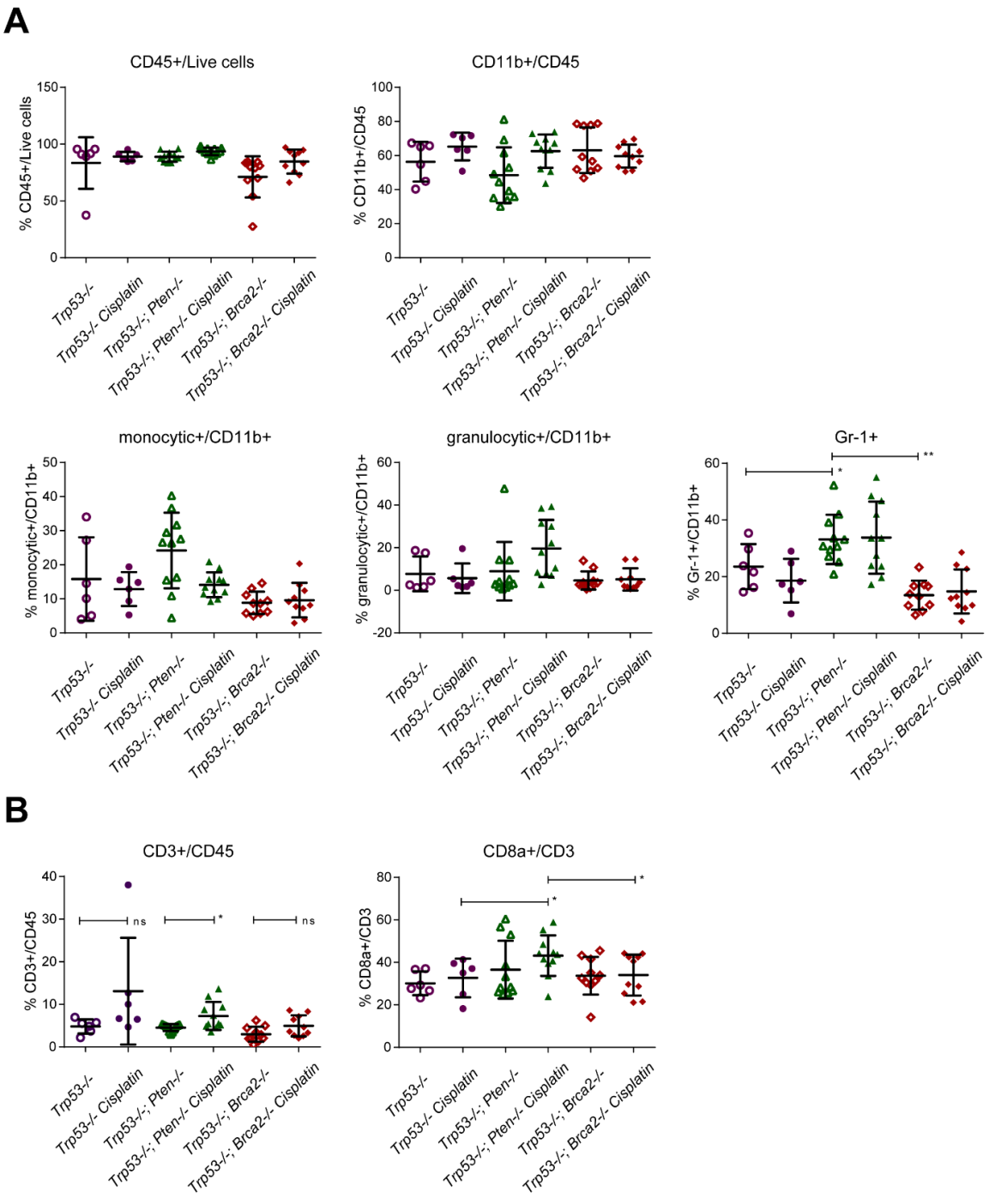

Figure 5.3 Flow cytometry analysis of ascites and following cisplatin treatment. **A**, Flow analysis showing no difference in CD45+ and CD11b+ populations between the groups. There was a significant increase in Ly6C+Ly6G+ (Gr-1) between the *Trp53-/-* and *Trp53-/-;Pten-/-* genotypes (*) and between *Trp53-/-;Brca2-/-* and *Trp53-/-;Pten-/-* (**). **B**, Flow analysis showing a significant increase in CD3+ between the *Trp53-/-;Pten-/-* (PBS treated) and *Trp53-/-;Pten-/-* (cisplatin treated) groups (*). There was a significant increase in CD8a+ between the *Trp53-/-* (cisplatin), *Trp53-/-;Brca2-/-* (cisplatin) and the *Trp53-/-;Pten-/-* (cisplatin) group (*) (*).

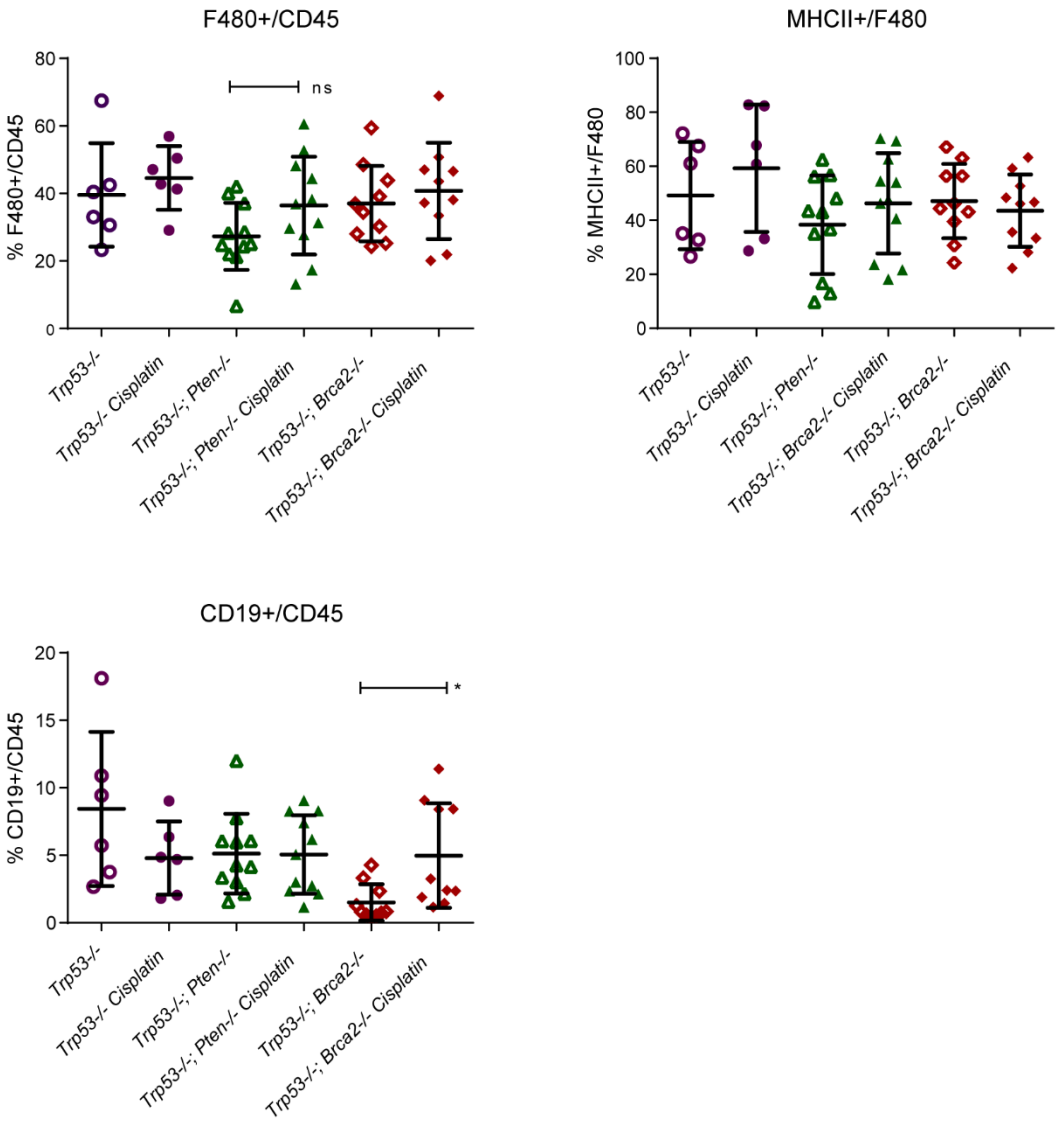

Figure 5.4 Flow cytometry analysis of ascites comparing the *Trp53-/-*, *Trp53-/-;Pten-/-*, *Trp53-/-;Brca2-/-* genotypes and following cisplatin treatment.
Flow analysis showing a non-significant increase in F4/80+ between the *Trp53-/-;Pten-/-* (PBS) and *Trp53-/-;Pten-/-* (cisplatin) groups. There was no significant difference in MHCII+/F480 levels between the genotypes and treatment groups. There was a significant increase in CD19+ between the *Trp53-/-;Brca2-/-* (PBS) and *Trp53-/-;Brca2-/-* (cisplatin) groups (*).

5.3 Tissue Microarrays

Three tissue microarrays (TMAs) were generated from the cisplatin *in vivo* experiment. Each TMA contained cores from at least four different genotypes and contained PBS and cisplatin treated cores (Methods – section 2.5) (Figure 5.5). The TMAs were stained for CD3, CD8a, F4/80, p-Akt, CD206 and iNOS (Figure 5.6) and scored using HALO software.

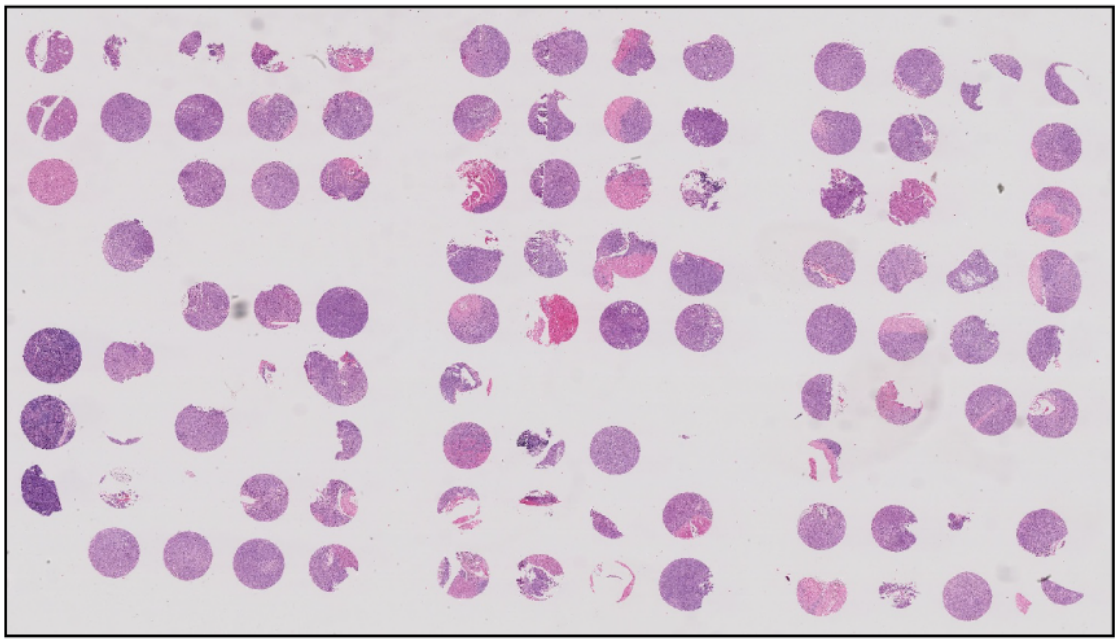

Figure 5.5: An example of one TMA from the cisplatin *in vivo* experiment.

The TMA was generated from 1mm cores from paraffin-embedded blocks. Four blocks were used per genotype and cisplatin group and three tumour cores were taken from each block. The cores were spread across three different TMAs.

5.3.1 CD3

CD3 staining of the murine tumour showed a significant increase in CD3 levels in the *Trp53-/-;Pten-/-* compared to the *Trp53-/-* genotype (*) and a non-significant increase in the *Trp53-/-;Brca2-/-;Pten-/-* genotype. There were no other significant differences between the genotypes. There were also no differences shown in CD3 levels in cisplatin treated samples (Figure 5.7).

When the PBS treated and cisplatin treated samples were combined there was a significant decrease in CD3 staining in the cisplatin group (*). The histoscores for CD3 were low with the majority scoring <5 (Figure 5.7).

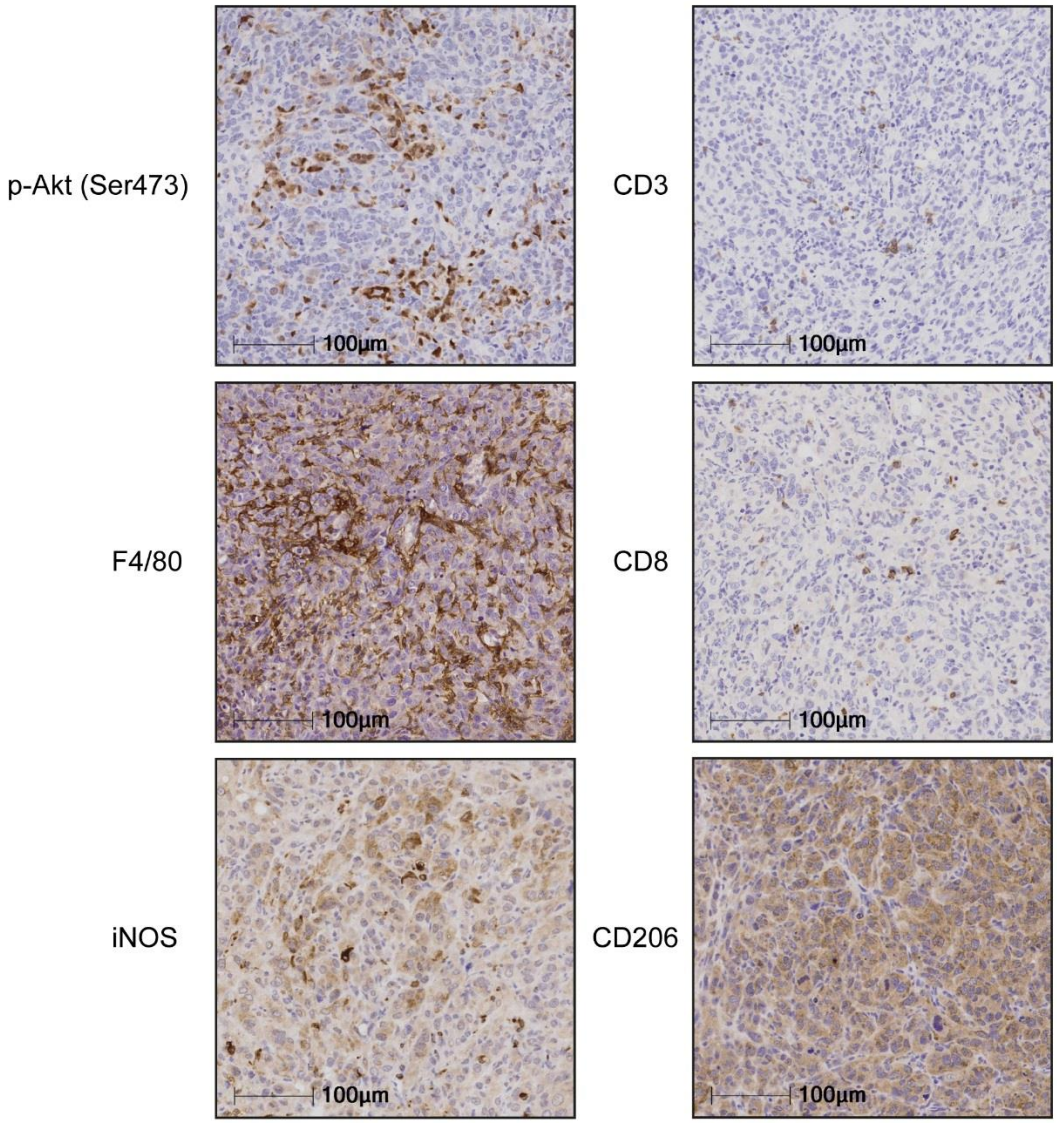

Figure 5.6: Examples of TMA staining.
Staining for p-Akt (Ser473), CD3, CD8a, F4/80, CD206 and iNOS (20x magnification).

5.3.2 CD8a

CD8a staining showed a non-significant increase in the *Trp53-/-;Pten-/-* compared to *Trp53-/-* genotype and a significant increase in the *Trp53-/-;Brca2-/-;Pten-/-* genotype (*). There were no other significant differences between the genotypes. There were also no differences shown in CD8a levels in cisplatin treated samples (Figure 5.8).

When the PBS treated and cisplatin treated samples were combined, there was no difference in CD8a staining between the groups. The histoscores for CD8a were low, with the majority scoring <2 (Figure 5.8).

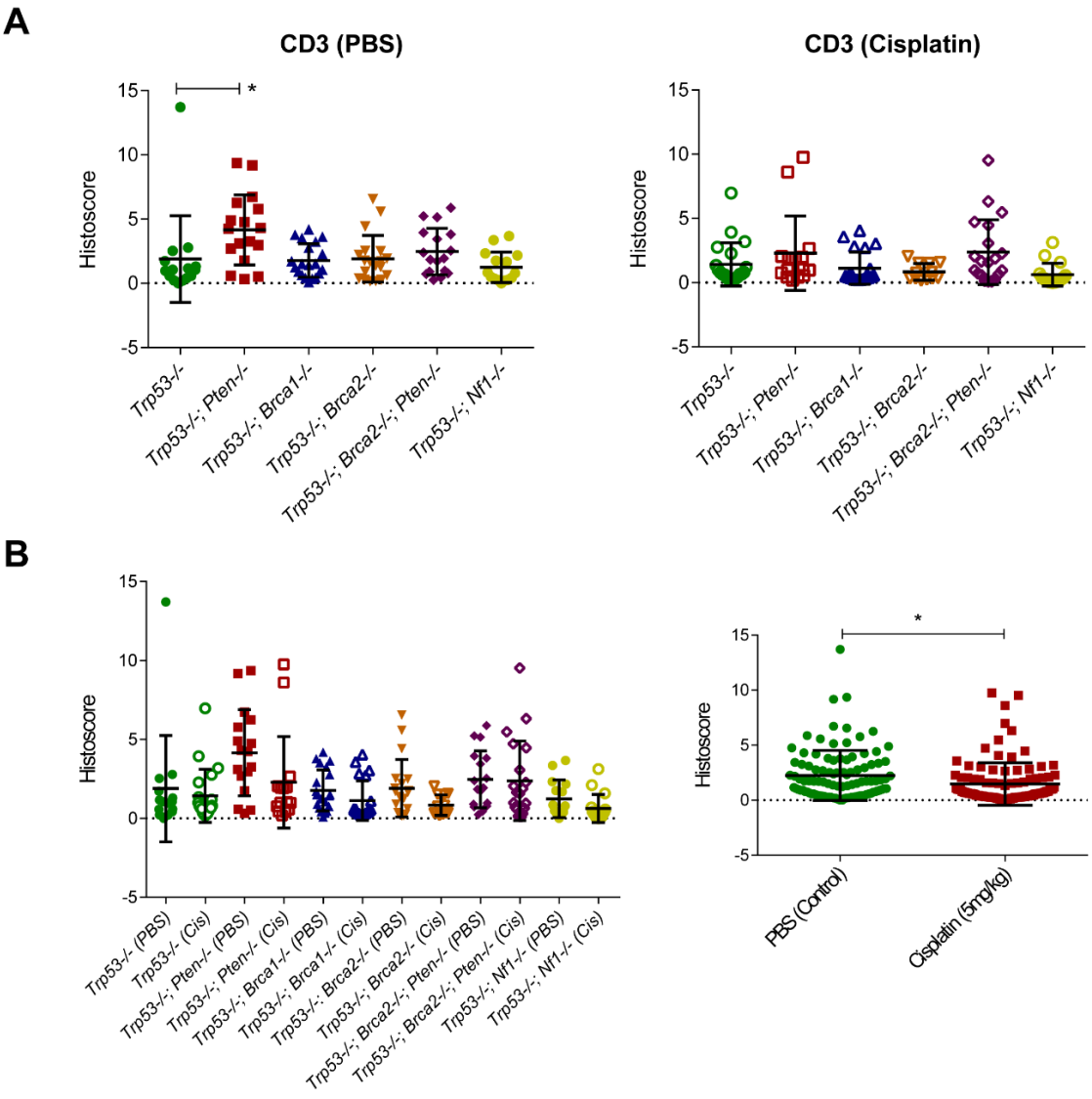

Figure 5.7: CD3 immunohistochemistry staining of tumour.

A, CD3 histoscores from PBS and cisplatin treated genotypes showing a significant increase in CD3 between the *Trp53-/-* and *Trp53-/-;Pten-/-* genotypes (*). **B**, CD3 histoscores showing the differences between the genotypes. There was a significant decrease in CD3 in the cisplatin treated group when the different genotypes were combined to show the overall cisplatin effect (*).

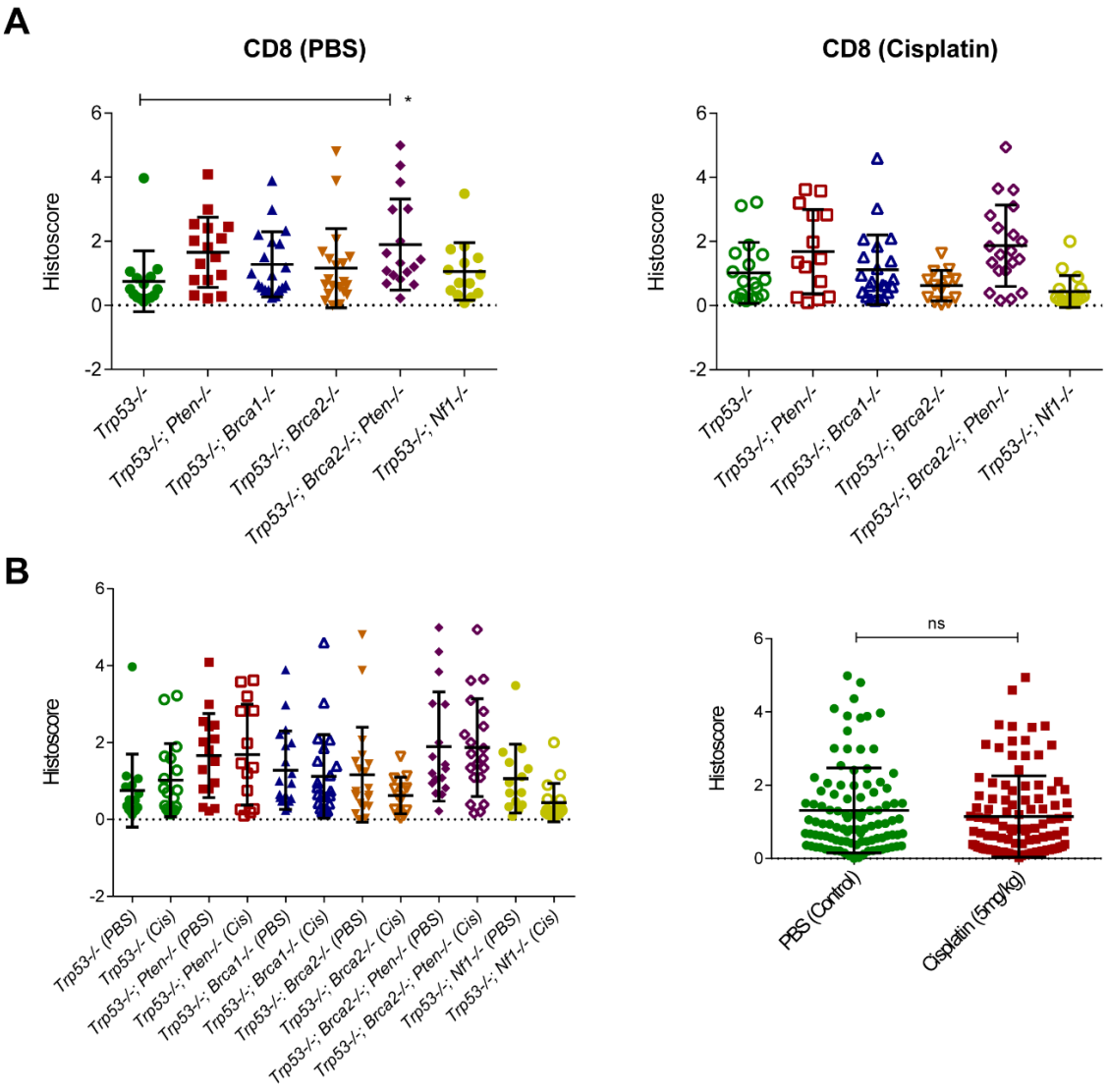

Figure 5.8: CD8a immunohistochemistry staining of tumour.

A, CD8 histoscores from PBS and cisplatin treated genotypes showing a non-significant increase in CD8 between the *Trp53-/-* and *Trp53-/-;Pten-/-* genotypes and a significant increase between the *Trp53-/-* and *Trp53-/-;Brca2-/-;Pten-/-* genotypes (*). **B**, CD8 histoscores showing the differences between the genotypes. There was no significant difference in CD8 staining between the two treatment groups when the different genotypes were combined to show the overall cisplatin effect.

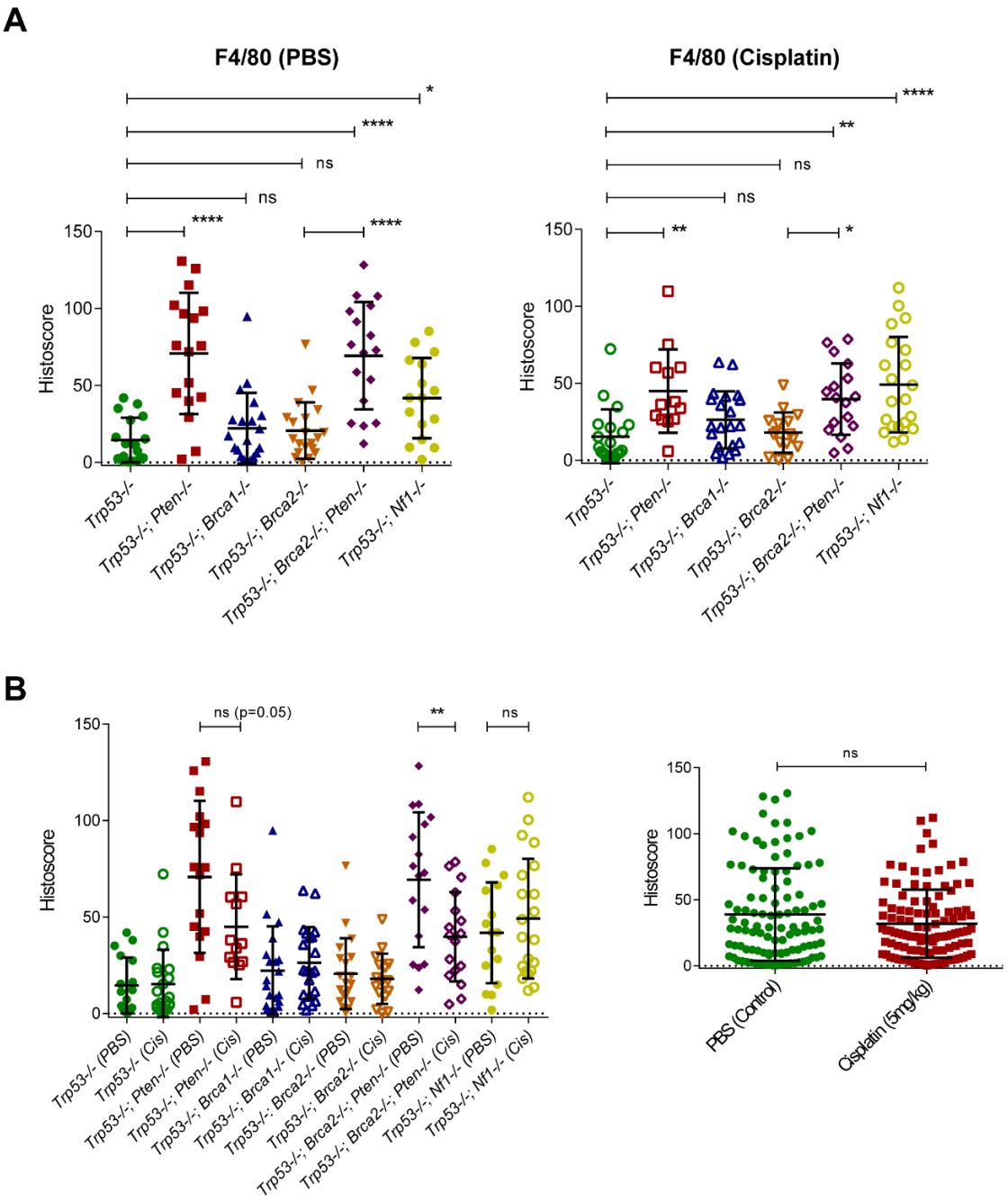

Figure 5.9: F4/80 immunohistochemistry staining of tumour.

A, F4/80 histoscores from PBS and cisplatin treated genotypes showing a significant increase in F4/80 between *Trp53-/-* and the *Trp53-/-;Pten-/-* (****) and *Trp53-/-;Brca2-/-;Pten-/-* (****) genotypes. There was also a significant increase in F4/80 between the *Trp53-/-;Brca2-/-* and *Trp53-/-;Brca2-/-;Pten-/-* genotype (****). **B**, F4/80 histoscores showing a non-significant decrease in F4/80 in the *Trp53-/-;Pten-/-* cisplatin group and significant decrease in the *Trp53-/-;Brca2-/-;Pten-/-* cisplatin group (**). There was a non-significant increase in F4/80 in the *Trp53-/-;Nf1-/-* cisplatin group.

5.3.3 F4/80 (macrophage marker)

F4/80 staining showed a significant increase in F4/80 levels in both the *Trp53-/-;Pten-/-* and *Trp53-/-;Brca2-/-;Pten-/-* (****) genotypes compared to *Trp53-/-* genotype (****). There was also a significant increase in F4/80 staining in the *Trp53-/-;Brca2-/-;Pten-/-* compared to the *Trp53-/-;Brca2-/-* genotype (****). F4/80 staining was significantly increased in the *Trp53-/-;Nf1-/-* compared to the *Trp53-/-* genotype (*) (Figure 5.9).

F4/80 levels were significantly increased in cisplatin-treated *Trp53-/-;Pten-/-* (**) and *Trp53-/-;Brca2-/-;Pten-/-* (**) tumours compared to the *Trp53-/-* cisplatin group. There was also a significant increase in F4/80 in the *Trp53-/-;Brca2-/-;Pten-/-* cisplatin-treated compared to the *Trp53-/-;Brca2-/-* cisplatin-treated genotype (*). F4/80 staining was significantly increased in the *Trp53-/-;Nf1-/-* cisplatin treated compared to the *Trp53-/-* cisplatin treated genotype (****) (Figure 5.9).

There was a non-significant decrease in F4/80 in the *Trp53-/-;Pten-/-* cisplatin group compared to the PBS treated *Trp53-/-;Pten-/-* group (p=0.05) and a significant decrease when comparing the PBS and cisplatin treated *Trp53-/-;Brca2-/-;Pten-/-* genotype (**). There was also a non-significant increase in F4/80 staining in the cisplatin treated *Trp53-/-;Nf1-/-* group compared to the PBS treated (Figure 5.9).

When the PBS treated and cisplatin treated samples were combined there was no difference in F4/80 staining between the groups (Figure 5.9).

5.4 RNA sequencing

RNA sequencing was performed on tumour samples from the cisplatin *in vivo* experiment. Tumour cellularity was checked prior to RNA extraction and RIN determined prior to sequencing (see Methods – section 2.6). RNA sequencing was performed on PBS-treated and cisplatin-treated tumour samples from the following genotypes: *Trp53*+/+, *Trp53*-/-, *Trp53*-/-;*Pten*-/-, *Trp53*-/-;*Brca1*-/-, *Trp53*-/-;*Brca2*-/- and *Trp53*-/-;*Nf1*-/-.

The percentage of reads mapped to the mouse genome ranged from 71.1-93% with the GC content ranging from 49-56% and duplicates from 6.9-20.7%. The mean Phred quality score for all samples and per sequence were >30 (base call accuracy 99.9%) (Appendix 1, Appendix 3 and Appendix 5).

Trp53 expression was reduced in the *Trp53*-/-, *Trp53*-/-;*Pten*-/-, *Trp53*-/-;*Brca1*-/-, *Trp53*-/-;*Brca2*-/- and *Trp53*-/-;*Nf1*-/- samples compared to the *Trp53*+/+ genotype. *Pten* expression was reduced in the *Trp53*-/-;*Pten*-/- genotype compared to the *Trp53*-/-. *Brca1* expression was reduced in the *Trp53*-/-;*Brca1*-/- samples compared to the *Trp53*-/- genotype. By contrast, the expression of *Brca2* was increased in the *Trp53*-/-;*Brca2*-/- samples compared to the *Trp53*-/- genotype and *Nf1* expression was increased in the *Trp53*-/-;*Nf1*-/- samples compared to *Trp53*-/- (Appendix 2, Appendix 4 and Appendix 6).

The top 50 significantly up regulated and down regulated genes in the different genotypes and following cisplatin treatment (R package – edgeR) are outlined in Appendix 7.

5.4.1 *Trp53*+/+, *Trp53*-/-

There were a significant number of genes up- and downregulated with the loss of *Trp53* when comparing the *Trp53*+/+ and *Trp53*-/- genotypes. The enrichment analysis showed the chemokine activity, genes involved in chromosomal stability and dsDNA binding to be amongst the pathways upregulated in the *Trp53*-/- genotype.

Only a small number of genes were downregulated in the *Trp53*-/- cisplatin treated group compared to the PBS treated group and therefore enrichment analysis was unable to be performed (Figure 5.10).

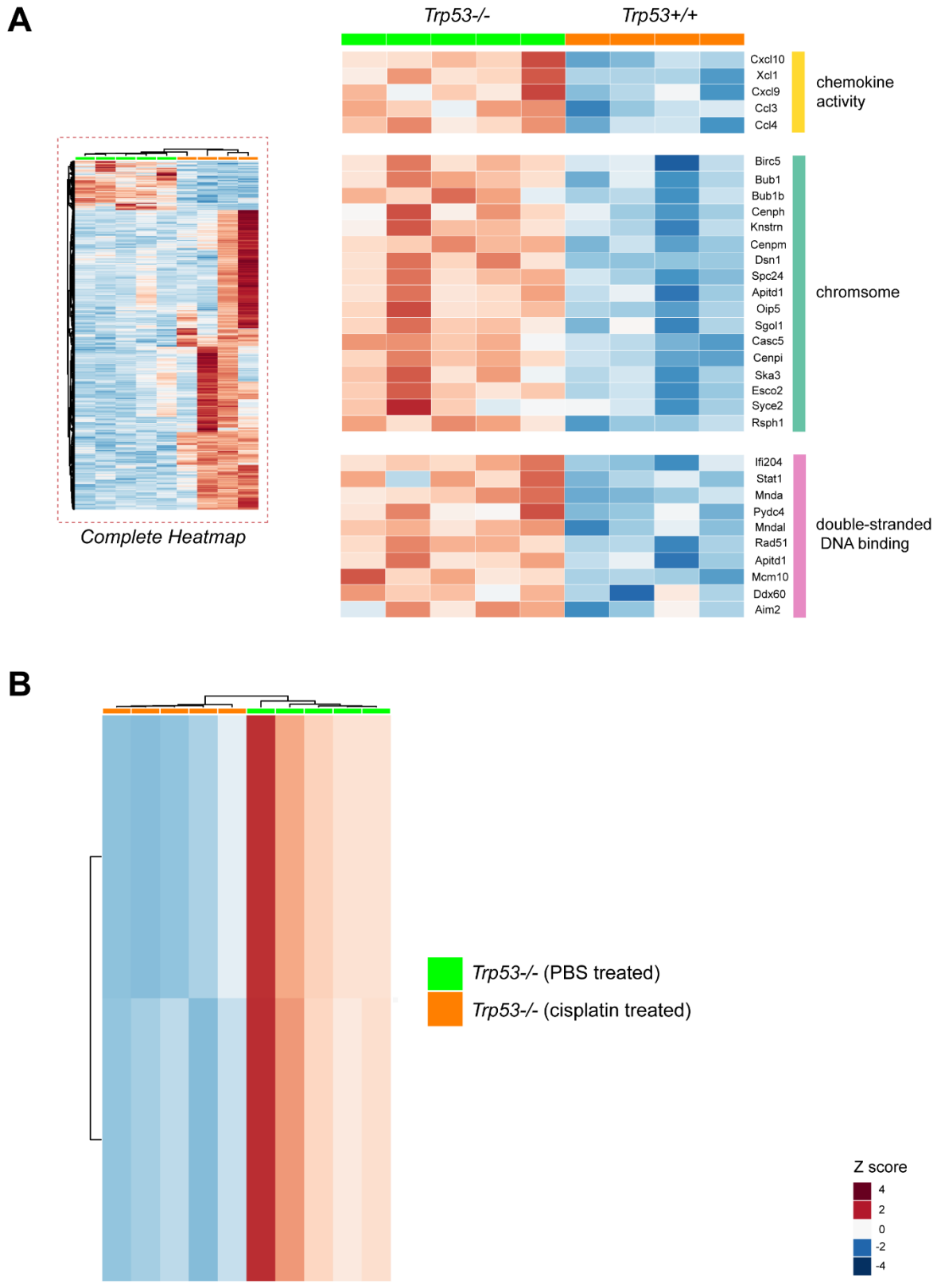

Figure 5.10: RNA sequencing of murine tumours from *Trp53*+/+, *Trp53*-/- (PBS treated) and *Trp53*-/- (cisplatin treated) genotypes.
A, Gene expression heat map comparing the *Trp53*+/+ and *Trp53*-/- groups and enrichment analysis showing an upregulation of pathways involved in chemokine activity, chromosome stability and dsDNA binding. **B**, Gene expression heat map comparing *Trp53*-/- (PBS treated) and *Trp53*-/- (cisplatin treated) samples and showing a limited number of downregulated genes in the *Trp53*-/- (cisplatin treated) group.

5.4.2 *Trp53-/-;Pten-/-*

There were a significant number of genes up- and downregulated with the loss of *Pten* when comparing the *Trp53-/-* and *Trp53-/-;Pten-/-* genotypes (see section 5.5, Figure 5.18).

Comparing the PBS-treated, and cisplatin-treated *Trp53-/-;Pten-/-* groups, an even greater number of genes were up- and downregulated following treatment. The enrichment analysis showed a downregulation in the chemokine activity and immune response and an upregulation in the canonical Wnt signalling pathway in the cisplatin treated samples (Figure 5.11).

5.4.3 *Trp53-/-;Brca1-/-* and *Brca2-/-*

The loss of *Brca1* and *Brca2* did not result in many significantly up- or downregulated genes when comparing both the *Trp53-/-;Brca1-/-* and *Trp53-/-;Brca2-/-* to the *Trp53-/-* genotype. A similar lack of altered gene expression was found when comparing the PBS treated and cisplatin treated samples from the two genotypes (Figure 5.12 and Figure 5.13).

Enrichment analysis of these genotypes was unable to be performed due to the lack of differences in gene expression.

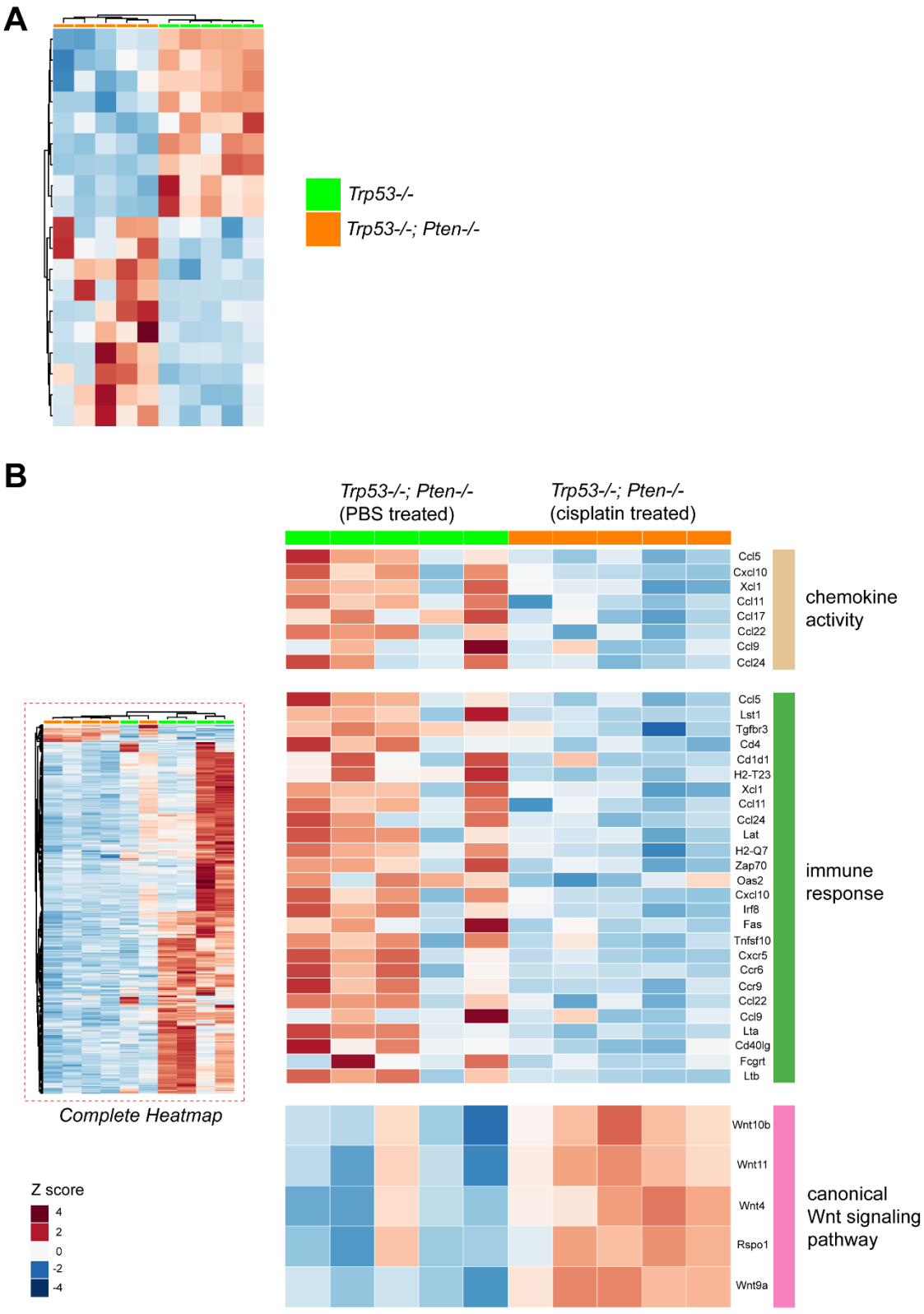

Figure 5.11: RNA sequencing of murine tumours from *Trp53-/-;Pten-/-* (PBS treated) and *Trp53-/-;Pten-/-* (cisplatin treated) genotypes.
A, Gene expression heat map comparing the *Trp53-/-* and *Trp53-/-;Pten-/-* genotypes, (see Figure 5.18 for enrichment analysis). **B**, Gene expression heat map comparing *Trp53-/-;Pten-/-* (PBS treated) and *Trp53-/-;Pten-/-* (cisplatin treated) samples and enrichment analysis showing a downregulation of pathways involved in chemokine activity and immune response, and upregulation in the canonical Wnt signalling pathway.

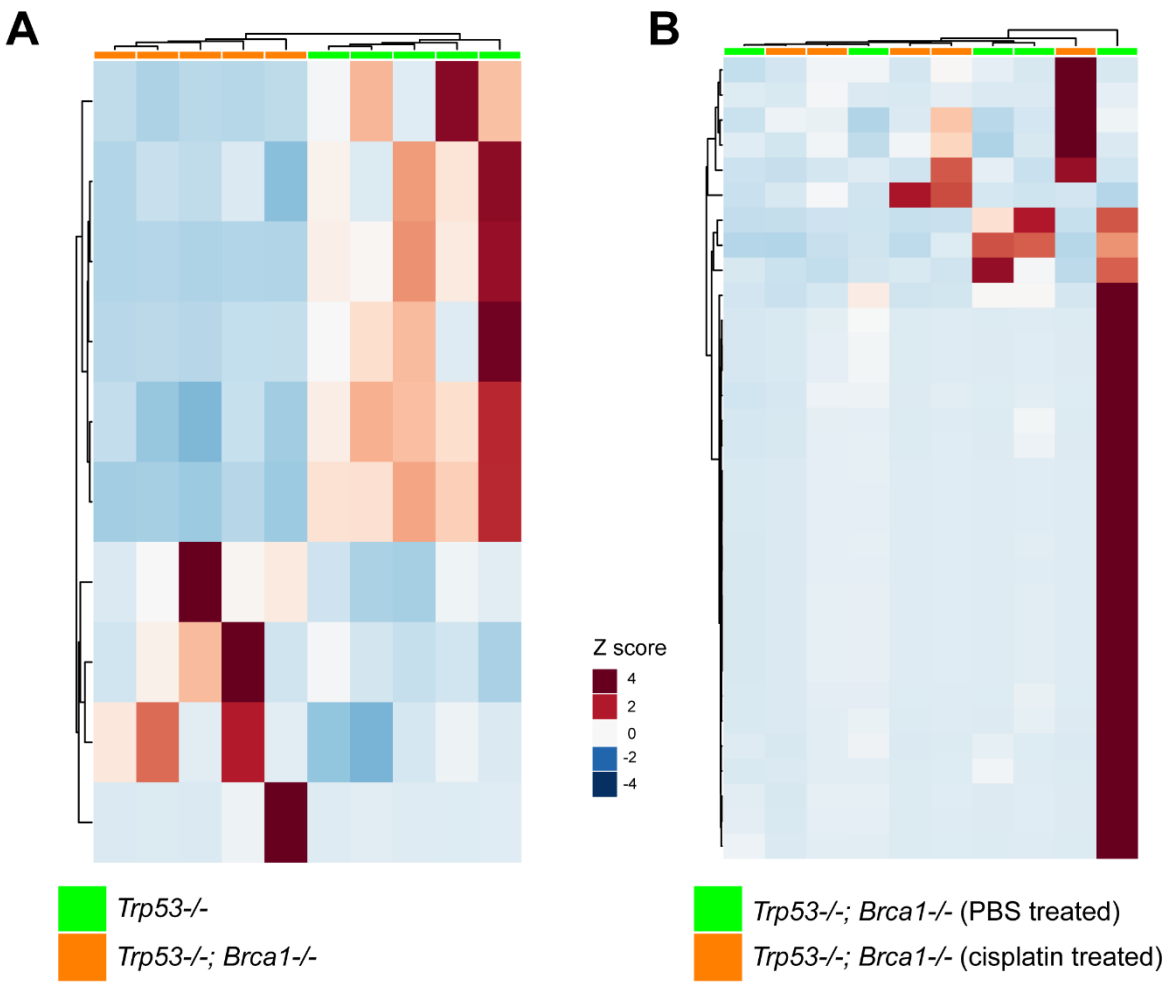

Figure 5.12: RNA sequencing of murine tumours from *Trp53-/-;Brca1-/-* (PBS treated) and *Trp53-/-;Brca1-/-* (cisplatin treated).
A, Gene expression heat map comparing the *Trp53-/-* and *Trp53-/-;Brca1-/-* genotypes. **B**, Gene expression heat map comparing the *Trp53-/-;Brca1-/-* (PBS treated) and *Trp53-/-;Brca1-/-* (cisplatin treated).

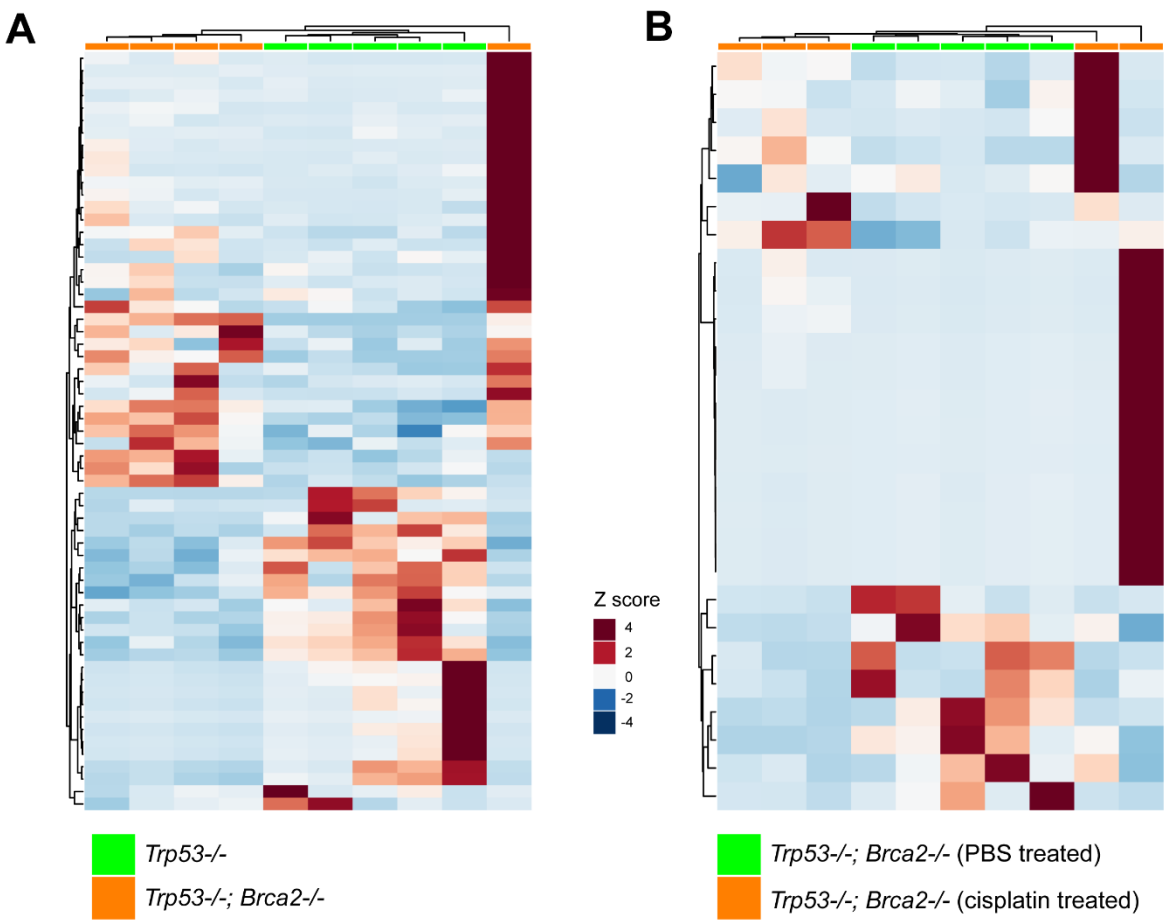

Figure 5.13: RNA sequencing of murine tumours from *Trp53-/-;Brca2-/-* (PBS treated) and *Trp53-/-;Brca2-/-* (cisplatin treated).
A, Gene expression heat map comparing the *Trp53-/-* and *Trp53-/-;Brca2-/-* genotypes. **B**, Gene expression heat map comparing the *Trp53-/-;Brca1-/-* (PBS treated) and *Trp53-/-;Brca2-/-* (cisplatin treated).

5.4.4 *Trp53-/-;Nf1-/-*

There were a significant number of genes up- and downregulated with the loss of *Nf1*. The enrichment analysis showed the chemokine activity and immune response to be amongst the pathways significantly downregulated and genes involved in neurotransmitter transport were significantly upregulated in the *Trp53-/-;Nf1-/-* genotype compared to *Trp53-/-* (Figure 5.14).

Comparing the PBS treated, and cisplatin treated *Trp53-/-;Nf1-/-* groups an even greater number of genes were up- and downregulated following treatment. The enrichment analysis showed a downregulation in genes responsible for the inflammatory response and chemotaxis and an upregulation in genes involved in the function of the cell junction in the cisplatin treated samples (Figure 5.15).

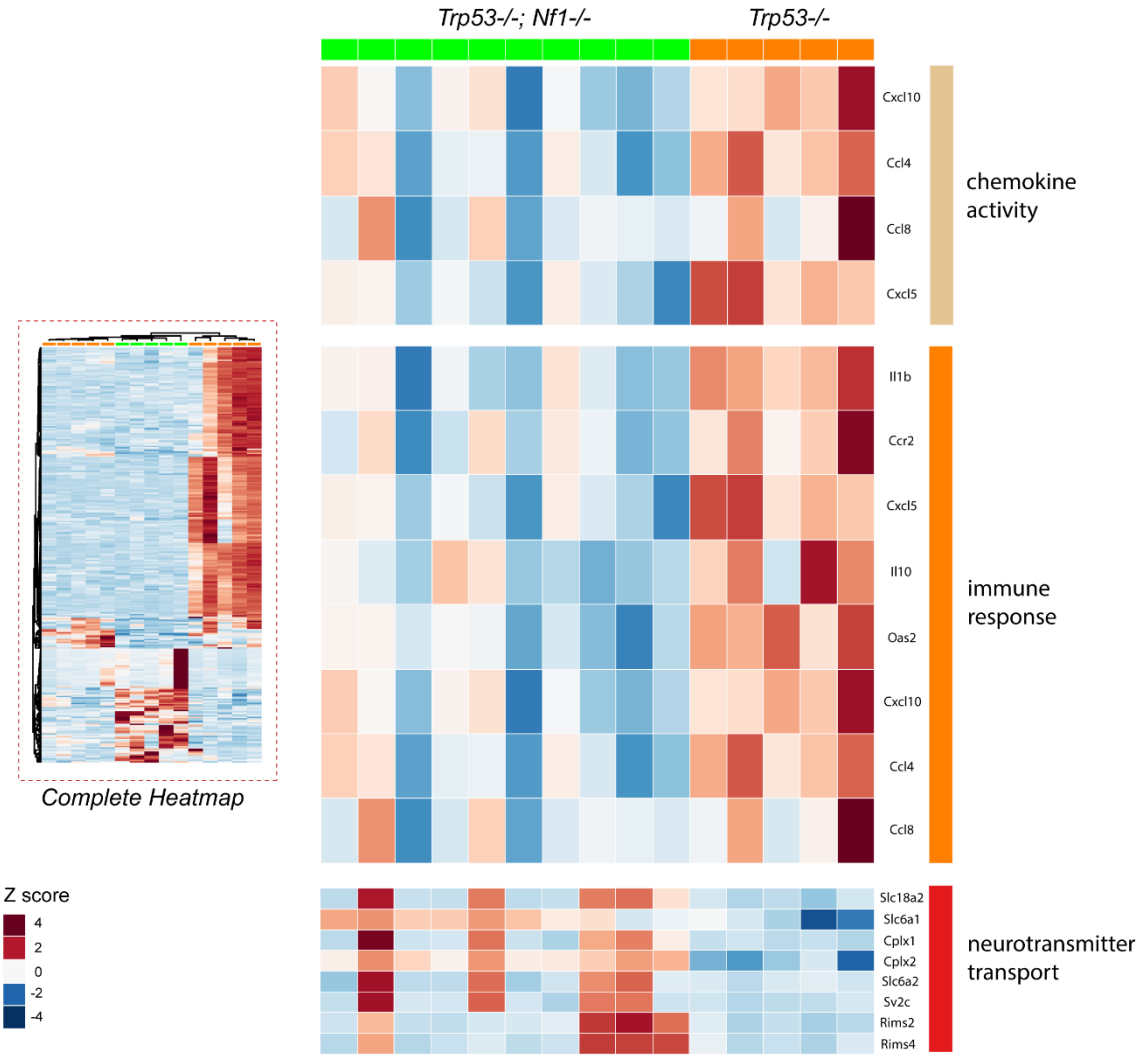

Figure 5.14: RNA sequencing of murine tumours from *Trp53-/-;Nf1-/-* genotype.

Gene expression heat map comparing the *Trp53-/-* and *Trp53-/-;Nf1-/-* groups. Enrichment analysis showing a downregulation of pathways involved in chemokine activity and immune response, and an upregulation in genes involved in neurotransmitter transport in the *Trp53-/-;Nf1-/-* genotype.

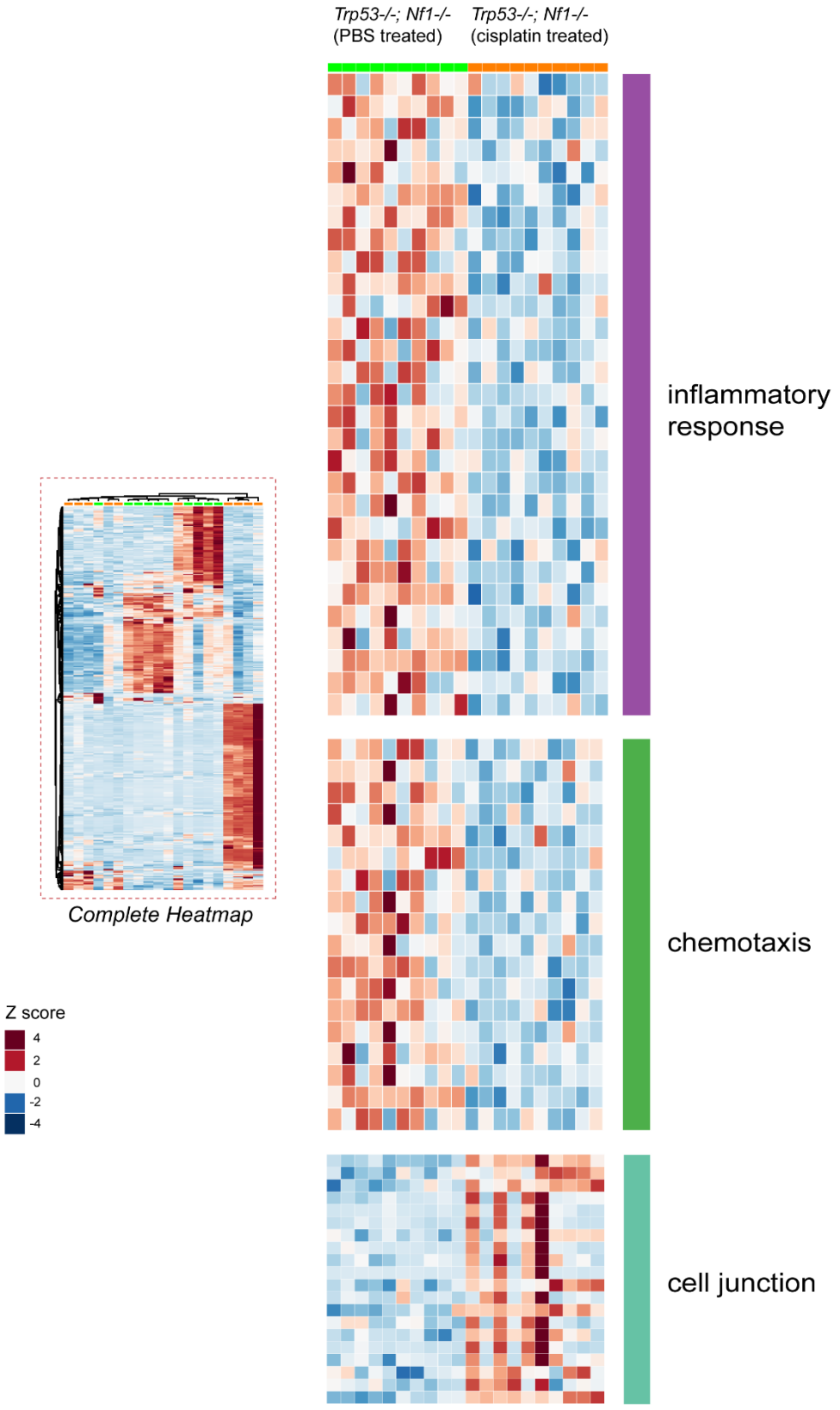

Figure 5.15: RNA sequencing of murine tumours from cisplatin treated *Trp53-/-;Nf1-/-* genotype.
Gene expression heat map comparing *Trp53-/-;Nf1-/-* (PBS treated) and *Trp53-/-;Nf1-/-* (cisplatin treated) samples. Enrichment analysis showing a downregulation of pathways involved in inflammatory response and chemotaxis, and an upregulation in genes involved in the function of the cell junction in the *Trp53-/-;Nf1-/-* (cisplatin treated) samples.

5.5 *Pten* loss

We focussed on the effect of loss of *Pten* and summarised the findings from flow cytometry, cytokine array, RNA seq, RT-qPCR and immunohistochemistry experiments.

Staining of the three TMAs for pAkt (Ser473) showed a significant increase in staining in the *Trp53-/-;Pten-/-* genotype compared to *Trp53-/-* (**). There was also a significant increase in pAkt staining in the *Trp53-/-;Brca2-/-;Pten-/-* genotype compared to *Trp53-/-;Brca2-/-* (****) (Figure 5.16).

An *in vitro* chemokine/cytokine array comparing the *Trp53-/-* and *Trp53-/-;Pten-/-* cell lines following serum starvation showed a significant increase in *Ccl2* and *Ccl7* expression and a significant reduction in *IL16* and *Thpo* expression in the *Trp53-/-;Pten-/-* group (Figure 5.17). These findings were confirmed by performing RT-qPCR on murine tumour samples looking at changes in *Ccl2*, *Ccl7* and *Pten* expression. In the *Trp53-/-;Pten-/-* genotype there was a decrease in *Pten* expression relative to the *Trp53-/-* samples (****) and an increase in *Ccl7* and *Ccl2* expression relative to the *Trp53-/-* samples (****) (Figure 5.17).

RNA sequencing was done on murine tumours from both *Trp53-/-* and *Trp53-/-;Pten-/-* genotypes. The enrichment analysis showed the chemokine activity, immune response, inflammatory response and T cell receptor signalling pathway to be upregulated in the *Trp53-/-;Pten-/-* genotype compared to *Trp53-/-* (Figure 5.18). Upregulated genes in the *Trp53-/-;Pten-/-* genotypes that are involved in the recruitment and function of tumour-associated macrophages include *Ccl2, 5, 8, 9, 17, 22* and *Cxcl9* and *10* and *IL-4* and *αTNF*. Upregulated genes in recruitment and function of myeloid-derived suppressor cells include *Ccl2, 5, 7* and *IL-4* and *αTNF* (Figure 5.18).

Following on from the chemokine/cytokine array and RT-qPCR data, the chemokines *Ccl2* and *Ccl7* from RNA seq analysis were also found to be overexpressed in the *Trp53-/-;Pten-/-* compared to *Trp53-/-* genotype (p=0.46). (Figure 5.18).

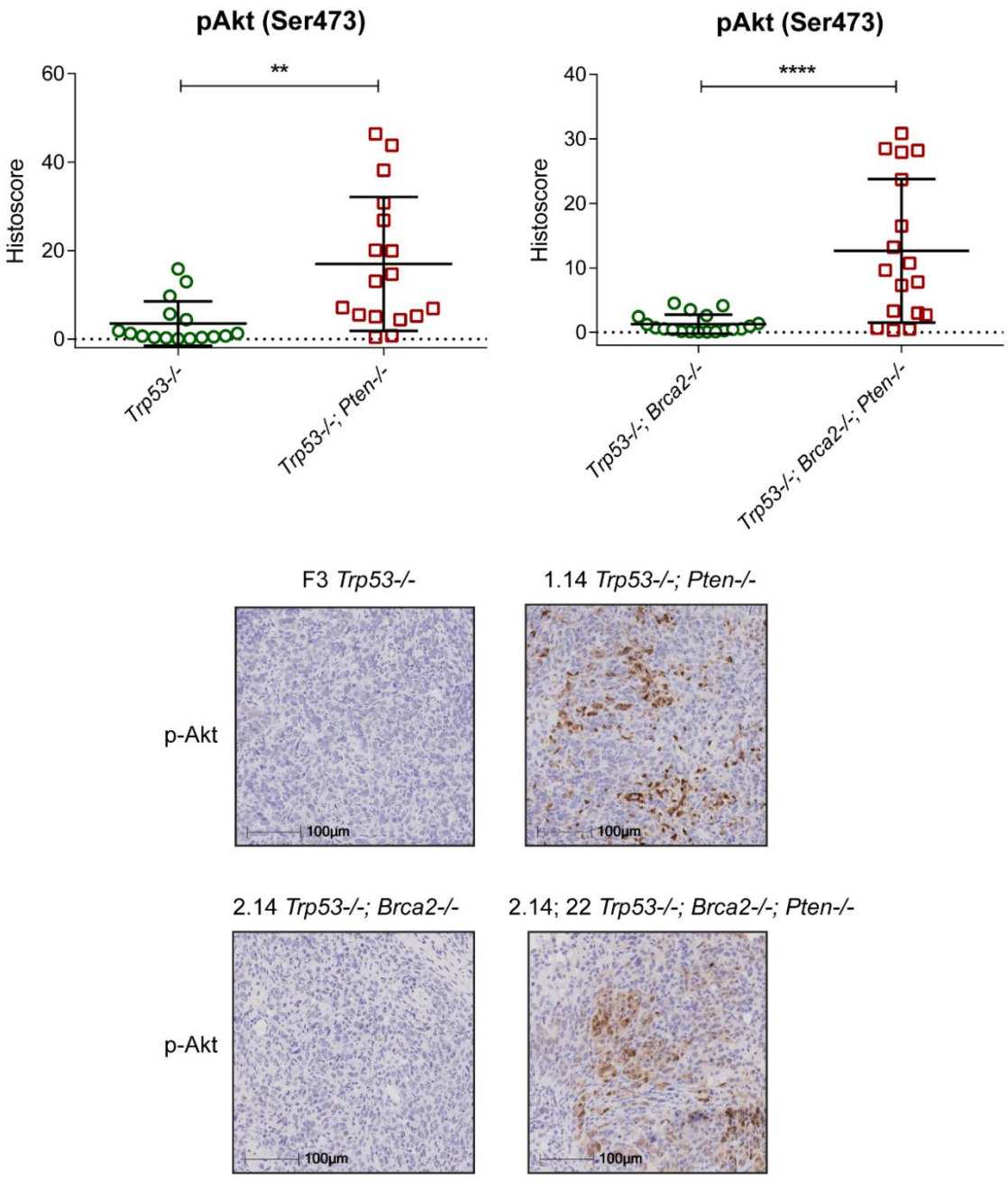

Figure 5.16: Data showing the effect of *Pten* loss.

p-Akt (Ser473) immunohistochemistry showing a significant increase in staining between the *Trp53-/-* and *Trp53-/-;Pten-/-* genotypes (**) and *Trp53-/-;Brca2-/-* and *Trp53-/-;Brca2-/-;Pten-/-* genotypes (****).

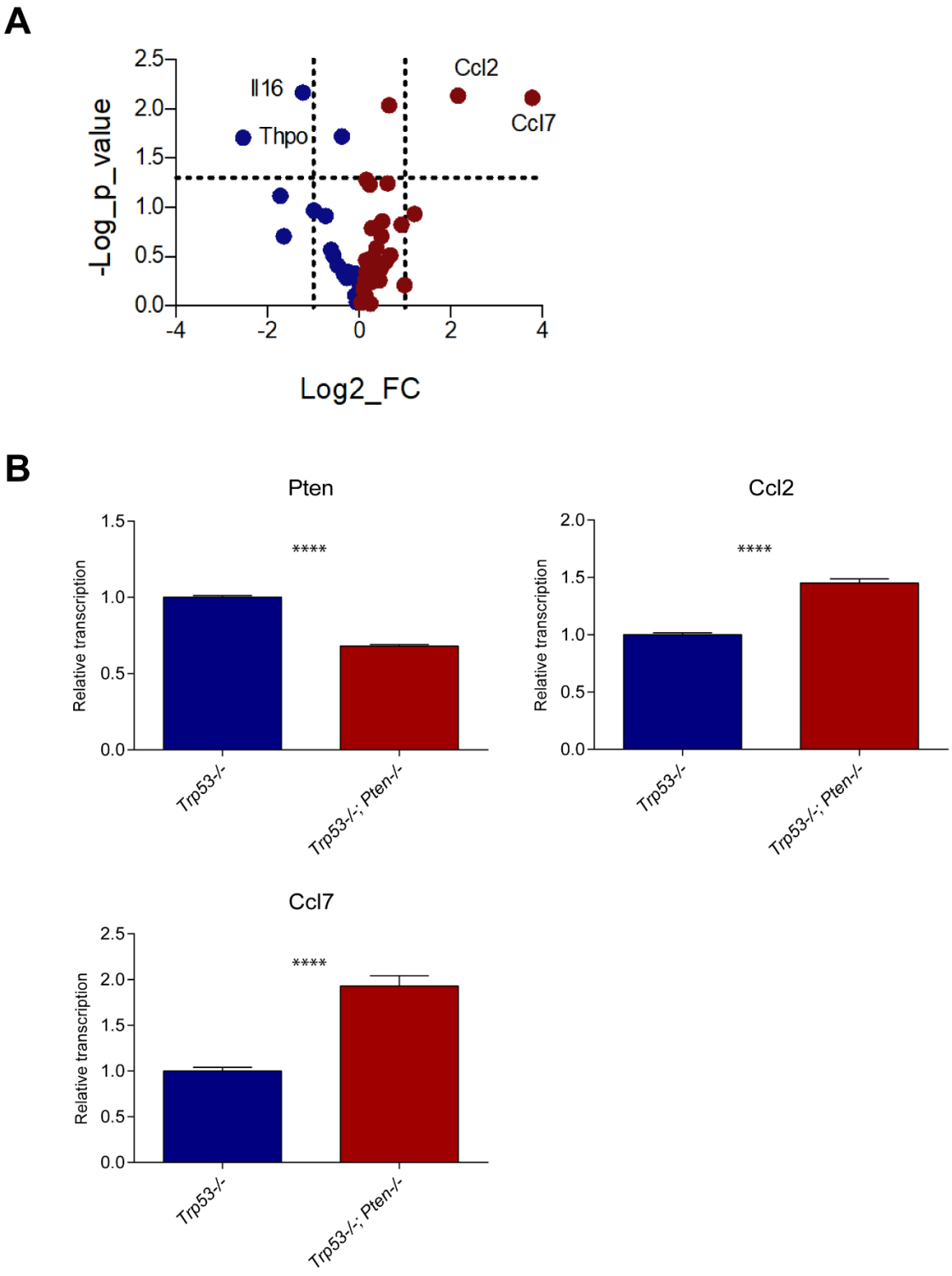

Figure 5.17: Chemokine/cytokine array on cell lines and RT-qPCR on tumour samples.
A, *In vitro* chemokine/cytokine array (performed by Josephine Walton) comparing the *Trp53-/-* vs *Trp53-/-;Pten-/-* cell lines following serum starvation, showing a significant increase in *Ccl2* and *Ccl7* and a significant decrease in *IL16* in the *Trp53-/-;Pten-/-* genotype. **B**, RT-qPCR murine samples comparing the *Trp53-/-* and *Trp53-/-;Pten-/-* genotypes. Values were normalised to *Rpl34*. There was a significant decrease in *Pten* expression relative to the *Trp53-/-* genotype (****) and a significant increase in *Ccl7* (****) and *Ccl2* (****) expression relative to the *Trp53-/-* genotype.

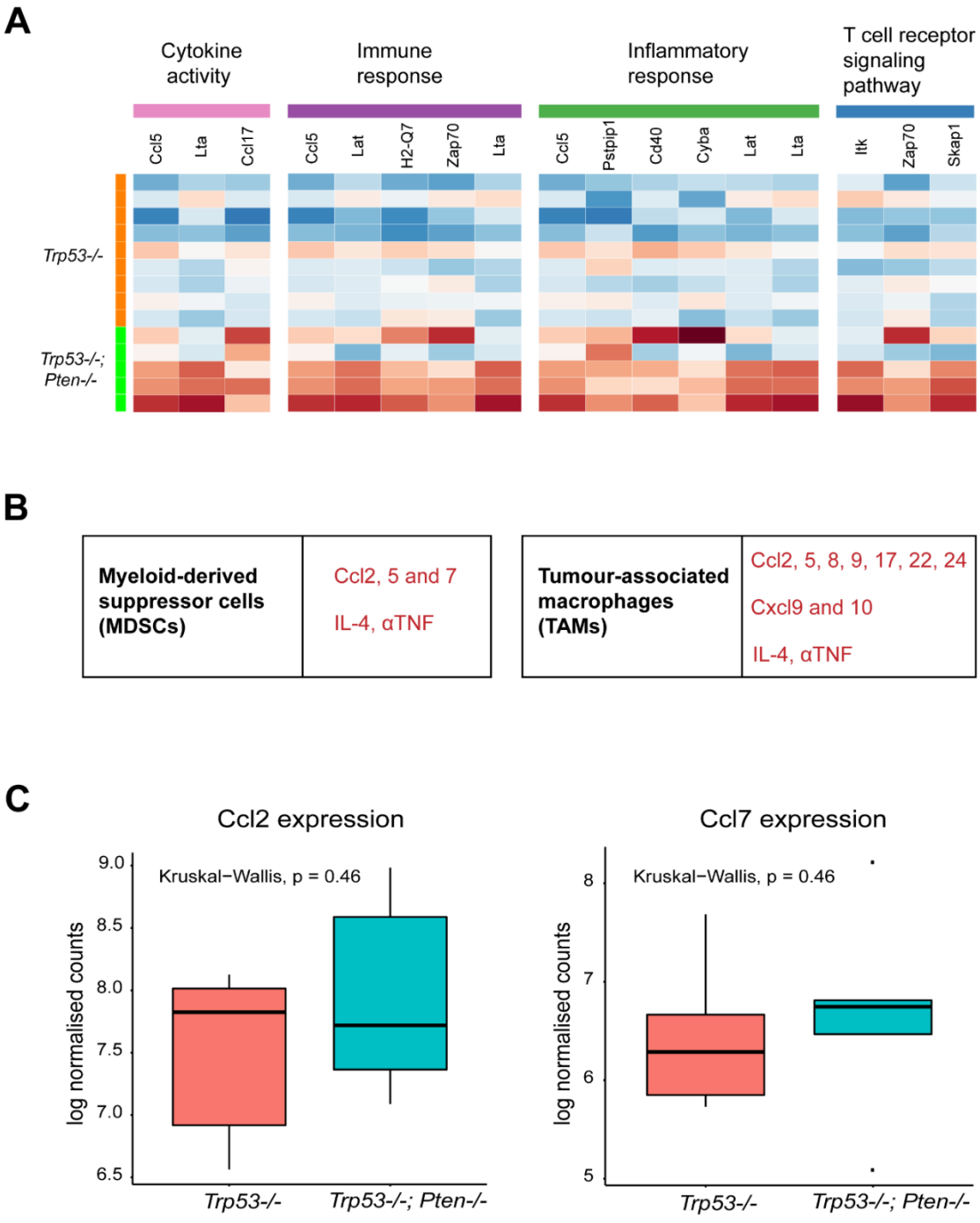

Figure 5.18: RNA sequencing of murine tumours from *Trp53-/-;Pten-/-* genotype

A, Gene expression heat map comparing *Trp53-/-* and *Trp53-/-;Pten-/-* samples and enrichment analysis showing an upregulation of genes involved in chemokine activity, immune response, inflammatory response and the T cell receptor signalling pathway. **B**, Upregulated chemokines/cytokines in the *Trp53-/-;Pten-/-* genotype responsible for recruitment and function of tumour-associated macrophages and myeloid-derived suppressor cells. **C**, *Ccl2* and *Ccl7* expression from RNA seq data showing a non-significant increase in the *Trp53-/-;Pten-/-* genotype.

Flow cytometry analysis of ascites from *in vivo* experiments showed a significant increase in Ly6C+Ly6G+ (Gr-1+) levels in the *Trp53-/-;Pten-/-* genotype compared to *Trp53-/-* (*). In the ascites samples, there was no significant difference in F4/80 levels between the samples (Figure 5.19).

Flow cytometry analysis of tumour samples from fresh *in vivo* experiments showed a significant increase in Gr-1+ levels in the *Trp53-/-;Pten-/-* genotype compared to *Trp53-/-* (**). There was also a significant increase in F4/80 levels in the *Trp53-/-;Pten-/-* samples (**) (Figure 5.19).

Consistent with flow cytometry data of tumour samples, staining of the three TMAs for F4/80 showed a significant increase in F4/80 levels in the *Trp53-/-;Pten-/-* genotype compared to *Trp53-/-* (****). There was also a significant increase in iNOS (M1 marker) (***) and CD206 (M2 marker) (**) staining in the *Trp53-/-;Pten-/-* genotype (Figure 5.20).

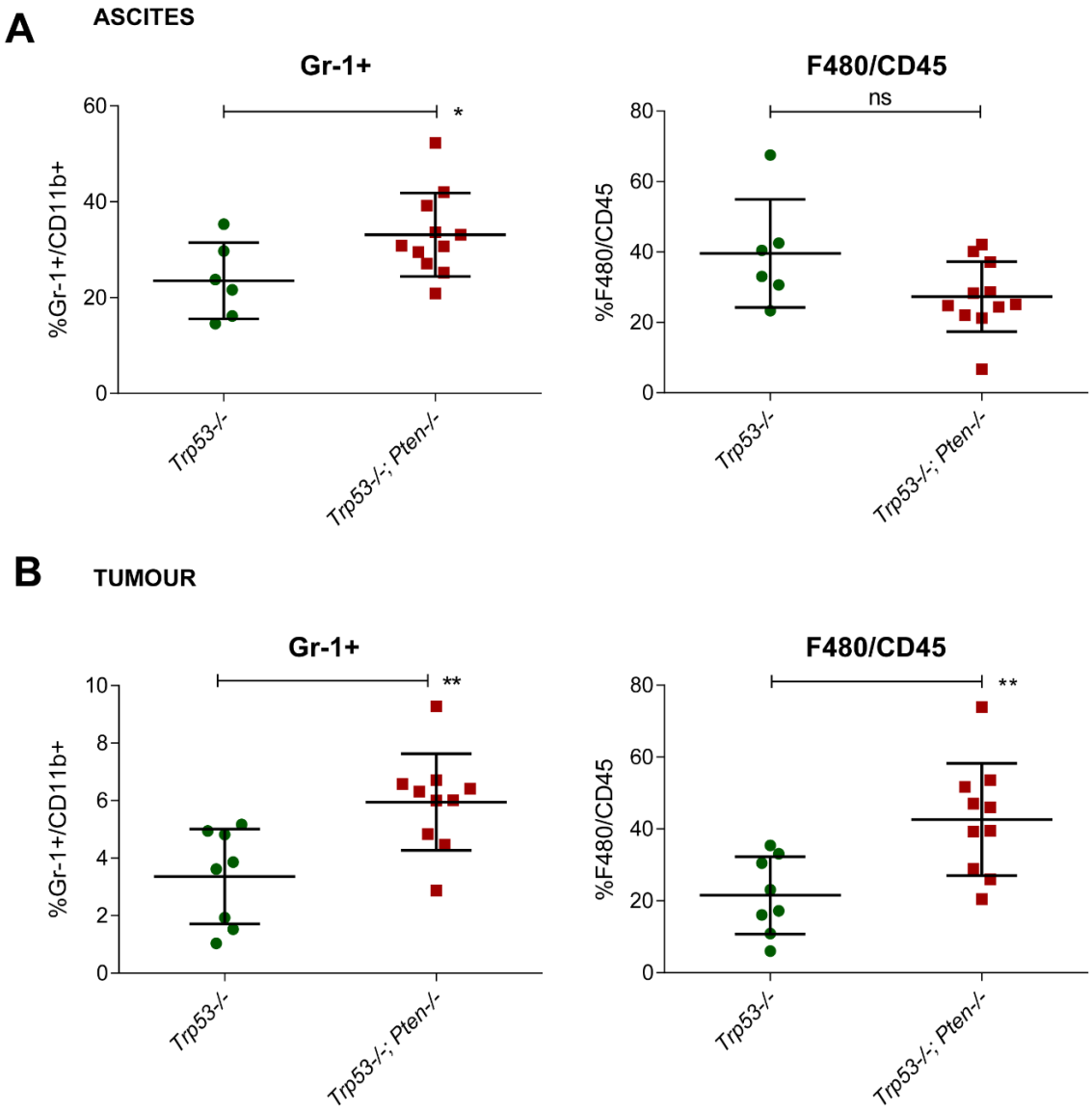

Figure 5.19: Flow cytometry analysis showing the effect of *Pten* loss.

A, Flow cytometry analysis of ascites, showing a significant increase in Ly6C+Ly6G+ (Gr-1+) levels in ascites in the *Trp53-/-;Pten-/-* genotype (*) but no significant difference in F4/80 levels. **B**, Flow cytometry analysis of murine tumour, showing a significant increase in Gr-1+ levels (**) in the *Trp53-/-; Pten-/-* genotype and a significant increase in F4/80 (**). Analysis of tumour samples was performed by Josephine Walton.

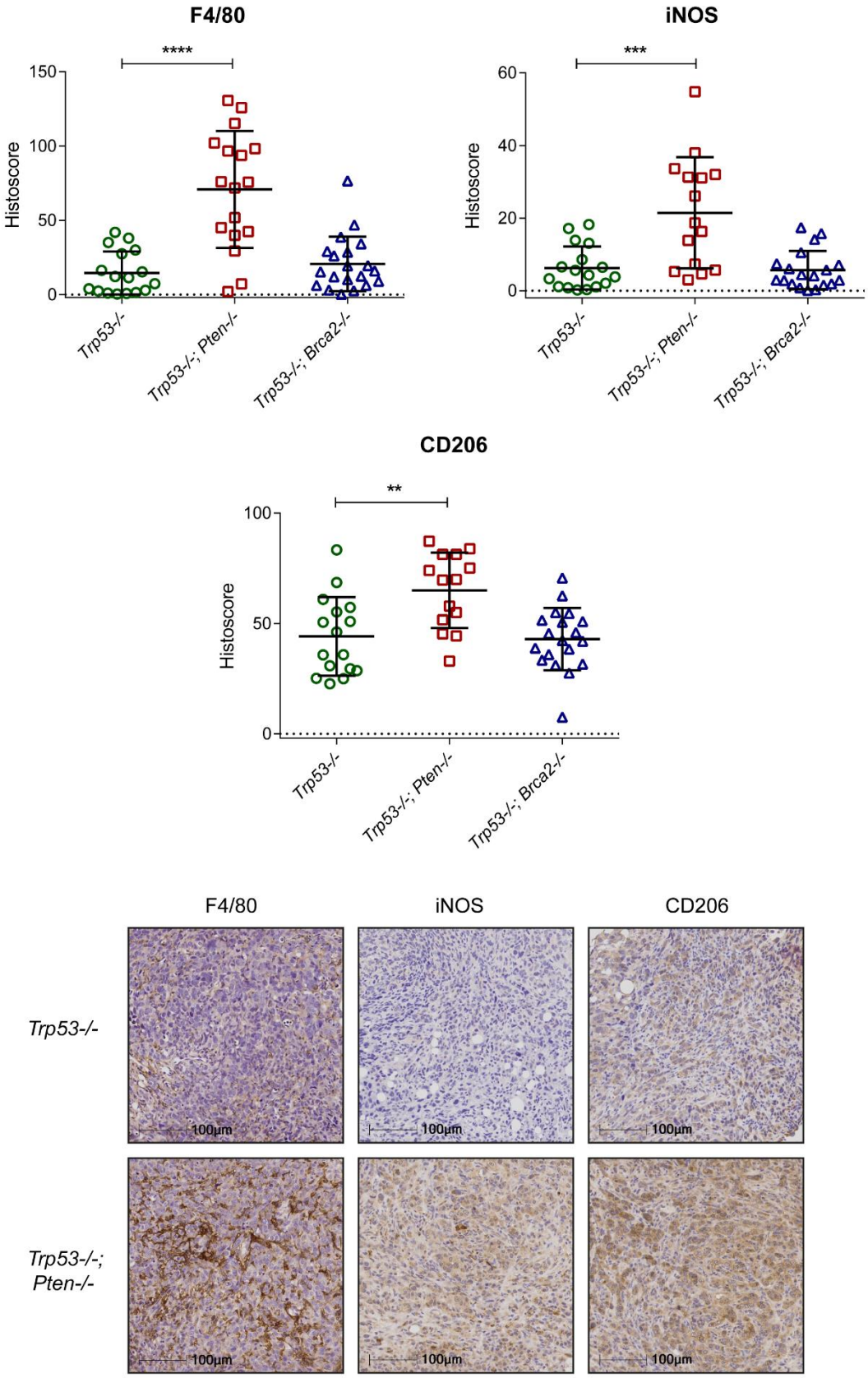

Figure 5.20 Immunohistochemistry of macrophage markers

Immunohistochemistry of TMAs from murine tumours showing a significant increase in F4/80, iNOS (M1-marker) and CD206 (M2 marker) with the loss of *Pten*.

5.6 Discussion

The tumour microenvironment is known to be important in tumour progression with non-malignant cells not only regulating tumour growth but facilitating its metastatic dissemination. In advanced ovarian cancer the widespread dissemination of disease within the peritoneal cavity results in an inflammatory response and the accumulation of ascites (Thibault et al., 2014). Ascites from ovarian cancer patients has been found to contain molecules that promote tumour activity by influencing the proliferation, angiogenesis and metastatic spread (Xu et al., 1995).

Similarly, the microenvironment within the tumour is known to influence disease progression with the presence of intratumoral T cells on immunohistochemistry found to be associated with an improved prognosis in advanced ovarian cancer (PFS HR 0.14, 95% CI 0.08-0.36, p=<0.001) (Zhang et al., 2003).

There is increasing evidence that the tumour microenvironment can be altered following treatment with platinum chemotherapy. Bohm et al showed that neo-adjuvant platinum-based chemotherapy might enhance the host immune response and therefore help to prolong survival (Bohm et al., 2016).

Flow cytometry was performed on ascites from the cisplatin experiment to investigate differences in the tumour microenvironment between genotypes and the influence of cisplatin chemotherapy. Samples were analysed from the *Trp53-/-*, *Trp53-/-;Pten-/-* (negative *in vivo* prognosis) and *Trp53-/-;Brca2-/-* (positive *in vivo* prognosis) genotypes.

From the ascites samples the MDSC monocytic (Ly6C+G-) but not MDSC granulocytic (Ly6C-G+) population was increased in the *Trp53-/-;Pten-/-* genotype and when these two populations were combined (Ly6C+Ly6G+) it was significantly increased compared to the *Trp53-/-* genotype (*). The loss of *Brca2* resulted in significantly lower Ly6C+Ly6G+ levels (**) and a non-significant reduction in CD19+ levels compared to the *Trp53-/-* genotype (Figure 5.3, Figure 5.4 and Figure 5.19).

This shows that the overall MDSC population is increased in the ascites following the loss of *Pten* which is associated with the worst prognosis whereas the MDSC levels were decreased following *Brca2* loss which is the group with the best prognosis. This suggests that the immunosuppressive environment created by increased MDSC levels are having an influence on *in vivo* survival.

Studies have found using transgenic mouse models for melanoma that elevated levels of MDSCs in addition to immunosuppression also stimulate tumourigenesis and tumour growth (Sevko and Umansky, 2013). There is currently no evidence that activation of the PI3K/AKT pathway influences MDSC infiltrates in ovarian cancer. A study by Garcia et al however found that *Pten* deletion in a prostate mouse model resulted in an increased inflammatory response and accumulation of MDSCs (Garcia et al., 2014).

The role of increased B cells (CD19+) in the *Trp53-/-;Brca2-/-* genotype was unclear. Flow cytometry was performed on frozen ascites samples and this may have influenced the granulocytic+ population as subsequent experiments on fresh samples have shown an increase in the *Trp53-/-;Pten-/-* genotype.

The CD3+ levels were significantly increased following cisplatin treatment in the *Trp53-/-;Pten-/-* genotype (*) and there was also a non-significant increase in all other genotypes. The CD8+ levels did not change significantly with cisplatin treatment however the *Trp53-/-;Pten-/-* cisplatin treated group had a significantly higher CD8+ level compared to the *Trp53-/-* cisplatin (*) and *Trp53-/-;Brca2-/-* cisplatin (*) groups (Figure 5.3).

The increase in CD3+ levels after cisplatin treatment is consistent with studies previously mentioned where both Böhm et al and Lo et al found neoadjuvant chemotherapy to be immune stimulatory in tumour samples (Bohm et al., 2016, Lo et al., 2017). A possible explanation for the high CD3+ and CD8+ levels after cisplatin with the loss of *Pten* may be as a counter response to the immunosuppressive environment discussed earlier.

Due to the small number of samples per genotype and variability within each genotype, the PBS treated, and cisplatin treated groups were combined to investigate whether there were any subtle differences in immune infiltrates following cisplatin treatment.

The CD45+, CD11b+, F4/80+, CD3+ and CD8+ populations were significantly increased with cisplatin treatment. The monocytic+ (Ly6C+G-) levels were significantly decreased (****) and granulocytic+ (Ly6C-G+) significantly increased (*) but when combined there was no significant difference in Ly6C+Ly6G+ levels after cisplatin treatment. PDL-1+ expression on CD3 cells was decreased after cisplatin treatment (p=0.05) and significantly decreased on CD19 cells (****) (Figure 5.1 and Figure 5.2).

The overall cisplatin effect found in the ascites samples supports the finding of an enhanced immune response discussed previously and found no difference in the overall MDSC population following treatment. The same studies from Böhm et al and Lo et also found an increase in PDL-1+ expression on T cells as a response to chemotherapy (Bohm et al., 2016, Lo et al., 2017). However, our data showed that PDL-1 was decreased but there were very low levels of CD3+/PDL1 expression in all samples.

The tissue microarrays (TMAs) allowed us to look at the tumour infiltrates within tumour samples. CD3 staining was significantly increased in the *Trp53-/-;Pten-/-* genotype (*) with a non-significant increase in the *Trp53-/-;Brca2-/-;Pten-/-* group. No difference was found in CD3 levels after cisplatin treatment between the genotypes. However, when the PBS and cisplatin groups were combined there was a significant decrease in CD3 staining in the cisplatin group (*) (Figure 5.7).

The CD8a levels were non-significantly increased in the *Trp53-/-;Pten-/-* genotype and significantly increased in the *Trp53-/-;Brca2-/-;Pten-/-* group (*). There were no differences in CD8a levels after cisplatin treatment or when the PBS and cisplatin groups were combined (Figure 5.8).

These results differ from our flow cytometry data of ascites, where no difference was found in CD3 and CD8 levels between genotypes but there was an increase in CD3+ levels across all genotypes and significantly *Trp53-/-;Pten-/-* after cisplatin treatment. The higher levels of CD3 and CD8 in the tumour with the loss of *Pten* may also be a counter response to the immunosuppressive environment. The reduced levels of CD3 in the tumour after cisplatin treatment is not consistent with studies that have suggested that platinum chemotherapy stimulates an immune response.

F4/80 (macrophage marker) staining was significantly increased in *Trp53-/-;Pten-/-* (****), *Trp53-/-;Brca2-/-;Pten-/-* (****) and *Trp53-/-;Nf1-/-* (*) genotypes compared to the *Trp53-/-* group. After cisplatin treatment the F4/80 staining was significantly increased in the *Trp53-/-;Pten-/-* (**), *Trp53-/-;Brca2-/-;Pten-/-* (**) and *Trp53-/-;Nf1-/-* (****) genotypes compared to the cisplatin treated *Trp53-/-* group (Figure 5.9).

When comparing the PBS and cisplatin treated groups, both *Trp53-/-;Pten-/-* (p=0.05) and *Trp53-/-;Brca2-/-;Pten-/-* (**) had a decrease in F4/80 staining after cisplatin treatment. However, the *Trp53-/-;Nf1-/-* genotype had a non-significant increase in F4/80 following cisplatin treatment (Figure 5.9).

This shows that, in addition to changes in the level of MDSCs, there is also a significant increase in tumour-associated macrophages (F4/80) with the loss of *Pten* and the loss of *Nf1*. These two genotypes had the worst *in vivo* survival, and this suggests that the macrophages may contribute to tumour progression (see Chapter 4 – Figure 4.3).

Tumour-associated macrophages have been shown to adopt pro-tumour properties *in vivo* and promote angiogenesis, tumour invasion and motility (Biswas and Mantovani, 2010). Coussens et al also found that TAMs can suppress the T cell response and can therefore lead to an immunosuppressive environment (Coussens et al., 2013). As discussed previously two states of polarised macrophages (M1 and M2) have been recognised both with distinct chemokine/cytokine profiles. M1-type macrophages are thought to inhibit cell proliferation and tissue repair whereas M2-type macrophages are thought to

promote cell proliferation, tissue remodelling and therefore tumour progression (Noy and Pollard, 2014). This is a useful but oversimplified model for classification as macrophages have been shown to adapt to a range of activation states depending on the signals present within the microenvironment (Heusinkveld and van der Burg, 2011).

F4/80 is a pan-macrophage marker and therefore does not differentiate between M1-like and M2-like states.

RNA sequencing of murine tumour samples allowed us to look at the differences between the genotypes and following cisplatin treatment at the transcript level. The *Trp53-/-* expression was reduced in all samples compared to the *Trp53+/+* genotype, which is expected as all samples had a background knockout of *Trp53*. Similarly, *Pten* expression was reduced in the *Trp53-/-;Pten-/-* and *Brca1* expression reduced in the *Trp53-/-;Brca1-/-* genotypes. However, the expression of *Brca2* was increased in the *Trp53-/-;Brca2-/-* and *Nf1-/-* increased in the *Trp53-/-;Nf1-/-* genotypes. A possible reason for this increase in expression is that there is reduced nonsense-mediated decay (NMD) taking place in the cells with *Brca2* and *Nf1* mutations. NMD is an mRNA surveillance pathway that degrades transcripts and the efficiency can vary between cells and between transcripts with some more prone to NMD than others. This can result in a deleterious gain-of-function with a compensatory increase in expression (Lindeboom et al., 2016) (Appendix 2, Appendix 4 and Appendix 6).

The enrichment analysis found that genes involved in cytokine activity, chromosomal stability and DNA binding were upregulated with the loss of *Trp53*. The treatment with cisplatin in the *Trp53-/-* group did not result in a significant up- or down-regulation of genes and therefore it is difficult to make any comment (Figure 5.10).

There was a significant number of genes up- and down- regulated in the *Trp53-/-;Pten-/-* genotype. Enrichment analysis found that in *Trp53-/-;Pten-/-* samples treated with cisplatin there was a downregulation in the immune response and an upregulation in the canonical Wnt signalling pathway. This is consistent with our immunohistochemistry data, which indicated a significant

decrease in CD3+ levels (*) following cisplatin treatment when the PBS and cisplatin groups were combined from all genotypes (Figure 5.7). The activation of the Wnt/ß-catenin pathway has been found to correlate with poor outcomes in HGSOC with a recent study showing that activation of the pathway is a critical driver in chemotherapy resistance (Nagaraj et al., 2015). This offers a possible explanation for the decreased *in vivo* platinum sensitivity with the loss of *Pten* (Figure 5.11).

RNA sequencing data from the *Trp53-/-;Brca1-/-* and *Trp53-/-;Brca2-/-* genotypes was relatively 'bland' with very few up- or downregulated genes compared to *Trp53-/-* and also following treatment with cisplatin. We had expected to find a down-regulation in genes responsible for double-stand DNA repair however it was not possible to perform enrichment analysis on these genotypes due to the limited number of altered genes (Figure 5.12 and Figure 5.13). This could be because both Brca1 and Brca2 have a much narrower activity and are therefore less likely to cause huge changes in overall gene expression. The RNA sequencing analysis included tumour and non-tumour cells so changes in DNA repair genes in tumour may be hard to quantify overall or it could be that the changes in these genes occur at a post-transcriptional level so would only be detected by protein-based assays.

The *Trp53-/-;Nf1-/-* genotype like the *Trp53-/-;Pten-/-* group had a significant number of genes up- and downregulated compared to *Trp53-/-* and also following cisplatin treatment. This is not surprising given that both Pten (PI3K/AKT pathway) and Nf1 (RAS/MAPK pathway) regulate complicated pathways. Enrichment analysis of *Trp53-/-;Nf1-/-* found the chemokine activity and immune response to be downregulated and pathways involved in neurotransmitter transport to be upregulated. This upregulation may be partially explained by the higher level of Nf1 rRNA in the *Nf1-/-* knockouts (Appendix 6). The RNA sequencing findings are the opposite to those found in the *Trp53-/-;Pten-/-* genotype (i.e. increased immune/inflammatory response) and although we previously found an increase in F4/80 with the loss of *Nf1-/-* the immunosuppressive environment may be achieved by a different mechanism to the *Pten* knockouts (Figure 5.14).

Trp53-/-;Nf1-/- samples treated with cisplatin showed a downregulation in the inflammatory response/chemotaxis and upregulation in genes responsible for the function of the cell junction (Figure 5.15). These enrichment findings are similar to the cisplatin treated *Trp53-/-;Pten-/-* samples where we also found from IH data a significant decrease in CD3+ levels after cisplatin treatment.

We focussed on the effect of *Pten* loss and summarised some of the findings that might explain its poor *in vivo* prognosis. Following on from previously published data that confirmed biallelic deletion of *Pten* and an increase in Akt phosphorylation on western blot in the *Trp53-/-;Pten-/-* genotype (Walton et al., 2017) we also showed a significant increase in p-Akt (Ser473) on immunohistochemistry in the *Trp53-/-;Pten-/-* and *Trp53-/-;Brca2-/-;Pten-/-* genotypes confirming the activation of the PI3K/AKT pathway (Figure 5.16).

An *in vitro* chemokine/cytokine array comparing the *Trp53-/-* and *Trp53-/-;Pten-/-* groups showed a significant increase in *Ccl2* and *Ccl7* in the *Trp53-/-;Pten-/-* genotype. This was also confirmed by RT-qPCR and RNA sequencing on murine tumour samples that showed an increase in expression of these cytokines with the loss of *Pten* (****) (Figure 5.17 and Figure 5.18).

Ccl2 has been shown to attract monocytic and granulocytic MDSCs in breast, colorectal and lung cancer and to maintain immunosuppressive activity (Sevko and Umansky, 2013). The recruitment of inflammatory monocytes and tumour-associated macrophages by tumour and stroma have been found to depend on *Ccl2* (Qian et al., 2011, Noy and Pollard, 2014). Studies have shown that inhibiting the CCL2-CCR2 signalling axis decreases the infiltration of TAMs and MDSCs and prolongs the survival in tumour-bearing mice (Qian et al., 2011, Zollo et al., 2012).

Ccl7 has been reported to be involved in monocytic recruitment with studies showing an important role for the chemokine in enrichment of MDSC in an *in vivo* colon cancer model (Sevko and Umansky, 2013, Ichikawa et al., 2011). The same study also showed that a reduction in *Ccl7*, *Ccl5* and *Cxcl1* and MDSC infiltration was associated with a significant reduction in tumour growth and metastasis (Ichikawa et al., 2011).

RNA sequencing was performed on the *Trp53-/-;Pten-/-* tumours. Enrichment analysis showed an upregulation in chemokine activity, inflammatory response and the T cell receptor signalling pathway compared to *Trp53-/-*. Upregulated genes in the *Trp53-/-;Pten-/-* tumours that are involved in the activity of tumour-associated macrophages and myeloid-derived suppressor cells were identified and summarised in Figure 5.18. These included *Ccl2, 5, 8, 9, 17, 22* and *Cxcl9* and *10* and *IL-4* and *TNFa* involved in tumour-associated macrophage function and *Ccl2, 5, 7* and *IL-4* and *TNFa* involved in myeloid-derived suppressor cell function.

As mentioned previously, *Ccl2* and *Ccl7* have been shown to influence MDSC infiltration but *Ccl5* has been found to be important in both MDSC recruitment and macrophage differentiation (Ugel et al., 2015). *IL-4* contributes to an immuno-suppressive phenotype by supporting the survival of both TAMs and MDSC (Ugel et al., 2015). *IL-4* activation of macrophages with the help of T_H2 cells induces the polarisation to M2-like macrophages (Coussens et al., 2013, Gocheva et al., 2010), whereas TNFα has been shown to mediate the generation of highly suppressive MDSCs from PBMCs and induce the polarisation to M1-like macrophages (Lechner et al., 2010, Mills, 2012).

In addition to *Ccl2*, *Ccl5* and *Ccl9* are known to recruit immature myeloid cells and been found to be expressed on tumour-associated macrophages (Kitamura et al., 2010, Liou et al., 2013). The polarisation of macrophages is guided by the surrounding cytokines. M1 and M2 macrophages promote T_H1 and T_H2 response respectively (Mills, 2012). Polarising chemokines that have been found in multiple studies to favour polarisation to M1-like macrophages include *Cxcl9*, *10* and *Ccl8* and those favouring polarisation to M2-like macrophages include *Ccl17, Ccl22, Ccl24* (Martinez et al., 2006, Biswas and Mantovani, 2010).

Flow cytometry analysis from both ascites and tumour showed a significant increase in MDSCs (Ly6C+Ly6G+) in ascites and tumour with the loss of *Pten*. There was also a significant increase in tumour F4/80 levels in the *Trp53-/-;Pten-/-* genotype from flow cytometry and immunohistochemistry analysis (Figure 5.19). Immunohistochemistry analysis showed a significant increase in

iNOS (M1-like marker) and CD206 (M2-like marker) staining in the same genotype but with no evidence of favouring an M2-like state (Figure 5.20). However, to confidently determine macrophage polarisation, analysis by flow cytometry or IHC staining for multiple markers is required.

These findings support the hypothesis that the loss of *Pten* and activation of the PI3K/AKT pathway leads to an immunosuppressive microenvironment that helps to drive tumour progression and impact survival. The environment is altered by specific chemokine/cytokine responses that result in increased levels of MDSC and tumour-associated macrophages. The macrophages are likely to be skewed towards an M2-like phenotype that encourages tumour growth and invasion.

In summary, data in this chapter show that the tumour microenvironment is different between genotypes and can be altered with the addition of platinum chemotherapy. The cisplatin effect was not necessarily the same in the ascites and tumour samples as evidenced by different levels of CD3/CD8. The subtle changes within the microenvironment offer potential explanations for differences in *in vivo* survival between the genotypes.

We decided to focus on *Pten* loss as this offered an exciting therapeutic target that could potentially have an impact clinically. The next step was to attempt to reverse the effect of *Pten* by targeting the chemokine/cytokine receptors and PI3K/AKT pathway.

6 Reversing the effect of *Pten* loss

6.1 Introduction

PTEN is a phosphatase that acts as a tumour suppressor. A deletion or loss of function mutation of *PTEN* results in the activation of the PI3K/AKT pathway that can lead to increased proliferation and cell growth. TCGA and ICGC data suggest the loss of *PTEN* to be a common event in HGSOC with up to 36% of tumours demonstrating at least heterozygous *PTEN* loss (Martins et al., 2014, Patch et al., 2015).

Loss of *PTEN* is a negative prognostic factor with a recent study showing the loss or downregulation of *PTEN* to be strongly associated with a worse overall survival (Martins et al., 2014). The activation of the PI3K/AKT pathway in ovarian cancer has also been associated with chemotherapy resistance in several studies (Kolasa et al., 2009, Yang et al., 2008).

As described in the previous chapters, we found that the knockout of *Pten* was associated with a poor prognosis in an *in vivo* model. We also showed that there were significant changes in the tumour microenvironment with increased levels of MDSCs and TAMs (see Chapter 4 and 5).

There are a broad range of drugs and potential targets that we could have used to attempt to reverse the effect of *Pten*. Isoform-specific PI3K inhibitors (e.g. p110α and p110β) have been shown in clinical trials to have fewer toxicities and result in a more complete inhibition of the PI3K/AKT pathway compared to pan-class I PI3K inhibitors (Furman et al., 2014). There is also evidence in *PTEN*-mutant tumours that p110α activity is suppressed and the PI3K pathway is driven by p110ß (Schwartz et al., 2015).

We decided to target both the cytokine/chemokine response directly by using a transgenic mouse model and the PI3K/AKT pathway by using a PI3K inhibitor p110ß. This chapter describes these two *in vivo* experiments to reverse the effect of *Pten*.

6.2 GGTACKO *in vivo* pilot experiment

A pilot experiment using only 17 mice was performed to establish whether this transgenic mouse model influenced the tumour microenvironment in the *Trp53-/-;Pten-/-* genotype and, if so, whether this altered the survival. The GGTACKO mice, which are on a C57Bl/6n background, have constitutive knockout of CCR1, 2, 3 and 5. These encode the chemokine receptors CCR1, 2, 3 and 5, which in turn are the receptors for a wide variety of chemokines, including *Ccl2* and *Ccl7* that were shown in the last chapter to be upregulated in *Trp53-/-;Pten-/-* ID8 cells and tumours.

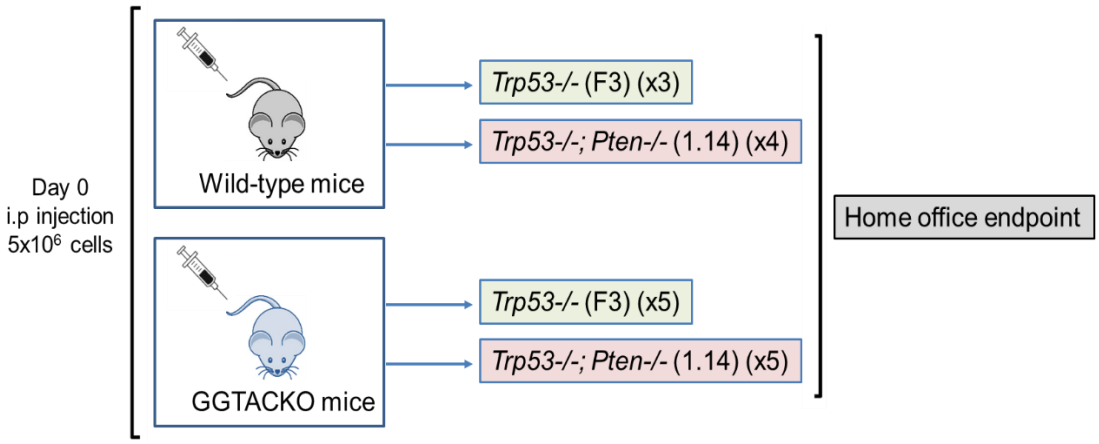

Figure 6.1: Outline of the GGTACKO *in-vivo* experiment.

GGTACKO mice were used to investigate the effect of knocking out CCR1, 2, 3 and 5 receptors on the tumour microenvironment. The C57BL/6n WT or KO (female) mice were injected i.p with $5x10^6$ cells of either the *Trp53-/-* or *Trp53-/-;Pten-/-* genotype. The mice were then taken at the Home office endpoint.

6.2.1 Survival

The 17 mice were injected intraperitoneally as described above (Figure 6.1). 7 wild-type mice were used, 3 injected with the *Trp53-/-* (F3) genotype and 4 injected with the *Trp53-/-;Pten-/-* (1.14) genotype. 10 knockout mice were used, 5 injected with *Trp53-/-* (F3) and 5 with *Trp53-/-;Pten-/-* (1.14) genotype. The mice were monitored daily and killed when they reached UK Home Office limits.

Both the wild-type and knockout mice injected with F3 (*Trp53-/-*) had a median survival of 53 days. The wild-type mice injected with 1.14 (*Trp53-/-;Pten-/-*)

had a median survival of 32 days compared to a median survival of 36 days in the knock-out mice injected with the 1.14 cell line (Figure 6.2 and Table 6.1); however, this difference was not significant.

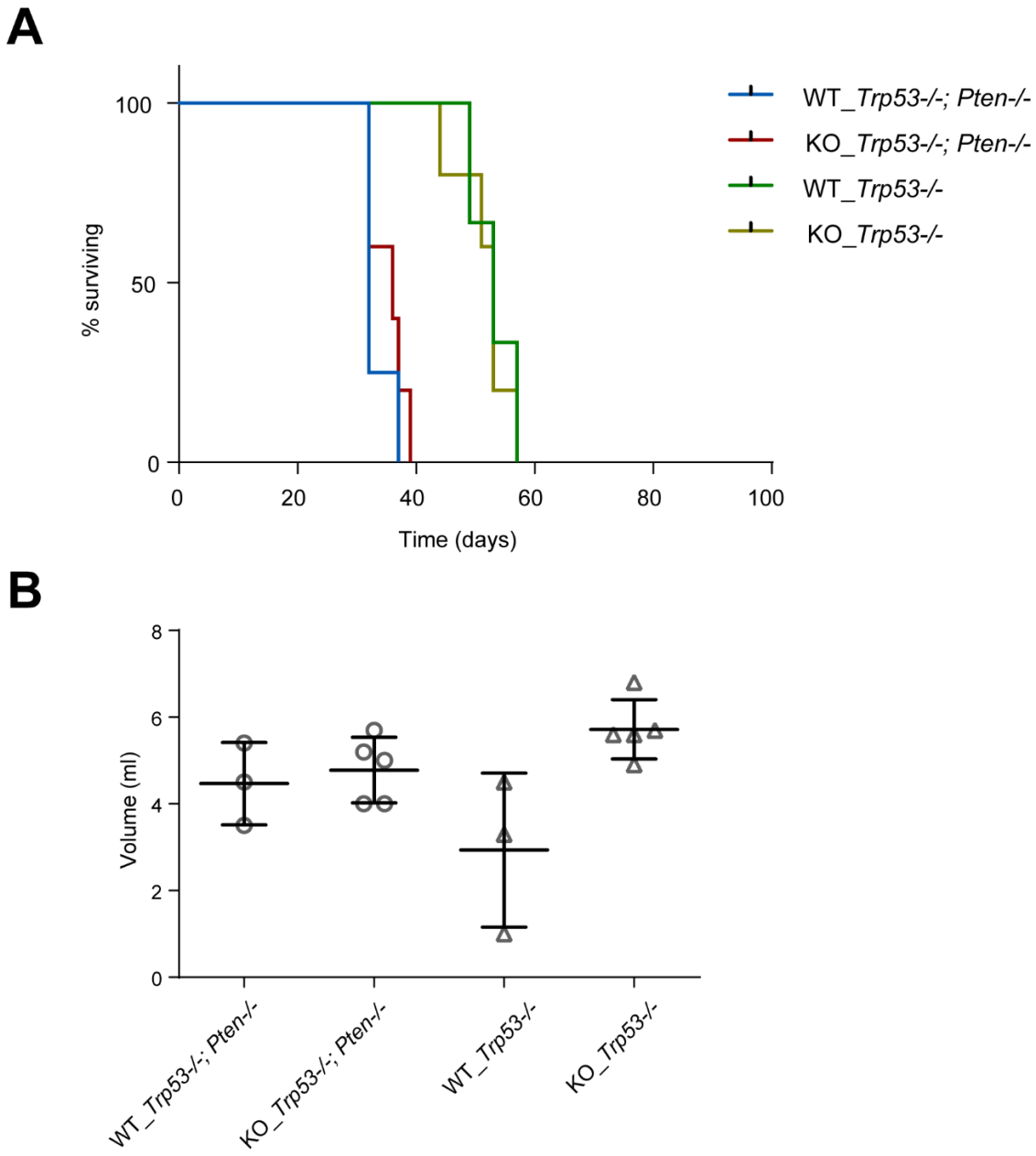

Figure 6.2: *In vivo* GGTACKO experiment showing the survival and ascites volumes

A, Kaplan-Meier survival curves comparing the WT and KO mice with either *Trp53-/-* or *Trp53-/-;Pten-/-* cell lines injected with the median survival (days) **B**, Ascites volumes from the different genotypes and WT/KO mice.

Table 6.1: GGTACKO Median Survival

Genotype	Median survival (days)
WT_*Trp53*-/-;*Pten*-/-	32
KO_*Trp53*-/-;*Pten*-/-	36
WT_*Trp53*-/-	53
KO_*Trp53*-/-	53

Ascites volumes between the different groups were similar however, there were significantly lower volumes in the WT_*Trp53*-/- group compared to the KO_*Trp53*-/- group (*) (Figure 6.2).

6.2.2 Flow cytometry

Flow cytometry analysis was performed on the fresh ascites and tumour samples using the same 12 antibody panel used previously (see Methods – Table 2.5).

There was no obvious difference in CD11b+ and F4/80 levels in the ascites samples between the different genotypes and between the wild-type and knock-out mice. The Ly6C+Ly6G+ (Gr-1+) levels appeared to be higher in the WT and KO mice injected with the *Trp53*-/-;*Pten*-/- cell line compared to the *Trp53*-/- genotype (Figure 6.3).

In the tumour samples, the F4/80, CD11b+ and Ly6C+Ly6G+ levels were higher in the WT mice injected with *Trp53*-/-;*Pten*-/- (1.14) with lower levels in the mice injected with *Trp53*-/- (F3). Although there was only one mouse tumour sample, there appeared to be a reduction in F4/80, CD11b+ and Ly6C+Ly6G+ levels in the *Trp53*-/-;*Pten*-/- tumours in the knockout mouse compared to the WT mice (Figure 6.3).

Due to the limited number of mice used for the experiment, statistical analysis was not performed to compare any differences.

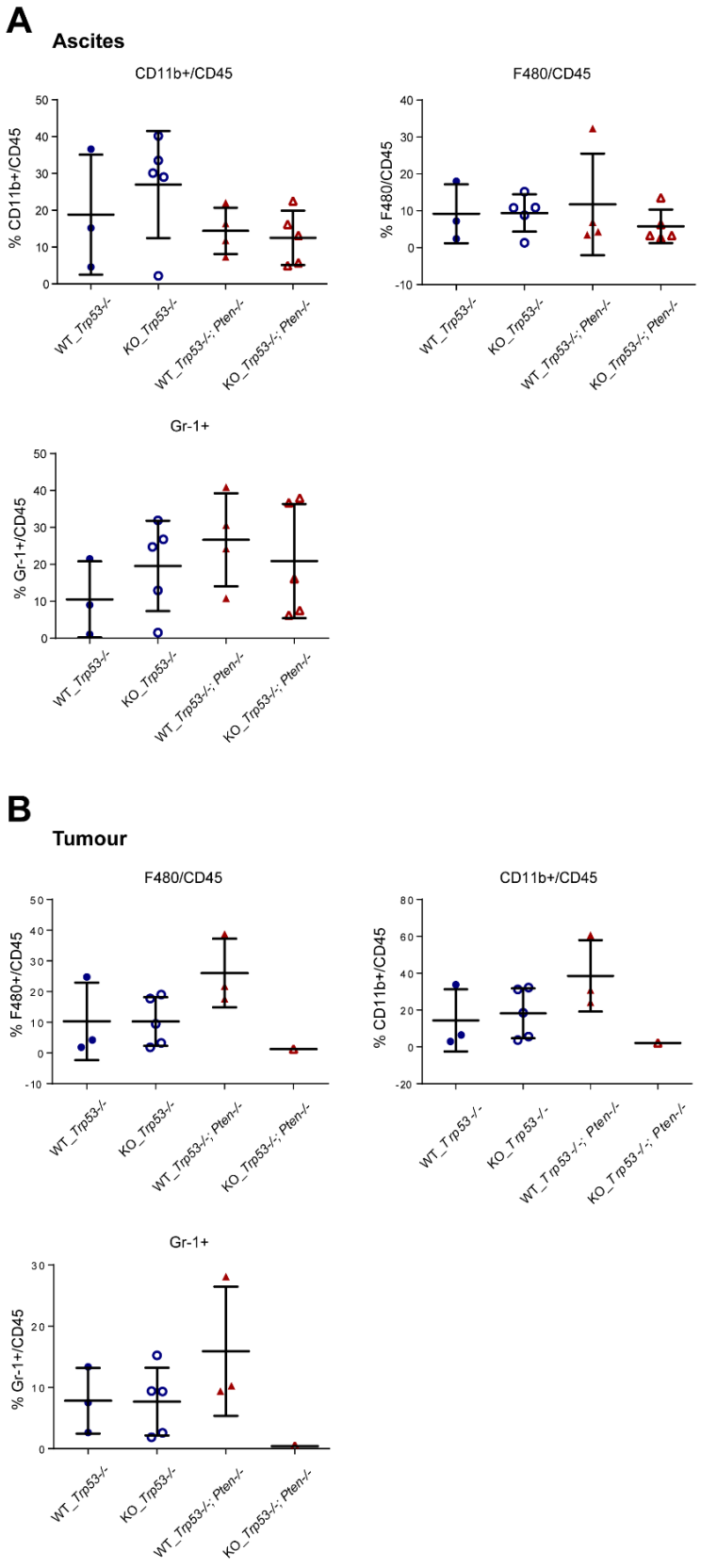

Figure 6.3: Flow cytometry analysis of ascites and murine tumour from the GGTACKO pilot experiment.
A, Ascites samples showing a higher level of Ly6C+Ly6G+ (Gr-1+) in the *Trp53-/-;Pten-/-* genotypes in both WT and KO mice. **B**, Tumour samples showing a higher level of CD11b+, F4/80 and Gr-1+ in the *Trp53-/-;Pten-/-* genotype in the WT mice compared to the KO mouse.

6.2.3 Full blood count

A full blood count was taken from each mouse once they had reached the Home Office endpoint. The HGB (haemoglobin), PLT (platelets) and NEUT:LYMPH ratio data are summarised in Figure 6.4. The WT and KO mice injected with the *Trp53-/-;Pten-/-* genotype had lower levels of HGB compared to the mice injected with the *Trp53-/-* cell line. There did not appear to be any difference in HGB levels between the wild-type and knockout mice (Figure 6.4).

There was no obvious difference in platelet levels between the WT and KO mice and the different genotypes.

The NEUT:LYMPH ratio showed a trend towards a higher level in the WT and KO mice injected with *Trp53-/-;Pten-/-* compared to those injected with the *Trp53-/-* genotype. There was also no obvious difference between the wild-type and knockout mice (Figure 6.4).

Statistical analysis was not performed to compare any differences again due to the limited number of mice used.

6.2.4 Immunohistochemistry

The GGTACKO murine tumours were stained for pAkt (Ser473), F4/80, iNOS and CD206. There was a significant increase in pAkt staining between the WT_*Trp53-/-* and WT_*Trp53-/-;Pten-/-* genotypes (*) and between the KO_*Trp53-/-* and KO_*Trp53-/-;Pten-/-* genotypes (**). There was no significant difference in F4/80, iNOS and CD206 levels between the wild-type and knockout mice and between different genotypes (Figure 6.5).

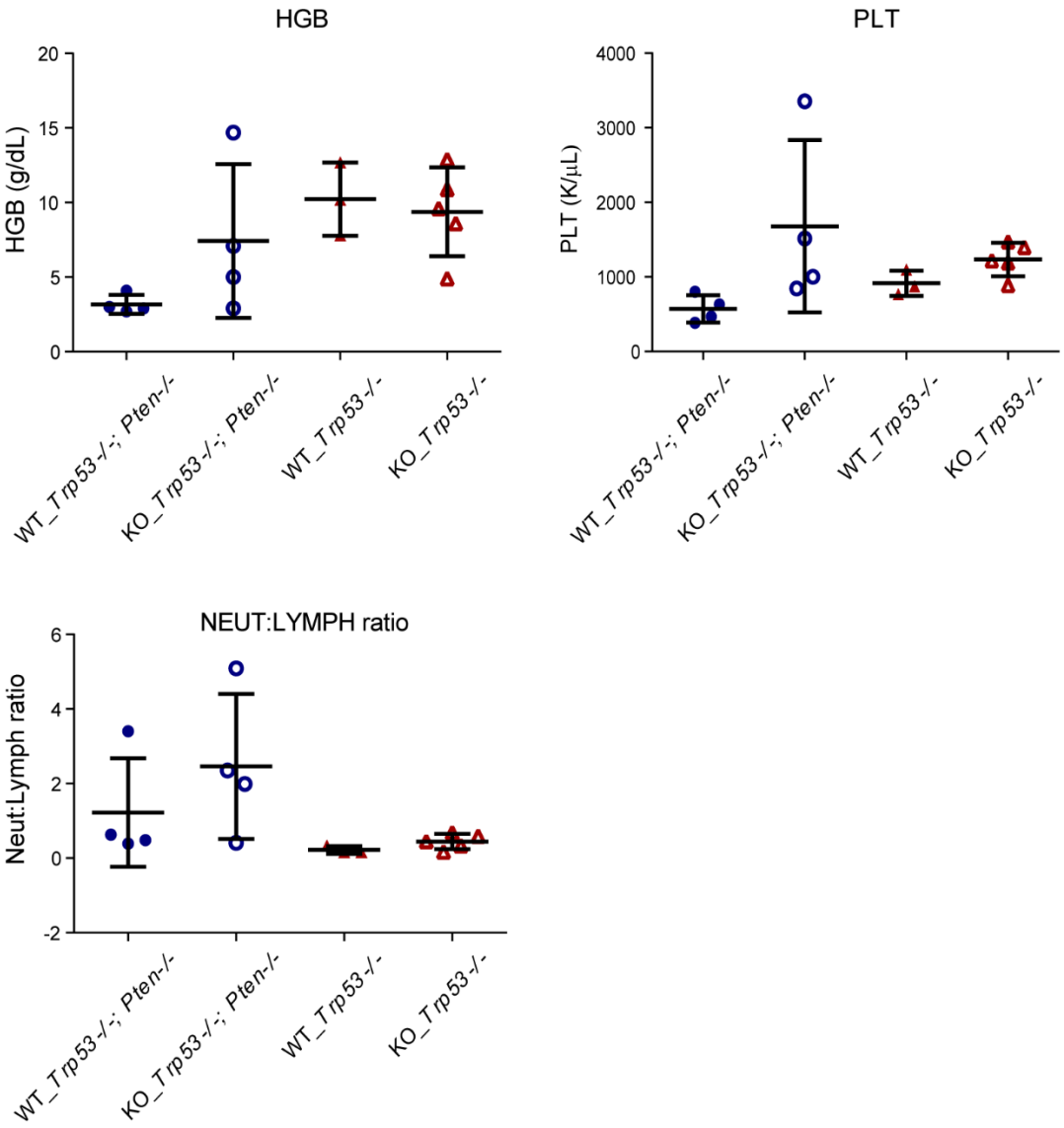

Figure 6.4: Full blood counts (FBC) from the GGTACKO mice.

The HGB (haemoglobin) is reduced in the 1.14 *Trp53-/-;Pten-/-* compared to the F3 *Trp53-/-* genotype. No obvious difference in platelets is observed and an increase is shown in the NEUT:LYMPH ratio in the 1.14 *Trp53-/-;Pten-/-* genotype.

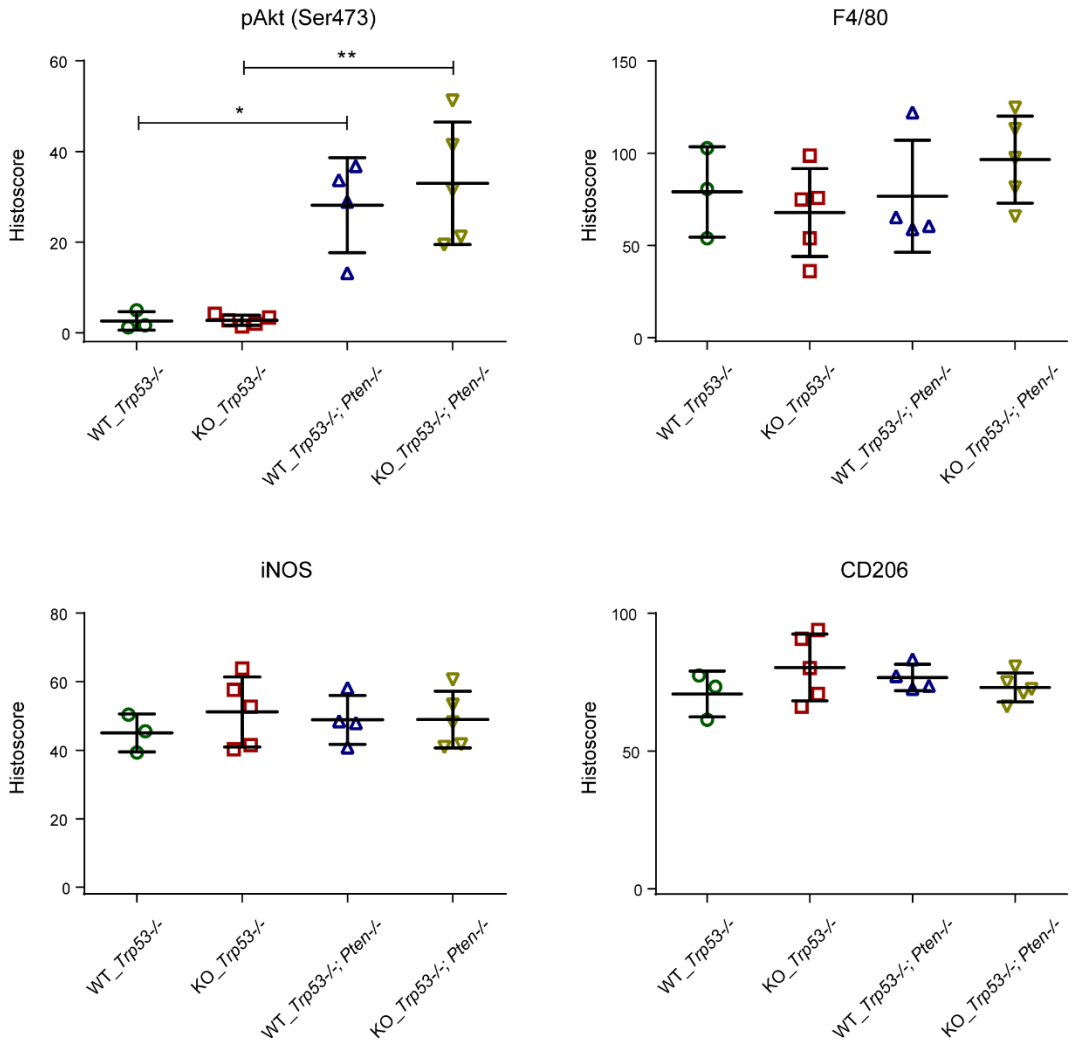

Figure 6.5: Immunohistochemistry from the GGTACKO pilot experiment

Immunohistochemistry from murine tumours showing a significant increase in pAkt in the *Trp53-/-;Pten-/-* in both the wild-type and knockout mice but no obvious difference in F4/80, iNOS (M1-marker) and CD206 (M2 marker) levels.

6.3 AZD8186 *in vivo* experiment

AZD8186 is a small molecule that selectively inhibits PI3Kβ signalling. It has been shown to reduce p-AKT (Ser473) levels and inhibit tumour growth in breast and prostate *in vivo PTEN*-null models (Hancox et al., 2015).

The aim of this initial experiment was to block the activated PI3K/AKT pathway in our *Pten* knockout cell lines and therefore reverse the changes we have previously described in the tumour microenvironment.

The injection and treatment protocol are described in the Methods section (Chapter 2, 2.7.3 and Figure 6.6).

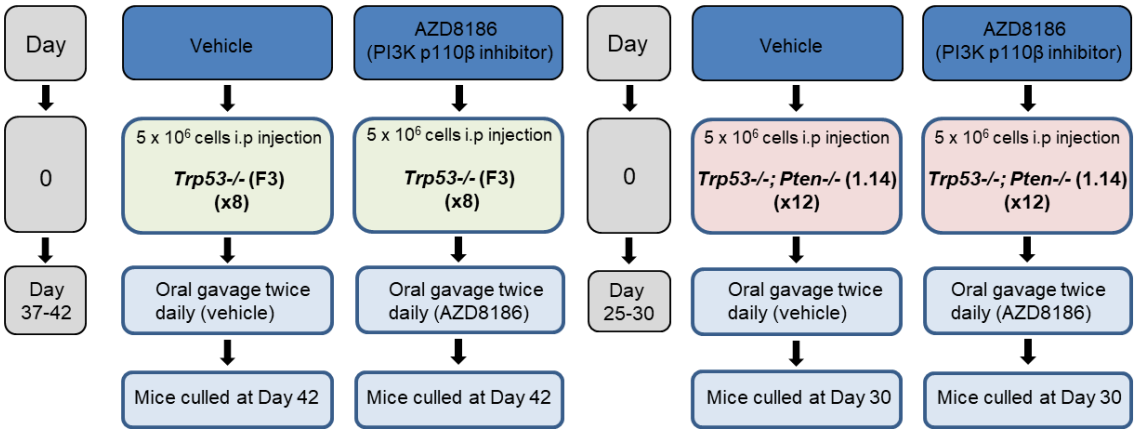

Figure 6.6: Outline of the AZD8186 *in vivo* experiment.

A p110β PI3K inhibitor (AZD8186) was used to block the PI3K/AKT pathway and attempt to reverse the *Pten* effect. C57BL/6 (female) mice were injected i.p with 5x10^6 cells of either the F3 (*Trp53*-/-) or 1.14 (*Trp53*-/-;*Pten*-/-) cell lines. The F3 mice were treated by twice daily oral gavage with either the control (0.5% hydroxyl-propyl-methycellulose + 0.1% tween-80) or AZD8186 from days 37 to 42 and then culled on day 42. The 1.14 mice were treated on days 25 to 30 and then culled on day 30.

The next step was to perform *in vitro* experiments to optimise the AZD8186 drug prior to under taking the *in vivo* experiment.

6.3.1 Optimisation of drug

The *in vitro* optimisation experiments were performed by Josephine Walton (post-doc). The 1.14 *Trp53-/-;Pten-/-* cell line was treated with the AZD8186 drug to determine the optimal concentration required to inhibit the PI3K/AKT pathway. The cells were serum starved overnight and treated for 2 hours in serum-free medium with a range of drug concentrations (10, 100, 250, 500, 1000nM). A western blot showed the minimum concentration required to prevent Akt (Ser473) phosphorylation was 100nM (Figure 6.7).

A time course showed that cells treated with 250nM of AZD8186 had a reduced expression of p-Akt for 2 hours but by 4 hours the expression was back to pre-treatment levels. This corresponded with RT-qPCR data that showed a reduction in *Ccl2* and *Ccl7* levels until 2 hours after treatment, after which there was a steady increase until back to pre-treatment levels after 24 hours (Figure 6.7).

A dose of 50mg/kg of AZD8186 had been previously published *in vivo* and showed pathway inactivation with no adverse toxicity (Hancox et al., 2015). I therefore used this dose for the *in vivo* experiment.

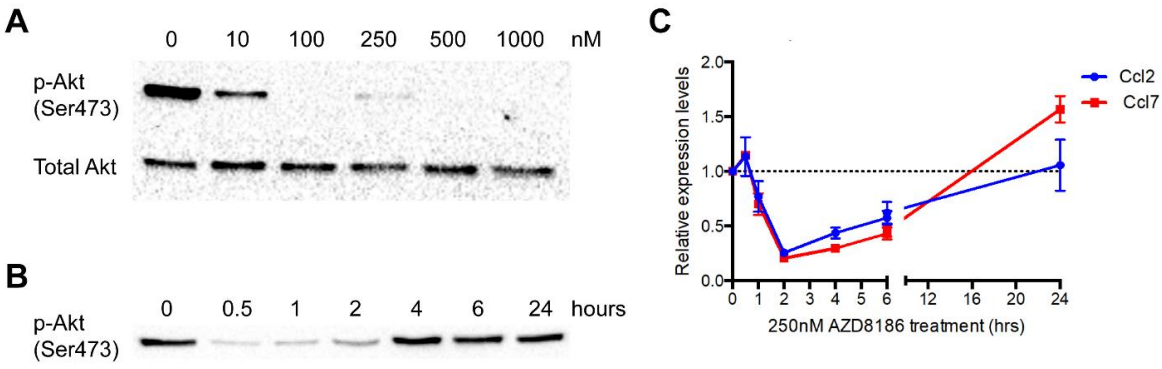

Figure 6.7: *In vitro* optimisation of the AZD8186 drug.

This experiment was performed by Josephine Walton (post-doc).
A, Western blot showing absent p-Akt (Ser473) expression after overnight serum-starvation and 2hrs treatment with AZD8186 (100nM) in the 1.14 cell line. **B,** A time course showing reduced p-Akt expression up until 4 hours on western blot after 2hrs treatment of the 1.14 cell line with AZD8186 (250nM). **C,** RT-qPCR showing the time course of expression of *Ccl2* and *Ccl7* following treatment with AZD8186 (250nM) relative to time 0.

6.3.2 Flow cytometry

Flow cytometry analysis was performed on the fresh ascites and tumour samples using the same 12 antibody panel used previously in the GGTACKO pilot experiment.

In the ascites samples, there was no obvious difference in the F4/80 levels in between the different genotypes and treatment groups. There was a non-significant increase in the Ly6C+Ly6G+ level in the 1.14 (*Trp53*-/-;*Pten*-/-) (control) compared to the F3 (*Trp53*-/-) (control) group. There was a non-significant decrease in Ly6C+Ly6G+ levels between the control and AZD8186 mice injected with F3 however there was a significant decrease in levels between the control and AZD8186 treated mice injected with 1.14 (***) (Figure 6.8).

In the tumour samples, there was again no obvious difference in the F4/80 levels between the different genotypes and treatment groups. There was a significant increase in the Ly6C+Ly6G+ level in the 1.14 (*Trp53*-/-;*Pten*-/-) (control) compared to the F3 (*Trp53*-/-) (control) group (***). Following treatment with AZD8186 there was a non-significant decrease in Gr-1+ levels in the 1.14 cell line (Figure 6.8).

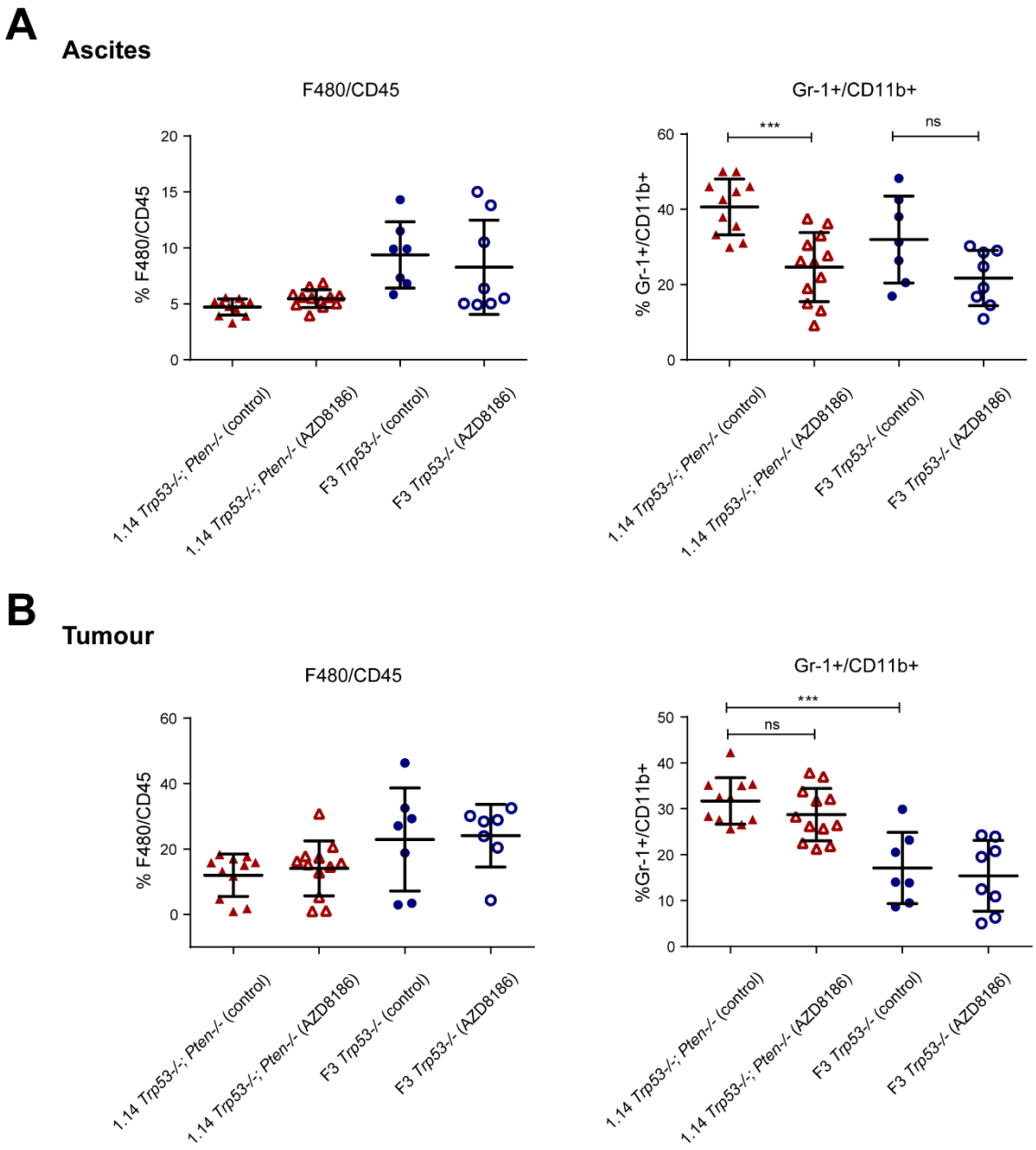

Figure 6.8: Flow cytometry analysis of ascites and murine tumour from the AZD8186 experiment.
A, Ascites samples showing a significant decrease in Ly6C+Ly6G+ (Gr-1+) levels following AZD8186 treatment in the *Trp53-/-;Pten-/-* (1.14) genotype but no difference in the F4/80 levels **B,** Tumour samples showing a non-significant decrease in Ly6C+Ly6G+ levels following AZD8186 treatment in the *Trp53-/-;Pten-/-* (1.14) genotype but again no difference in the F4/80 levels.

6.3.3 Full blood count

A full blood count was taken from each mouse once they had reached the Home Office endpoint. There was no difference in HGB between the control and AZD8186 treated mice injected with F3 (*Trp53*-/-). The HGB was significantly increased in the AZD8186 treated group compared to the control group in mice injected with 1.14 (*Trp53*-/-;*Pten*) (****). There was also a significant reduction in HGB levels between the F3 and 1.14 (control) groups (Figure 6.9).

The platelet levels were not significantly different between the genotypes or between different treatment groups.

There was no significant difference in the NEUT:LYMPH ratio between the 1.14 (control) compared to the F3 (control) group. There was a significant reduction in the AZD8186 treatment groups (F3 and 1.14) compared to both the controls (**) (Figure 6.9).

6.3.4 RT-qPCR

The RT-qPCR from the tumours showed a decrease in *Pten* expression and an increase in *Ccl2* and *Ccl7* when comparing the F3 (control) and 1.14 (control), which is comparable to our previous *in vivo* data (****) (Figure 6.10).

AZD8186 treatment did not alter *Pten* expression in the *Trp53*-/-;*Pten*-/- tumours, but did decrease *Ccl2* and *Ccl7* expression (****). Interestingly, *Ccl2* and *Ccl7* also reduced in the *Trp53*-/- tumours following AZD8186 (****). When comparing both genotypes treated with AZD8186 the levels of *Ccl2* (***) and *Ccl7* (****) were still higher in the *Trp53*-/-;*Pten*-/- tumours (Figure 6.10).

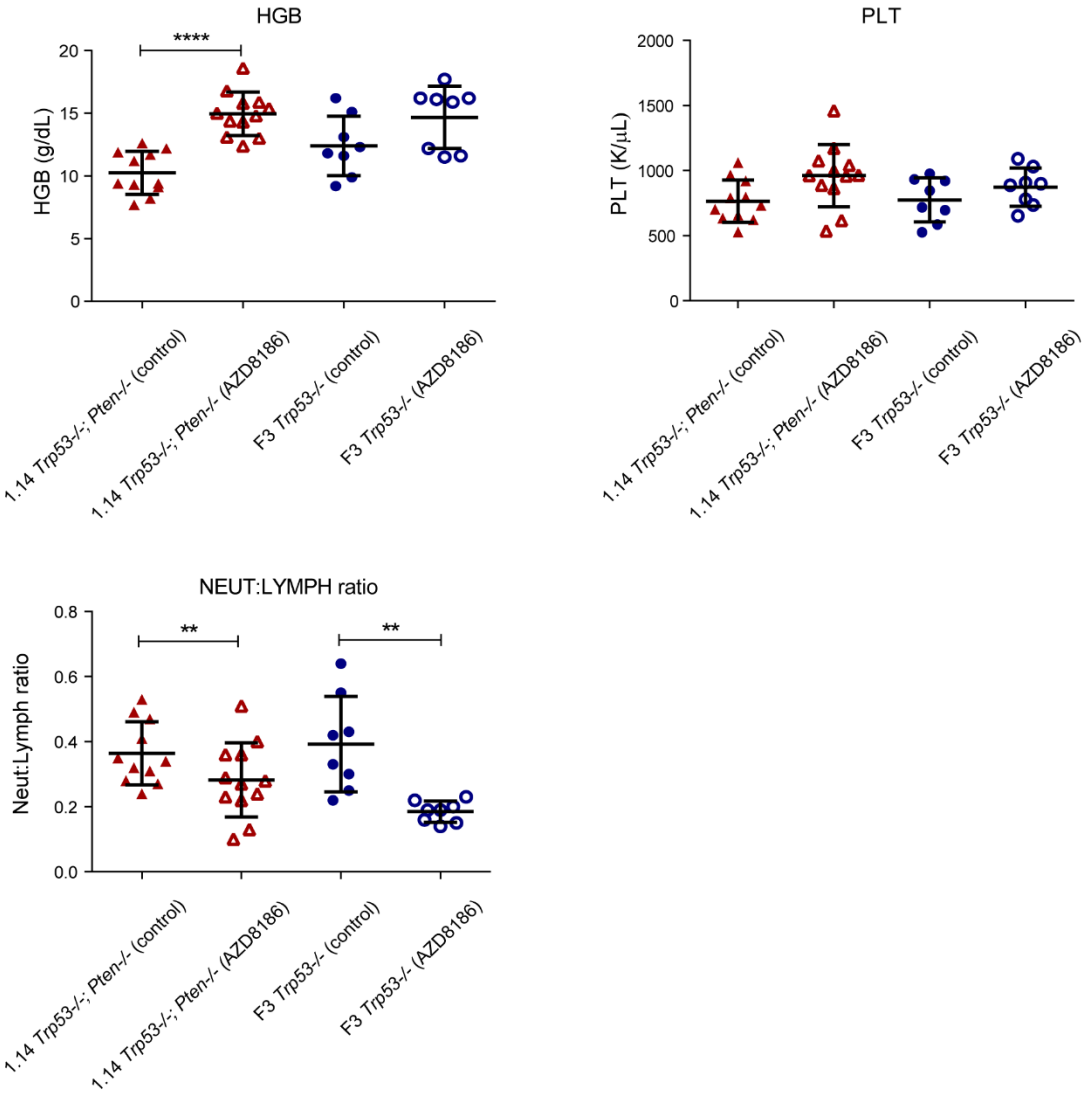

Figure 6.9: Full blood counts (FBC) from the AZD8186 experiment.

Each dot represents the FBC from one mouse. The HGB (haemoglobin) levels are reduced in the 1.14 *Trp53-/-;Pten-/-* compared to the F3 *Trp53-/-* genotype as shown in previous *in vivo* data. There is a significant increase in the HGB level in the 1.14 cell line following treatment with AZD8186 (****). No obvious difference in platelets is observed. A significant reduction in the NEUT:LYMPH ratio is shown in both the F3 and 1.14 cell line following AZD8186 treatment (**).

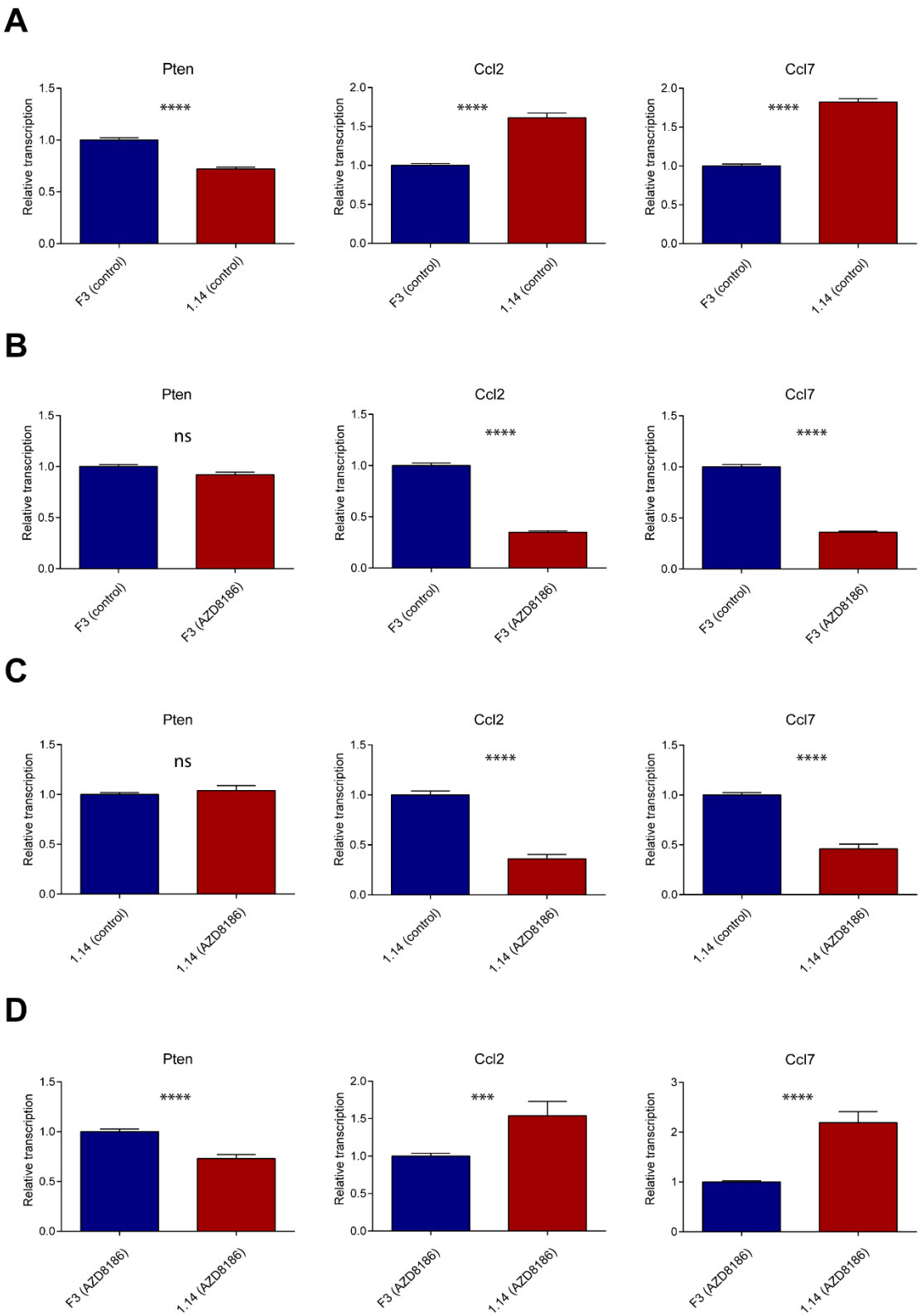

Figure 6.10 RT-qPCR on murine tumour samples from the AZD8186 experiment.

A, F3 (control) vs 1.14 (control) showing reduced expression of *Pten* and increased *Ccl2* and *Ccl7* expression. **B,** F3 (control) vs F3 (AZD8186) showing no change in *Pten* expression and reduced expression of *Ccl2* and *Ccl7*. **C,** 1.14 (control) vs 1.14 (AZD8186) showing no change in *Pten* and reduced expression of *Ccl2* and *Ccl7* following AZD8186 treatment. **D,** F3 (AZD8186) vs 1.14 (AZD8186) showing reduced expression of *Pten* and increased *Ccl2* and *Ccl7* expression.

6.3.5 Immunohistochemistry

The AZD8186 treated and untreated murine samples were stained for BrDU, pAkt (Ser473), F4/80, iNOS and CD206. There was no significant difference in BrDU levels between the genotypes treated with vehicle or following treatment with AZD8186. As previously shown there was a significant increase in p-Akt (Ser473) in the *Trp53-/-;Pten-/-* compared to the *Trp53-/-* genotype. Phospho-Akt staining was reduced in the *Trp53-/-;Pten-/-* tumours after AZD8186 treatment, although not significantly.

There was a non-significant increase in F4/80 levels in the *Trp53-/-;Pten-/-* control group compared to the *Trp53-/-* control group. However, treatment with AZD8186 did not alter these levels significantly.

The *Trp53-/-;Pten-/-* genotype had a significantly lower level of iNOS staining (M1-marker) compared to the *Trp53-/-* genotype with a non-significant decrease in levels in the same genotype after treatment with AZD8186. There was no significant difference in CD206 levels between the genotypes or after treatment (Figure 6.11).

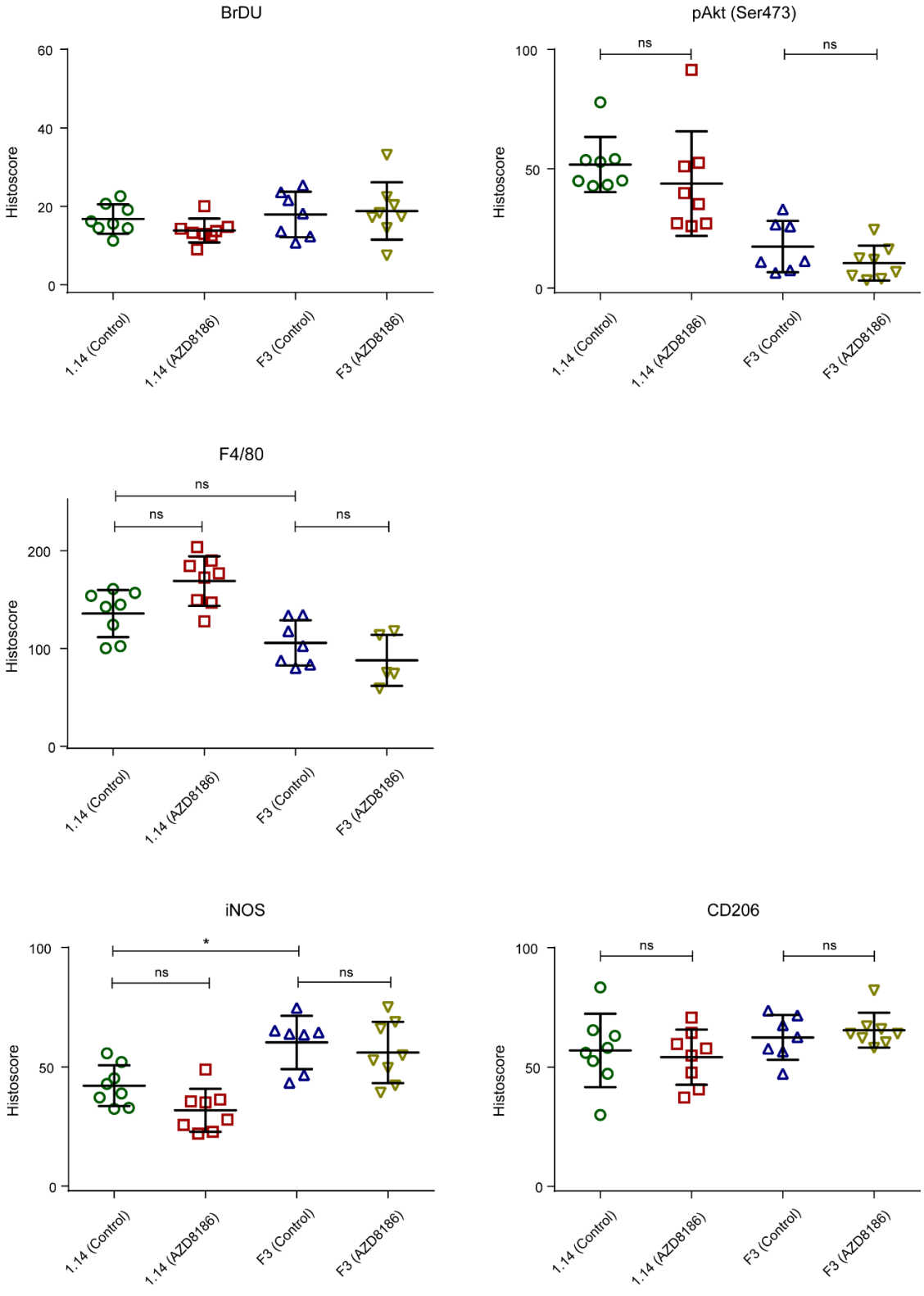

Figure 6.11: Immunohistochemistry from the AZD8186 experiment

Immunohistochemistry from murine tumours showing no significant difference in BrDU, F4/80, iNOS and CD206 levels following treatment with AZD8186 in both genotypes and a non-significant decrease in p-Akt (Ser473) levels in the *Trp53-/-;Pten-/-* genotype after AZD8186 treatment. The iNOS level (M1-type) was significantly reduced in the *Trp53-/-;Pten-/-* (1.14) compared to the *Trp53-/-* (F3) genotype.

6.4 Discussion

A complex chemokine network within the tumour microenvironment has been shown to influence the phenotype of the immune infiltrates and impact on tumour growth and migration as reviewed by Balkwill et al (Balkwill, 2004). The GGTACKO mice have constitutive deletions in CCR1, 2, 3 and 5 and these mice allowed us to target the chemokine/cytokine response directly.

Inhibition of CCR1 has been shown to block the accumulation of immature myeloid cells resulting in reduced tumour dissemination and significantly prolonging survival in a colon cancer mouse model (Kitamura et al., 2010). CCL2/CCR2 chemokine axis is critical in the recruitment and mobilisation of inflammatory monocytes in tumour. In pancreatic cancer in mice, CCR2 blockade has been found to reduce the levels of both inflammatory monocytes and macrophages resulting in decreased tumour growth (Sanford et al., 2013).

CCR3 expression has been found on cells that are important for M2-like polarisation these include T_{reg}, T_H2 cells, eosinophils and basophils (Mantovani et al., 2004b). The CCL5/CCR5 axis has been shown to be a significant regulator of immunosuppressive myeloid cells. Studies have found the absence of CCL5 or CCR5 to delay tumour progression with a reduction in both monocytic and granulocytic myeloid-derived suppressor cells and tumour-associated macrophages (Schlecker et al., 2012, Ban et al., 2017).

Our previous findings have found an increase in MDSCs and TAMs with the loss of *Pten*. By using this GGTACKO transgenic *in vivo* model that targeted specifically the CCR1, 2, 3, and 5 receptors we hoped to reduce the level of these immune infiltrates and therefore prolong survival in the *Pten*-/- genotype.

The wild-type mice injected with the F3 cell line (*Trp53*-/-) had a median survival of 53 days compared to the knock-out mice with a median survival of 53 days. The wild-type mice injected with the 1.14 cell line (*Trp53*-/-;*Pten*-/-) had a median survival of 32 days and this was compared to 36 days in the knock-out mice (Figure 6.2).

The difference in survival between the *Trp53*-/- and *Trp53*-/-;*Pten*-/- genotypes in the wild-type mice is comparable with previous *in vivo* data (see Chapter 4, Figure 4.2). There was no obvious difference in survival with the *Trp53*-/- genotype between the WT and KO mice. The *Trp53*-/-;*Pten*-/- genotype in the KO mice extended survival by 4 days compared to the wild-type mice with the same genotype, however this was not significant. A larger experiment would be required to demonstrate whether there was a real difference in survival.

Flow cytometry from ascites showed a trend towards a higher level of Ly6C+Ly6G+ expression in both the WT and KO mice injected with the *Trp53*-/-;*Pten*-/- compared to *Trp53*-/- cell line (Figure 6.3). This was similar to previous flow cytometry analysis of ascites (see Chapter 5, Figure 5.19). However, no difference was seen in Ly6C+Ly6G+ expression when comparing the WT and KO mice.

Flow cytometry performed on fresh tumour samples showed a trend towards a higher level of CD11b+, Ly6C+Ly6G+ and F4/80+ expression in the WT mice injected with *Trp53*-/-;*Pten*-/- compared to the WT and KO mice injected with *Trp53*-/-. No obvious difference in expression levels in the tumour between the KO and WT mice injected with F3 (*Trp53*-/) were found. However, there appeared to be a reduction in the level of CD11b+, Ly6C+Ly6G+ and F4/80 expression in the tumour in the KO mouse injected with 1.14 (*Trp53*-/-;*Pten*-/-) (Figure 6.3). Unfortunately, only one tumour sample from the KO mice injected with the 1.14 cell line was analysed and it is therefore difficult to make any valid conclusions.

A full blood count (FBC) was taken from each mouse when they were culled at the Home Office endpoint. The WT and KO mice with *Trp53*-/-;*Pten*-/- were more anaemic with lower levels of haemoglobin compared to the mice injected with the *Trp53*-/- cell line (Figure 6.4). There was no difference in ascites volumes or bloody appearance of the ascites between the mice that might have explained the anaemia (Figure 6.2). Previous *in vivo* experiments using the *Trp53*-/-;*Pten*-/- genotype had shown the mice to be anaemic but there was no

obvious reversal in this experiment using these knockout mice, implying that signalling via CCR1, 2, 3 or 5 was not responsible for the anaemia.

Thrombocytosis has been found to be associated with advanced disease and a worse overall survival in ovarian cancer (Stone et al., 2012). We found no difference in platelet levels between the mice. A high neutrophil to lymphocyte ratio has also been shown to be associated with an adverse overall survival in many solid tumours including ovarian cancer (Templeton et al., 2014, Cho et al., 2009). There was a trend towards a higher NEUT:LYMPH ratio in the *Trp53-/-;Pten-/-* compared to the *Trp53-/-* genotype but there was no obvious difference between the WT and KO mice (Figure 6.4).

Immunohistochemistry staining of the GGTACKO tumours showed no obvious differences in the F4/80, iNOS and CD206 staining between the wild-type and knockout mice. We also were unable to show increased levels of these macrophage markers in the *Trp53-/-;Pten-/-* although the numbers analysed were small (Figure 6.5).

The GGTACKO *in vivo* experiment was a pilot experiment to determine whether the knockout of these CCR receptors influenced not only the immune infiltrates within the tumour but also survival. The early results were encouraging but a repeat experiment is required before valid conclusions can be made. It is possible that knocking out specific CCR receptors may have a limited impact on macrophage and MDSC levels and that the function and recruitment of these infiltrates is more complicated.

In the AZD8186 *in vivo* experiment we used an alternative approach to reverse the effect of *Pten* by targeting the PI3K/AKT pathway. The *in vitro* optimisation determined the optimal concentration of drug to inhibit p-Akt (Ser473) and change the cytokine profile. The p-Akt (Ser473) expression was inhibited but returned to pre-treatment levels after 4 hours and *Ccl2* and *7* were at their lowest level at 2 hours post-treatment. These findings confirmed that the mice needed to be culled no later than 2 hours after the final treatment dose so as we could identify any changes within the tumour.

From recent AZD8186 *in vivo* studies on PTEN null tumour xenograft models (786-0 renal and U87-MG glioma), 5 days of twice daily treatment (50mg/kg) was found to reduce tumour growth by 87% compared to 93% with constant dosing (Hancox et al., 2015). From this information and our recent *in vitro* data, we decided on a treatment regime of twice daily gavage (50mg/kg) for 5 days and culling of the mice 2 hours after their final dose. The timing of the treatment was determined by previous *in vivo* survival data (see Chapter 4, Figure 4.2).

Flow cytometry showed similar data to previous *in vivo* experiments with a significantly higher level of Ly6C+Ly6G+ in both the ascites and tumour in the 1.14 mice (*Trp53-/-;Pten-/-*) compared to mice injected with F3 (*Trp53-/-*). However we were unable to replicate the high levels of F4/80 we had previously seen in the *Trp53-/-;Pten-/-* genotype. We showed no obvious difference in Ly6C+Ly6G+ and F4/80 levels between the control and AZD8186 treated mice injected with F3 (*Trp53-/-*). However, there was a significant reduction in Ly6C+Ly6G+ levels in the ascites in the AZD8186 treated group injected with 1.14 (*Trp53-/;Pten-/-*) compared to the control group and a non-significant decrease in levels in the tumour samples. As mentioned there was no obvious difference in F4/80 levels between the samples (Figure 6.8).

These data show that the AZD8186 drug has started to reverse some of the immunosuppressive changes we had previously described in the tumour microenvironment with the loss of *Pten*. The reason for the low F4/80 levels between all samples is unknown.

A full blood count from these mice showed no difference between the control and AZD8186 treated mice injected with F3. However, there was a reduction in the level of anaemia in the AZD8186 treated group injected with the 1.14 clone with an increase in haemoglobin (HGB) levels compared to the control. These changes suggest that the AZD8186 drug has reversed the anaemic state previously seen in the *Trp53-/-;Pten-/-* genotype, the exact mechanism of this is unclear (Figure 6.9).

As discussed previously the NEUT:LYMPH ratio is associated with a worse prognosis. Both AZD8186 treatment groups (F3 and 1.14) had a significant reduction in the ratio compared to the control. However we did not show a higher baseline level in the 1.14 control group which previous *in vivo* data had shown. This reduction in the ratio with AZD8186 treatment is difficult to explain for both genotypes as the drug inhibits the PI3K/AKT pathway which has been shown not to be activated in the F3 (*Trp53*-/-) genotype. The drug may be having some off-target effects that influence the circulating leukocyte population (Figure 6.9).

The RT-qPCR from the murine tumours showed a decrease in *Pten* expression and an increase in *Ccl2* and *Ccl7* expression when comparing the F3 (control) and 1.14 (control), which is comparable to our previous *in vivo* data (****). However, when comparing the 1.14 (AZD8186) and 1.14 (control) samples there was no change in *Pten* expression but a decrease in *Ccl2* and *Ccl7* expression (****). This shows that in addition to AZD8186 reversing the level of MDSCs the expression of specific cytokines associated with macrophage and MDSC activity are reduced. Similar cytokine changes were seen when comparing the F3 (control) and F3 (AZD8186) samples that suggests that the AZD8186 drug is having an overall effect on cytokine levels. We also compared the two AZD8186 treatment groups (F3 and 1.14) and showed that the *Ccl2* (***) and *Ccl7* (****) levels remained higher in the 1.14 (*Trp53*-/-;*Pten*-/-) genotype (Figure 6.10).

As shown previously immunohistochemistry analysis from the murine tumours showed a higher level of p-Akt (Ser473) in the *Trp53*-/-;*Pten*-/- (1.14) genotype and a non-significant decrease in levels following AZD8186 treatment. This non-significant reduction may show that the PI3K/AKT pathway has been partially inhibited by the drug and could be due to inadequate treatment length or alternative mechanisms leading to on-going activation of the pathway. Staining with BrDU did not show any differences between the genotypes, suggesting that the more aggressive tumour behaviour seen in the *Trp53*-/-;*Pten*-/- genotype is not because of increased cell proliferation (Figure 6.11).

The *Trp53*-/-;*Pten*-/- genotype showed higher levels of F4/80 as shown previously but a significantly lower level of iNOS staining (M1-marker) with no

difference in CD206 levels (M2-marker). The differences in iNOS staining were not seen on the TMAs but this result does provide some evidence of polarisation of the *Trp53-/-;Pten-/-* genotype to a pro-tumour M2-like state. Consistent with the flow cytometry data, there was no significant difference in F4/80 levels following treatment with AZD8186 and this could be as result of incomplete inactivation of the PI3K/AKT pathway (Figure 6.11).

In summary, we have shown by these two *in vivo* experiments that it is possible to reverse the effect of *Pten* loss, at least partially. We targeted the PI3K/AKT pathway and showed that the immunosuppressive microenvironment can be reversed. The GGTACKO experiment targeted the chemokine/cytokine response directly and although only a pilot showed encouraging data that supports this as a potential target. A repeat of the GGTACKO experiment is on-going and an *in vivo* AZD8186 survival experiment is the next step to establish whether by altering the tumour microenvironment we can improve survival in the *Trp53-/-;Pten-/-* genotype.

7 Final Discussion

The treatment of high grade serous ovarian cancer has improved over the last 30 years with the introduction of platinum and taxane-based chemotherapy. Platinum chemotherapy often leads to an initial clinical response, however most patients will ultimately relapse and there remains a sub-group of patients who are intrinsically resistant to platinum (Galluzzi et al., 2012). Improving our understanding of these resistant mechanisms will help us to develop alternative therapeutic strategies.

Until recently there was a 'one size fits all' approach to ovarian cancer management with no acknowledgement of the histological subtypes and how these differed in terms of chemotherapy response, survival, genetics and tissue of origin. Most cases of high grade serous ovarian cancer are now thought to originate from the fallopian tube. This has important implications for future management in terms of prevention, early detection and surgical intervention (Labidi-Galy et al., 2017b).

An improved understanding of the molecular diversity and tumour microenvironment has allowed us to make progress in drug development. PARP inhibitors and VEGF inhibitors (bevacizumab) are the first new drugs for use in ovarian cancer for over 20 years.

The Cancer Genome Atlas (TCGA) has helped to map out the genetic landscape of HGSOC. Homologous recombination is known to be an important pathway in the repair of double-strand DNA and in addition to *BRCA1* and *BRCA2* mutations, defective homologous recombination is thought to be present in up to 50% of cases. This has important therapeutic implications as PARP inhibitors currently have FDA approval in patients with known *BRCA1/2* mutations and last year have been approved for use in non-*BRCA* patients with recurrent epithelial ovarian cancer who had a complete or partial response to platinum-based chemotherapy.

A greater understanding of the genetic landscape has helped to identify the most common but also least frequently mutated genes in HGSOC. *BRCA1/2* mutations in ovarian cancer are well known and tend to respond well to both platinum chemotherapy and PARP inhibitors. However, knowledge regarding

prognosis and chemotherapy response in tumours with less frequently mutated genes such as *RB1*, *NF1* and *PTEN* is limited.

These ID8 CRISPR-generated models represent a novel and simple tool to investigate the biology of HGSOC. In this thesis I have shown that a defective homologous recombination pathway is associated in most cases with a greater sensitivity to platinum chemotherapy and PARP inhibitors. However, when I combine data from other ovarian cancer cell lines with known HR status the relationship between cisplatin sensitivity and defective homologous recombination is more complicated.

We know from clinical data that around 15% of women with a *BRCA1/2* mutation are refractory or resistant to platinum chemotherapy (Alsop et al., 2012). Our data has shown that although the *Brca1-/-* and *Brca2-/-* ID8 derivatives are more sensitive to cisplatin, there is a greater sensitivity in clones with mutations in the PALB2 domain compared to the BRCT2 domain. In addition, the loss of *Pten* in the *Trp53-/-;Brca2-/-* genotype was shown to reduce sensitivity to cisplatin. These findings show that the location of the mutation and presence of confounding mutations in *Brca1-/-* and *Brca2-/-* can influence the sensitivity to platinum chemotherapy and might explain why a sub-group of these patients respond poorly to conventional treatment.

The *in vivo* data showed that the *Brca1-/-* and *Brca2-/-* genotypes responded the best to platinum chemotherapy and the *Pten-/-* and *Nf1-/-* genotypes had the worst prognosis. This correlates well with what we know about clinical responses to platinum chemotherapy. As this was a transplantable *in vivo* model it allowed us to look closely at the tumour microenvironment and how this differed between the genotypes and following treatment with cisplatin. At present we know that certain mutations in women are associated with a worse prognosis but in most cases, we don't know the exact mechanism for this treatment resistance. This ID8 model offered a unique opportunity to investigate this further.

The tumour microenvironment is known to play an important role in the tumour progression and metastatic spread of disease. The interaction between the non-

malignant and malignant cells within this environment is thought to offer a potential therapeutic target. In ovarian cancer particularly, the tumour has a predisposition for the omentum and its dissemination is aided by the circulating ascites within the peritoneal cavity (Thibault et al., 2014).

I have shown that treatment with cisplatin alters the tumour microenvironment and as well as an overall cisplatin effect there are also differences between genotypes. When all genotypes were combined there was a significant increase in CD45+, CD11b+, CD3+, CD8+ and F4/80+ levels in the ascites after cisplatin treatment. The monocytic+ level was decreased, granulocytic+ level increased but overall the MDSC level (Ly6C+Ly6G+) was not changed following cisplatin treatment. In the *Pten*-/- genotype there was an increase in CD3+ levels and although not increased the CD8+ level was higher compared to the other genotypes. The MDSCs also remained high despite cisplatin treatment in the *Pten*-/- genotype.

However, RNA sequencing of the tumours showed that cisplatin suppressed the immune response in all genotypes, and this was further supported by a decrease in tumour CD3+ levels by immunohistochemistry. These findings show that cisplatin can induce an immuno-stimulatory response in the ascites and an immuno-inhibitory response within the tumour and these two opposing responses may contribute to chemotherapy resistance. The cisplatin treatment does not appear to influence the MDSC level in the *Pten*-/- genotype and this may explain its poor prognosis. The influence of cisplatin chemotherapy is summarised in Figure 7.1.

I showed that changes in both the ascites and tumour supported an immunosuppressive microenvironment in the *Pten*-/- and *Nf1*-/- genotypes which were associated with the worst *in vivo* survival. We decided to focus on the loss of *Pten*. The hypothesis was that *Pten* loss created an immunosuppressive microenvironment that helps to drive tumour progression and result in a poor prognosis. Our data from flow cytometry, RNA sequencing, RT-qPCR and immunohistochemistry supported this hypothesis. We found a significant increase in the MDSCs population in both ascites and tumour samples from flow cytometry and an increase in TAMs in tumour samples from

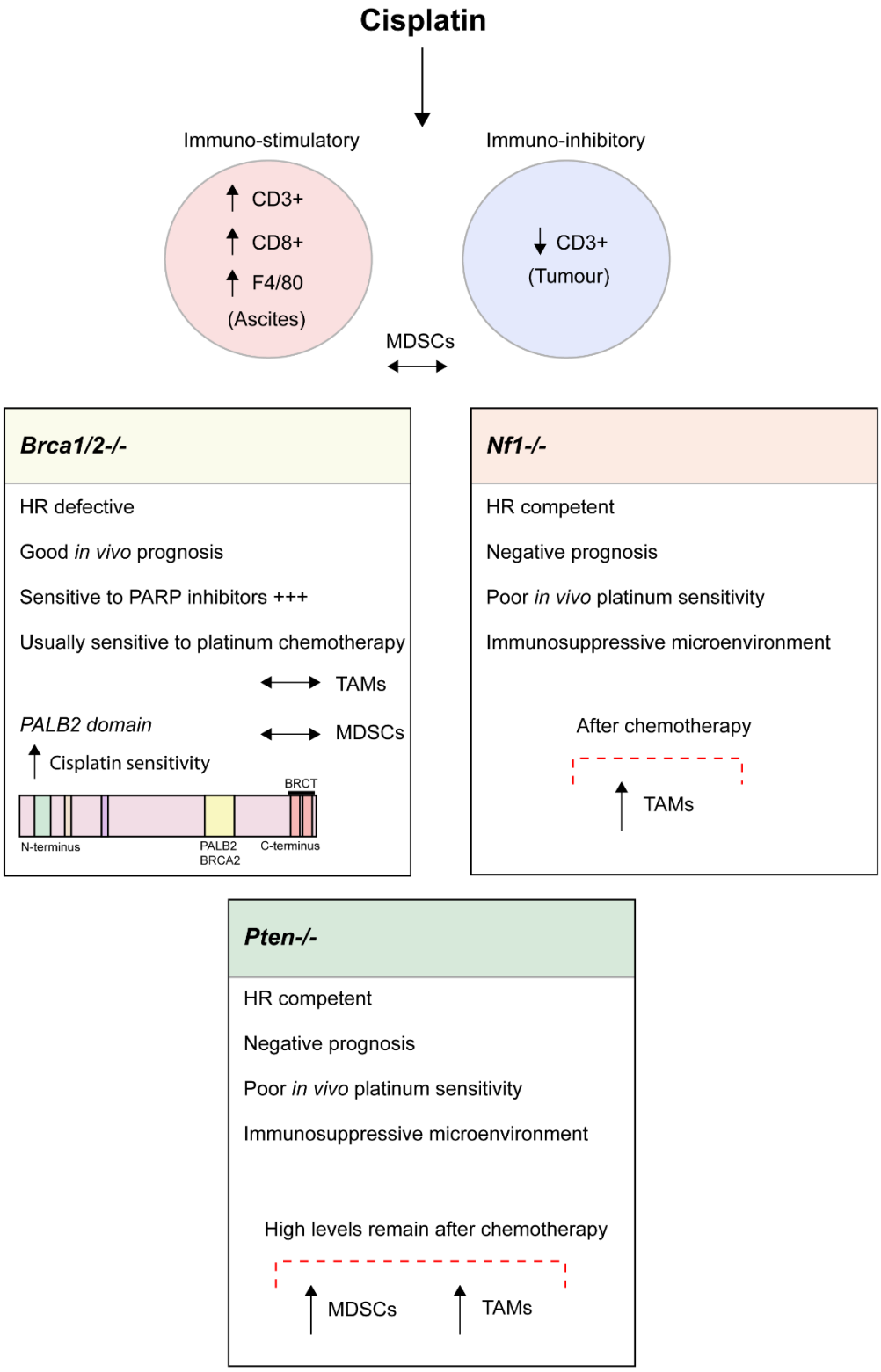

Figure 7.1: Summary of the influence of platinum chemotherapy

Cisplatin showing an immune-stimulatory response in ascites and an immune-stimulatory response in tumour. The MDSC and TAM populations are unchanged following cisplatin treatment in the *BRCA1* and *BRCA2* genotypes (positive prognosis) but clones with mutations within the PALB2 domain show greater sensitivity. The TAMs are increased in the *Nf1-/-* genotype (poor prognosis) and both MDSCs and TAMs although not increased, remain high in the *Pten-/-* genotype (poor prognosis) after treatment.

flow cytometry and immunohistochemistry data. From cytokine array and RT-qPCR, we showed specific chemokines (*Ccl2* and *Ccl7*) involved in MDSC and TAM recruitment to be upregulated in the *Pten*-/- genotype. This was further supported by RNA sequencing of murine tumours that showed a range of upregulated cytokine/chemokines important in MDSC activity, TAM recruitment and polarisation.

We also showed evidence of TAM polarisation to a pro-tumour M2-like state with the loss of *Pten*. RNA sequencing of tumours highlighted several chemokine/cytokines present in both M1 and M2-like macrophages. Specifically, *Ccl2* which was identified in the chemokine array and confirmed on RT-qPCR and RNA seq to be significantly upregulated. This chemokine is important in polarisation of macrophages to an M2-like state. However immunohistochemistry data from the TMAs showed a significant increase in both iNOS (M1-marker) and CD206 (M2-marker) with the loss of *Pten* but no obvious polarisation to an M2-like state.

Pten offers an attractive therapeutic target. We have shown that this immunosuppressive microenvironment is a possible explanation for the more aggressive tumour progression and poor prognosis in the *Pten*-/- genotype. The next step was to attempt to reverse the effect of *Pten* with the eventual goal of improving survival. The AZD8186 *in vivo* experiment targeted the PI3K/AKT pathway directly by selectively inhibiting PI3Kβ whereas the GGTACKO *in vivo* experiment directly targeted CCR receptors involved in both MDSC and TAM activity.

We showed from the initial GGTACKO pilot experiment that by inhibiting the receptors CCR1, 2, 3, and 5 the MDSC and TAM populations were reduced in the *Pten*-/- genotype and survival was extended. This experiment is currently being repeated to confirm these findings. The AZD8186 experiment showed that by inhibiting PI3Kβ, that the MDSCs that had previously been increased were reduced in the *Pten*-/- genotype. In addition, *Ccl2* and *Ccl7* were reduced and iNOS levels (M1-like) were reduced showing some evidence to support an M2-like macrophage state. The effect of *Pten* loss is summarised in Figure 7.2.

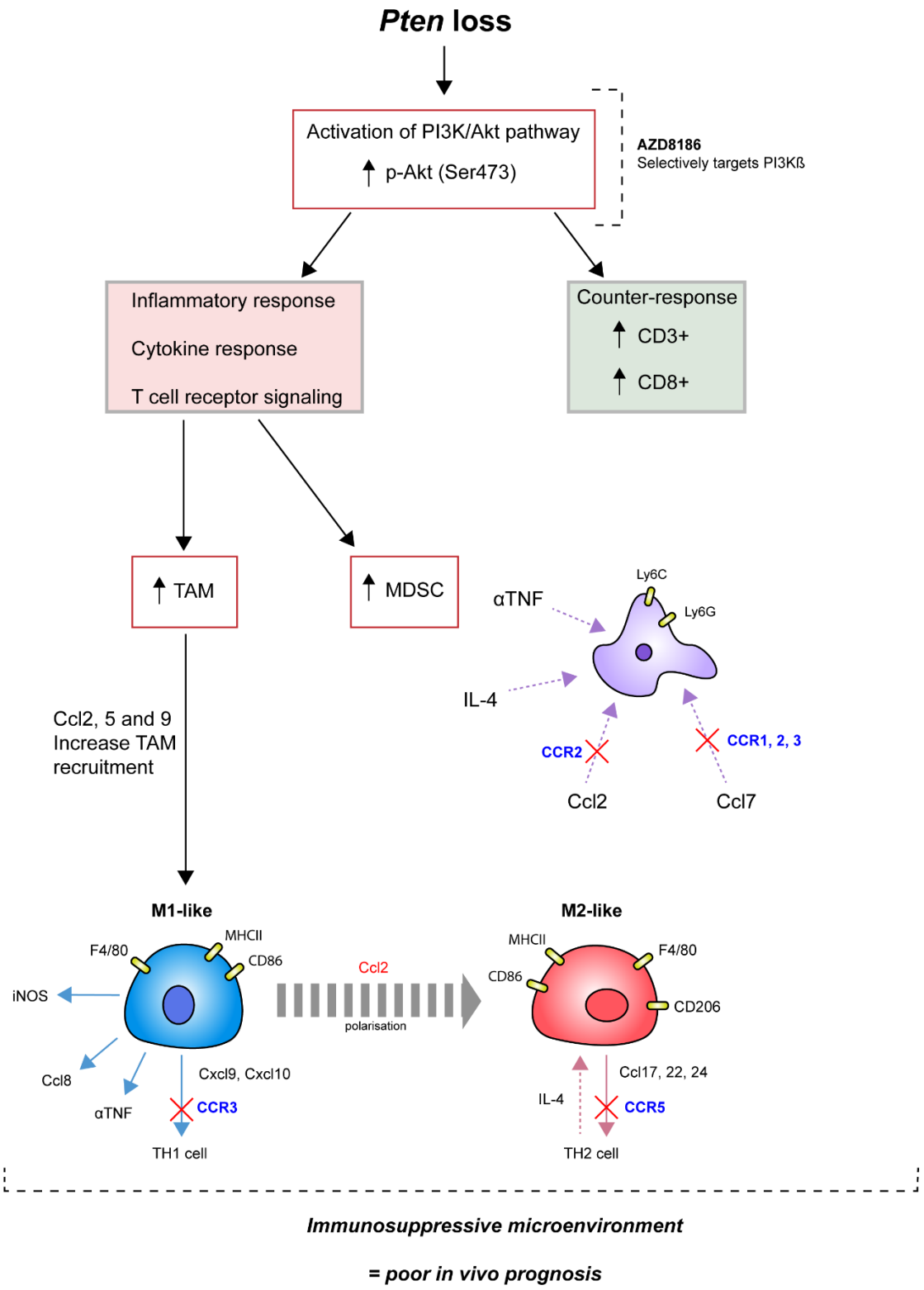

Figure 7.2: Summary of *Pten* loss

Pten loss showing the activation of the PI3K/AKT pathway resulting in an inflammatory response and an increase in MDSCs and TAMs. A counter-response is shown with an increase in CD3 and CD8. The loss of *Pten* also results in polarisation of TAMS to an M2-like state (pro-tumour). The CCR receptors (blue) knocked out in the GGTACKO mice that are involved in MDSC and TAM activity are shown.

In this thesis, I have looked to improve the understanding of platinum sensitivity and the influence of the tumour microenvironment in high grade serous ovarian cancer. I established that cisplatin sensitivity is more complicated than simply a defective homologous recombination pathway and is likely to involve a multitude of factors, particularly the tumour microenvironment. I have used a transplantable *in vivo* model for HGSOC to investigate potential mechanisms of platinum sensitivity and identified poor prognostic genotypes. Finally, I have found *Pten* loss to be associated with an immunosuppressive microenvironment and by targeting the activated PI3K/AKT pathway and CCR receptors we can begin to reverse the effect of *Pten*. The next *in vivo* experiment will be to determine whether reversing the immunosuppressive microenvironment in the *Pten*-/- genotype with AZD8186 results in a prolonged survival.

The research undertaken in this thesis has helped to further our knowledge of HGSOC and will hopefully contribute to the ovarian cancer research community. Ovarian cancer is one of the most lethal malignancies and results in a poor prognostic outlook for many patients. However the management is going to change significantly in the next 20 years. TCGA has increased our knowledge of the mutational landscape of ovarian cancer and is likely to lead to a transformation in personalised strategies. We have identified poor prognostic groups (*Pten*, *Nf1*) and potential therapeutic targets in an *in vivo* model. The next step will be to confirm these findings on other *in vivo* models and primary tissue. By identifying patients with specific mutations, we can tailor treatment to the individual and hopefully begin to improve survival dramatically.

8 References

8.1 Journal Articles

AGHAJANIAN, C., BLANK, S. V., GOFF, B. A., JUDSON, P. L., TENERIELLO, M. G., HUSAIN, A., SOVAK, M. A., YI, J. & NYCUM, L. R. 2012. OCEANS: a randomized, double-blind, placebo-controlled phase III trial of chemotherapy with or without bevacizumab in patients with platinum-sensitive recurrent epithelial ovarian, primary peritoneal, or fallopian tube cancer. *J Clin Oncol,* 30**,** 2039-45.

AHMED, A. A., ETEMADMOGHADAM, D., TEMPLE, J., LYNCH, A. G., RIAD, M., SHARMA, R., STEWART, C., FEREDAY, S., CALDAS, C., DEFAZIO, A., BOWTELL, D. & BRENTON, J. D. 2010. Driver mutations in TP53 are ubiquitous in high grade serous carcinoma of the ovary. *J Pathol,* 221**,** 49-56.

AHMED, F., GOODMAN, M. T., KOSARY, C., RUIZ, B., WU, X. C., CHEN, V. W. & CORREA, C. N. 2006. Excess risk of subsequent primary cancers among colorectal carcinoma survivors, 1975-2001. *Cancer,* 107**,** 1162-71.

ALCAZAR, J. L. 2016. Ultrasound-based IOTA simple rules allow accurate malignancy risk estimation for adnexal masses. *Evid Based Med,* 21**,** 197.

ALETTI, G. D., GOSTOUT, B. S., PODRATZ, K. C. & CLIBY, W. A. 2006. Ovarian cancer surgical resectability: relative impact of disease, patient status, and surgeon. *Gynecol Oncol,* 100**,** 33-7.

ALITALO, K. 2011. The lymphatic vasculature in disease. *Nat Med,* 17**,** 1371-80.

ALLEN, D. G., HEINTZ, A. P. & TOUW, F. W. 1995. A meta-analysis of residual disease and survival in stage III and IV carcinoma of the ovary. *Eur J Gynaecol Oncol,* 16**,** 349-56.

ALSOP, K., FEREDAY, S., MELDRUM, C., DEFAZIO, A., EMMANUEL, C., GEORGE, J., DOBROVIC, A., BIRRER, M. J., WEBB, P. M., STEWART, C., FRIEDLANDER, M., FOX, S., BOWTELL, D. & MITCHELL, G. 2012. BRCA mutation frequency and patterns of treatment response in BRCA mutation-positive women with ovarian cancer: a report from the Australian Ovarian Cancer Study Group. *J Clin Oncol,* 30**,** 2654-63.

AOGS 1971. Classification and staging of malignant tumours in the female pelvis. *Acta Obstet Gynecol Scand,* 50**,** 1-7.

ARMSTRONG, D. K., BUNDY, B., WENZEL, L., HUANG, H. Q., BAERGEN, R., LELE, S., COPELAND, L. J., WALKER, J. L., BURGER, R. A. & GYNECOLOGIC ONCOLOGY, G. 2006. Intraperitoneal cisplatin and paclitaxel in ovarian cancer. *N Engl J Med,* 354**,** 34-43.

BAEKELANDT, M., KRISTENSEN, G. B., NESLAND, J. M., TROPE, C. G. & HOLM, R. 1999. Clinical significance of apoptosis-related factors p53, Mdm2, and Bcl-2 in advanced ovarian cancer. *J Clin Oncol,* 17**,** 2061.

BALKWILL, F. 2004. Cancer and the chemokine network. *Nat Rev Cancer,* 4**,** 540-50.

BALKWILL, F., CHARLES, K. A. & MANTOVANI, A. 2005. Smoldering and polarized inflammation in the initiation and promotion of malignant disease. *Cancer Cell,* 7**,** 211-7.

BALKWILL, F. R., CAPASSO, M. & HAGEMANN, T. 2012. The tumor microenvironment at a glance. *J Cell Sci,* 125**,** 5591-6.

BAMIAS, A., SOTIROPOULOU, M., ZAGOURI, F., TRACHANA, P., SAKELLARIOU, K., KOSTOUROS, E., KAKOYIANNI, K., RODOLAKIS, A., VLAHOS, G., HAIDOPOULOS, D., THOMAKOS, N., ANTSAKLIS, A. & DIMOPOULOS, M. A. 2012. Prognostic evaluation of tumour type and other histopathological characteristics in advanced epithelial ovarian cancer, treated with surgery and paclitaxel/carboplatin chemotherapy: cell type is the most useful prognostic factor. *Eur J Cancer,* 48**,** 1476-83.

BAN, Y., MAI, J., LI, X., MITCHELL-FLACK, M., ZHANG, T., ZHANG, L., CHOUCHANE, L., FERRARI, M., SHEN, H. & MA, X. 2017. Targeting Autocrine CCL5-CCR5 Axis Reprograms Immunosuppressive Myeloid Cells and Reinvigorates Antitumor Immunity. *Cancer Res,* 77**,** 2857-2868.

BASHASHATI, A., HA, G., TONE, A., DING, J., PRENTICE, L. M., ROTH, A., ROSNER, J., SHUMANSKY, K., KALLOGER, S., SENZ, J., YANG, W., MCCONECHY, M., MELNYK, N., ANGLESIO, M., LUK, M. T., TSE, K., ZENG, T., MOORE, R., ZHAO, Y., MARRA, M. A., GILKS, B., YIP, S., HUNTSMAN, D. G., MCALPINE, J. N. & SHAH, S. P. 2013. Distinct evolutionary trajectories of primary high-grade serous ovarian cancers revealed through spatial mutational profiling. *J Pathol,* 231**,** 21-34.

BAST, R. C., JR., KLUG, T. L., ST JOHN, E., JENISON, E., NILOFF, J. M., LAZARUS, H., BERKOWITZ, R. S., LEAVITT, T., GRIFFITHS, C. T., PARKER, L., ZURAWSKI, V. R., JR. & KNAPP, R. C. 1983. A radioimmunoassay using a

monoclonal antibody to monitor the course of epithelial ovarian cancer. *N Engl J Med,* 309**,** 883-7.

BERAL, V., DOLL, R., HERMON, C., PETO, R. & REEVES, G. 2008. Ovarian cancer and oral contraceptives: collaborative reanalysis of data from 45 epidemiological studies including 23,257 women with ovarian cancer and 87,303 controls. *Lancet,* 371**,** 303-14.

BERAL, V., GAITSKELL, K., HERMON, C., MOSER, K. & REEVES, G. 2015. Menopausal hormone use and ovarian cancer risk: individual participant meta-analysis of 52 epidemiological studies. *The Lancet,* 385**,** 1835-1842.

BERAL, V., GAITSKELL, K., HERMON, C., MOSER, K., REEVES, G. & PETO, R. 2012. Ovarian cancer and smoking: individual participant meta-analysis including 28,114 women with ovarian cancer from 51 epidemiological studies : Collaborative Group on Epidemiological Studies of Ovarian Cancer. *Lancet Oncol,* 13**,** 946-56.

BISWAS, S. K. & MANTOVANI, A. 2010. Macrophage plasticity and interaction with lymphocyte subsets: cancer as a paradigm. *Nat Immunol,* 11**,** 889-96.

BOHM, S., MONTFORT, A., PEARCE, O. M., TOPPING, J., CHAKRAVARTY, P., EVERITT, G. L., CLEAR, A., MCDERMOTT, J. R., ENNIS, D., DOWE, T., FITZPATRICK, A., BROCKBANK, E. C., LAWRENCE, A. C., JEYARAJAH, A., FARUQI, A. Z., MCNEISH, I. A., SINGH, N., LOCKLEY, M. & BALKWILL, F. R. 2016. Neoadjuvant Chemotherapy Modulates the Immune Microenvironment in Metastases of Tubo-Ovarian High-Grade Serous Carcinoma. *Clin Cancer Res,* 22**,** 3025-36.

BOLTON, K. L., CHENEVIX-TRENCH, G., GOH, C., SADETZKI, S., RAMUS, S. J., KARLAN, B. Y., LAMBRECHTS, D., DESPIERRE, E., BARROWDALE, D., MCGUFFOG, L., HEALEY, S., EASTON, D. F., SINILNIKOVA, O., BENITEZ, J., GARCIA, M. J., NEUHAUSEN, S., GAIL, M. H., HARTGE, P., PEOCK, S., FROST, D., EVANS, D. G., EELES, R., GODWIN, A. K., DALY, M. B., KWONG, A., MA, E. S., LAZARO, C., BLANCO, I., MONTAGNA, M., D'ANDREA, E., NICOLETTO, M. O., JOHNATTY, S. E., KJAER, S. K., JENSEN, A., HOGDALL, E., GOODE, E. L., FRIDLEY, B. L., LOUD, J. T., GREENE, M. H., MAI, P. L., CHETRIT, A., LUBIN, F., HIRSH-YECHEZKEL, G., GLENDON, G., ANDRULIS, I. L., TOLAND, A. E., SENTER, L., GORE, M. E., GOURLEY, C., MICHIE, C. O., SONG, H., TYRER, J., WHITTEMORE, A. S., MCGUIRE, V., SIEH, W., KRISTOFFERSSON, U., OLSSON, H., BORG, A., LEVINE, D. A., STEELE, L., BEATTIE, M. S., CHAN,

S., NUSSBAUM, R. L., MOYSICH, K. B., GROSS, J., CASS, I., WALSH, C., LI, A. J., LEUCHTER, R., GORDON, O., GARCIA-CLOSAS, M., GAYTHER, S. A., CHANOCK, S. J., ANTONIOU, A. C., PHAROAH, P. D., EMBRACE, KCONFAB, I. & CANCER GENOME ATLAS RESEARCH, N. 2012. Association between BRCA1 and BRCA2 mutations and survival in women with invasive epithelial ovarian cancer. *JAMA,* 307**,** 382-90.

BOOKMAN, M. A., BRADY, M. F., MCGUIRE, W. P., HARPER, P. G., ALBERTS, D. S., FRIEDLANDER, M., COLOMBO, N., FOWLER, J. M., ARGENTA, P. A., DE GEEST, K., MUTCH, D. G., BURGER, R. A., SWART, A. M., TRIMBLE, E. L., ACCARIO-WINSLOW, C. & ROTH, L. M. 2009. Evaluation of new platinum-based treatment regimens in advanced-stage ovarian cancer: a Phase III Trial of the Gynecologic Cancer Intergroup. *J Clin Oncol,* 27**,** 1419-25.

BRYANT, H. E., SCHULTZ, N., THOMAS, H. D., PARKER, K. M., FLOWER, D., LOPEZ, E., KYLE, S., MEUTH, M., CURTIN, N. J. & HELLEDAY, T. 2005. Specific killing of BRCA2-deficient tumours with inhibitors of poly(ADP-ribose) polymerase. *Nature,* 434**,** 913-7.

BUISSON, R., DION-COTE, A. M., COULOMBE, Y., LAUNAY, H., CAI, H., STASIAK, A. Z., STASIAK, A., XIA, B. & MASSON, J. Y. 2010. Cooperation of breast cancer proteins PALB2 and piccolo BRCA2 in stimulating homologous recombination. *Nat Struct Mol Biol,* 17**,** 1247-54.

BURGER, R. A., BRADY, M. F., BOOKMAN, M. A., FLEMING, G. F., MONK, B. J., HUANG, H., MANNEL, R. S., HOMESLEY, H. D., FOWLER, J., GREER, B. E., BOENTE, M., BIRRER, M. J., LIANG, S. X. & GYNECOLOGIC ONCOLOGY, G. 2011. Incorporation of bevacizumab in the primary treatment of ovarian cancer. *N Engl J Med,* 365**,** 2473-83.

CALDERON-MARGALIT, R., FRIEDLANDER, Y., YANETZ, R., KLEINHAUS, K., PERRIN, M. C., MANOR, O., HARLAP, S. & PALTIEL, O. 2009. Cancer risk after exposure to treatments for ovulation induction. *Am J Epidemiol,* 169**,** 365-75.

CANCER GENOME ATLAS RESEARCH, N. 2011. Intergrated genome analyses of ovarian carcinoma. *Nature,* 474**,** 609-15.

CANDIDO-DOS-REIS, F. J., SONG, H., GOODE, E. L., CUNNINGHAM, J. M., FRIDLEY, B. L., LARSON, M. C., ALSOP, K., DICKS, E., HARRINGTON, P., RAMUS, S. J., DE FAZIO, A., MITCHELL, G., FEREDAY, S., BOLTON, K. L., GOURLEY, C., MICHIE, C., KARLAN, B., LESTER, J., WALSH, C., CASS, I., OLSSON, H., GORE,

M., BENITEZ, J. J., GARCIA, M. J., ANDRULIS, I., MULLIGAN, A. M., GLENDON, G., BLANCO, I., LAZARO, C., WHITTEMORE, A. S., MCGUIRE, V., SIEH, W., MONTAGNA, M., ALDUCCI, E., SADETZKI, S., CHETRIT, A., KWONG, A., KJAER, S. K., JENSEN, A., HOGDALL, E., NEUHAUSEN, S., NUSSBAUM, R., DALY, M., GREENE, M. H., MAI, P. L., LOUD, J. T., MOYSICH, K., TOLAND, A. E., LAMBRECHTS, D., ELLIS, S., FROST, D., BRENTON, J. D., TISCHKOWITZ, M., EASTON, D. F., ANTONIOU, A., CHENEVIX-TRENCH, G., GAYTHER, S. A., BOWTELL, D., PHAROAH, P. D., FOR, E., KCONFAB, I. & AUSTRALIAN OVARIAN CANCER STUDY, G. 2015. Germline mutation in BRCA1 or BRCA2 and ten-year survival for women diagnosed with epithelial ovarian cancer. *Clin Cancer Res,* 21**,** 652-7.

CANEVARI, S., GARIBOLDI, M., REID, J. F., BONGARZONE, I. & PIEROTTI, M. A. 2006. Molecular predictors of response and outcome in ovarian cancer. *Crit Rev Oncol Hematol,* 60**,** 19-37.

CHEE, J. L., SAIDIN, S., LANE, D. P., LEONG, S. M., NOLL, J. E., NEILSEN, P. M., PHUA, Y. T., GABRA, H. & LIM, T. M. 2013. Wild-type and mutant p53 mediate cisplatin resistance through interaction and inhibition of active caspase-9. *Cell Cycle,* 12**,** 278-88.

CHIEN, J., KUANG, R., LANDEN, C. & SHRIDHAR, V. 2013. Platinum-sensitive recurrence in ovarian cancer: the role of tumor microenvironment. *Front Oncol,* 3**,** 251.

CHO, H., HUR, H. W., KIM, S. W., KIM, S. H., KIM, J. H., KIM, Y. T. & LEE, K. 2009. Pre-treatment neutrophil to lymphocyte ratio is elevated in epithelial ovarian cancer and predicts survival after treatment. *Cancer Immunol Immunother,* 58**,** 15-23.

CICCIA, A. & ELLEDGE, S. J. 2010. The DNA damage response: making it safe to play with knives. *Mol Cell,* 40**,** 179-204.

COLE, A. J., DWIGHT, T., GILL, A. J., DICKSON, K. A., ZHU, Y., CLARKSON, A., GARD, G. B., MAIDENS, J., VALMADRE, S., CLIFTON-BLIGH, R. & MARSH, D. J. 2016. Assessing mutant p53 in primary high-grade serous ovarian cancer using immunohistochemistry and massively parallel sequencing. *Sci Rep,* 6**,** 26191.

COLEMAN, R. L., OZA, A. M., LORUSSO, D., AGHAJANIAN, C., OAKNIN, A., DEAN, A., COLOMBO, N., WEBERPALS, J. I., CLAMP, A., SCAMBIA, G., LEARY, A., HOLLOWAY, R. W., GANCEDO, M. A., FONG, P. C., GOH, J. C., O'MALLEY,

D. M., ARMSTRONG, D. K., GARCIA-DONAS, J., SWISHER, E. M., FLOQUET, A., KONECNY, G. E., MCNEISH, I. A., SCOTT, C. L., CAMERON, T., MALONEY, L., ISAACSON, J., GOBLE, S., GRACE, C., HARDING, T. C., RAPONI, M., SUN, J., LIN, K. K., GIORDANO, H., LEDERMANN, J. A. & INVESTIGATORS, A. 2017. Rucaparib maintenance treatment for recurrent ovarian carcinoma after response to platinum therapy (ARIEL3): a randomised, double-blind, placebo-controlled, phase 3 trial. *Lancet,* 390**,** 1949-1961.

COLLABORATIVE GROUP ON EPIDEMIOLOGICAL STUDIES OF OVARIAN CANCER 2012. Ovarian cancer and body size: individual participant meta-analysis including 25,157 women with ovarian cancer from 47 epidemiological studies. *PLoS Med,* 9**,** e1001200.

COLLINSON, F., QIAN, W., FOSSATI, R., LISSONI, A., WILLIAMS, C., PARMAR, M., LEDERMANN, J., COLOMBO, N., SWART, A. & COLLABORATORS, I. 2014. Optimal treatment of early-stage ovarian cancer. *Ann Oncol,* 25**,** 1165-71.

COUSSENS, L. M., ZITVOGEL, L. & PALUCKA, A. K. 2013. Neutralizing tumor-promoting chronic inflammation: a magic bullet? *Science,* 339**,** 286-91.

CURIEL, T. J., COUKOS, G., ZOU, L., ALVAREZ, X., CHENG, P., MOTTRAM, P., EVDEMON-HOGAN, M., CONEJO-GARCIA, J. R., ZHANG, L., BUROW, M., ZHU, Y., WEI, S., KRYCZEK, I., DANIEL, B., GORDON, A., MYERS, L., LACKNER, A., DISIS, M. L., KNUTSON, K. L., CHEN, L. & ZOU, W. 2004. Specific recruitment of regulatory T cells in ovarian carcinoma fosters immune privilege and predicts reduced survival. *Nat Med,* 10**,** 942-9.

DASARI, S. & TCHOUNWOU, P. B. 2014. Cisplatin in cancer therapy: molecular mechanisms of action. *Eur J Pharmacol,* 740**,** 364-78.

DE GRAEFF, P., CRIJNS, A. P., DE JONG, S., BOEZEN, M., POST, W. J., DE VRIES, E. G., VAN DER ZEE, A. G. & DE BOCK, G. H. 2009. Modest effect of p53, EGFR and HER-2/neu on prognosis in epithelial ovarian cancer: a meta-analysis. *Br J Cancer,* 101**,** 149-59.

DE LORENZO, S. B., PATEL, A. G., HURLEY, R. M. & KAUFMANN, S. H. 2013. The Elephant and the Blind Men: Making Sense of PARP Inhibitors in Homologous Recombination Deficient Tumor Cells. *Front Oncol,* 3**,** 228.

DENARDO, D. G., BRENNAN, D. J., REXHEPAJ, E., RUFFELL, B., SHIAO, S. L., MADDEN, S. F., GALLAGHER, W. M., WADHWANI, N., KEIL, S. D., JUNAID, S. A., RUGO, H. S., HWANG, E. S., JIRSTROM, K., WEST, B. L. & COUSSENS, L.

M. 2011. Leukocyte complexity predicts breast cancer survival and functionally regulates response to chemotherapy. *Cancer Discov,* 1**,** 54-67.

DI PALMA, T., LUCCI, V., DE CRISTOFARO, T., FILIPPONE, M. G. & ZANNINI, M. 2014. A role for PAX8 in the tumorigenic phenotype of ovarian cancer cells. *BMC Cancer,* 14**,** 292.

DIJKGRAAF, E. M., HEUSINKVELD, M., TUMMERS, B., VOGELPOEL, L. T., GOEDEMANS, R., JHA, V., NORTIER, J. W., WELTERS, M. J., KROEP, J. R. & VAN DER BURG, S. H. 2013. Chemotherapy alters monocyte differentiation to favor generation of cancer-supporting M2 macrophages in the tumor microenvironment. *Cancer Res,* 73**,** 2480-92.

DROST, R., BOUWMAN, P., ROTTENBERG, S., BOON, U., SCHUT, E., KLARENBEEK, S., KLIJN, C., VAN DER HEIJDEN, I., VAN DER GULDEN, H., WIENTJENS, E., PIETERSE, M., CATTEAU, A., GREEN, P., SOLOMON, E., MORRIS, J. R. & JONKERS, J. 2011. BRCA1 RING function is essential for tumor suppression but dispensable for therapy resistance. *Cancer Cell,* 20**,** 797-809.

DUIKER, E. W., MOM, C. H., DE JONG, S., WILLEMSE, P. H., GIETEMA, J. A., VAN DER ZEE, A. G. & DE VRIES, E. G. 2006. The clinical trail of TRAIL. *Eur J Cancer,* 42**,** 2233-40.

DUIKER, E. W., VAN DER ZEE, A. G., DE GRAEFF, P., BOERSMA-VAN EK, W., HOLLEMA, H., DE BOCK, G. H., DE JONG, S. & DE VRIES, E. G. 2010. The extrinsic apoptosis pathway and its prognostic impact in ovarian cancer. *Gynecol Oncol,* 116**,** 549-55.

DUNCAN, T. J., AL-ATTAR, A., ROLLAND, P., SCOTT, I. V., DEEN, S., LIU, D. T., SPENDLOVE, I. & DURRANT, L. G. 2008. Vascular endothelial growth factor expression in ovarian cancer: a model for targeted use of novel therapies? *Clin Cancer Res,* 14**,** 3030-5.

EISENHAUER, E. A., VERMORKEN, J. B. & VAN GLABBEKE, M. 1997. Predictors of response to subsequent chemotherapy in platinum pretreated ovarian cancer: a multivariate analysis of 704 patients [seecomments]. *Ann Oncol,* 8**,** 963-8.

EITAN, R., LEVINE, D. A., ABU-RUSTUM, N., SONODA, Y., HUH, J. N., FRANKLIN, C. C., STEVENS, T. A., BARAKAT, R. R. & CHI, D. S. 2005. The clinical significance of malignant pleural effusions in patients with optimally debulked ovarian carcinoma. *Cancer,* 103**,** 1397-401.

EREZ, N., TRUITT, M., OLSON, P., ARRON, S. T. & HANAHAN, D. 2010. Cancer-Associated Fibroblasts Are Activated in Incipient Neoplasia to Orchestrate Tumor-Promoting Inflammation in an NF-kappaB-Dependent Manner. *Cancer Cell,* 17**,** 135-47.

ETEMADMOGHADAM, D., DEFAZIO, A., BEROUKHIM, R., MERMEL, C., GEORGE, J., GETZ, G., TOTHILL, R., OKAMOTO, A., RAEDER, M. B., HARNETT, P., LADE, S., AKSLEN, L. A., TINKER, A. V., LOCANDRO, B., ALSOP, K., CHIEW, Y. E., TRAFICANTE, N., FEREDAY, S., JOHNSON, D., FOX, S., SELLERS, W., URASHIMA, M., SALVESEN, H. B., MEYERSON, M., BOWTELL, D. & GROUP, A. S. 2009. Integrated genome-wide DNA copy number and expression analysis identifies distinct mechanisms of primary chemoresistance in ovarian carcinomas. *Clin Cancer Res,* 15**,** 1417-27.

ETEMADMOGHADAM, D., WEIR, B. A., AU-YEUNG, G., ALSOP, K., MITCHELL, G., GEORGE, J., AUSTRALIAN OVARIAN CANCER STUDY, G., DAVIS, S., D'ANDREA, A. D., SIMPSON, K., HAHN, W. C. & BOWTELL, D. D. 2013. Synthetic lethality between CCNE1 amplification and loss of BRCA1. *Proc Natl Acad Sci U S A,* 110**,** 19489-94.

EZZATI, M., ABDULLAH, A., SHARIFTABRIZI, A., HOU, J., KOPF, M., STEDMAN, J. K., SAMUELSON, R. & SHAHABI, S. 2014. Recent Advancements in Prognostic Factors of Epithelial Ovarian Carcinoma. *Int Sch Res Notices,* 2014**,** 953509.

FABER, M. T., KJAER, S. K., DEHLENDORFF, C., CHANG-CLAUDE, J., ANDERSEN, K. K., HOGDALL, E., WEBB, P. M., JORDAN, S. J., AUSTRALIAN CANCER, S., AUSTRALIAN OVARIAN CANCER STUDY, G., ROSSING, M. A., DOHERTY, J. A., LURIE, G., THOMPSON, P. J., CARNEY, M. E., GOODMAN, M. T., NESS, R. B., MODUGNO, F., EDWARDS, R. P., BUNKER, C. H., GOODE, E. L., FRIDLEY, B. L., VIERKANT, R. A., LARSON, M. C., SCHILDKRAUT, J., CRAMER, D. W., TERRY, K. L., VITONIS, A. F., BANDERA, E. V., OLSON, S. H., KING, M., CHANDRAN, U., KIEMENEY, L. A., MASSUGER, L. F., VAN ALTENA, A. M., VERMEULEN, S. H., BRINTON, L., WENTZENSEN, N., LISSOWSKA, J., YANG, H. P., MOYSICH, K. B., ODUNSI, K., KASZA, K., ODUNSI-AKANJI, O., SONG, H., PHARAOH, P., SHAH, M., WHITTEMORE, A. S., MCGUIRE, V., SIEH, W., SUTPHEN, R., MENON, U., GAYTHER, S. A., RAMUS, S. J., GENTRY-MAHARAJ, A., PEARCE, C. L., WU, A. H., PIKE, M. C., RISCH, H. A., JENSEN, A. & OVARIAN CANCER ASSOCIATION, C. 2013. Cigarette smoking and risk of

ovarian cancer: a pooled analysis of 21 case-control studies. *Cancer Causes Control,* 24**,** 989-1004.

FARMER, H., MCCABE, N., LORD, C. J., TUTT, A. N., JOHNSON, D. A., RICHARDSON, T. B., SANTAROSA, M., DILLON, K. J., HICKSON, I., KNIGHTS, C., MARTIN, N. M., JACKSON, S. P., SMITH, G. C. & ASHWORTH, A. 2005. Targeting the DNA repair defect in BRCA mutant cells as a therapeutic strategy. *Nature,* 434**,** 917-21.

FERLAY, J., SOERJOMATARAM, I., DIKSHIT, R., ESER, S., MATHERS, C., REBELO, M., PARKIN, D. M., FORMAN, D. & BRAY, F. 2015. Cancer incidence and mortality worldwide: sources, methods and major patterns in GLOBOCAN 2012. *Int J Cancer,* 136**,** E359-86.

FERRARA, N. 1995. The role of vascular endothelial growth factor in pathological angiogenesis. *Breast Cancer Res Treat,* 36**,** 127-37.

FERRY, K. V., HAMILTON, T. C. & JOHNSON, S. W. 2000. Increased nucleotide excision repair in cisplatin-resistant ovarian cancer cells: role of ERCC1-XPF. *Biochem Pharmacol,* 60**,** 1305-13.

FONG, P. C., BOSS, D. S., YAP, T. A., TUTT, A., WU, P., MERGUI-ROELVINK, M., MORTIMER, P., SWAISLAND, H., LAU, A., O'CONNOR, M. J., ASHWORTH, A., CARMICHAEL, J., KAYE, S. B., SCHELLENS, J. H. & DE BONO, J. S. 2009. Inhibition of poly(ADP-ribose) polymerase in tumors from BRCA mutation carriers. *N Engl J Med,* 361**,** 123-34.

FOULKES, W. D. 2006. BRCA1 and BRCA2: chemosensitivity, treatment outcomes and prognosis. *Fam Cancer,* 5**,** 135-42.

FRANTZ, C., STEWART, K. M. & WEAVER, V. M. 2010. The extracellular matrix at a glance. *J Cell Sci,* 123**,** 4195-200.

FRASER, M., ZHAO, H., LUOTO, K. R., LUNDIN, C., COACKLEY, C., CHAN, N., JOSHUA, A. M., BISMAR, T. A., EVANS, A., HELLEDAY, T. & BRISTOW, R. G. 2012. PTEN deletion in prostate cancer cells does not associate with loss of RAD51 function: implications for radiotherapy and chemotherapy. *Clin Cancer Res,* 18**,** 1015-27.

FREEMAN, G. J., LONG, A. J., IWAI, Y., BOURQUE, K., CHERNOVA, T., NISHIMURA, H., FITZ, L. J., MALENKOVICH, N., OKAZAKI, T., BYRNE, M. C., HORTON, H. F., FOUSER, L., CARTER, L., LING, V., BOWMAN, M. R., CARRENO, B. M., COLLINS, M., WOOD, C. R. & HONJO, T. 2000. Engagement of the PD-1

immunoinhibitory receptor by a novel B7 family member leads to negative regulation of lymphocyte activation. *J Exp Med,* 192**,** 1027-34.

FURMAN, R. R., SHARMAN, J. P., COUTRE, S. E., CHESON, B. D., PAGEL, J. M., HILLMEN, P., BARRIENTOS, J. C., ZELENETZ, A. D., KIPPS, T. J., FLINN, I., GHIA, P., ERADAT, H., ERVIN, T., LAMANNA, N., COIFFIER, B., PETTITT, A. R., MA, S., STILGENBAUER, S., CRAMER, P., AIELLO, M., JOHNSON, D. M., MILLER, L. L., LI, D., JAHN, T. M., DANSEY, R. D., HALLEK, M. & O'BRIEN, S. M. 2014. Idelalisib and rituximab in relapsed chronic lymphocytic leukemia. *N Engl J Med,* 370**,** 997-1007.

GADDUCCI, A., COSIO, S., TANA, R. & GENAZZANI, A. R. 2009. Serum and tissue biomarkers as predictive and prognostic variables in epithelial ovarian cancer. *Crit Rev Oncol Hematol,* 69**,** 12-27.

GALLUZZI, L., BUQUE, A., KEPP, O., ZITVOGEL, L. & KROEMER, G. 2015. Immunological Effects of Conventional Chemotherapy and Targeted Anticancer Agents. *Cancer Cell,* 28**,** 690-714.

GALLUZZI, L., SENOVILLA, L., VITALE, I., MICHELS, J., MARTINS, I., KEPP, O., CASTEDO, M. & KROEMER, G. 2012. Molecular mechanisms of cisplatin resistance. *Oncogene,* 31**,** 1869-83.

GARCIA, A. J., RUSCETTI, M., ARENZANA, T. L., TRAN, L. M., BIANCI-FRIAS, D., SYBERT, E., PRICEMAN, S. J., WU, L., NELSON, P. S., SMALE, S. T. & WU, H. 2014. Pten null prostate epithelium promotes localized myeloid-derived suppressor cell expansion and immune suppression during tumor initiation and progression. *Mol Cell Biol,* 34**,** 2017-28.

GEISLER, J. P., GEISLER, H. E., MILLER, G. A., WIEMANN, M. C., ZHOU, Z. & CRABTREE, W. 2000. p53 and bcl-2 in epithelial ovarian carcinoma: their value as prognostic indicators at a median follow-up of 60 months. *Gynecol Oncol,* 77**,** 278-82.

GEOMINI, P., KRUITWAGEN, R., BREMER, G. L., CNOSSEN, J. & MOL, B. W. 2009. The accuracy of risk scores in predicting ovarian malignancy: a systematic review. *Obstet Gynecol,* 113**,** 384-94.

GO, R. S. & ADJEI, A. A. 1999. Review of the comparative pharmacology and clinical activity of cisplatin and carboplatin. *J Clin Oncol,* 17**,** 409-22.

GOCHEVA, V., WANG, H. W., GADEA, B. B., SHREE, T., HUNTER, K. E., GARFALL, A. L., BERMAN, T. & JOYCE, J. A. 2010. IL-4 induces cathepsin protease

activity in tumor-associated macrophages to promote cancer growth and invasion. *Genes Dev,* 24**,** 241-55.

GODOY, H. E., KHAN, A. N., VETHANAYAGAM, R. R., GRIMM, M. J., SINGEL, K. L., KOLOMEYEVSKAYA, N., SEXTON, K. J., PARAMESWARAN, A., ABRAMS, S. I., ODUNSI, K. & SEGAL, B. H. 2013. Myeloid-derived suppressor cells modulate immune responses independently of NADPH oxidase in the ovarian tumor microenvironment in mice. *PLoS One,* 8**,** e69631.

GOLDING, S. E., ROSENBERG, E., KHALIL, A., MCEWEN, A., HOLMES, M., NEILL, S., POVIRK, L. F. & VALERIE, K. 2004. Double strand break repair by homologous recombination is regulated by cell cycle-independent signaling via ATM in human glioma cells. *J Biol Chem,* 279**,** 15402-10.

GOODSELL, D. S. 2006. The molecular perspective: cisplatin. *Oncologist,* 11**,** 316-7.

HANAHAN, D. & COUSSENS, L. M. 2012. Accessories to the crime: functions of cells recruited to the tumor microenvironment. *Cancer Cell,* 21**,** 309-22.

HANCOX, U., COSULICH, S., HANSON, L., TRIGWELL, C., LENAGHAN, C., ELLSTON, R., DRY, H., CRAFTER, C., BARLAAM, B., FITZEK, M., SMITH, P. D., OGILVIE, D., D'CRUZ, C., CASTRIOTTA, L., WEDGE, S. R., WARD, L., POWELL, S., LAWSON, M., DAVIES, B. R., HARRINGTON, E. A., FOSTER, E., CUMBERBATCH, M., GREEN, S. & BARRY, S. T. 2015. Inhibition of PI3Kbeta signaling with AZD8186 inhibits growth of PTEN-deficient breast and prostate tumors alone and in combination with docetaxel. *Mol Cancer Ther,* 14**,** 48-58.

HANSEN, J. M., COLEMAN, R. L. & SOOD, A. K. 2016. Targeting the tumour microenvironment in ovarian cancer. *Eur J Cancer,* 56**,** 131-43.

HARRELL, M. I., IRITANI, B. M. & RUDDELL, A. 2007. Tumor-induced sentinel lymph node lymphangiogenesis and increased lymph flow precede melanoma metastasis. *Am J Pathol,* 170**,** 774-86.

HARTER, P., SEHOULI, J. & LORUSSO, D. 2017. LION: Lymphadenectomy in ovarian neoplasms. *2017 ASCO Annual Meeting, Chicago*.

HEFLER, L. A., ZEILLINGER, R., GRIMM, C., SOOD, A. K., CHENG, W. F., GADDUCCI, A., TEMPFER, C. B. & REINTHALLER, A. 2006. Preoperative serum vascular endothelial growth factor as a prognostic parameter in ovarian cancer. *Gynecol Oncol,* 103**,** 512-7.

HEUSINKVELD, M. & VAN DER BURG, S. H. 2011. Identification and manipulation of tumor associated macrophages in human cancers. *J Transl Med,* 9**,** 216.

HEW, K. E., MILLER, P. C., EL-ASHRY, D., SUN, J., BESSER, A. H., INCE, T. A., GU, M., WEI, Z., ZHANG, G., BRAFFORD, P., GAO, W., LU, Y., MILLS, G. B., SLINGERLAND, J. M. & SIMPKINS, F. 2016. MAPK Activation Predicts Poor Outcome and the MEK Inhibitor, Selumetinib, Reverses Antiestrogen Resistance in ER-Positive High-Grade Serous Ovarian Cancer. *Clin Cancer Res,* 22**,** 935-47.

HILEY, C. T. & SWANTON, C. 2014. Spatial and temporal cancer evolution: causes and consequences of tumour diversity. *Clin Med,* 14 Suppl 6**,** s33-7.

HOGDALL, E. V., CHRISTENSEN, L., KJAER, S. K., BLAAKAER, J., CHRISTENSEN, I. J., GAYTHER, S., JACOBS, I. J. & HOGDALL, C. K. 2007. Expression level of Wilms tumor 1 (WT1) protein has limited prognostic value in epithelial ovarian cancer: from the Danish "MALOVA" ovarian cancer study. *Gynecol Oncol,* 106**,** 318-24.

HONGO, A., SEKI, S., AKIYAMA, K. & KUDO, T. 1994. A comparison of *in vitro* platinum-DNA adduct formation between carboplatin and cisplatin. *Int J Biochem,* 26**,** 1009-16.

HORAK, P., PILS, D., KAIDER, A., PINTER, A., ELANDT, K., SAX, C., ZIELINSKI, C. C., HORVAT, R., ZEILLINGER, R., REINTHALLER, A. & KRAINER, M. 2005. Perturbation of the tumor necrosis factor--related apoptosis-inducing ligand cascade in ovarian cancer: overexpression of FLIPL and deregulation of the functional receptors DR4 and DR5. *Clin Cancer Res,* 11**,** 8585-91.

HSIAO, M. C., PIOTROWSKI, A., CALLENS, T., FU, C., WIMMER, K., CLAES, K. B. & MESSIAEN, L. 2015. Decoding NF1 Intragenic Copy-Number Variations. *Am J Hum Genet,* 97**,** 238-49.

HUEN, M. S., SY, S. M. & CHEN, J. 2010. BRCA1 and its toolbox for the maintenance of genome integrity. *Nat Rev Mol Cell Biol,* 11**,** 138-48.

HUNT, C. R., GUPTA, A., HORIKOSHI, N. & PANDITA, T. K. 2012. Does PTEN loss impair DNA double-strand break repair by homologous recombination? *Clin Cancer Res,* 18**,** 920-2.

ICHIKAWA, M., WILLIAMS, R., WANG, L., VOGL, T. & SRIKRISHNA, G. 2011. S100A8/A9 activate key genes and pathways in colon tumor progression. *Mol Cancer Res,* 9**,** 133-48.

INGHAM, S. L., WARWICK, J., BUCHAN, I., SAHIN, S., O'HARA, C., MORAN, A., HOWELL, A. & EVANS, D. G. 2013. Ovarian cancer among 8,005 women from a breast cancer family history clinic: no increased risk of invasive ovarian cancer in families testing negative for BRCA1 and BRCA2. *J Med Genet,* 50**,** 368-72.

IOANNIDES, C. G., PLATSOUCAS, C. D., RASHED, S., WHARTON, J. T., EDWARDS, C. L. & FREEDMAN, R. S. 1991. Tumor cytolysis by lymphocytes infiltrating ovarian malignant ascites. *Cancer Res,* 51**,** 4257-65.

JACOBS, I. & BAST, R. C., JR. 1989. The CA 125 tumour-associated antigen: a review of the literature. *Hum Reprod,* 4**,** 1-12.

JAIN, R. K. 2005. Normalization of tumor vasculature: an emerging concept in antiangiogenic therapy. *Science,* 307**,** 58-62.

JAYSON, G. C., KOHN, E. C., KITCHENER, H. C. & LEDERMANN, J. A. 2014. Ovarian cancer. *Lancet,* 384**,** 1376-88.

JENSEN, A., SHARIF, H., FREDERIKSEN, K. & KJAER, S. K. 2009. Use of fertility drugs and risk of ovarian cancer: Danish Population Based Cohort Study. *BMJ,* 338**,** b249.

JERVIS, S., SONG, H., LEE, A., DICKS, E., TYRER, J., HARRINGTON, P., EASTON, D. F., JACOBS, I. J., PHAROAH, P. P. & ANTONIOU, A. C. 2014. Ovarian cancer familial relative risks by tumour subtypes and by known ovarian cancer genetic susceptibility variants. *J Med Genet,* 51**,** 108-13.

KANCHI, K. L., JOHNSON, K. J., LU, C., MCLELLAN, M. D., LEISERSON, M. D., WENDL, M. C., ZHANG, Q., KOBOLDT, D. C., XIE, M., KANDOTH, C., MCMICHAEL, J. F., WYCZALKOWSKI, M. A., LARSON, D. E., SCHMIDT, H. K., MILLER, C. A., FULTON, R. S., SPELLMAN, P. T., MARDIS, E. R., DRULEY, T. E., GRAUBERT, T. A., GOODFELLOW, P. J., RAPHAEL, B. J., WILSON, R. K. & DING, L. 2014. Integrated analysis of germline and somatic variants in ovarian cancer. *Nat Commun,* 5**,** 3156.

KANG, H. J., CHUN, S. M., KIM, K. R., SOHN, I. & SUNG, C. O. 2013. Clinical relevance of gain-of-function mutations of p53 in high-grade serous ovarian carcinoma. *PLoS One,* 8**,** e72609.

KANG, S., JU, W., KIM, J. W., PARK, N. H., SONG, Y. S., KIM, S. C., PARK, S. Y., KANG, S. B. & LEE, H. P. 2006. Association between excision repair cross-complementation group 1 polymorphism and clinical outcome of platinum-

based chemotherapy in patients with epithelial ovarian cancer. *Exp Mol Med,* 38**,** 320-4.

KAYE, S. B., LUBINSKI, J., MATULONIS, U., ANG, J. E., GOURLEY, C., KARLAN, B. Y., AMNON, A., BELL-MCGUINN, K. M., CHEN, L. M., FRIEDLANDER, M., SAFRA, T., VERGOTE, I., WICKENS, M., LOWE, E. S., CARMICHAEL, J. & KAUFMAN, B. 2012. Phase II, open-label, randomized, multicenter study comparing the efficacy and safety of olaparib, a poly (ADP-ribose) polymerase inhibitor, and pegylated liposomal doxorubicin in patients with BRCA1 or BRCA2 mutations and recurrent ovarian cancer. *J Clin Oncol,* 30**,** 372-9.

KEHOE, S., HOOK, J., NANKIVELL, M., JAYSON, G. C., KITCHENER, H., LOPES, T., LUESLEY, D., PERREN, T., BANNOO, S., MASCARENHAS, M., DOBBS, S., ESSAPEN, S., TWIGG, J., HEROD, J., MCCLUGGAGE, G., PARMAR, M. & SWART, A. M. 2015. Primary chemotherapy versus primary surgery for newly diagnosed advanced ovarian cancer (CHORUS): an open-label, randomised, controlled, non-inferiority trial. *Lancet*.

KIM, H. S., KIM, T. H., CHUNG, H. H. & SONG, Y. S. 2014. Risk and prognosis of ovarian cancer in women with endometriosis: a meta-analysis. *Br J Cancer,* 110**,** 1878-90.

KIM, J., COFFEY, D. M., CREIGHTON, C. J., YU, Z., HAWKINS, S. M. & MATZUK, M. M. 2012. High-grade serous ovarian cancer arises from fallopian tube in a mouse model. *Proc Natl Acad Sci U S A,* 109**,** 3921-6.

KIRKEGAARD, T., EDWARDS, J., TOVEY, S., MCGLYNN, L. M., KRISHNA, S. N., MUKHERJEE, R., TAM, L., MUNRO, A. F., DUNNE, B. & BARTLETT, J. M. 2006. Observer variation in immunohistochemical analysis of protein expression, time for a change? *Histopathology,* 48**,** 787-94.

KITAMURA, T., FUJISHITA, T., LOETSCHER, P., REVESZ, L., HASHIDA, H., KIZAKA-KONDOH, S., AOKI, M. & TAKETO, M. M. 2010. Inactivation of chemokine (C-C motif) receptor 1 (CCR1) suppresses colon cancer liver metastasis by blocking accumulation of immature myeloid cells in a mouse model. *Proc Natl Acad Sci U S A,* 107**,** 13063-8.

KOBEL, M., KALLOGER, S. E., BOYD, N., MCKINNEY, S., MEHL, E., PALMER, C., LEUNG, S., BOWEN, N. J., IONESCU, D. N., RAJPUT, A., PRENTICE, L. M., MILLER, D., SANTOS, J., SWENERTON, K., GILKS, C. B. & HUNTSMAN, D.

2008. Ovarian carcinoma subtypes are different diseases: implications for biomarker studies. *PLoS Med,* 5**,** e232.

KOLASA, I. K., REMBISZEWSKA, A., FELISIAK, A., ZIOLKOWSKA-SETA, I., MURAWSKA, M., MOES, J., TIMOREK, A., DANSONKA-MIESZKOWSKA, A. & KUPRYJANCZYK, J. 2009. PIK3CA amplification associates with resistance to chemotherapy in ovarian cancer patients. *Cancer Biol Ther,* 8**,** 21-6.

KONSTANTINOPOULOS, P. A., CECCALDI, R., SHAPIRO, G. I. & D'ANDREA, A. D. 2015. Homologous Recombination Deficiency: Exploiting the Fundamental Vulnerability of Ovarian Cancer. *Cancer Discov,* 5**,** 1137-54.

KORKOLOPOULOU, P., VASSILOPOULOS, I., KONSTANTINIDOU, A. E., ZORZOS, H., PATSOURIS, E., AGAPITOS, E. & DAVARIS, P. 2002. The combined evaluation of p27Kip1 and Ki-67 expression provides independent information on overall survival of ovarian carcinoma patients. *Gynecol Oncol,* 85**,** 404-14.

LABIDI-GALY, S. I., OLIVIER, T., RODRIGUES, M., FERRAIOLI, D., DERBEL, O., BODMER, A., PETIGNAT, P., RAK, B., CHOPIN, N., TREDAN, O., HEUDEL, P. E., STUCKELBERGER, S., MEEUS, P., MERALDI, P., VIASSOLO, V., AYME, A., CHAPPUIS, P. O., STERN, M. H., HOUDAYER, C., STOPPA-LYONNET, D., BUISSON, A., GOLMARD, L., BONADONA, V. & RAY-COQUARD, I. 2017a. Location of Mutation in BRCA2 Gene and Survival in Patients with Ovarian Cancer. *Clin Cancer Res*.

LABIDI-GALY, S. I., PAPP, E., HALLBERG, D., NIKNAFS, N., ADLEFF, V., NOE, M., BHATTACHARYA, R., NOVAK, M., JONES, S., PHALLEN, J., HRUBAN, C. A., HIRSCH, M. S., LIN, D. I., SCHWARTZ, L., MAIRE, C. L., TILLE, J. C., BOWDEN, M., AYHAN, A., WOOD, L. D., SCHARPF, R. B., KURMAN, R., WANG, T. L., SHIH, I. M., KARCHIN, R., DRAPKIN, R. & VELCULESCU, V. E. 2017b. High grade serous ovarian carcinomas originate in the fallopian tube. *Nat Commun,* 8**,** 1093.

LE PAGE, C., HUNTSMAN, D. G., PROVENCHER, D. M. & MES-MASSON, A. M. 2010. Predictive and prognostic protein biomarkers in epithelial ovarian cancer: recommendation for future studies. *Cancers (Basel),* 2**,** 913-54.

LECHNER, M. G., LIEBERTZ, D. J. & EPSTEIN, A. L. 2010. Characterization of cytokine-induced myeloid-derived suppressor cells from normal human peripheral blood mononuclear cells. *J Immunol,* 185**,** 2273-84.

LEDERMANN, J., HARTER, P., GOURLEY, C., FRIEDLANDER, M., VERGOTE, I., RUSTIN, G., SCOTT, C., MEIER, W., SHAPIRA-FROMMER, R., SAFRA, T.,

MATEI, D., MACPHERSON, E., WATKINS, C., CARMICHAEL, J. & MATULONIS, U. 2012. Olaparib maintenance therapy in platinum-sensitive relapsed ovarian cancer. *N Engl J Med,* 366**,** 1382-92.

LEDERMANN, J., HARTER, P., GOURLEY, C., FRIEDLANDER, M., VERGOTE, I., RUSTIN, G., SCOTT, C. L., MEIER, W., SHAPIRA-FROMMER, R., SAFRA, T., MATEI, D., FIELDING, A., SPENCER, S., DOUGHERTY, B., ORR, M., HODGSON, D., BARRETT, J. C. & MATULONIS, U. 2014. Olaparib maintenance therapy in patients with platinum-sensitive relapsed serous ovarian cancer: a preplanned retrospective analysis of outcomes by BRCA status in a randomised phase 2 trial. *Lancet Oncol,* 15**,** 852-61.

LEE, J. Y., JEON, I., KIM, J. W., SONG, Y. S., YOON, J. M. & PARK, S. M. 2013. Diabetes mellitus and ovarian cancer risk: a systematic review and meta-analysis of observational studies. *Int J Gynecol Cancer,* 23**,** 402-12.

LEE, S., CHOI, E. J., JIN, C. & KIM, D. H. 2005. Activation of PI3K/Akt pathway by PTEN reduction and PIK3CA mRNA amplification contributes to cisplatin resistance in an ovarian cancer cell line. *Gynecol Oncol,* 97**,** 26-34.

LEE, Y., MIRON, A., DRAPKIN, R., NUCCI, M. R., MEDEIROS, F., SALEEMUDDIN, A., GARBER, J., BIRCH, C., MOU, H., GORDON, R. W., CRAMER, D. W., MCKEON, F. D. & CRUM, C. P. 2007. A candidate precursor to serous carcinoma that originates in the distal fallopian tube. *J Pathol,* 211**,** 26-35.

LEUNG, C. C. & GLOVER, J. N. 2011. BRCT domains: easy as one, two, three. *Cell Cycle,* 10**,** 2461-70.

LEVY-LAHAD, E., CATANE, R., EISENBERG, S., KAUFMAN, B., HORNREICH, G., LISHINSKY, E., SHOHAT, M., WEBER, B. L., BELLER, U., LAHAD, A. & HALLE, D. 1997. Founder BRCA1 and BRCA2 mutations in Ashkenazi Jews in Israel: frequency and differential penetrance in ovarian cancer and in breast-ovarian cancer families. *Am J Hum Genet,* 60**,** 1059-67.

LINDEBOOM, R. G., SUPEK, F. & LEHNER, B. 2016. The rules and impact of nonsense-mediated mRNA decay in human cancers. *Nat Genet,* 48**,** 1112-8.

LIOU, G. Y., DOPPLER, H., NECELA, B., KRISHNA, M., CRAWFORD, H. C., RAIMONDO, M. & STORZ, P. 2013. Macrophage-secreted cytokines drive pancreatic acinar-to-ductal metaplasia through NF-kappaB and MMPs. *J Cell Biol,* 202**,** 563-77.

LO, C. S., SANII, S., KROEGER, D. R., MILNE, K., TALHOUK, A., CHIU, D. S., RAHIMI, K., SHAW, P. A., CLARKE, B. A. & NELSON, B. H. 2017. Neoadjuvant

Chemotherapy of Ovarian Cancer Results in Three Patterns of Tumor-Infiltrating Lymphocyte Response with Distinct Implications for Immunotherapy. *Clin Cancer Res,* 23**,** 925-934.

LORD, C. J. & ASHWORTH, A. 2013. Mechanisms of resistance to therapies targeting BRCA-mutant cancers. *Nat Med,* 19**,** 1381-8.

LUKANOVA, A. & KAAKS, R. 2005. Endogenous hormones and ovarian cancer: epidemiology and current hypotheses. *Cancer Epidemiol Biomarkers Prev,* 14**,** 98-107.

LYNCH, H. T., SNYDER, C. & CASEY, M. J. 2013. Hereditary ovarian and breast cancer: what have we learned? *Ann Oncol,* 24 Suppl 8**,** viii83-viii95.

MACKAY, H. J., BRADY, M. F., OZA, A. M., REUSS, A., PUJADE-LAURAINE, E., SWART, A. M., SIDDIQUI, N., COLOMBO, N., BOOKMAN, M. A., PFISTERER, J., DU BOIS, A. & GYNECOLOGIC CANCER, I. 2010. Prognostic relevance of uncommon ovarian histology in women with stage III/IV epithelial ovarian cancer. *Int J Gynecol Cancer,* 20**,** 945-52.

MADORE, J., REN, F., FILALI-MOUHIM, A., SANCHEZ, L., KOBEL, M., TONIN, P. N., HUNTSMAN, D., PROVENCHER, D. M. & MES-MASSON, A. M. 2010. Characterization of the molecular differences between ovarian endometrioid carcinoma and ovarian serous carcinoma. *J Pathol,* 220**,** 392-400.

MANTOVANI, A., ALLAVENA, P., SOZZANI, S., VECCHI, A., LOCATI, M. & SICA, A. 2004a. Chemokines in the recruitment and shaping of the leukocyte infiltrate of tumors. *Semin Cancer Biol,* 14**,** 155-60.

MANTOVANI, A., SICA, A., SOZZANI, S., ALLAVENA, P., VECCHI, A. & LOCATI, M. 2004b. The chemokine system in diverse forms of macrophage activation and polarization. *Trends Immunol,* 25**,** 677-86.

MARKMAN, M., ROTHMAN, R., HAKES, T., REICHMAN, B., HOSKINS, W., RUBIN, S., JONES, W., ALMADRONES, L. & LEWIS, J. L., JR. 1991. Second-line platinum therapy in patients with ovarian cancer previously treated with cisplatin. *J Clin Oncol,* 9**,** 389-93.

MARTIN, L. P., HAMILTON, T. C. & SCHILDER, R. J. 2008. Platinum resistance: the role of DNA repair pathways. *Clin Cancer Res,* 14**,** 1291-5.

MARTINEZ, F. O., GORDON, S., LOCATI, M. & MANTOVANI, A. 2006. Transcriptional profiling of the human monocyte-to-macrophage differentiation and

polarization: new molecules and patterns of gene expression. *J Immunol,* 177**,** 7303-11.

MARTINS, F. C., SANTIAGO, I., TRINH, A., XIAN, J., GUO, A., SAYAL, K., JIMENEZ-LINAN, M., DEEN, S., DRIVER, K., MACK, M., ASLOP, J., PHAROAH, P. D., MARKOWETZ, F. & BRENTON, J. D. 2014. Combined image and genomic analysis of high-grade serous ovarian cancer reveals PTEN loss as a common driver event and prognostic classifier. *Genome Biol,* 15**,** 526.

MCELLIN, B., CAMACHO, C. V., MUKHERJEE, B., HAHM, B., TOMIMATSU, N., BACHOO, R. M. & BURMA, S. 2010. PTEN loss compromises homologous recombination repair in astrocytes: implications for glioblastoma therapy with temozolomide or poly(ADP-ribose) polymerase inhibitors. *Cancer Res,* 70**,** 5457-64.

MCGUIRE, W. P., HOSKINS, W. J., BRADY, M. F., KUCERA, P. R., PARTRIDGE, E. E., LOOK, K. Y., CLARKE-PEARSON, D. L. & DAVIDSON, M. 1996. Cyclophosphamide and cisplatin compared with paclitaxel and cisplatin in patients with stage III and stage IV ovarian cancer. *N Engl J Med,* 334**,** 1-6.

MENDES-PEREIRA, A. M., MARTIN, S. A., BROUGH, R., MCCARTHY, A., TAYLOR, J. R., KIM, J. S., WALDMAN, T., LORD, C. J. & ASHWORTH, A. 2009. Synthetic lethal targeting of PTEN mutant cells with PARP inhibitors. *EMBO Mol Med,* 1**,** 315-22.

MERRITT, W. M., LIN, Y. G., HAN, L. Y., KAMAT, A. A., SPANNUTH, W. A., SCHMANDT, R., URBAUER, D., PENNACCHIO, L. A., CHENG, J. F., NICK, A. M., DEAVERS, M. T., MOURAD-ZEIDAN, A., WANG, H., MUELLER, P., LENBURG, M. E., GRAY, J. W., MOK, S., BIRRER, M. J., LOPEZ-BERESTEIN, G., COLEMAN, R. L., BAR-ELI, M. & SOOD, A. K. 2008. Dicer, Drosha, and outcomes in patients with ovarian cancer. *N Engl J Med,* 359**,** 2641-50.

MICHAUD, M., MARTINS, I., SUKKURWALA, A. Q., ADJEMIAN, S., MA, Y., PELLEGATTI, P., SHEN, S., KEPP, O., SCOAZEC, M., MIGNOT, G., RELLO-VARONA, S., TAILLER, M., MENGER, L., VACCHELLI, E., GALLUZZI, L., GHIRINGHELLI, F., DI VIRGILIO, F., ZITVOGEL, L. & KROEMER, G. 2011. Autophagy-dependent anticancer immune responses induced by chemotherapeutic agents in mice. *Science,* 334**,** 1573-7.

MILLS, C. D. 2012. M1 and M2 Macrophages: Oracles of Health and Disease. *Crit Rev Immunol,* 32**,** 463-88.

MIRZA, M. R., MONK, B. J., HERRSTEDT, J., OZA, A. M., MAHNER, S., REDONDO, A., FABBRO, M., LEDERMANN, J. A., LORUSSO, D., VERGOTE, I., BEN-BARUCH, N. E., MARTH, C., MADRY, R., CHRISTENSEN, R. D., BEREK, J. S., DORUM, A., TINKER, A. V., DU BOIS, A., GONZALEZ-MARTIN, A., FOLLANA, P., BENIGNO, B., ROSENBERG, P., GILBERT, L., RIMEL, B. J., BUSCEMA, J., BALSER, J. P., AGARWAL, S., MATULONIS, U. A. & INVESTIGATORS, E.-O. N. 2016. Niraparib Maintenance Therapy in Platinum-Sensitive, Recurrent Ovarian Cancer. *N Engl J Med,* 375**,** 2154-2164.

MUKHOPADHYAY, A., ELATTAR, A., CERBINSKAITE, A., WILKINSON, S. J., DREW, Y., KYLE, S., LOS, G., HOSTOMSKY, Z., EDMONDSON, R. J. & CURTIN, N. J. 2010. Development of a functional assay for homologous recombination status in primary cultures of epithelial ovarian tumor and correlation with sensitivity to poly(ADP-ribose) polymerase inhibitors. *Clin Cancer Res,* 16**,** 2344-51.

MULLER, P. A. & VOUSDEN, K. H. 2013. p53 mutations in cancer. *Nat Cell Biol,* 15**,** 2-8.

MULLER, P. A. & VOUSDEN, K. H. 2014. Mutant p53 in cancer: new functions and therapeutic opportunities. *Cancer Cell,* 25**,** 304-17.

NAGARAJ, A. B., JOSEPH, P., KOVALENKO, O., SINGH, S., ARMSTRONG, A., REDLINE, R., RESNICK, K., ZANOTTI, K., WAGGONER, S. & DIFEO, A. 2015. Critical role of Wnt/beta-catenin signaling in driving epithelial ovarian cancer platinum resistance. *Oncotarget,* 6**,** 23720-34.

NEUFELD, G., TESSLER, S., GITAY-GOREN, H., COHEN, T. & LEVI, B. Z. 1994. Vascular endothelial growth factor and its receptors. *Prog Growth Factor Res,* 5**,** 89-97.

NIEMAN, K. M., KENNY, H. A., PENICKA, C. V., LADANYI, A., BUELL-GUTBROD, R., ZILLHARDT, M. R., ROMERO, I. L., CAREY, M. S., MILLS, G. B., HOTAMISLIGIL, G. S., YAMADA, S. D., PETER, M. E., GWIN, K. & LENGYEL, E. 2011. Adipocytes promote ovarian cancer metastasis and provide energy for rapid tumor growth. *Nat Med,* 17**,** 1498-503.

NORQUIST, B. M., BRADY, M. F., HARRELL, M. I., WALSH, T., LEE, M. K., GULSUNER, S., BERNARDS, S. S., CASADEI, S., BURGER, R. A., TEWARI, K. S., BACKES, F. J., MANNEL, R. S., GLASER, G., BAILEY, C., RUBIN, S. C., SOPER, J. T., LANKES, H. A., RAMIREZ, N. C., KING, M. C., BIRRER, M. J. & SWISHER, E. M. 2017. Mutations in Homologous Recombination Genes and Outcomes in

Ovarian Carcinoma Patients in GOG 218: an NRG Oncology/Gynecologic Oncology Group Study. *Clin Cancer Res*.

NOY, R. & POLLARD, J. W. 2014. Tumor-associated macrophages: from mechanisms to therapy. *Immunity,* 41**,** 49-61.

O'KEEFFE, M. B., DEVLIN, A. H., BURNS, A. J., GARDINER, T. A., LOGAN, I. D., HIRST, D. G. & MCKEOWN, S. R. 2008. Investigation of pericytes, hypoxia, and vascularity in bladder tumors: association with clinical outcomes. *Oncol Res,* 17**,** 93-101.

OBERMAJER, N., MUTHUSWAMY, R., ODUNSI, K., EDWARDS, R. P. & KALINSKI, P. 2011. PGE(2)-induced CXCL12 production and CXCR4 expression controls the accumulation of human MDSCs in ovarian cancer environment. *Cancer Res,* 71**,** 7463-70.

OBERMUELLER, E., VOSSELER, S., FUSENIG, N. E. & MUELLER, M. M. 2004. Cooperative autocrine and paracrine functions of granulocyte colony-stimulating factor and granulocyte-macrophage colony-stimulating factor in the progression of skin carcinoma cells. *Cancer Res,* 64**,** 7801-12.

OHTA, T., OHMICHI, M., HAYASAKA, T., MABUCHI, S., SAITOH, M., KAWAGOE, J., TAKAHASHI, K., IGARASHI, H., DU, B., DOSHIDA, M., MIREI, I. G., MOTOYAMA, T., TASAKA, K. & KURACHI, H. 2006. Inhibition of phosphatidylinositol 3-kinase increases efficacy of cisplatin in *in vivo* ovarian cancer models. *Endocrinology,* 147**,** 1761-9.

OMURA, G. A., BRADY, M. F., HOMESLEY, H. D., YORDAN, E., MAJOR, F. J., BUCHSBAUM, H. J. & PARK, R. C. 1991. Long-term follow-up and prognostic factor analysis in advanced ovarian carcinoma: the Gynecologic Oncology Group experience. *J Clin Oncol,* 9**,** 1138-50.

OUELLET, V., LE PAGE, C., MADORE, J., GUYOT, M. C., BARRES, V., LUSSIER, C., TONIN, P. N., PROVENCHER, D. M. & MES-MASSON, A. M. 2007. An apoptotic molecular network identified by microarray: on the TRAIL to new insights in epithelial ovarian cancer. *Cancer,* 110**,** 297-308.

OZA, A. M., COOK, A. D., PFISTERER, J., EMBLETON, A., LEDERMANN, J. A., PUJADE-LAURAINE, E., KRISTENSEN, G., CAREY, M. S., BEALE, P., CERVANTES, A., PARK-SIMON, T. W., RUSTIN, G., JOLY, F., MIRZA, M. R., PLANTE, M., QUINN, M., POVEDA, A., JAYSON, G. C., STARK, D., SWART, A. M., FARRELLY, L., KAPLAN, R., PARMAR, M. K., PERREN, T. J. & INVESTIGATORS, I. T. 2015. Standard chemotherapy with or without

bevacizumab for women with newly diagnosed ovarian cancer (ICON7): overall survival results of a phase 3 randomised trial. *Lancet Oncol*, 16, 928-36.

OZOLS, R. F., GARVIN, A. J., COSTA, J., SIMON, R. M. & YOUNG, R. C. 1980. Advanced ovarian cancer: correlation of histologic grade with response to therapy and survival. *Cancer,* 45, 572-81.

PANICI, P. B., MAGGIONI, A., HACKER, N., LANDONI, F., ACKERMANN, S., CAMPAGNUTTA, E., TAMUSSINO, K., WINTER, R., PELLEGRINO, A., GREGGI, S., ANGIOLI, R., MANCI, N., SCAMBIA, G., DELL'ANNA, T., FOSSATI, R., FLORIANI, I., ROSSI, R. S., GRASSI, R., FAVALLI, G., RASPAGLIESI, F., GIANNARELLI, D., MARTELLA, L. & MANGIONI, C. 2005. Systematic aortic and pelvic lymphadenectomy versus resection of bulky nodes only in optimally debulked advanced ovarian cancer: a randomized clinical trial. *J Natl Cancer Inst,* 97, 560-6.

PARMAR, M. K., LEDERMANN, J. A., COLOMBO, N., DU BOIS, A., DELALOYE, J. F., KRISTENSEN, G. B., WHEELER, S., SWART, A. M., QIAN, W., TORRI, V., FLORIANI, I., JAYSON, G., LAMONT, A., TROPE, C., ICON & COLLABORATORS, A. G. O. 2003. Paclitaxel plus platinum-based chemotherapy versus conventional platinum-based chemotherapy in women with relapsed ovarian cancer: the ICON4/AGO-OVAR-2.2 trial. *Lancet,* 361, 2099-106.

PATCH, A. M., CHRISTIE, E. L., ETEMADMOGHADAM, D., GARSED, D. W., GEORGE, J., FEREDAY, S., NONES, K., COWIN, P., ALSOP, K., BAILEY, P. J., KASSAHN, K. S., NEWELL, F., QUINN, M. C., KAZAKOFF, S., QUEK, K., WILHELM-BENARTZI, C., CURRY, E., LEONG, H. S., AUSTRALIAN OVARIAN CANCER STUDY, G., HAMILTON, A., MILESHKIN, L., AU-YEUNG, G., KENNEDY, C., HUNG, J., CHIEW, Y. E., HARNETT, P., FRIEDLANDER, M., QUINN, M., PYMAN, J., CORDNER, S., O'BRIEN, P., LEDITSCHKE, J., YOUNG, G., STRACHAN, K., WARING, P., AZAR, W., MITCHELL, C., TRAFICANTE, N., HENDLEY, J., THORNE, H., SHACKLETON, M., MILLER, D. K., ARNAU, G. M., TOTHILL, R. W., HOLLOWAY, T. P., SEMPLE, T., HARLIWONG, I., NOURSE, C., NOURBAKHSH, E., MANNING, S., IDRISOGLU, S., BRUXNER, T. J., CHRIST, A. N., POUDEL, B., HOLMES, O., ANDERSON, M., LEONARD, C., LONIE, A., HALL, N., WOOD, S., TAYLOR, D. F., XU, Q., FINK, J. L., WADDELL, N., DRAPKIN, R., STRONACH, E., GABRA, H., BROWN, R., JEWELL, A., NAGARAJ, S. H., MARKHAM, E., WILSON, P. J., ELLUL, J., MCNALLY, O., DOYLE, M. A.,

VEDURURU, R., STEWART, C., LENGYEL, E., PEARSON, J. V., WADDELL, N., DEFAZIO, A., GRIMMOND, S. M. & BOWTELL, D. D. 2015. Whole-genome characterization of chemoresistant ovarian cancer. *Nature,* 521**,** 489-94.

PATHAK, A. P., ARTEMOV, D., NEEMAN, M. & BHUJWALLA, Z. M. 2006. Lymph node metastasis in breast cancer xenografts is associated with increased regions of extravascular drain, lymphatic vessel area, and invasive phenotype. *Cancer Res,* 66**,** 5151-8.

PENNINGTON, K. P., WALSH, T., HARRELL, M. I., LEE, M. K., PENNIL, C. C., RENDI, M. H., THORNTON, A., NORQUIST, B. M., CASADEI, S., NORD, A. S., AGNEW, K. J., PRITCHARD, C. C., SCROGGINS, S., GARCIA, R. L., KING, M. C. & SWISHER, E. M. 2014. Germline and somatic mutations in homologous recombination genes predict platinum response and survival in ovarian, fallopian tube, and peritoneal carcinomas. *Clin Cancer Res,* 20**,** 764-75.

PERREN, T. J., SWART, A. M., PFISTERER, J., LEDERMANN, J. A., PUJADE-LAURAINE, E., KRISTENSEN, G., CAREY, M. S., BEALE, P., CERVANTES, A., KURZEDER, C., DU BOIS, A., SEHOULI, J., KIMMIG, R., STAHLE, A., COLLINSON, F., ESSAPEN, S., GOURLEY, C., LORTHOLARY, A., SELLE, F., MIRZA, M. R., LEMINEN, A., PLANTE, M., STARK, D., QIAN, W., PARMAR, M. K., OZA, A. M. & INVESTIGATORS, I. 2011. A phase 3 trial of bevacizumab in ovarian cancer. *N Engl J Med,* 365**,** 2484-96.

PFISTERER, J., PLANTE, M., VERGOTE, I., DU BOIS, A., HIRTE, H., LACAVE, A. J., WAGNER, U., STAHLE, A., STUART, G., KIMMIG, R., OLBRICHT, S., LE, T., EMERICH, J., KUHN, W., BENTLEY, J., JACKISCH, C., LUCK, H. J., ROCHON, J., ZIMMERMANN, A. H., EISENHAUER, E., AGO, O., NCIC, C. T. G. & EORTC, G. C. G. 2006. Gemcitabine plus carboplatin compared with carboplatin in patients with platinum-sensitive recurrent ovarian cancer: an intergroup trial of the AGO-OVAR, the NCIC CTG, and the EORTC GCG. *J Clin Oncol,* 24**,** 4699-707.

PRADEEP, S., KIM, S. W., WU, S. Y., NISHIMURA, M., CHALUVALLY-RAGHAVAN, P., MIYAKE, T., PECOT, C. V., KIM, S. J., CHOI, H. J., BISCHOFF, F. Z., MAYER, J. A., HUANG, L., NICK, A. M., HALL, C. S., RODRIGUEZ-AGUAYO, C., ZAND, B., DALTON, H. J., ARUMUGAM, T., LEE, H. J., HAN, H. D., CHO, M. S., RUPAIMOOLE, R., MANGALA, L. S., SEHGAL, V., OH, S. C., LIU, J., LEE, J. S., COLEMAN, R. L., RAM, P., LOPEZ-BERESTEIN, G., FIDLER, I. J. & SOOD,

A. K. 2014. Hematogenous metastasis of ovarian cancer: rethinking mode of spread. *Cancer Cell,* 26**,** 77-91.

PRAT, J. 2012. Ovarian carcinomas: five distinct diseases with different origins, genetic alterations, and clinicopathological features. *Virchows Arch,* 460**,** 237-49.

PRAT, J. 2015. Abridged republication of FIGO's staging classification for cancer of the ovary, fallopian tube, and peritoneum; Figo Committee on Gynecologic Oncology. *Cancer,* 121**,** 3452-4.

PUJADE-LAURAINE, E., HILPERT, F., WEBER, B., REUSS, A., POVEDA, A., KRISTENSEN, G., SORIO, R., VERGOTE, I., WITTEVEEN, P., BAMIAS, A., PEREIRA, D., WIMBERGER, P., OAKNIN, A., MIRZA, M. R., FOLLANA, P., BOLLAG, D. & RAY-COQUARD, I. 2014. Bevacizumab combined with chemotherapy for platinum-resistant recurrent ovarian cancer: The AURELIA open-label randomized phase III trial. *J Clin Oncol,* 32**,** 1302-8.

PUJADE-LAURAINE, E., WAGNER, U., AAVALL-LUNDQVIST, E., GEBSKI, V., HEYWOOD, M., VASEY, P. A., VOLGGER, B., VERGOTE, I., PIGNATA, S., FERRERO, A., SEHOULI, J., LORTHOLARY, A., KRISTENSEN, G., JACKISCH, C., JOLY, F., BROWN, C., LE FUR, N. & DU BOIS, A. 2010. Pegylated liposomal Doxorubicin and Carboplatin compared with Paclitaxel and Carboplatin for patients with platinum-sensitive ovarian cancer in late relapse. *J Clin Oncol,* 28**,** 3323-9.

QIAN, B. Z., LI, J., ZHANG, H., KITAMURA, T., ZHANG, J., CAMPION, L. R., KAISER, E. A., SNYDER, L. A. & POLLARD, J. W. 2011. CCL2 recruits inflammatory monocytes to facilitate breast-tumour metastasis. *Nature,* 475**,** 222-5.

RATNER, N. & MILLER, S. J. 2015. A RASopathy gene commonly mutated in cancer: the neurofibromatosis type 1 tumour suppressor. *Nat Rev Cancer,* 15**,** 290-301.

RESTLE, A., FARBER, M., BAUMANN, C., BOHRINGER, M., SCHEIDTMANN, K. H., MULLER-TIDOW, C. & WIESMULLER, L. 2008. Dissecting the role of p53 phosphorylation in homologous recombination provides new clues for gain-of-function mutants. *Nucleic Acids Res,* 36**,** 5362-75.

RIGHETTI, S. C., DELLA TORRE, G., PILOTTI, S., MENARD, S., OTTONE, F., COLNAGHI, M. I., PIEROTTI, M. A., LAVARINO, C., CORNAROTTI, M., ORIANA, S., BOHM, S., BRESCIANI, G. L., SPATTI, G. & ZUNINO, F. 1996. A comparative study of p53 gene mutations, protein accumulation, and

response to cisplatin-based chemotherapy in advanced ovarian carcinoma. *Cancer Res,* 56**,** 689-93.

ROA, B. B., BOYD, A. A., VOLCIK, K. & RICHARDS, C. S. 1996. Ashkenazi Jewish population frequencies for common mutations in BRCA1 and BRCA2. *Nat Genet,* 14**,** 185-7.

ROBY, K. F., TAYLOR, C. C., SWEETWOOD, J. P., CHENG, Y., PACE, J. L., TAWFIK, O., PERSONS, D. L., SMITH, P. G. & TERRANOVA, P. F. 2000. Development of a syngeneic mouse model for events related to ovarian cancer. *Carcinogenesis,* 21**,** 585-91.

ROSENBERG, E., DEMOPOULOS, R. I., ZELENIUCH-JACQUOTTE, A., YEE, H., SORICH, J., SPEYER, J. L. & NEWCOMB, E. W. 2001. Expression of cell cycle regulators p57(KIP2), cyclin D1, and cyclin E in epithelial ovarian tumors and survival. *Hum Pathol,* 32**,** 808-13.

ROSSING, M. A., DALING, J. R., WEISS, N. S., MOORE, D. E. & SELF, S. G. 1994. Ovarian tumors in a cohort of infertile women. *N Engl J Med,* 331**,** 771-6.

ROY, R., CHUN, J. & POWELL, S. N. 2011. BRCA1 and BRCA2: different roles in a common pathway of genome protection. *Nat Rev Cancer,* 12**,** 68-78.

RUST, K., SPILIOPOULOU, P., TANG, C. Y., BELL, C., STIRLING, D., PHANG, T. H. F., DAVIDSON, R., MACKEAN, M., NUSSEY, F., GLASSPOOL, R., REED, N., SADOZYE, A., PORTEOUS, M., MCGOLDRICK, T., FERGUSON, M., MIEDZYBRODZKA, Z., MCNEISH, I. A. & GOURLEY, C. 2018. Routine germline BRCA1 and BRCA2 testing in ovarian carcinoma patients: analysis of the Scottish real life experience. *BJOG*.

RUSTIN, G. J. 2003. Use of CA-125 to assess response to new agents in ovarian cancer trials. *J Clin Oncol,* 21**,** 187s-193s.

RUSTIN, G. J., VERGOTE, I., EISENHAUER, E., PUJADE-LAURAINE, E., QUINN, M., THIGPEN, T., DU BOIS, A., KRISTENSEN, G., JAKOBSEN, A., SAGAE, S., GREVEN, K., PARMAR, M., FRIEDLANDER, M., CERVANTES, A., VERMORKEN, J. & GYNECOLOGICAL CANCER, I. 2011. Definitions for response and progression in ovarian cancer clinical trials incorporating RECIST 1.1 and CA 125 agreed by the Gynecological Cancer Intergroup (GCIG). *Int J Gynecol Cancer,* 21**,** 419-23.

SAKAI, W., SWISHER, E. M., KARLAN, B. Y., AGARWAL, M. K., HIGGINS, J., FRIEDMAN, C., VILLEGAS, E., JACQUEMONT, C., FARRUGIA, D. J., COUCH, F. J., URBAN, N. & TANIGUCHI, T. 2008. Secondary mutations as a

mechanism of cisplatin resistance in BRCA2-mutated cancers. *Nature,* 451**,** 1116-20.

SANFORD, D. E., BELT, B. A., PANNI, R. Z., MAYER, A., DESHPANDE, A. D., CARPENTER, D., MITCHEM, J. B., PLAMBECK-SUESS, S. M., WORLEY, L. A., GOETZ, B. D., WANG-GILLAM, A., EBERLEIN, T. J., DENARDO, D. G., GOEDEGEBUURE, S. P. & LINEHAN, D. C. 2013. Inflammatory monocyte mobilization decreases patient survival in pancreatic cancer: a role for targeting the CCL2/CCR2 axis. *Clin Cancer Res,* 19**,** 3404-15.

SANNER, K., CONNER, P., BERGFELDT, K., DICKMAN, P., SUNDFELDT, K., BERGH, T., HAGENFELDT, K., JANSON, P. O., NILSSON, S. & PERSSON, I. 2009. Ovarian epithelial neoplasia after hormonal infertility treatment: long-term follow-up of a historical cohort in Sweden. *Fertil Steril,* 91**,** 1152-8.

SATO, E., OLSON, S. H., AHN, J., BUNDY, B., NISHIKAWA, H., QIAN, F., JUNGBLUTH, A. A., FROSINA, D., GNJATIC, S., AMBROSONE, C., KEPNER, J., ODUNSI, T., RITTER, G., LELE, S., CHEN, Y. T., OHTANI, H., OLD, L. J. & ODUNSI, K. 2005. Intraepithelial CD8+ tumor-infiltrating lymphocytes and a high CD8+/regulatory T cell ratio are associated with favorable prognosis in ovarian cancer. *Proc Natl Acad Sci U S A,* 102**,** 18538-43.

SCARLETT, U. K., RUTKOWSKI, M. R., RAUWERDINK, A. M., FIELDS, J., ESCOVAR-FADUL, X., BAIRD, J., CUBILLOS-RUIZ, J. R., JACOBS, A. C., GONZALEZ, J. L., WEAVER, J., FIERING, S. & CONEJO-GARCIA, J. R. 2012. Ovarian cancer progression is controlled by phenotypic changes in dendritic cells. *J Exp Med,* 209**,** 495-506.

SCHLECKER, E., STOJANOVIC, A., EISEN, C., QUACK, C., FALK, C. S., UMANSKY, V. & CERWENKA, A. 2012. Tumor-infiltrating monocytic myeloid-derived suppressor cells mediate CCR5-dependent recruitment of regulatory T cells favoring tumor growth. *J Immunol,* 189**,** 5602-11.

SCHONFELD, S. J., BERRINGTON DE GONZALEZ, A., VISVANATHAN, K., PFEIFFER, R. M. & ANDERSON, W. F. 2013. Declining second primary ovarian cancer after first primary breast cancer. *J Clin Oncol,* 31**,** 738-43.

SCHWARTZ, S., WONGVIPAT, J., TRIGWELL, C. B., HANCOX, U., CARVER, B. S., RODRIK-OUTMEZGUINE, V., WILL, M., YELLEN, P., DE STANCHINA, E., BASELGA, J., SCHER, H. I., BARRY, S. T., SAWYERS, C. L., CHANDARLAPATY, S. & ROSEN, N. 2015. Feedback suppression of PI3Kalpha signaling in PTEN-

mutated tumors is relieved by selective inhibition of PI3Kbeta. *Cancer Cell,* 27**,** 109-22.

SCHWARZ, R. F., NG, C. K., COOKE, S. L., NEWMAN, S., TEMPLE, J., PISKORZ, A. M., GALE, D., SAYAL, K., MURTAZA, M., BALDWIN, P. J., ROSENFELD, N., EARL, H. M., SALA, E., JIMENEZ-LINAN, M., PARKINSON, C. A., MARKOWETZ, F. & BRENTON, J. D. 2015. Spatial and temporal heterogeneity in high-grade serous ovarian cancer: a phylogenetic analysis. *PLoS Med,* 12**,** e1001789.

SEVKO, A. & UMANSKY, V. 2013. Myeloid-derived suppressor cells interact with tumors in terms of myelopoiesis, tumorigenesis and immunosuppression: thick as thieves. *J Cancer,* 4**,** 3-11.

SHEN, G. H., GHAZIZADEH, M., KAWANAMI, O., SHIMIZU, H., JIN, E., ARAKI, T. & SUGISAKI, Y. 2000. Prognostic significance of vascular endothelial growth factor expression in human ovarian carcinoma. *Br J Cancer,* 83**,** 196-203.

SHIH IE, M. & KURMAN, R. J. 2004. Ovarian tumorigenesis: a proposed model based on morphological and molecular genetic analysis. *Am J Pathol,* 164**,** 1511-8.

SHIMIZU, Y., KAMOI, S., AMADA, S., HASUMI, K., AKIYAMA, F. & SILVERBERG, S. G. 1998. Toward the development of a universal grading system for ovarian epithelial carcinoma. I. Prognostic significance of histopathologic features--problems involved in the architectural grading system. *Gynecol Oncol,* 70**,** 2-12.

SOBIN, L. 2009. *TNM classification of malignant tumors; UICC International Union Against Cancer*, Wiley-Blackwell.

SPAETH, E. L., DEMBINSKI, J. L., SASSER, A. K., WATSON, K., KLOPP, A., HALL, B., ANDREEFF, M. & MARINI, F. 2009. Mesenchymal stem cell transition to tumor-associated fibroblasts contributes to fibrovascular network expansion and tumor progression. *PLoS One,* 4**,** e4992.

STARUP-LINDE, J., KARLSTAD, O., ERIKSEN, S. A., VESTERGAARD, P., BRONSVELD, H. K., DE VRIES, F., ANDERSEN, M., AUVINEN, A., HAUKKA, J., HJELLVIK, V., BAZELIER, M. T., BOER, A., FURU, K. & DE BRUIN, M. L. 2013. CARING (CAncer Risk and INsulin analoGues): the association of diabetes mellitus and cancer risk with focus on possible determinants - a systematic review and a meta-analysis. *Curr Drug Saf,* 8**,** 296-332.

STONE, R. L., NICK, A. M., MCNEISH, I. A., BALKWILL, F., HAN, H. D., BOTTSFORD-MILLER, J., RUPAIRMOOLE, R., ARMAIZ-PENA, G. N., PECOT, C. V., COWARD,

J., DEAVERS, M. T., VASQUEZ, H. G., URBAUER, D., LANDEN, C. N., HU, W., GERSHENSON, H., MATSUO, K., SHAHZAD, M. M., KING, E. R., TEKEDERELI, I., OZPOLAT, B., AHN, E. H., BOND, V. K., WANG, R., DREW, A. F., GUSHIKEN, F., LAMKIN, D., COLLINS, K., DEGEEST, K., LUTGENDORF, S. K., CHIU, W., LOPEZ-BERESTEIN, G., AFSHAR-KHARGHAN, V. & SOOD, A. K. 2012. Paraneoplastic thrombocytosis in ovarian cancer. *N Engl J Med,* 366**,** 610-8.

SWARTZ, M. A. & LUND, A. W. 2012. Lymphatic and interstitial flow in the tumour microenvironment: linking mechanobiology with immunity. *Nat Rev Cancer,* 12**,** 210-9.

SWISHER, E. M., SAKAI, W., KARLAN, B. Y., WURZ, K., URBAN, N. & TANIGUCHI, T. 2008. Secondary BRCA1 mutations in BRCA1-mutated ovarian carcinomas with platinum resistance. *Cancer Res,* 68**,** 2581-6.

TEMPLETON, A. J., MCNAMARA, M. G., SERUGA, B., VERA-BADILLO, F. E., ANEJA, P., OCANA, A., LEIBOWITZ-AMIT, R., SONPAVDE, G., KNOX, J. J., TRAN, B., TANNOCK, I. F. & AMIR, E. 2014. Prognostic role of neutrophil-to-lymphocyte ratio in solid tumors: a systematic review and meta-analysis. *J Natl Cancer Inst,* 106**,** dju124.

THIBAULT, B., CASTELLS, M., DELORD, J. P. & COUDERC, B. 2014. Ovarian cancer microenvironment: implications for cancer dissemination and chemoresistance acquisition. *Cancer Metastasis Rev,* 33**,** 17-39.

TOMASEK, J. J., GABBIANI, G., HINZ, B., CHAPONNIER, C. & BROWN, R. A. 2002. Myofibroblasts and mechano-regulation of connective tissue remodelling. *Nat Rev Mol Cell Biol,* 3**,** 349-63.

TRIMBOS, J. B., PARMAR, M., VERGOTE, I., GUTHRIE, D., BOLIS, G., COLOMBO, N., VERMORKEN, J. B., TORRI, V., MANGIONI, C., PECORELLI, S., LISSONI, A., SWART, A. M., INTERNATIONAL COLLABORATIVE OVARIAN, N., EUROPEAN ORGANISATION FOR, R. & TREATMENT OF CANCER COLLABORATORS-ADJUVANT CHEMOTHERAPY UN OVARIAN, N. 2003. International Collaborative Ovarian Neoplasm trial 1 and Adjuvant ChemoTherapy In Ovarian Neoplasm trial: two parallel randomized phase III trials of adjuvant chemotherapy in patients with early-stage ovarian carcinoma. *J Natl Cancer Inst,* 95**,** 105-12.

UGEL, S., DE SANCTIS, F., MANDRUZZATO, S. & BRONTE, V. 2015. Tumor-induced myeloid deviation: when myeloid-derived suppressor cells meet tumor-associated macrophages. *J Clin Invest,* 125**,** 3365-76.

VACCHELLI, E., ARANDA, F., EGGERMONT, A., GALON, J., SAUTES-FRIDMAN, C., CREMER, I., ZITVOGEL, L., KROEMER, G. & GALLUZZI, L. 2014. Trial Watch: Chemotherapy with immunogenic cell death inducers. *Oncoimmunology,* 3**,** e27878.

VASEY, P. A. 2003. Resistance to chemotherapy in advanced ovarian cancer: mechanisms and current strategies. *Br J Cancer,* 89 Suppl 3**,** S23-8.

VASEY, P. A., JAYSON, G. C., GORDON, A., GABRA, H., COLEMAN, R., ATKINSON, R., PARKIN, D., PAUL, J., HAY, A., KAYE, S. B. & SCOTTISH GYNAECOLOGICAL CANCER TRIALS, G. 2004. Phase III randomized trial of docetaxel-carboplatin versus paclitaxel-carboplatin as first-line chemotherapy for ovarian carcinoma. *J Natl Cancer Inst,* 96**,** 1682-91.

VERGOTE, I., TROPE, C. G., AMANT, F., KRISTENSEN, G. B., EHLEN, T., JOHNSON, N., VERHEIJEN, R. H., VAN DER BURG, M. E., LACAVE, A. J., PANICI, P. B., KENTER, G. G., CASADO, A., MENDIOLA, C., COENS, C., VERLEYE, L., STUART, G. C., PECORELLI, S., REED, N. S., EUROPEAN ORGANIZATION FOR, R., TREATMENT OF CANCER-GYNAECOLOGICAL CANCER, G. & GROUP, N. C. T. 2010. Neoadjuvant chemotherapy or primary surgery in stage IIIC or IV ovarian cancer. *N Engl J Med,* 363**,** 943-53.

VERGOTE, I. B., JIMENO, A., JOLY, F., KATSAROS, D., COENS, C., DESPIERRE, E., MARTH, C., HALL, M., STEER, C. B., COLOMBO, N., LESOIN, A., CASADO, A., REINTHALLER, A., GREEN, J., BUCK, M., RAY-COQUARD, I., FERRERO, A., FAVIER, L., REED, N. S., CURE, H. & PUJADE-LAURAINE, E. 2014. Randomized phase III study of erlotinib versus observation in patients with no evidence of disease progression after first-line platin-based chemotherapy for ovarian carcinoma: a European Organisation for Research and Treatment of Cancer-Gynaecological Cancer Group, and Gynecologic Cancer Intergroup study. *J Clin Oncol,* 32**,** 320-6.

WALTON, J., BLAGIH, J., ENNIS, D., LEUNG, E., DOWSON, S., FARQUHARSON, M., TOOKMAN, L. A., ORANGE, C., ATHINEOS, D., MASON, S., STEVENSON, D., BLYTH, K., STRATHDEE, D., BALKWILL, F. R., VOUSDEN, K., LOCKLEY, M. & MCNEISH, I. A. 2016. CRISPR/Cas9-Mediated Trp53 and Brca2 Knockout to

Generate Improved Murine Models of Ovarian High-Grade Serous Carcinoma. *Cancer Res*.

WALTON, J. B., FARQUHARSON, M., MASON, S., PORT, J., KRUSPIG, B., DOWSON, S., STEVENSON, D., MURPHY, D., MATZUK, M., KIM, J., COFFELT, S., BLYTH, K. & MCNEISH, I. A. 2017. CRISPR/Cas9-derived models of ovarian high grade serous carcinoma targeting Brca1, Pten and Nf1, and correlation with platinum sensitivity. *Sci Rep,* 7**,** 16827.

WILLIAMS, G. J., LEES-MILLER, S. P. & TAINER, J. A. 2010. Mre11-Rad50-Nbs1 conformations and the control of sensing, signaling, and effector responses at DNA double-strand breaks. *DNA Repair (Amst),* 9**,** 1299-306.

WOO, E. Y., CHU, C. S., GOLETZ, T. J., SCHLIENGER, K., YEH, H., COUKOS, G., RUBIN, S. C., KAISER, L. R. & JUNE, C. H. 2001. Regulatory CD4(+)CD25(+) T cells in tumors from patients with early-stage non-small cell lung cancer and late-stage ovarian cancer. *Cancer Res,* 61**,** 4766-72.

XIAO, X., MELTON, D. W. & GOURLEY, C. 2014. Mismatch repair deficiency in ovarian cancer -- molecular characteristics and clinical implications. *Gynecol Oncol,* 132**,** 506-12.

XU, Y., GAUDETTE, D. C., BOYNTON, J. D., FRANKEL, A., FANG, X. J., SHARMA, A., HURTEAU, J., CASEY, G., GOODBODY, A., MELLORS, A. & ET AL. 1995. Characterization of an ovarian cancer activating factor in ascites from ovarian cancer patients. *Clin Cancer Res,* 1**,** 1223-32.

YANG, D., KHAN, S., SUN, Y., HESS, K., SHMULEVICH, I., SOOD, A. K. & ZHANG, W. 2011. Association of BRCA1 and BRCA2 mutations with survival, chemotherapy sensitivity, and gene mutator phenotype in patients with ovarian cancer. *JAMA,* 306**,** 1557-65.

YANG, H., KONG, W., HE, L., ZHAO, J. J., O'DONNELL, J. D., WANG, J., WENHAM, R. M., COPPOLA, D., KRUK, P. A., NICOSIA, S. V. & CHENG, J. Q. 2008. MicroRNA expression profiling in human ovarian cancer: miR-214 induces cell survival and cisplatin resistance by targeting PTEN. *Cancer Res,* 68**,** 425-33.

YAP, Y. S., MCPHERSON, J. R., ONG, C. K., ROZEN, S. G., TEH, B. T., LEE, A. S. & CALLEN, D. F. 2014. The NF1 gene revisited - from bench to bedside. *Oncotarget,* 5**,** 5873-92.

YONENAGA, Y., MORI, A., ONODERA, H., YASUDA, S., OE, H., FUJIMOTO, A., TACHIBANA, T. & IMAMURA, M. 2005. Absence of smooth muscle actin-

positive pericyte coverage of tumor vessels correlates with hematogenous metastasis and prognosis of colorectal cancer patients. *Oncology,* 69**,** 159-66.

ZAINO, R. J., BRADY, M. F., LELE, S. M., MICHAEL, H., GREER, B. & BOOKMAN, M. A. 2011. Advanced stage mucinous adenocarcinoma of the ovary is both rare and highly lethal: a Gynecologic Oncology Group study. *Cancer,* 117**,** 554-62.

ZHANG, F., MA, J., WU, J., YE, L., CAI, H., XIA, B. & YU, X. 2009. PALB2 links BRCA1 and BRCA2 in the DNA-damage response. *Curr Biol,* 19**,** 524-9.

ZHANG, L., CONEJO-GARCIA, J. R., KATSAROS, D., GIMOTTY, P. A., MASSOBRIO, M., REGNANI, G., MAKRIGIANNAKIS, A., GRAY, H., SCHLIENGER, K., LIEBMAN, M. N., RUBIN, S. C. & COUKOS, G. 2003. Intratumoral T cells, recurrence, and survival in epithelial ovarian cancer. *N Engl J Med,* 348**,** 203-13.

ZOLLO, M., DI DATO, V., SPANO, D., DE MARTINO, D., LIGUORI, L., MARINO, N., VASTOLO, V., NAVAS, L., GARRONE, B., MANGANO, G., BIONDI, G. & GUGLIELMOTTI, A. 2012. Targeting monocyte chemotactic protein-1 synthesis with bindarit induces tumor regression in prostate and breast cancer animal models. *Clin Exp Metastasis,* 29**,** 585-601.

8.2 Webpages

www.cancerresearchuk.org [Online]. [Accessed 12.06.17].

http://teachmeanatomy.info/pelvis/female-reproductive-tract/fallopian-tubes/ [Online]. [Accessed 20.08.16].

National Cancer Institute (2016) SEER Stat Fact Sheets: Ovarian Cancer. [Accessed 03/08/2016]. Available from: http://seer.cancer.gov/statfacts/html/ovary.html.

National Institute for Health and Care Excellence (NICE). Ovarian cancer: the recognition and initial management of ovarian cancer. 2011. Available from: http://www.nice.org.uk/guidance/CG122. [Accessed 12.06.17].

9 Appendices

Appendix 1: Quality scores and GC content from the RNAseq data of ID8 *Trp53+/+*, *Trp53-/-* and *Trp53-/-;Pten-/-* tumours.

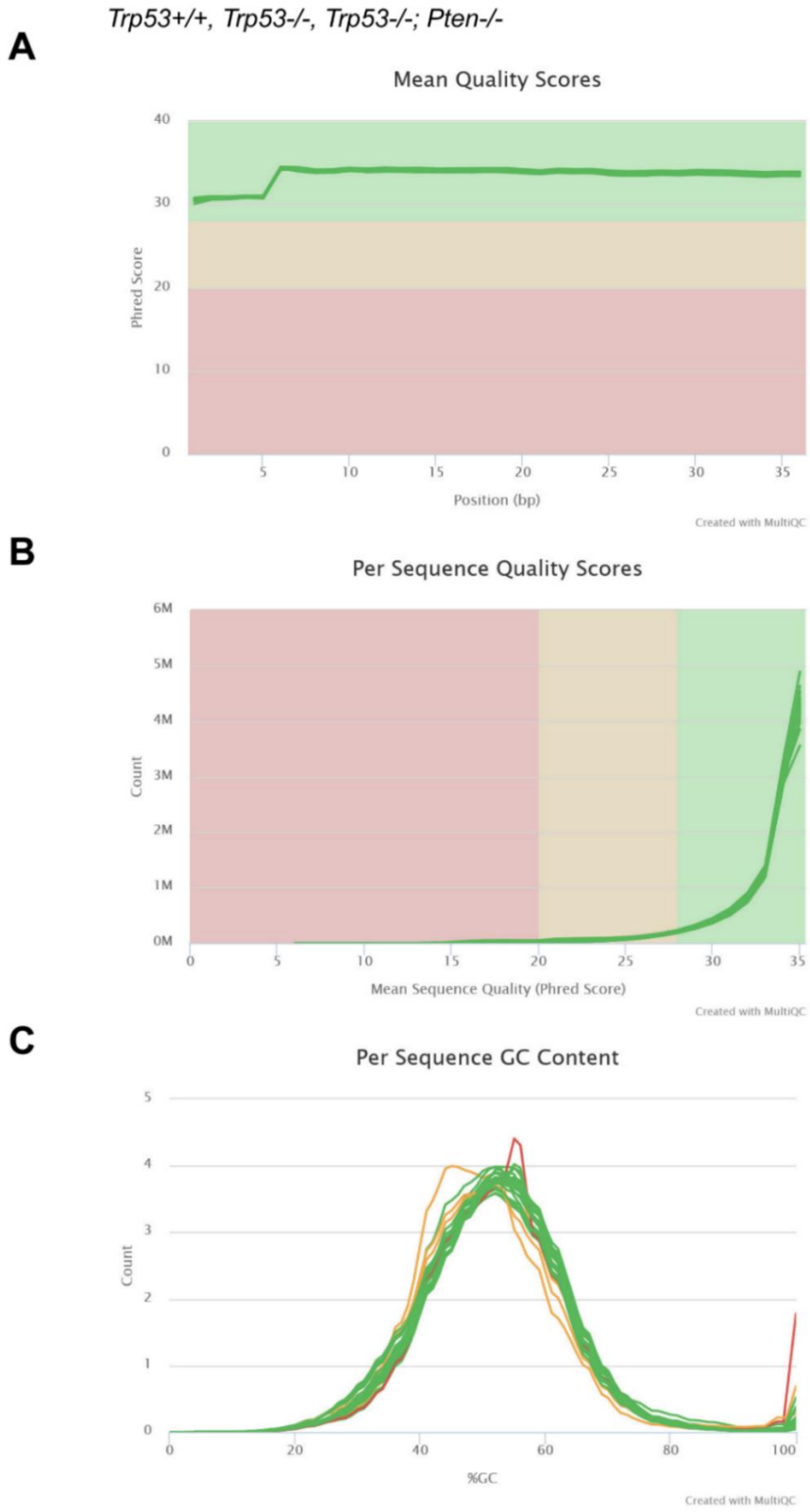

A, Mean Quality Scores **B,** Per Sequence Quality Scores **C,** Per Sequence GC Content

Appendix 2: *Trp53* and *Pten* expression from the RNAseq of ID8 *Trp53*+/+ tumours and in the *Trp53*-/- and *Trp53*-/-;*Pten*-/- tumours treated with cisplatin or PBS.

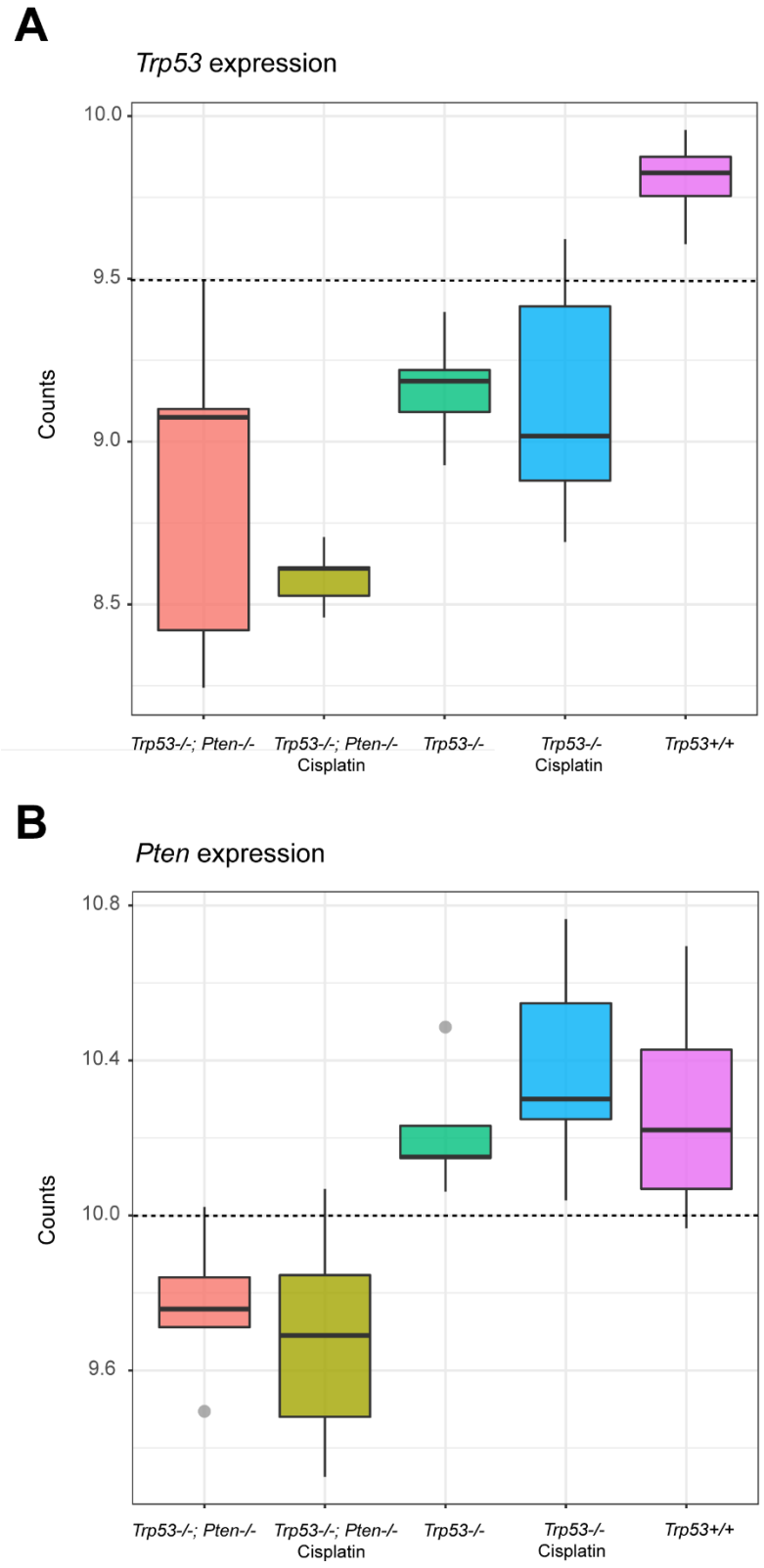

A, *Trp53* expression **B,** *Pten* expression

Appendix 3: Quality scores and GC content from the RNAseq data of ID8 *Trp53-/-;Brca1-/-* and *Trp53-/-;Brca2-/-*tumours.

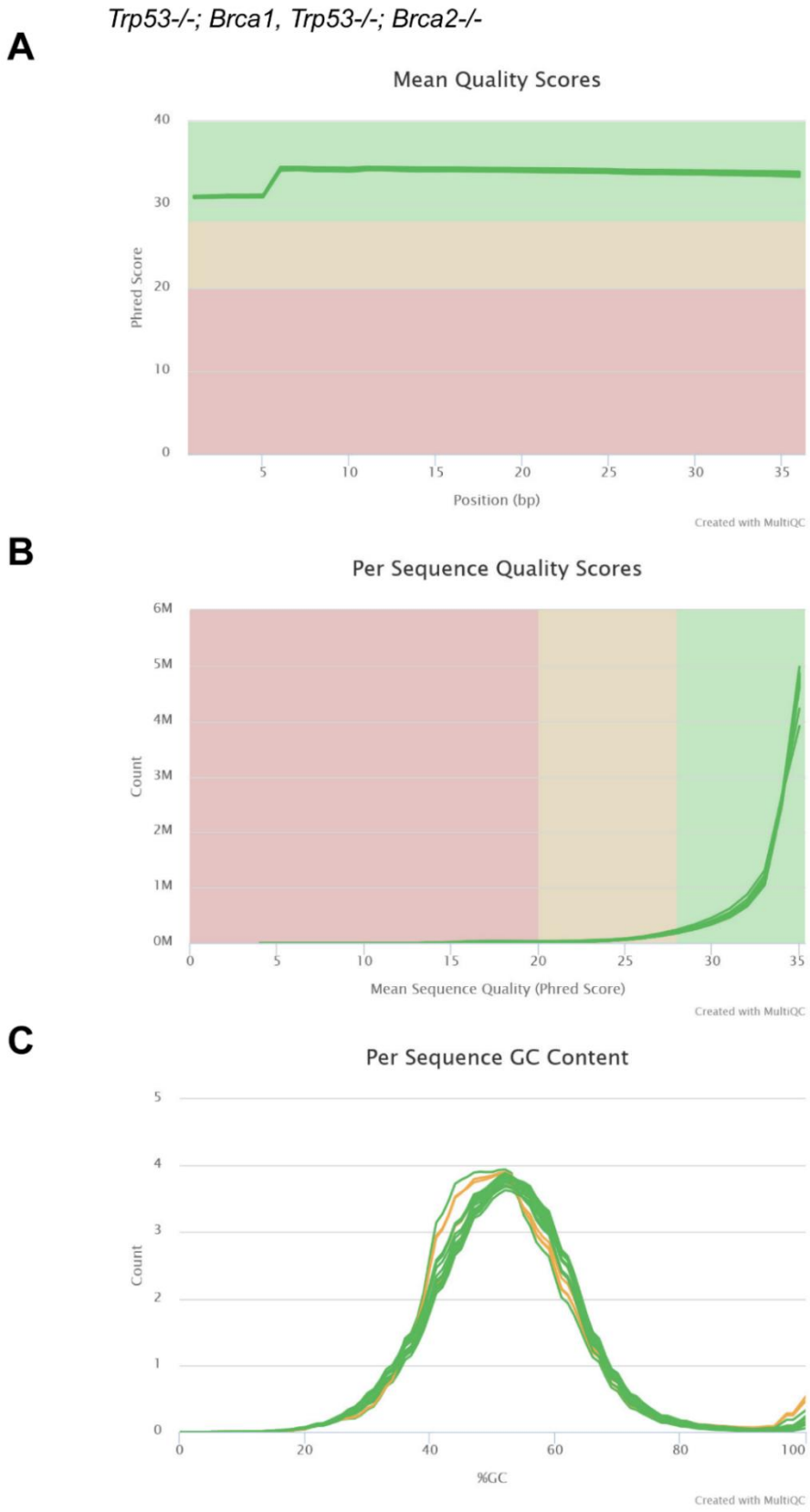

A, Mean Quality Scores **B,** Per Sequence Quality Scores **C,** Per Sequence GC Content

Appendix 4: *Trp53*, *Brca1* and *Brca2* expression from the RNAseq of ID8 *Trp53*+/+ and *Trp53*-/- tumours and in the *Trp53*-/-;*Brca1*-/- and *Trp53*-/-;*Brca2*-/- tumours treated with cisplatin or PBS.

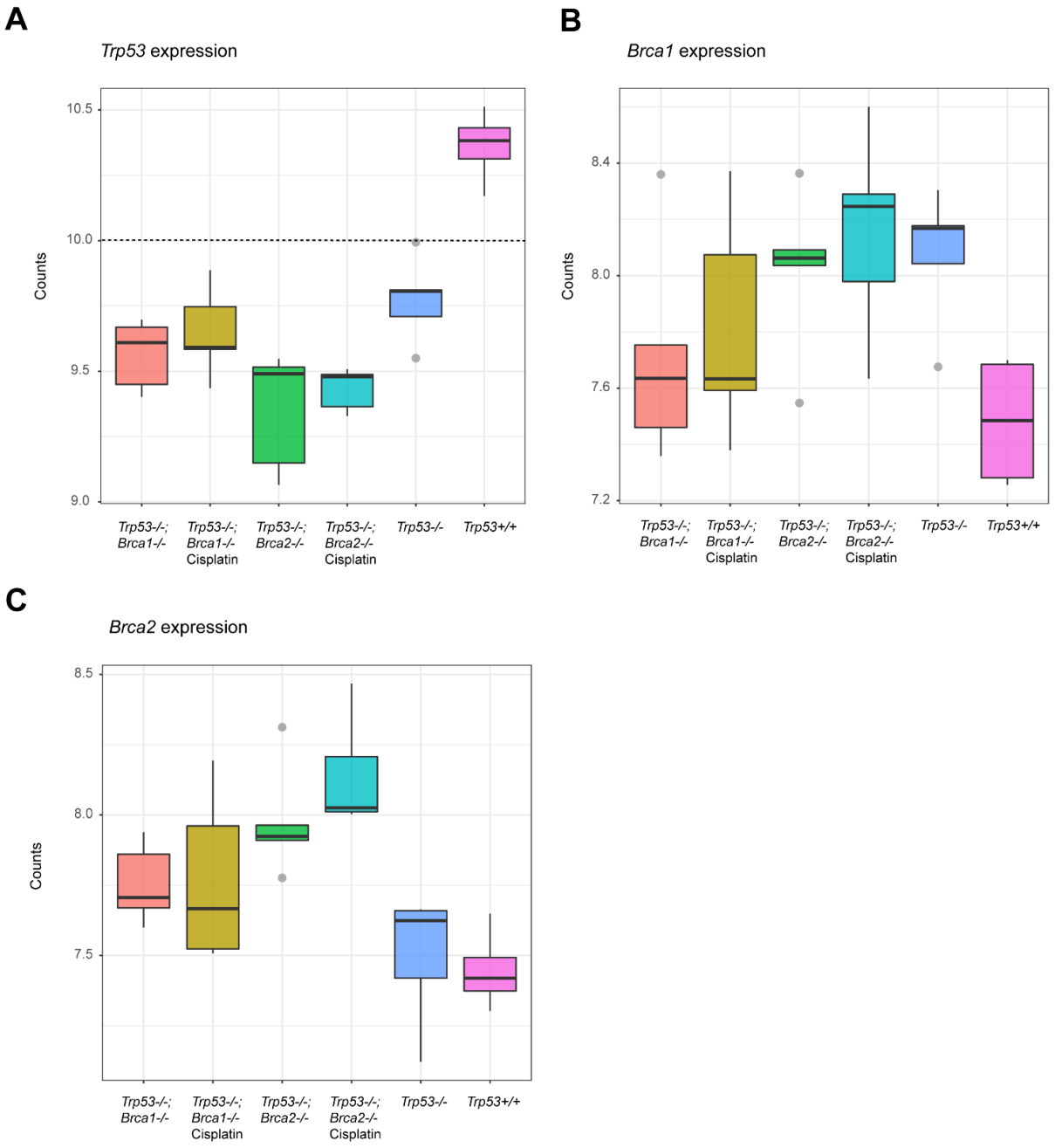

A, *Trp53* expression **B,** *Brca1* expression **C,** *Brca2* expression

Appendix 5: Quality scores and GC content from the RNAseq data of ID8 *Trp53-/-;Nf1-/-* tumours.

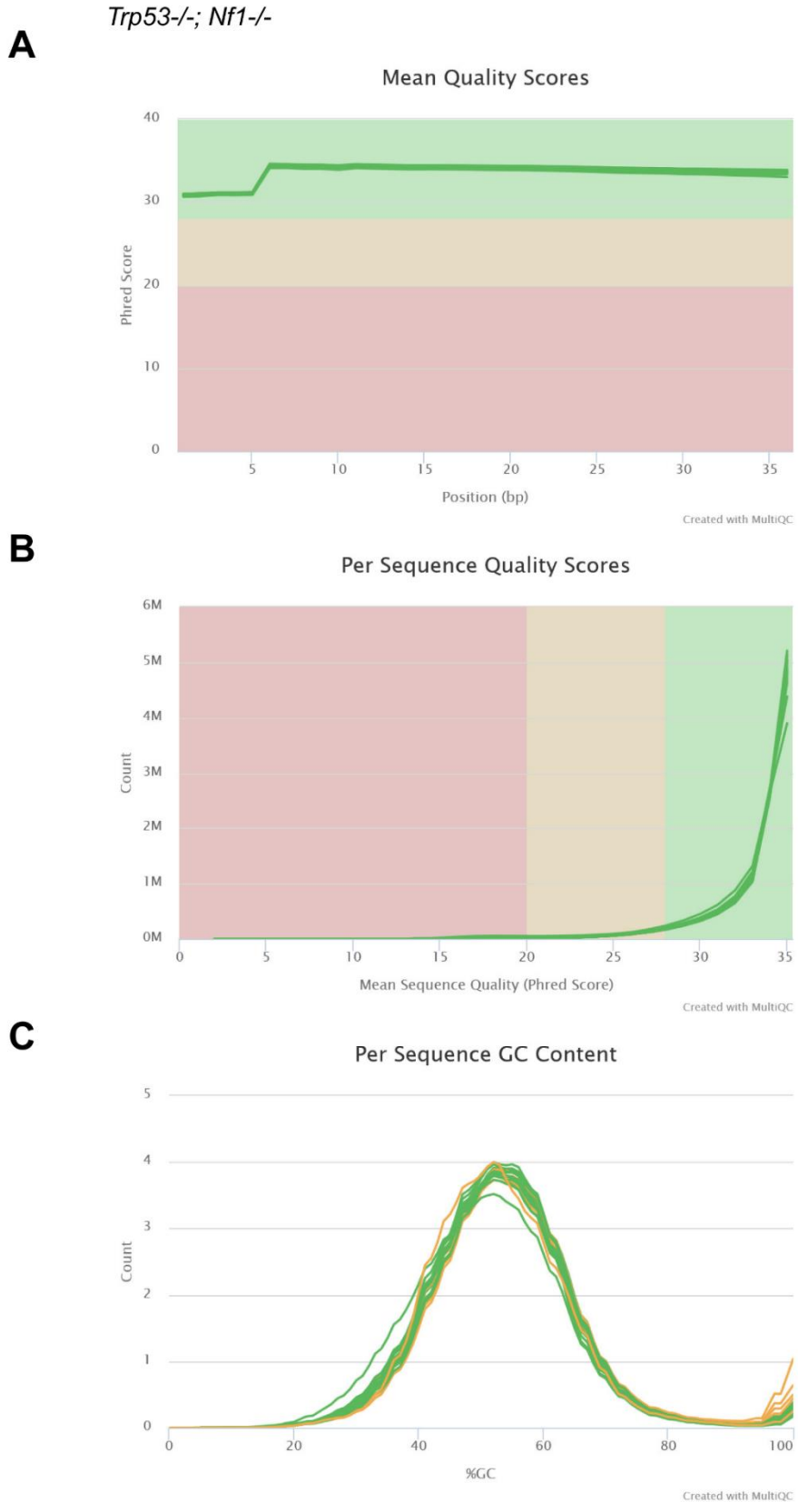

A, Mean Quality Scores **B,** Per Sequence Quality Scores **C,** Per Sequence GC Content

Appendix 6: *Trp53* and *Nf1* expression from the RNAseq of ID8 *Trp53*+/+ and *Trp53*-/- tumours and in the *Trp53*-/-;*Nf1*-/- tumours treated with cisplatin or PBS.

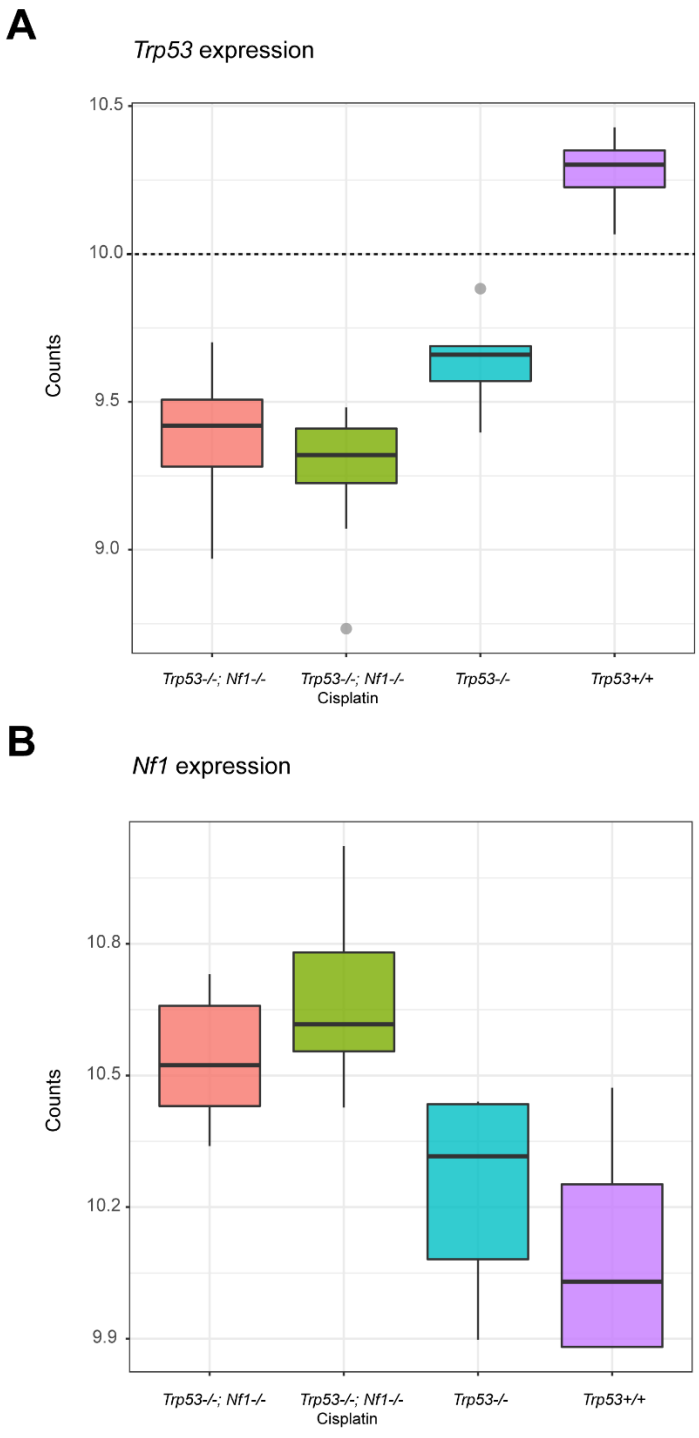

A, *Trp53* expression **B,** *Nf1* expression

Appendix 7: Tables outlining differential gene expression from RNA sequencing analysis.

The tables below outlines the significantly up-regulated and down-regulated genes in the different genotypes and following cisplatin treatment (R package – edgeR). Only the top 50 most significant genes are shown in the tables below.

Wild-type versus *Trp53-/-*

Down-regulated		
Gene	**Adjusted P value**	**Log2 fold change**
Rn7sk	4.09E-18	434.007
Mup16	8.18E-18	11.985
Znrf4	6.98E-17	103.561
H2-K1	7.63E-16	15422.589
Mup17	9.27E-16	67.447
Cd82	1.10E-14	2565.646
Cryaa	4.16E-14	53.711
Mup18	5.17E-14	37.603
Alppl2	8.95E-14	54.592
Fam118a	2.88E-13	558.879
2610528A11Rik	6.49E-12	162.618
Cdhr1	6.47E-12	144.108
Olfr1372-ps1	6.97E-12	140.887
Ndp	6.09E-11	72.072
Gm14002	2.46E-10	29.694
H2-D1	4.91E-10	12701.864
Lctl	5.83E-10	433.105
Piwil4	6.46E-10	59.802
B2m	8.55E-10	15222.523
1700008I05Rik	9.73E-10	33.858
Plxnb3	9.95E-10	363.467
Rprl2	1.19E-09	42.726
A430093F15Rik	8.12E-09	31.079
Cotl1	9.75E-09	3308.428
Topaz1	1.25E-08	24.307
Dut	1.62E-08	803.345
5033428I22Rik	2.05E-08	36.130
Xaf1	2.74E-08	445.615
3110035E14Rik	3.60E-08	136.472
Zbp1	3.66E-08	502.549
Oas1g	4.47E-08	81.932
Irf7	4.69E-08	1160.636
Aire	5.78E-08	23.867
AY036118	7.11E-08	19.674
AA467197	8.80E-08	752.896
Sin3b	1.21E-07	1709.481
Amz1	1.97E-07	107.759
Slc12a1	2.79E-07	21.647
Bst2	3.39E-07	1883.359
Rsph1	3.47E-07	63.303
Rad51	3.52E-07	211.430
Rai14	3.77E-07	2466.851
AU018091	4.09E-07	18.097
Gm14088	4.38E-07	37.944
AI848285	4.56E-07	861.049
Slc27a6	5.23E-07	235.274
Slfn4	5.37E-07	79.010
AI427809	7.69E-07	36.285
Ceacam15	8.49E-07	34.922
Edn2	8.70E-07	191.592

Up-regulated		
Gene	**Adjusted P value**	**Log2 fold change**
Lrrc4	3.51E-26	51.644
Tnni3	2.28E-23	96.870
Cacna1h	7.87E-20	167.554
Prrg3	1.92E-17	170.836
Unc13b	2.14E-17	205.296
Sez6l	4.43E-17	184.755
Bnc1	5.82E-17	79.158
Tmem132a	6.28E-17	296.963
Wnt5a	1.04E-16	236.776
Gata5	1.27E-16	46.387
Ccnjl	8.57E-16	23.344
Krt10	1.21E-15	5279.469
Slc12a2	7.79E-15	361.260
Mboat2	1.06E-14	92.736
Wnt9a	2.00E-14	198.809
Pla2g5	1.34E-13	59.919
Kcnd2	9.09E-13	48.328
Fa2h	9.72E-13	86.169
Kif1a	1.12E-12	96.067
Slmap	1.81E-12	1251.860
Dnajc14	3.38E-12	749.179
Ccdc64	4.14E-12	354.466
Mecom	7.95E-12	95.464
Nxph3	1.55E-11	20.846
Myh11	1.96E-11	2222.835
Cacnb2	3.35E-11	28.716
Fut2	3.77E-11	90.820
Col23a1	6.24E-11	115.533
Emx2os	1.90E-10	13.876
Rcan2	1.99E-10	393.842
Arnt2	2.13E-10	49.833
B3gnt7	2.96E-10	68.267
Scn5a	2.97E-10	44.835
9330159F19Rik	3.23E-10	45.142
Gas6	3.44E-10	3542.796
Spock2	3.42E-10	148.687
Cst6	5.86E-10	161.398
Epcam	9.91E-10	155.559
Gpr116	9.27E-10	805.607
Jazf1	9.39E-10	20.020
Krt1	9.93E-10	4281.354
Tns1	1.18E-09	3591.463
Sobp	1.25E-09	46.559
Lurap1	1.31E-09	64.704
Sgpp2	1.37E-09	101.683
Map4k3	1.42E-09	704.668
Tmtc1	1.64E-09	296.648
Cttnbp2	1.72E-09	21.758
Efs	2.00E-09	72.397
Bmp6	2.11E-09	77.898

***Trp53-/-* (PBS) versus *Trp53-/-* (cisplatin)**

Up-regulated		
Gene	**Adjusted P value**	**Log2 fold change**
Rn7sk	1.06E-16	434.007
Rprl2	7.66E-10	42.726

Trp53-/- versus *Trp53-/-;Pten-/-*

Down-regulated		
Gene	**Adjusted P value**	**Log2 fold change**
Ighv9-4	1.24E-12	146.619
Mmel1	4.49E-08	39.674
Ighv1-81	1.90E-07	164.629
Igkv1-110	2.15E-07	148.708
Igkv3-7	1.56E-06	56.303
Haus7	6.02E-06	264.559
Ucp1	2.47E-05	330.522
Igkv8-24	2.85E-05	38.618
Prr5	4.12E-05	134.867
Scand1	4.11E-05	546.245
Utp3	4.00E-05	528.331
Ighv1-12	5.63E-05	11.927
Ighv1-19	6.27E-05	116.894
Igkv1-135	0.000100894	79.656
Unc119	0.000111335	478.892

Up-regulated		
Gene	**Adjusted P value**	**Log2 fold change**
Gprasp2	1.52E-13	52.042
Rn7sk	3.49E-12	434.007
Tmem255a	1.69E-11	914.593
Rprl2	2.79E-10	42.726
Sema5a	2.30E-09	1186.711
Slc4a11	1.50E-07	484.154
Cntln	5.06E-07	184.020
Mylk3	4.74E-07	178.748
Adam33	8.67E-07	603.247
Pcdhb19	8.12E-07	38.584
0610007N19Rik	1.01E-06	429.547
Wnt9a	2.19E-06	198.809
Kif5c	2.94E-06	79.869
Espn	3.41E-06	392.377
Ermp1	8.31E-06	1693.199
Stx1b	1.30E-05	76.738
2610028E06Rik	2.72E-05	8.989
Crip3	3.58E-05	80.822
Olfm4	3.67E-05	21.366
Pkhd1l1	6.33E-05	1009.668
5033428I22Rik	9.93E-05	36.130
Bcam	0.000107477	2589.363
Zfp644	0.000111501	414.867

Trp53-/-;Pten-/- (PBS) versus *Trp53-/-;Pten-/-* (cisplatin)

Down-regulated		
Gene	**Adjusted P value**	**Log2 fold change**
Wnt9a	2.25E-12	198.809
Dync1i1	6.28E-11	326.445
Upk3b	1.27E-10	2409.312
Tmem255a	8.23E-09	914.593
Gm7361	1.05E-08	25.926
Espnl	8.78E-08	9.858
Slc48a1	1.01E-07	1998.491
Dlg2	1.98E-07	100.079
Pkhd1l1	5.06E-07	1009.668
Wwtr1	5.53E-07	1706.562
Tmx4	1.13E-06	391.649
Tmtc4	1.45E-06	297.300
Gdf6	1.69E-06	217.186
Lgals1	2.66E-06	24111.167
Hmcn1	2.72E-06	181.143
Arhgap29	2.82E-06	2263.335
Ermp1	3.09E-06	1693.199
B3galnt2	3.47E-06	558.775
Txnrd1	3.51E-06	1826.192
Ttll1	5.91E-06	208.509
Garnl3	7.96E-06	362.842
Scn5a	7.83E-06	44.835
Rab6a	1.08E-05	1350.036
Bcam	1.24E-05	2589.363
Srxn1	1.25E-05	882.293
Hs6st2	1.78E-05	261.346
Mrgprf	1.81E-05	137.662
Pcdh9	1.80E-05	21.563
Sema5a	1.89E-05	1186.711
Carhsp1	1.99E-05	2121.817
Dcbld2	1.98E-05	1449.347
Wnt4	2.04E-05	2225.340
Il10	2.22E-05	23.252
Zfp647	2.25E-05	51.704
Galc	2.37E-05	378.377
Sgtb	2.50E-05	51.397
Apbb1	2.59E-05	186.966
Mmel1	2.60E-05	39.674
Ttll5	2.75E-05	302.777
2610203C20	3.06E-05	818.638
Axin2	3.13E-05	462.676
Dnah7b	3.33E-05	27.466
Cercam	5.11E-05	554.322
Pcdhb20	4.88E-05	61.716
Ppp2r5b	5.09E-05	1031.640
Wnt11	4.92E-05	869.925
Sv2a	5.38E-05	181.766
Gm996	6.06E-05	76.243
Nebl	6.14E-05	643.940
Pcdhb19	6.42E-05	38.584

Up-regulated		
Gene	**Adjusted P value**	**Log2 fold change**
Mup18	1.72E-22	37.603
Gm13775	2.29E-20	31.618
Igkv4-55	1.85E-12	172.989
Ighv9-4	7.04E-10	146.619
Timd4	9.93E-10	66.700
Pla2g4d	3.13E-09	23.753
Adam11	3.00E-08	78.438
Agr2	4.48E-08	44.873
Siglech	1.23E-07	35.621
Plac8	1.49E-07	513.427
Defb4	2.38E-07	23.215
Ighv1-81	2.37E-07	164.629
Cd209b	3.38E-07	134.677
Cd209f	3.80E-07	50.011
Sorcs1	4.43E-07	68.119
Bst2	4.81E-07	1883.359
Ighm	6.56E-07	9010.879
Igkv3-7	7.02E-07	56.303
Fcer2a	9.67E-07	110.152
Plbd1	1.24E-06	729.267
Igkv9-124	1.39E-06	90.814
Bace2	1.48E-06	205.233
Susd1	1.55E-06	74.004
Irf9	1.87E-06	697.860
Faim3	2.01E-06	121.881
Rasgrp2	2.01E-06	265.191
Gm11131	3.02E-06	25.370
Aff3	3.29E-06	57.007
Aven	3.54E-06	201.596
AW011738	3.30E-06	40.000
Ighv5-16	3.39E-06	47.420
Wdr86	3.78E-06	19.533
Il4i1	3.89E-06	123.828
Itpr2	4.33E-06	367.308
Zap70	4.48E-06	106.657
Trafd1	4.67E-06	1228.205
Lyz1	5.11E-06	80.785
Acp5	5.57E-06	753.817
Ltb	5.40E-06	185.251
Ly6d	5.57E-06	443.159
Adrbk2	6.74E-06	155.383
Cxcr5	6.89E-06	66.186
Bcl7a	7.24E-06	110.001
Bank1	8.02E-06	93.303
Cd19	7.68E-06	229.494
Cd209g	8.21E-06	18.688
Zfp629	8.27E-06	188.246
Flywch2	8.65E-06	12.817
H2-Q7	8.62E-06	538.454
Batf3	9.34E-06	32.383

Trp53-/- versus *Trp53-/-;Brca1-/-*

Down-regulated		
Gene	**Adjusted P value**	**Log2 fold change**
Cotl1	4.33E-24	6408.518
Cd82	7.39E-23	4614.267
H2-D1	9.00E-23	19093.937
Cryaa	1.34E-21	308.248
H2-K1	2.14E-21	22837.618
Alppl2	1.15E-20	109.063
Samhd1	1.81E-19	3817.135
Znrf4	2.93E-19	157.767
Hat1	8.03E-19	1333.544
Tapbp	2.30E-18	10010.628
Cdhr1	1.25E-17	386.363
Atp1a3	5.38E-17	1120.143
Gm14002	8.10E-17	54.216
Stk32b	1.13E-16	316.030
Arrb2	7.85E-16	1096.714
Rai14	1.64E-15	4048.789
Tap2	4.49E-15	2115.504
Flt4	1.63E-14	2731.462
Cdt1	2.06E-14	592.664
Dut	2.03E-14	1380.501
B2m	2.70E-14	22869.500
Piwil4	3.54E-14	170.075
AI427809	1.22E-13	80.262
Ndp	2.76E-13	127.377
Gpsm3	4.81E-13	553.824
Tap1	5.84E-13	1928.616
Dpy19l3	6.88E-13	1688.500
H2-T22	7.91E-13	1424.198
Mcm8	9.47E-13	252.573
Ogfr	1.27E-12	1594.347
Piwil2	1.67E-12	1134.610
Fam118a	2.02E-12	1018.080
Foxs1	2.79E-12	601.151
Ece2	5.52E-12	460.551
Gpr176	6.56E-12	797.340
Cxcl10	6.65E-12	526.369
Olfr1372-ps1	7.34E-12	259.597
Cdca7	7.73E-12	674.462
Usp18	1.25E-11	431.760
E2f1	1.30E-11	514.711
Lig1	1.66E-11	1316.464
Palm3	1.67E-11	353.388
Zbp1	1.89E-11	652.588
Oas1a	2.04E-11	306.588
Lpar2	2.29E-11	1062.748
Exosc8	3.70E-11	521.103
Dsn1	3.74E-11	326.966
Rcc2	4.26E-11	3453.340
Unc5c	4.81E-11	118.524
Bub1b	4.99E-11	1267.941

Up-regulated		
Gene	**Adjusted P value**	**Log2 fold change**
Rn7sk	2.44E-24	550.386
AY036118	9.85E-11	22.681
Rprl2	8.30E-11	54.093
Gm5210	1.39E-08	6.834
Klhl5	3.53E-06	718.336
n-R5-8s1	4.49E-06	83.774
Rmrp	3.94E-06	22.828
Acbd4	1.07E-05	555.954
Pex13	1.18E-05	626.057
Rps3a3	1.22E-05	22.241
Gpr135	3.12E-05	13.571
Nxt2	3.37E-05	253.855
Gm14420	6.14E-05	72.569
Gm20721	5.89E-05	58.048
Ndfip1	5.47E-05	3153.819

Trp53-/-;Brca1-/- (PBS) versus *Trp53-/-;Brca1-/-* (cisplatin)

Down-regulated		
Gene	**Adjusted P value**	**Log2 fold change**
Igkv6-13	2.98E-06	50.813
Lypd8	4.82E-06	52.806
Gkn3	1.44E-05	90.152
Muc5ac	4.87E-05	71.568
Clca3	7.93E-05	27.535
Muc6	7.81E-05	45.467

Up-regulated		
Gene	**Adjusted P value**	**Log2 fold change**
Gm1110	1.33E-15	24.189
Tceal7	9.63E-14	37.803
Kprp	2.46E-12	397.555
Lce1f	2.32E-11	154.745
Casp14	7.00E-11	193.716
Hrnr	6.74E-10	229.869
Lce1d	8.25E-10	227.115
Lce3a	4.95E-09	76.030
Serpinb3a	8.70E-09	146.206
Lce1a2	3.03E-08	201.170
Tmprss11f	8.20E-08	28.920
Flg	2.65E-07	197.834
Lce1b	4.82E-07	144.190
Usp18	5.05E-07	431.760
Lce1c	5.88E-07	182.904
Lce1a1	7.36E-07	232.437
Oas1a	8.16E-07	306.588
Klk5	2.61E-06	93.799
Isg15	6.42E-06	703.111
Lce1e	1.01E-05	104.485
Lce3b	1.04E-05	51.419
Lce3c	9.87E-06	77.348
Lce1i	1.38E-05	74.684
Hamp	2.01E-05	595.306
Gm6548	2.36E-05	356.728
Lce1g	2.38E-05	98.590
Lce1l	3.00E-05	89.023
2310050C0	4.20E-05	122.882
Bst2	7.09E-05	2378.200
2810007J2	8.09E-05	511.086
Irf7	7.88E-05	1632.101
Myh8	8.36E-05	1696.772

Trp53-/- versus *Trp53-/-; Brca2-/-*

Down-regulated		
Gene	**Adjusted P value**	**Log2 fold change**
Cryaa	1.13E-24	308.248
Cd82	9.25E-23	4614.267
Cotl1	2.84E-22	6408.518
Stk32b	7.32E-22	316.030
Cdhr1	3.91E-21	386.363
H2-D1	4.63E-20	19093.937
Alppl2	2.11E-19	109.063
Atp1a3	2.17E-19	1120.143
Hat1	1.04E-18	1333.544
H2-K1	1.38E-17	22837.618
Znrf4	2.65E-17	157.767
Tapbp	9.91E-17	10010.628
Piwil4	5.46E-16	170.075
Gm14002	8.27E-16	54.216
Trmt6	4.02E-15	1117.218
Rap2a	5.74E-15	1911.118
Samhd1	5.72E-15	3817.135
Ccdc109b	1.27E-14	637.137
Dut	2.45E-14	1380.501
Mgarp	3.50E-14	486.669
Ece2	3.60E-14	460.551
Crnkl1	6.04E-14	975.243
Gpsm3	1.27E-13	553.824
Ager	1.66E-13	144.429
Exosc8	1.93E-13	521.103
Flt4	3.90E-13	2731.462
Dsn1	1.08E-12	326.966
Gpr176	1.24E-12	797.340
5033428I22Rik	1.40E-12	77.663
Nras	1.95E-12	1785.705
Rab32	2.39E-12	920.261
Arrb2	4.81E-12	1096.714
Dpy19l3	5.19E-12	1688.500
Snx7	5.64E-12	707.379
Myl12b	6.28E-12	2741.539
Lig1	6.72E-12	1316.464
Ogfr	8.08E-12	1594.347
Slc7a6	1.03E-11	1460.934
Palm3	1.89E-11	353.388
AI427809	2.34E-11	80.262
Lpar2	2.33E-11	1062.748
Piwil2	2.33E-11	1134.610
Olfr1372-ps1	2.53E-11	259.597
Trim59	2.57E-11	651.506
Acd	4.60E-11	580.008
Mcm8	5.13E-11	252.573
Tap2	5.09E-11	2115.504
Grin2d	6.50E-11	419.963
B230314M03Rik	6.67E-11	38.594
Rnf181	6.67E-11	3655.727

Up-regulated		
Gene	**Adjusted P value**	**Log2 fold change**
Rn7sk	7.07E-20	550.386
AY036118	2.29E-11	22.681
Lce1f	1.83E-10	154.745
Lce1d	5.16E-09	227.115
Espn	2.03E-08	463.067
Gm5210	6.99E-08	6.834
Rprl2	9.62E-08	54.093
Lce1a2	1.11E-07	201.170
Sis	2.51E-07	20.199
Lce1a1	1.97E-06	232.437
Lce1b	2.77E-06	144.190
Gpaa1	3.05E-06	916.159
Flg	3.99E-06	197.834
Rmrp	4.02E-06	22.828
n-R5-8s1	7.85E-06	83.774
Lce1l	1.48E-05	89.023
Lce1m	1.54E-05	254.072
Pmaip1	1.66E-05	183.431
Hoxc12	1.86E-05	21.620
Fignl2	2.82E-05	124.982
Igkv3-5	2.77E-05	177.153
Lce1i	3.99E-05	74.684
Rgs16	3.89E-05	519.892
Vegfa	4.65E-05	6962.023
Igkv4-72	4.89E-05	87.393
Lce1e	7.06E-05	104.485
Mdfi	6.83E-05	208.531
Lrp2bp	7.52E-05	15.171
Trp53	9.69E-05	848.680
Nrgn	0.000108574	106.482
Cish	0.000118576	470.397
mt-Nd6	0.000120758	137.465
AY761184	0.000156889	5.988
Gm15408	0.000178273	26.624
Chac2	0.000245043	98.191
Socs2	0.000254748	387.902
Fras1	0.000281598	119.964
Mdm2	0.000280551	820.719
Tdrkh	0.000290448	57.217
Nmral1	0.000350786	110.119
Col27a1	0.000374875	224.970
Igkv4-63	0.000445103	29.757

Trp53-/-;Brca2-/- (PBS) versus *Trp53-/-;Brca2-/-* (cisplatin)

Down-regulated		
Gene	**Adjusted P value**	**Log2 fold change**
Lce1f	3.12E-11	154.745
Lce1d	4.88E-10	227.115
Lce1a2	2.32E-08	201.170
Flg	5.06E-07	197.834
Lce1a1	4.03E-07	232.437
Lce1b	4.45E-07	144.190
Lce1m	4.12E-07	254.072
Hmcn1	2.77E-06	349.734
P2ry12	8.15E-06	97.603
Lce1e	1.20E-05	104.485
Lce1i	1.33E-05	74.684
Lce1l	1.14E-05	89.023
Tubb1	1.30E-05	15.701
Prokr1	3.47E-05	17.498
Lce1j	5.13E-05	33.192
Nrgn	6.01E-05	106.482
2310050C09Rik	6.48E-05	122.882
Igkv3-12	6.34E-05	111.468
Igfbp5	7.41E-05	7358.120
Bai2	0.000105091	686.892
Map3k7	0.00010421	1285.324
Ptpn4	0.000115634	183.851
Tagap	0.000115911	166.907
Ppbp	0.000120648	31.628
Ighg3	0.000129718	1208.547
Igkv8-16	0.000125743	76.664

Up-regulated		
Gene	**Adjusted P value**	**Log2 fold change**
Brf2	2.02E-08	172.044
Mybphl	2.12E-07	310.013
Sprr2a3	4.69E-07	34.116
Ighv1-7	1.48E-06	122.526
Tm2d2	1.71E-06	1015.913
Ing2	7.03E-06	227.023
Tmem66	7.02E-06	2871.151
2310045N01Rik	7.51E-06	415.645
Tmem35	1.22E-05	179.679
Ash2l	1.50E-05	982.941
Ddx49	1.82E-05	718.805
Uba52	2.16E-05	348.022
Prosc	2.32E-05	1119.941
Mvb12a	2.48E-05	933.663
Sema7a	2.77E-05	1194.781
Frg1	3.25E-05	466.821
Prap1	3.35E-05	32.328
Fkbp8	4.10E-05	4924.168
Shh	6.75E-05	13.794
Ripply1	7.16E-05	50.849
1700019B21Rik	7.97E-05	13.514
AU015836	8.58E-05	12.300
Pgls	0.000121278	1268.693
Igkv16-104	0.000127456	368.995
Cfdp1	0.000151444	1434.303

Trp53-/- versus *Trp53-/-;Nf1-/-*

Down-regulated		
Gene	**Adjusted P value**	**Log2 fold change**
Alppl2	1.73E-35	140.139
Atp1a3	7.63E-23	971.421
Znrf4	9.47E-23	143.101
Ager	2.29E-22	151.542
Flt4	5.45E-22	2470.028
Piwil4	5.23E-22	138.614
Dut	1.25E-21	1082.358
Cd82	3.70E-21	4341.341
Cdhr1	8.60E-19	297.321
Edn2	1.11E-18	198.711
Slc7a6	1.32E-18	1251.347
Galnt10	1.58E-18	2504.629
Cplx2	3.08E-18	791.801
Lig1	5.02E-18	1307.545
Cryaa	7.38E-18	160.528
Cotl1	1.85E-17	4642.167
Dpy19l3	1.79E-17	1457.185
Grin2d	5.71E-16	343.614
Olfr1372-ps1	9.59E-16	203.311
Sox8	1.34E-15	709.133
Rai14	1.88E-15	3758.100
Snx7	2.37E-15	571.793
Fam118a	8.97E-15	839.886
Haus4	9.11E-15	347.859
Slc27a6	1.16E-14	391.486
Foxs1	2.12E-14	633.250
Syt9	2.88E-14	262.895
Ece2	3.61E-14	396.742
Plscr1	4.15E-14	874.397
Carhsp1	6.52E-14	3172.978
Lrp8	8.35E-14	162.354
Plxdc1	1.04E-13	1391.992
Rnf181	1.85E-13	3866.419
Gpr176	3.82E-13	534.229
Runx2	4.38E-13	257.287
Flnb	5.35E-13	7221.178
Camk2n2	5.42E-13	135.054
Gm14002	8.04E-13	48.387
Slc35b4	1.69E-12	1334.078
Nubp2	1.73E-12	759.778
4930486L24Rik	2.95E-12	287.834
Limk1	3.59E-12	654.290
Samhd1	4.65E-12	2872.506
Trmt6	5.13E-12	943.312
Eya2	5.30E-12	322.264
Scube3	5.85E-12	2040.003
Chrd	6.97E-12	615.260
Mgarp	7.15E-12	473.038
Adamts14	8.34E-12	513.091
H13	1.14E-11	4129.792

Up-regulated		
Gene	**Adjusted P value**	**Log2 fold change**
Rn7sk	4.14E-24	505.652
E330013P04Rik	5.06E-21	72.339
Casp14	1.31E-20	181.917
Rspo1	3.65E-15	912.587
Il1f5	6.38E-15	293.535
Cpq	1.76E-12	1756.715
Klk7	1.63E-12	133.523
Lce1e	9.42E-12	100.132
Lctl	1.78E-11	458.530
Pgc	1.09E-10	157.537
Gm10664	3.21E-10	17.775
AY036118	1.60E-09	23.501
Kcnt1	2.35E-09	549.226
Casp3	3.72E-09	404.724
Rmrp	6.50E-09	22.361
Spon2	7.66E-09	482.432
Aadacl3	9.50E-09	27.532
Upk3b	1.05E-08	2756.311
Lce1k	1.22E-08	49.925
Crot	2.15E-08	1846.395
Nr2e3	2.29E-08	18.060
Mdfi	2.47E-08	183.402
Rprl2	2.69E-08	48.755
n-R5-8s1	3.49E-08	76.783
Lcn11	3.84E-08	21.393
Hs6st2	4.49E-08	253.494
Slc13a4	4.77E-08	104.749
Casp1	5.02E-08	341.339
BC023105	5.65E-08	27.202
Gm12979	8.11E-08	13.984
Il17re	9.25E-08	107.163
Pkhd1l1	9.86E-08	1094.131
Klra2	1.30E-07	87.693
Igfbp5	1.54E-07	5436.266
Cers4	2.25E-07	693.162
Fxyd3	2.58E-07	386.865
Gng13	2.84E-07	27.489
Lce1g	3.16E-07	98.194
Pmaip1	3.56E-07	138.986
Aire	3.79E-07	18.144
Clec7a	3.78E-07	311.615
Arhgap29	4.18E-07	2533.610
Ptges3	4.54E-07	457.206
Gm15536	4.67E-07	25.713
Pilrb1	5.28E-07	19.121
Gm5210	5.86E-07	6.941
Gbp10	6.20E-07	24.903
Ndp	6.35E-07	63.136
Gm8430	7.50E-07	22.255
Ccdc64	8.45E-07	403.388

Trp53-/-;Nf1-/- (PBS) versus *Trp53-/-;Nf1* (cisplatin)

Down-regulated		
Gene	**Adjusted P value**	**Log2 fold change**
Casp14	9.08E-33	181.917
Rspo1	6.72E-32	912.587
Il1f5	1.33E-28	293.535
Upk3b	4.54E-26	2756.311
Lce1e	6.63E-22	100.132
Klk7	6.26E-21	133.523
Podxl	2.61E-18	6104.929
Gpr37	1.16E-17	115.243
Aadacl3	4.05E-16	27.532
Wwtr1	4.57E-16	2245.709
Lce1k	5.93E-16	49.925
Neo1	8.73E-16	2910.924
Wt1	9.24E-16	6819.456
E330013P04Rik	4.98E-15	72.339
Dcbld2	9.80E-15	1536.604
Wnt11	9.32E-15	1280.586
Asic3	1.24E-14	91.026
Cdon	1.47E-14	3605.485
Add3	1.61E-14	2661.938
Zbtb8a	3.18E-14	219.002
Abca4	5.55E-14	83.324
Slc13a4	8.46E-14	104.749
Unc13c	2.38E-13	64.176
Faim	2.48E-13	278.874
Kdelc2	3.47E-13	699.360
Necab3	7.22E-13	54.871
Ctxn1	7.95E-13	440.477
Klk5	8.59E-13	85.762
Lgals1	8.60E-13	28725.739
Al314831	1.26E-12	542.271
Lce1g	2.65E-12	98.194
Cldn26	3.31E-12	55.806
Ttll5	4.93E-12	424.464
Smim1	5.13E-12	1570.112
Wfikkn2	7.00E-12	253.485
Gxylt2	1.13E-11	456.425
Maged2	1.13E-11	6061.217
Crb2	1.60E-11	2058.946
Lrrn4	1.73E-11	412.909
Pkhd1l1	2.00E-11	1094.131
Wnt10b	2.41E-11	278.974
Pcnxl2	2.60E-11	393.452
Cers4	2.75E-11	693.162
Sv2a	2.75E-11	306.539
Kcnab1	3.13E-11	673.662
Gng13	3.21E-11	27.489
Pappa	4.81E-11	279.079
Lce1j	5.00E-11	32.551
Cercam	5.95E-11	664.033
Tyro3	6.79E-11	2796.784

Up-regulated		
Gene	**Adjusted P value**	**Log2 fold change**
Ccrl2	3.45E-14	63.643
Fas	3.15E-12	165.662
Acp2	4.70E-11	916.040
St3gal1	7.13E-11	1600.100
Ppbp	2.91E-10	33.260
C6	3.29E-10	164.606
Lrrc32	6.13E-10	525.178
Zfp422	8.00E-10	128.324
Dhx58	8.20E-10	240.781
Tspan11	9.56E-10	207.986
Timd4	1.04E-09	61.422
Adam23	1.79E-09	159.039
Susd4	1.94E-09	34.118
Trim25	2.00E-09	1974.371
Rnf130	3.07E-09	699.686
Fam167b	3.27E-09	89.317
Clec14a	3.75E-09	217.326
Ednrb	4.47E-09	374.221
Slco1a1	6.63E-09	247.914
Pcdh17	8.39E-09	112.046
Col27a1	9.50E-09	219.086
Pros1	9.67E-09	768.242
Cd163	1.27E-08	477.921
Serpine1	1.37E-08	4182.702
Bcl6b	1.46E-08	130.107
Cd97	1.52E-08	1143.120
Colec12	1.72E-08	629.259
Scarf1	1.89E-08	168.395
Cd209a	1.91E-08	20.999
S1pr3	2.37E-08	231.377
Nrep	2.40E-08	556.933
Jam2	2.94E-08	452.216
Fgf1	3.22E-08	970.377
Itga9	3.21E-08	885.601
Kdr	3.17E-08	904.306
Scn8a	4.34E-08	11.640
Emr4	4.75E-08	42.756
Kalrn	4.84E-08	739.429
Kcnj8	5.72E-08	226.150
Efna1	6.12E-08	500.496
Rnf114	6.43E-08	1169.358
Fam46a	7.14E-08	388.151
Gm13705	7.54E-08	15.158
Angptl4	8.47E-08	1564.356
2210016F16Rik	9.84E-08	259.453
Lrp3	9.98E-08	191.548
Itga1	1.19E-07	360.352
Tcf24	1.21E-07	20.752
Ldb2	1.44E-07	100.033
Fancf	1.59E-07	26.130